NASA Tech Briefs

National
Aeronautics and
Space
Administration



Beginning with the results of NASA work in ferrofluids, a New Hampshire corporation extended the state of the art in this area and found new applications, such as using ferromagnetic fluids to enhance the performance of the loudspeakers shown here. *[See page A1.]*

Vol. 4, No. 4

Winter 1979

About the NASA Technology Utilization Program

The National Aeronautics and Space Act of 1958, which established NASA and the United States civilian space program, requires that "The Administration shall provide for the widest practicable and appropriate dissemination of information concerning its activities and the results thereof."

To help carry out this objective, NASA's Technology Utilization (TU) Program was established in 1962. Now, as an element of NASA's Technology Transfer Division, this program offers a variety of valuable services to help transfer aerospace technology to nonaerospace applications, thus assuring American taxpayers maximum return on their investment in space research; thousands of spinoffs of NASA research have already occurred in virtually every area of our economy.

The TU program has worked for engineers, scientists, technicians, and businessmen; and it can work for you.

NASA Tech Briefs

Tech Briefs is published quarterly and is free to engineers in U.S. industry and to other domestic technology transfer agents. It is both a current-awareness medium and a problem-solving tool. Potential products . . . industrial processes . . . basic and applied research . . . shop and lab techniques . . . computer software . . . new sources of technical data . . . concepts . . . can be found here. The short section on New Product Ideas highlights a few of the potential new products contained in this issue. The remainder of the volume is organized by technical category to help you quickly review new developments in your areas of interest. Finally, a subject index makes each issue a convenient reference file.

Further Information on Innovations

Although some new technology announcements are complete in themselves, most are backed up by Technical Support Packages (TSP's). TSP's are available without charge and may be ordered by simply completing a TSP Request Card found at the back of this volume. Further information on some innovations is available for a nominal fee from other sources, as indicated. In addition, Technology Utilization Officers at NASA Field Centers will often be able to lend necessary guidance and assistance.

Patent Licenses

Patents have been issued to NASA on some of the inventions described, and patent applications have been submitted on others. Each announcement indicates patent status, if applicable.

Other Technology Utilization Services

To assist engineers, industrial researchers, business executives, city officials, and other potential users in applying space technology to their problems, NASA sponsors Industrial Applications Centers. Their services are described on page A6. In addition, an extensive library of computer programs is available through COSMIC, the Technology Utilization Program's outlet for NASA-developed software.

Applications Program

NASA conducts applications engineering projects to help solve public-sector problems in such areas as safety, health, transportation, and environmental protection. Applications teams, staffed by professionals from a variety of disciplines, assist in this effort by working with Federal agencies and health organizations to identify critical problems amenable to solution by the application of existing NASA technology.

Reader Feedback

We hope you find the information in *NASA Tech Briefs* useful. A reader-feedback card has been included because we want your comments and suggestions on how we can further help you apply NASA innovations and technology to your needs. Please use it; or if you need more space, write to the Director, Technology Transfer Division, P. O. Box 8757, Baltimore/Washington International Airport, Maryland 21240.

NASA Tech Briefs

National Aeronautics and Space Administration

WINTER 1979
Volume 4, Number 4

NASA TU Services	A3	Technology Utilization services that can assist you in learning about and applying NASA technology.
New Product Ideas	A9	A summary of selected innovations of value to manufacturers for the development of new products.
Tech Briefs	461	**Electronic Components and Circuits**
	479	**Electronic Systems**
	485	**Physical Sciences**
	501	**Materials**
	513	**Life Sciences**
	519	**Mechanics**
	543	**Machinery**
	553	**Fabrication Technology**
	581	**Mathematics and Information Sciences**
Subject Index	587	Items in this issue are indexed by subject; a cumulative index will be published yearly.

COVERS: The photographs on the front and back covers illustrate developments by NASA and its contractors that resulted in commercial and nonaerospace spinoffs. You can use the TSP Request Card at the end of this issue to learn more about the Ferrofluid Applications [Circle 75] and the Emergency Lighting System [Circle 76].

About This NASA Publication

NASA Tech Briefs, a quarterly publication, is distributed free to qualified U.S. citizens to encourage commercial application of U.S. space technology. For information on publications and services available through the NASA Technology Utilization Program, write to the Director, Technology Transfer Division, P. O. Box 8757, Baltimore/Washington International Airport, Maryland 21240.

"The Administrator of National Aeronautics and Space Administration has determined that the publication of this periodical is necessary in the transaction of the public business required by law of this Agency. Use of funds for printing this periodical has been approved by the Director of the Office of Management and Budget."

Change of Address

If you wish to have NASA Tech Briefs forwarded to your new address, use one of the Subscriptions cards enclosed in the back of this volume of NASA Tech Briefs. Be sure to check the appropriate box indicating change of address.

Communications Concerning Editorial Matter

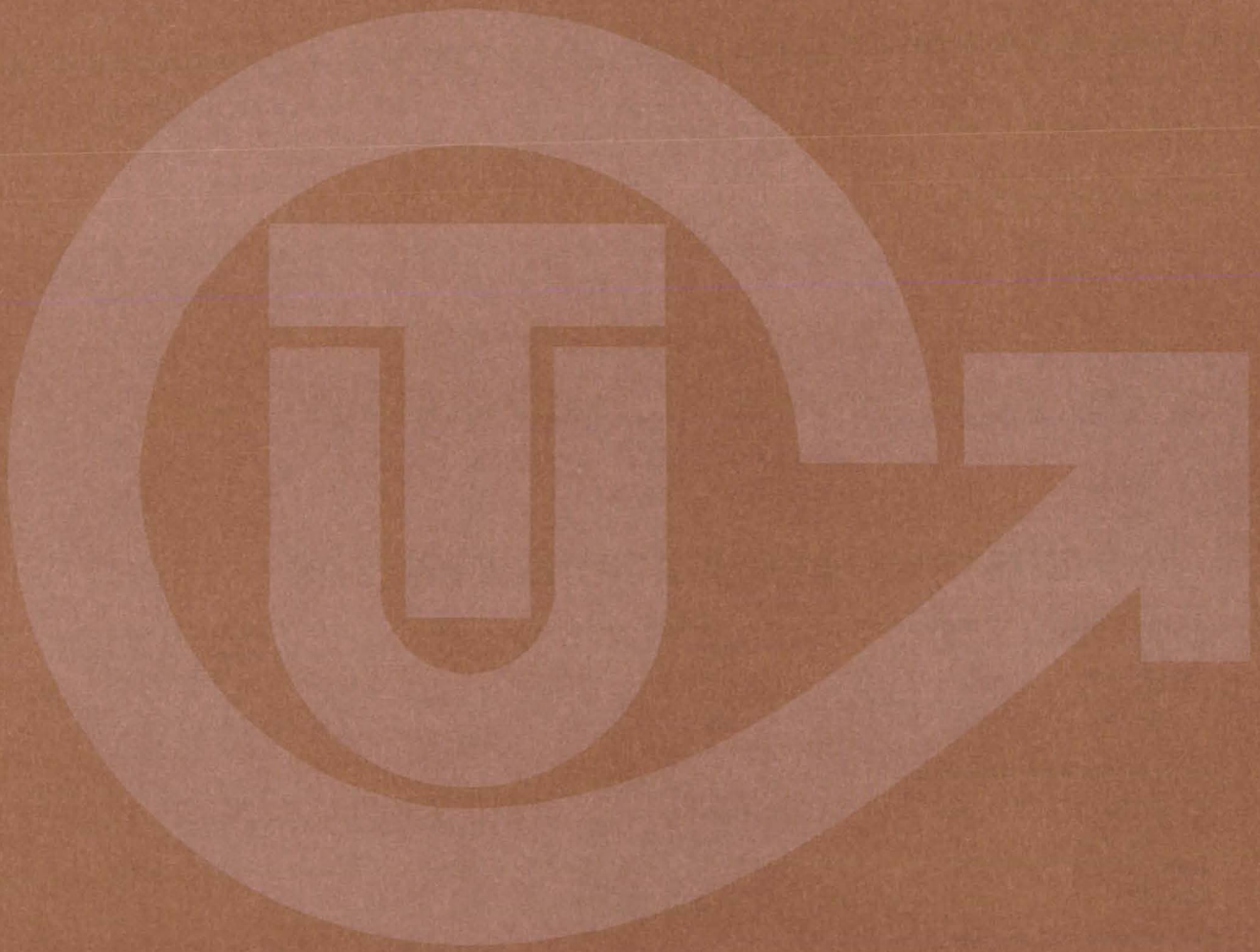
For editorial comments or general communications about NASA Tech Briefs, you may use the Feedback card in the back of NASA Tech Briefs, or write to: The Publications Manager, Technology Transfer Division (ETD-6), NASA Headquarters, Washington, DC 20546. Technical questions concerning specific articles should be directed to the Technology Utilization Officer of the sponsoring NASA Center (addresses listed on page A4).

Acknowledgements

NASA Tech Briefs is published quarterly by the National Aeronautics and Space Administration, Technology Utilization Branch, Washington, DC: Administrator: **Robert A. Frosch;** Director, Technology Transfer Division: **Floyd I. Roberson;** Publications Manager: **D. W. Orrick.** Prepared for the National Aeronautics and Space Administration by **Logical Technical Services Corp.:** Editor-in-Chief: **Graham L. Gross;** Art Director: **Ernest Gillespie;** Managing Editor: **Jay Kirschenbaum;** Senior Editor: **Donald Blattner;** Chief Copy Editor: **Oden Browne;** Staff Editors: **Jerry Rosen, Ted Selinsky, George Watson;** Graphics: **Concetto Auditore, Luis Martinez, Pat McDermond;** Editorial & Production: **Richard Johnson, Rose Giglietti, Beth Rogers, Vincent Susinno, John Tucker, Ernestine Walker.**

This document was prepared under the sponsorship of the National Aeronautics and Space Administration.. Neither the United States Government nor any person acting on behalf of the United States Government assumes any liability resulting from the use of the information contained in this document, or warrants that such use will be free from privately owned rights.

NASA TU SERVICES



NASA TECHNOLOGY UTILIZATION NETWORK

★ TECHNOLOGY UTILIZATION OFFICERS

Charles C. Kubokawa
Ames Research Center
Code AU: 240-2
Moffett Field, CA 94035
(415) 965-5333

Gussie Anderson
Hugh L. Dryden Flight Research Center
Code OD/TU Office - Room 2015
Post Office Box 273
Edwards, CA 93523
(805) 258-3311, Ext. 787

Donald S. Friedman
Goddard Space Flight Center
Code 702.1
Greenbelt, MD 20771
(301) 344-6242

John T. Wheeler
Lyndon B. Johnson Space Center
Code AT-3
Houston, TX 77058
(713) 483-3809

Raymond J. Cerrato
John F. Kennedy Space Center
Code AA-SA-1
Kennedy Space Center, FL 32899
(305) 867-2780

John Samos
Langley Research Center
Mail Stop 139A
Hampton, VA 23665
(804) 827-3281

Paul Foster
Lewis Research Center
Mail Stop 3-19
21000 Brookpark Road
Cleveland, OH 44135
(216) 433-4000, Ext. 6422

Aubrey D. Smith
George C. Marshall Space Flight Center
Code AT01
Marshall Space Flight Center, AL 35812
(205) 453-2224

D. W. Orrick
NASA Headquarters
Code ETD-6
Washington, DC 20546
(202) 755-2244

John H. Warden
NASA Pasadena Office
4800 Oak Grove Drive
Pasadena, CA 91103
(213) 354-6420

Gilmore H. Trafford
Wallops Flight Center
Code OD
Wallops Island, VA 23337
(804) 824-3411, Ext. 201

● INDUSTRIAL APPLICATIONS CENTERS

Aerospace Research Applications Center
1201 East 38th Street
Indianapolis, IN 46205
E. G. Buck, director
(317) 264-4644

Computer Software Management and Information Center (COSMIC)
Suite 112, Barrow Hall
University of Georgia
Athens, GA 30602
(404) 542-3265

Kerr Industrial Applications Center
Southeastern Oklahoma State University
Durant, OK 74701
Robert Oliver, director
(405) 924-0121, Ext. 413

NASA Industrial Applications Center
LIS Building
University of Pittsburgh
Pittsburgh, PA 15260
Edmond Howie, director
(412) 624-5211

New England Research Applications Center
Mansfield Professional Park
Storrs, CT 06268
Daniel Wilde, director
(203) 486-4533

North Carolina Science and Technology Research Center
Post Office Box 12235
Research Triangle Park, NC 27709
Peter J. Chenery, director
(919) 549-0671

Technology Applications Center
University of New Mexico
Albuquerque, NM 87131
Stanley Morain, director
(505) 277-3622

Western Research Applications Center
University of Southern California
University Park
Los Angeles, CA 90007
Robert Mixer, acting director
(213) 741-6132

■ STATE TECHNOLOGY APPLICATIONS CENTERS

NASA/University of Florida
State Technology Applications Center
311 Weil Hall
University of Florida
Gainesville, FL 32611
Ronald J. Thornton, director
Gainesville: (904) 392-6760
Orlando: (305) 275-2706
Tampa: (813) 974-2499

NASA/University of Kentucky
State Technology Applications Program
109 Kinkead Hall
University of Kentucky
Lexington, KY 40506
William R. Strong, manager
(606) 258-4632



◆ PATENT COUNSELS

Robert F. Kempf
Asst. Gen. Counsel for patent matters
NASA Headquarters
Code GP-4
400 Maryland Avenue, S.W.
Washington, DC 20546
(202) 755-3954

Darrell G. Brekke
Ames Research Center
Mail Code: 200-11A
Moffett Field, CA 94035
(415) 965-5104

Paul F. McCaul
Hugh L. Dryden Flight Research Center
Code OD/TU Office - Room 2015
Post Office Box 273
Edwards, CA 93523
(213) 354-2734

John O. Tresansky
Goddard Space Flight Center
Mail Code: 204
Greenbelt, MD 20771
(301) 344-7351

Marvin F. Matthews
Lyndon B. Johnson Space Center
Mail Code: AM
Houston, TX 77058
(713) 483-4871

James O. Harrell
John F. Kennedy Space Center
Mail Code: SA-PAT
Kennedy Space Center, FL 32899
(305) 867-2544

Howard J. Osborn
Langley Research Center
Mail Code: 279
Hampton, VA 23665
(804) 827-3725

Norman T. Musial
Lewis Research Center
Mail Code: 500-311
21000 Brookpark Road
Cleveland, OH 44135
(216) 433-4000, Ext. 346

Leon D. Wofford, Jr.
George C. Marshall Space Flight Center
Mail Code: CC01
Marshall Space Flight Center, AL 35812
(205) 453-0020

Monte F. Mott
NASA Pasadena Office
Mail Code: 180-601
4800 Oak Grove Drive
Pasadena, CA 91103
(213) 354-2700

▲ APPLICATION TEAMS

William N. Fetzner, director
Advisory Center for Medical Technology and Systems
University of Wisconsin
1500 Johnson Drive
Madison, WI 53706
(608) 263-2735

Edmund R. Bangs, director
IIT Research Institute
10 West 35th Street
Chicago, IL 60616
(312) 567-4191

Doris Rouse, director
Research Triangle Institute
Post Office Box 12194
Research Triangle Park, NC 27709
(919) 541-6256

Tom Anyos, director
SRI International
333 Ravenswood Avenue
Menlo Park, CA 94026
(415) 326-6200, Ext. 2864

Eugene Schmidt, program coordinator
Stanford University School of Medicine
Cardiology Division
Biomedical Technology Transfer
703 Welch Road, Suite E-4
Palo Alto, CA 94304
(415) 497-5353

David MacFadyen, project director
Technology + Economics
2225 Massachusetts Avenue
Cambridge, MA 02140
(617) 491-1500

TECHNOLOGY UTILIZATION OFFICERS

Technology transfer experts can help you apply the innovations in NASA Tech Briefs.

The Technology Utilization Officer at each NASA Field Center is an applications engineer who can help you make use of new technology developed at his center. He brings you NASA Tech Briefs and other special publications, sponsors conferences, and arranges for expert assistance in solving technical problems.

Technical assistance, in the form of further information about NASA innovations and technology, is one of the services available from the TUO. Together with NASA scientists and engineers, he can often help you find and implement NASA technology to meet your specific needs.

Technical Support Packages (TSP's) are prepared by the center TUO's. They provide further technical details for articles in NASA Tech Briefs. This additional material can help you evaluate and use NASA technology. You may receive most TSP's free of charge by using the TSP Request Card found at the back of this issue.

Technical questions about articles *in NASA Tech Briefs are answered in the TSP's. When no TSP is available, or you have further questions, contact the Technology Utilization Officer at the center that sponsored the research* [see page A4].

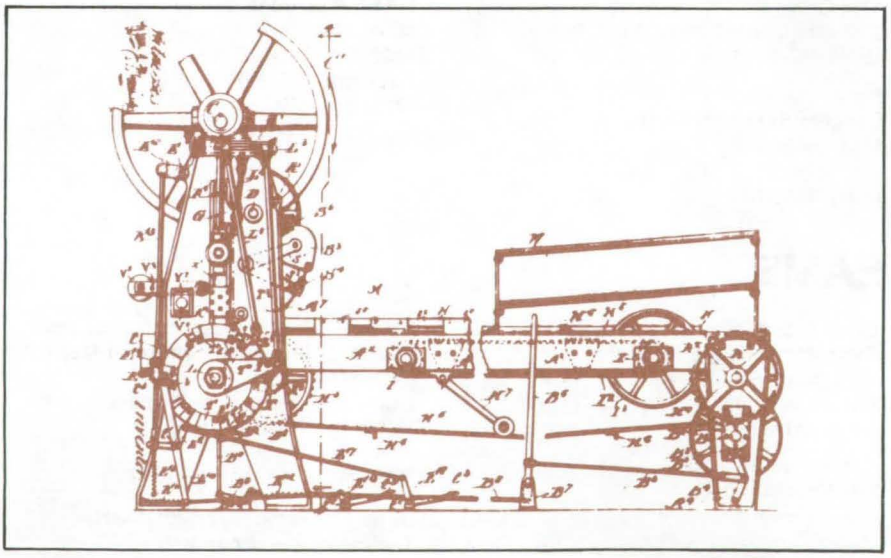


NASA INVENTIONS AVAILABLE FOR LICENSING

Over 3,500 NASA inventions are available for licensing in the United States — both exclusive and nonexclusive.

Nonexclusive licenses for commercial use of NASA inventions are encouraged to promote competition and to achieve the widest use of inventions. They must be used by a negotiated target date but are usually royalty-free.

Exclusive licenses may be granted to encourage early commercial development of NASA inventions, especially when considerable private investment is required. These are generally for 5 to 10 years and usually require royalties based on sales or use.



Additional licenses available include those of NASA-owned foreign patents. In addition to inventions described in NASA Tech Briefs, *"NASA Patent Abstract Bibliography"* (PAB), containing abstracts of all NASA inventions, can be purchased from National Technical Information Service, Springfield, VA 22161. The PAB is updated semiannually.

Patent licenses for Tech Briefs *are frequently available. Many of the inventions reported in NASA Tech Briefs are patented or are under consideration for a patent at the time they are published. The current patent status is described at the end of the article; otherwise, there is no statement about patents. If you want to know more about the patent program or are interested in licensing a particular invention, contact the Patent Counsel at the NASA Field Center that sponsored the research* [see page A5]. *Be sure to refer to the NASA reference number at the end of the Tech Brief.*

APPLICATION TEAMS

Technology-matching and problem-solving assistance to public-sector organizations

Application engineering projects are conducted by NASA to help solve public-sector problems in such areas as safety, health, transportation, and environmental protection. Some application teams specialize in biomedical disciplines; others, in engineering and scientific problems. Staffed by professionals from various disciplines, these teams work with other Federal agencies and health organizations to identify critical problems amenable to solution by the application of existing NASA technology.



Public-sector organization *representatives can learn more about application teams by contacting a nearby NASA Field Center Technology Utilization Office* [*see page A4*].

INDUSTRIAL APPLICATIONS CENTERS

Computerized access to nearly 10 million documents worldwide

Computerized information retrieval from one of the world's largest banks of technical data is available from NASA's network of Industrial Applications Centers (IAC's). The IAC's give you access to 1,800,000 technical reports in the NASA data base and to more than 10 times that many reports and articles found in 140 other computerized data bases.

The major sources include:

- *750,000 NASA Technical Reports*
- *Selected Water Resources Abstracts*
- *NASA Scientific and Technical Aerospace Reports*
- *Air Pollution Technical Information Center*
- *NASA International Aerospace Abstracts*
- *Chem Abstracts Condensates*
- *Engineering Index*
- *Energy Research Abstracts*
- *NASA Tech Briefs*
- *Government Reports Announcements*

and many other specialized files on food technology, textile technology, metallurgy, medicine, business, economics, social sciences, and physical science.

The IAC services range from tailored literature searches through expert technical assistance:



- *Retrospective Searches:* Published or unpublished literature is screened, and documents are identified according to your interest profile. IAC engineers tailor results to your specific needs and furnish abstracts considered the most pertinent. Complete reports are available upon request.
- *Current-Awareness Searches:* IAC engineers will help design a program to suit your needs. You will receive selected monthly or quarterly abstracts on new developments in your area of interest.
- *Technical Assistance:* IAC engineers will help you evaluate the results of your literature searches. They can help find answers to your technical problems and put you in touch with scientists and engineers at appropriate NASA Field Centers.

Prospective clients *can obtain more information about the services offered by NASA IAC's by contacting the nearest IAC* [*see page A4*] *or by checking the IAC box on a TSP Request Card in this issue.*

STATE TECHNOLOGY APPLICATIONS CENTERS

Technical information services for industry and state and local government agencies

Local government and industry in Florida and Kentucky can utilize the services of NASA's State Technology Applications Centers (STAC's). The STAC's differ from the Industrial Applications Centers described on page A7, primarily in that they are integrated into existing state technical assistance programs and serve only the host state, whereas the IAC's serve multistate regions.

Many data bases, including the NASA base and several commercial bases, are available for automatic data retrieval through the STAC's. Other services such as document retrieval and special searches are also provided. (The STAC's normally charge a fee for their services.)

To obtain information *about the services offered by NASA STAC's, write or call the STAC in your state* [*see page A4*].

COSMIC®

An economical source of computer programs developed by NASA and other government agencies

A vast software library is maintained by COSMIC — the Computer Software Management and Information Center. COSMIC gives you access to approximately 1,600 computer programs developed for NASA and the Department of Defense and selected programs for other government agencies. Programs and documentation are available at reasonable cost.



Available programs range from management (PERT scheduling) to information science (retrieval systems) and computer operations (hardware and software). Hundreds of engineering programs perform such tasks as structural analysis, electronic circuit design, chemical analysis, and the design of fluid systems. Others determine building energy requirements and optimize mineral exploration.

COSMIC services go beyond the collection and storage of software packages. Programs are checked for completeness; special announcements and an indexed software catalog are prepared; and programs are reproduced for distribution. Customers are helped to identify their software needs; and COSMIC follows up to determine the successes and problems and to provide updates and error corrections. In some cases, NASA engineers can offer guidance to users in installing or running a program.

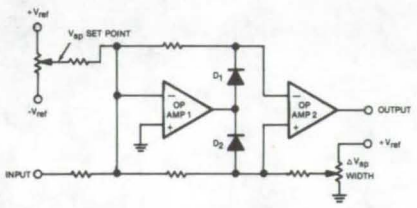
Information about programs *described in NASA Tech Briefs articles can be obtained by completing the COSMIC Request Card at the back of this issue. Just circle the letters that correspond to the programs in which you are interested.*

NEW PRODUCT IDEAS



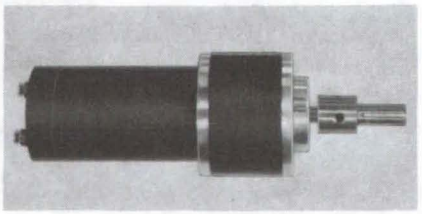
NEW PRODUCT IDEAS are just a few of the many innovations described in this issue of NASA Tech Briefs and having promising commercial applications. Each is discussed further on the referenced page in the appropriate section in this issue. If you are interested in developing a product from these or other NASA innovations, you can receive further technical information by requesting the TSP referenced at the end of the full-length article or by writing the Technology Utilization Office of the sponsoring NASA center (see page A4). NASA's patent-licensing program to encourage commercial development is described on page A6.

Window Comparator for Voltages



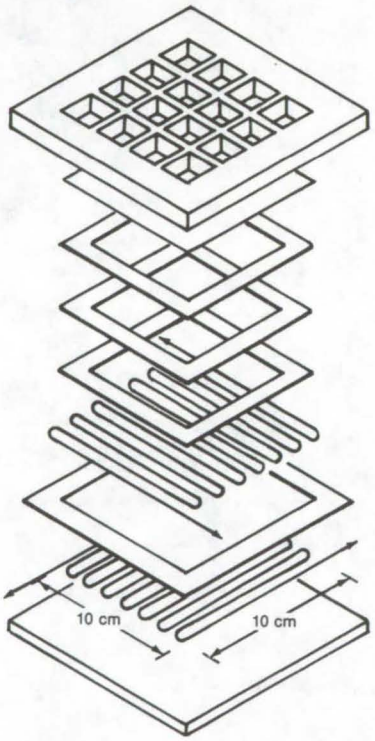
A very simple circuit determines whether an input voltage is within a preselected range. The circuit requires few components and is relatively immune to errors from reference-voltage drift. It could be useful in process-control circuitry, measuring instruments, and checkout equipment. The circuit uses two op amps and two switching diodes. One op amp subtracts the input signal from a set-point voltage. The other subtracts the difference output of the first op amp from the preselected window-width voltage. Unlike window comparators that consist of two simple level comparators, the stability requirements on the reference voltage are not great.
(See page 464.)

Miniature Motor-Driven Instrument Valve



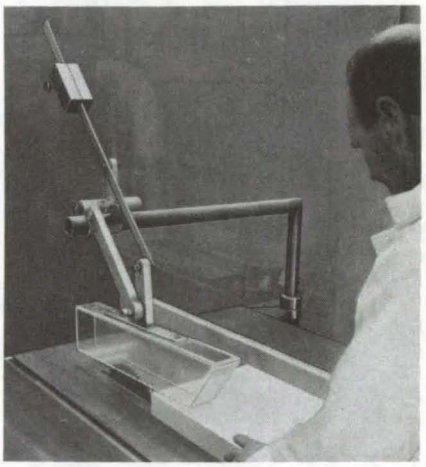
A remotely controlled valve can connect pressure transducers to calibration pressure sources. The valve can withstand up to 600 psi. It was developed for use in wind tunnels and engine test stands, but could be used in any application requiring pilot valves for control devices. Compared to other high-pressure instrument valves it requires less-precise machining and uses less power. It is essentially a small geared reversible motor operated by a momentary contact closure. The motor rotates a shaft and also moves it linearly, causing ports to be connected and disconnected. The control circuit consists of limit switches and relays.
(See page 547.)

Sealed High-Pressure X-Ray Detector



A new imaging hard X-ray detector operates for a long period of time with a single gas filling. Conventionally, a continuous gas flow has been requred to sweep out contaminants. This sealed detector has potential applications in nuclear medicine for use with radioactive tracers and could also be useful in X- and gamma-ray astronomy. The sealed detector can remain free of interfering contaminants because components are vacuum-baked before assembly to reduce outgassing, and passive "getters" are included within the package.
(See page 495.)

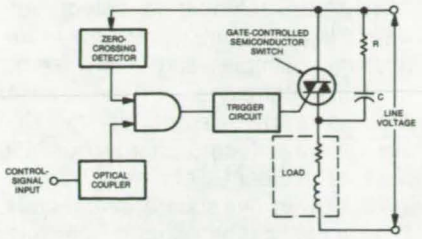
Improved Table-Saw Guard



A transparent plastic safety guard for table saws is counterbalanced to reduce damage to fragile materials (e.g., foams). The counterbalance causes less force to be applied to the workpiece as it is pushed under the guard. The overhead support makes is possible to perform slot and step cuts with the guard in place. This is not usually possible with a conventional guard that is supported by struts through the saw slot.
(See page 549.)

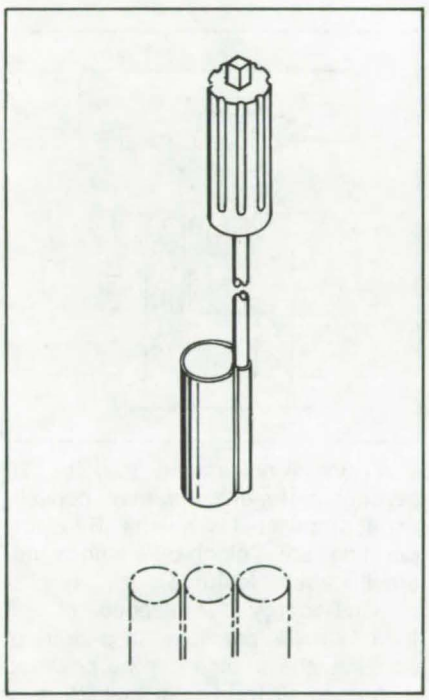
Low-EMI Solid-State Relay

A proposed solid-state relay could reduce the electromagnetic interference (EMI) generated when ac power is switched to a load. It could be used wherever the elimination of electrical noise is a concern. The input is optically coupled to the circuit. The input signal turns on a trigger circuit that fires a gate-controlled semiconductor switch, which switches current



to the load. In this way the load is turned on at zero voltage, and the semiconductor switch turns off at nearly zero current.
(See page 465.)

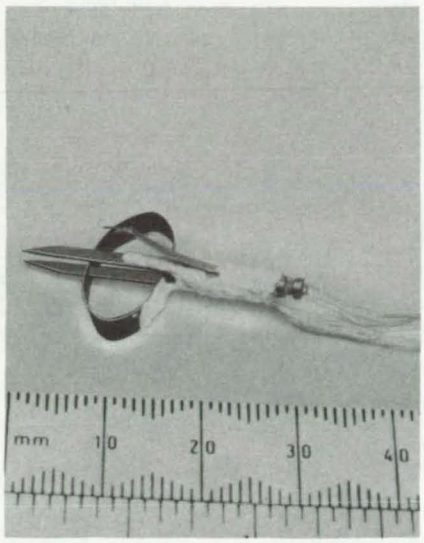
Tool for Installation and Removal of Cylindrical Baffles



A simple tool, similar to an automobile oil wrench, can be used to install and remove cylindrical baffles. The tool is essentially a curled metal sheet brazed onto a handgrip. The handgrip can be driven by wrench or other convenient tool. The curled metal sheet is slipped over a thread-on baffle and is twisted to advance the baffle. A separate mirror-image tool is used to remove a baffle.
(See page 551.)

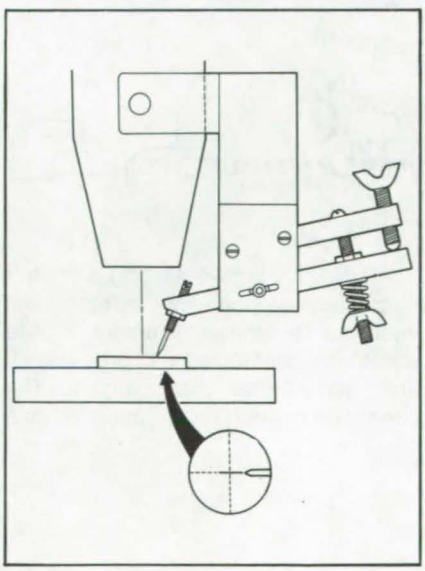
Trifunctional Transducer for Myocardial Monitoring

The prototype of a new myocardial transducer measures force, displacement, and thickness of the heart



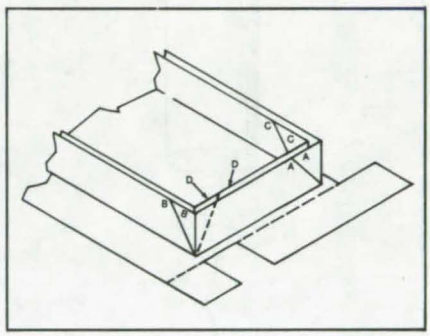
muscle simultaneously. The transducer, which has been tested on dogs, has a specially-designed tine system. Two tines, indented for retention by the muscle, have a lower compliance than the muscle fiber. This causes the fiber to apply stresses to the point where the tines are joined, where a piezoelectric transducer is placed. In addition, a high-compliance elliptical loop is attached to one tine. Changes in the thickness of the muscle compress the loop; compression is measured by a piezoelectric transducer. A third, high-compliance, tine detects linear displacement of the muscle fiber between the other two tines.
(See page 517.)

Precision Scriber



A precise tool can be used with a toolmaker's microscope to enscribe fine lines on flat or round surfaces. It was originally used to draw very accurate gage marks for a materials-testing program. This simply constructed tool can be screwed or clamped onto the lens column without altering the microscope. The scribe point is alined with the vertical crosshair of the eyepiece, and a line is drawn by moving the microscope slide table. The depth and width of the scribed line can be adjusted. When not needed, the scriber can be swung out of the way, allowing the microscope to be used for other purposes.
(See page 563.)

Structurally-Continuous Composite Corners



A simple technique for making boxes of plies of composite materials eliminates the overlapping edges that make the corners thicker than the walls for conventionally made containers. A proposed folding pattern produces uniform corners, and the cuts are structured so that shear loads are transferred from ply to ply instead of across one surface. This technique has been proposed for an aircraft aileron rib made from composite plies alternately oriented plus and minus 45°.
(See page 578.)

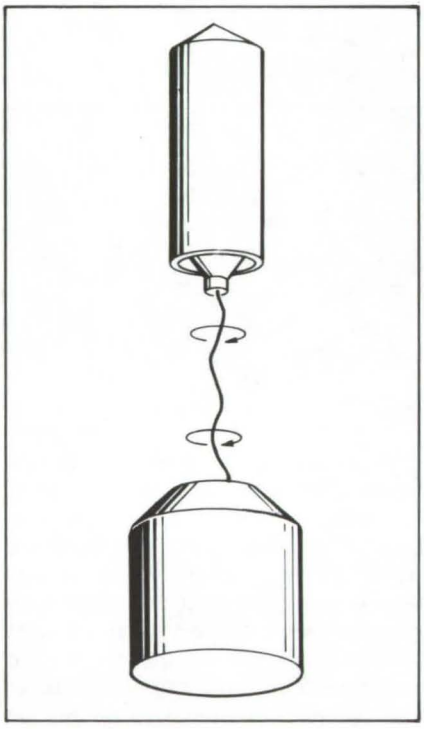
Plasma-Sprayed Valve Coating

A fused cobalt and tungsten carbide coating can reduce wear and improve the performance and life of valves, poppets, and other intricately shaped components. Developed to protect nickel alloy parts in the main engine of NASA's Space Shuttle, the coating could be useful in the manufacture of

(continued on next page)

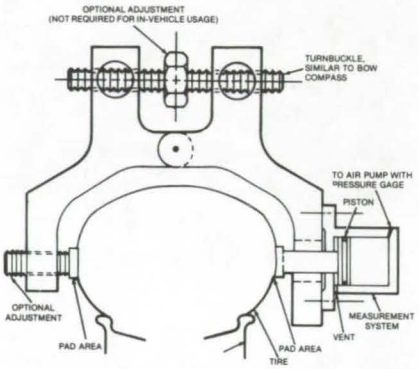
motors, automotive parts, and high-speed machinery. The dense and wear-resistant coating can be applied in controlled thicknesses. Coated parts resist spalling, flaking, thermal shock, and mechanical shock. The coating is applied with a plasma gun. On nickel parts, a nickel/boron/silicon braze alloy is applied first, followed by application of a mixture of the braze alloy with the cobalt and carbide coating material. The coating is subsequently fused at 1,050° C in a vacuum or inert atmosphere.
(See page 565.)

High-Acceleration Cable Deployment



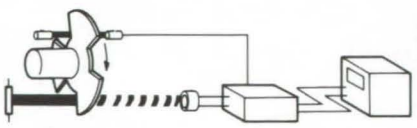
A cable-deployment projectile can withstand accelerations up to 20,000 g's and can operate at a velocity up to 500 ft/s. It was developed as a communications link for an instrument probe to be fired 40 ft into the surface of Mars. The forebody is a ballistic casing with a plastic drag funnel mounted over the rear opening. The cable is coiled within, in a single layer on a cylindrical spool. The cable is a tensile-strong beryllium and copper alloy with good elongation and low electrical resistivity. A tough lightweight coating similar to enamel is used as insulation. The projectile can be powered by a rocket or other suitable means.
(See page 545.)

New Tire-Pressure Gage



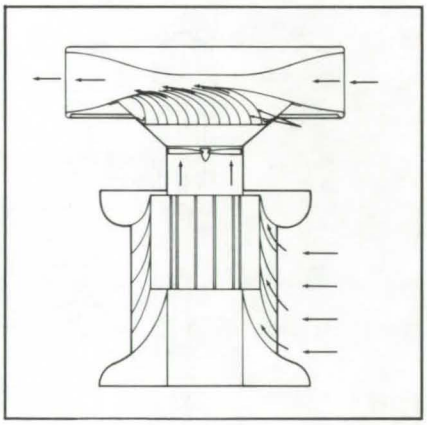
The tire pressure on aircraft and other vehicles could be rapidly measured with a proposed device that contacts only the tire walls. Since the device is not actually inserted into the airspace, no air is lost during the measurement, and continuous monitoring of pressure is possible. The pressure-sensing device consists of two pads that contact the inner and outer tire walls. One pad is connected to a pressure gage, and the load on that pad is increased until the tire deflects. At that point, the externally applied pressure is approximately equal to the internal tire pressure.
(See page 524.)

Sensor/Amplifier for Weak Light Sources



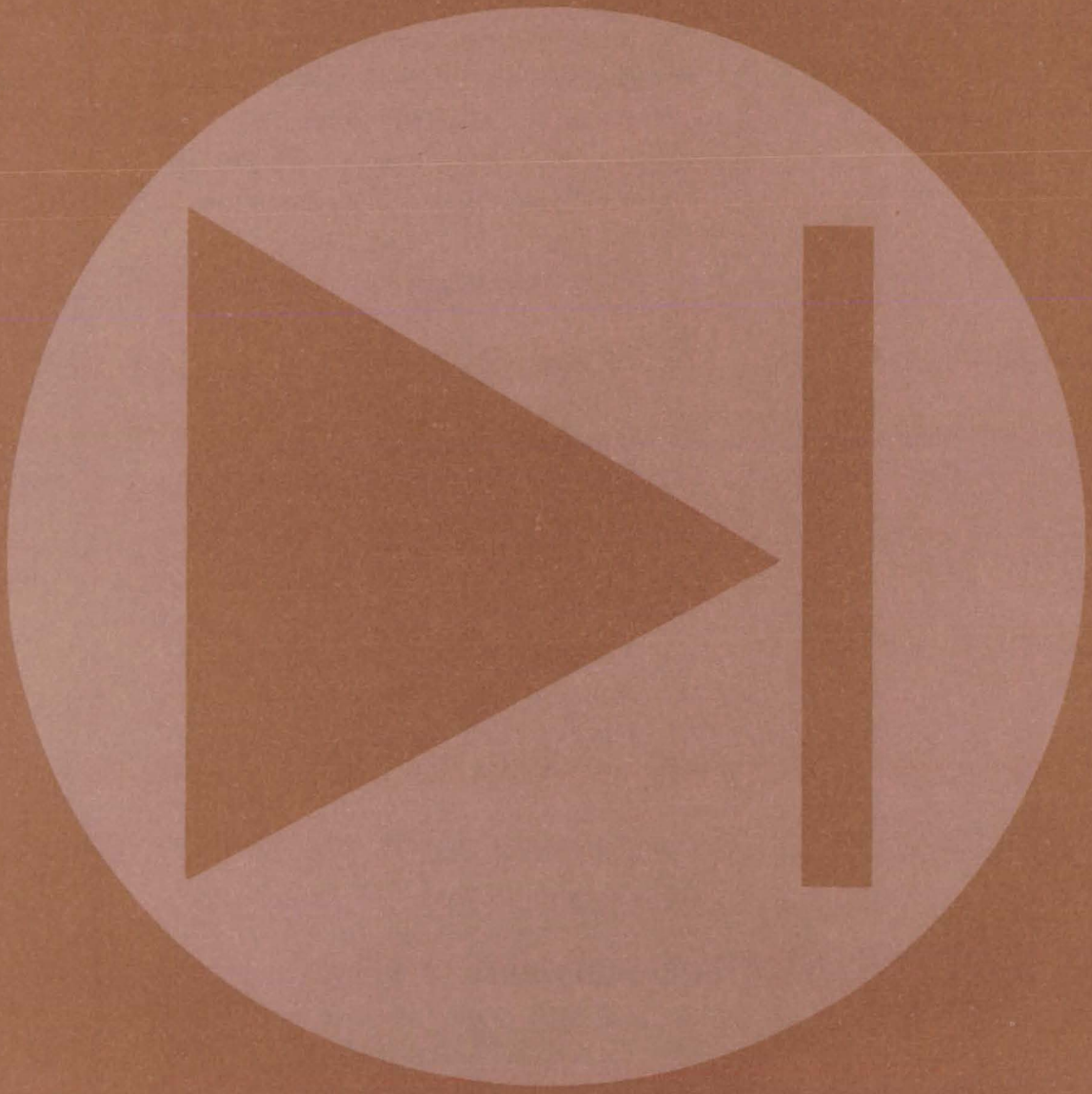
A sensitive light-detecting amplifier circuit developed for astronomical instruments could be useful in fire detectors, photographic processing, and many other applications. The sensor and circuit can operate in a "noisy" environment to detect very weak light signals; yet they are relatively simple and use readily available components. The sensor itself is a pyroelectric crystal that develops an electric charge from the heat of incident light (as little as 3×10^{-10} watt per square centimeter). The amplification circuit converts sensor outputs as low as 0.1 microvolt to millivolts. The circuit has worked without electric shielding in a room with fluorescent lights, which would generate considerable electrical interference for most sensitive amplifiers.
(See page 467.)

High-Efficiency Wind Turbine



A new wind turbine may be 20 percent more efficient than conventional propeller-driven units. By incorporating anti-"pinch-off" and wind-amplification features, the turbine delivers energy at windspeeds of less than 13 miles per hour. In periods of no wind, the turbine can be powered by heated air from solar collectors or by flue gas from chimneys. The wind amplifier directs the airflow into a spiral before it reaches the turbine blades. This increases the wind velocity and introduces air turbulence that hugs the blades for a longer distance before separating. The turbine exhausts into an expansion chamber that improves efficiency by reducing back pressure.
(See page 489.)

Electronic Components and Circuits



Hardware, Techniques, and Processes

463 Variable-Resolution Counter
464 Window Comparator for Voltages
465 Low-EMI Solid-State Relay
465 Real-Time Digital Integrator
466 Biased-Receiver Digital Interface
467 Sensor/Amplifier for Weak Light Sources
468 Overload Protection for Switching Regulators
469 Azimuth Correlator Design for IC Chip
470 Rise-Time Control in Saturated Amplifiers
472 Low-Cost, Lightweight RF Transfer Switch
472 A Reliable Solid-State RF Transfer Switch

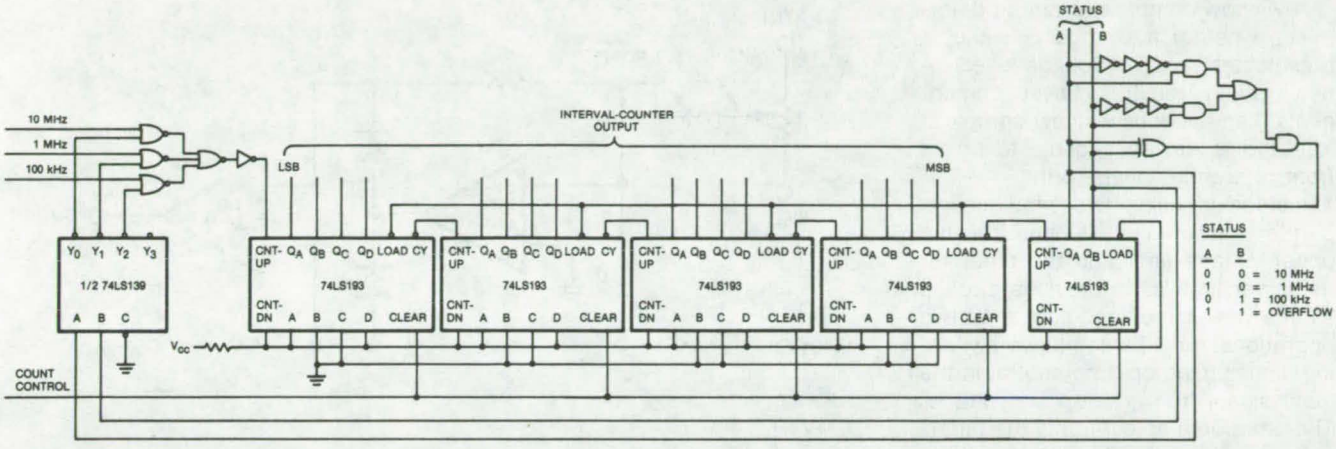
Books and Reports

473 Semiconductor Step-Stress Testing
474 JANTX1N645-1 Diode
474 JANTX1N649-1 Diode
474 JANTX1N746A Diode
475 JANTX1N759A Voltage-Regulating Diode
475 JANTX1N937B Zener Diode
475 JANTX1N972B Zener Diode
475 JANTX1N981B Zener Diode
475 JANTX1N1202A Switching Diode
476 JANTX1N3893 Diode
476 JANTX1N4570A Zener Diode
476 JANTX1N5415 Diode
476 JANTX1N5417 Diode
476 JANTX1N5420 Diode
476 JANTX1N5550 Switching Diode
477 JANTX1N5552 Switching Diode
477 JANTX1N5554 Switching Diode
477 JANTX1N5614 Switching Diode
477 JANTX1N5615 Switching Diode
478 JANTX1N5618 Switching Diode
478 JANTX1N5619 Diode

Variable-Resolution Counter

Multivalue clock signals reduce number of counter stages.

Langley Research Center, Hampton, Virginia



Variable-Resolution Counter Circuit utilizes three input clock frequencies to allow a single 2-bit binary counter to measure time intervals that would normally require additional circuitry.

A variable-resolution counter increases the time interval that an n-bit binary counter can measure by using a multivalue input clock. The circuit allows the measurement of time intervals beyond the capability of a single n-bit counter while maintaining a reasonable resolution. Obtaining similar time measurements with conventional techniques would require extra counters, increasing the number of data bits and making data handling more difficult.

The circuit provides a digital quantity that when multiplied by the clock resolution measures time intervals of 1 microsecond to 655.35 milliseconds. Three input clock frequencies are used, providing timing resoultions shown in the table.

A 16-bit binary counter with parallel data load is used for the interval counter, and a 2-bit binary counter is used as a clock status counter (see figure). The clock signals are switched by a 2-line to 4-line decoder and the appropriate random logic. With an initial condition of all counter outputs equal to zero, the status counter sets the 2-line to 4-line decoder output, Y_0, low, activating the 10-MHz clock.

Clock Frequency	Timing Resolution	Time Interval
10 MHz	100 ns	1 μs to 6.5535 ms
1 MHz	1 μs	6.5535 to 65.535 ms
100 kHz	10 μs	65.535 to 655.35 ms

Timing Resolution of a variable-resolution counter is shown for three input clock frequencies. Interval measurements below 1 microsecond result in reduced timing accuracy.

If the count control is low, the interval counter counts at the 10-MHz rate until the end of the interval to be timed or until an overflow is produced. The overflow increments the status counter; the output of the status counter sets the decoder output, Y_1, low; and the 1-MHz clock signal is switched to the interval counter. At overflow, the value of 6,553 is loaded into the interval counter to adjust the counter to the value where it would have been, had it been operating at the 1-MHz rate from the beginning of the timed interval.

An additional overflow increments the status counter; the 100-kHz clock signal is switched in; the value of 6,553 is loaded into the interval counter; and the counting resumes. Another overflow increments the status counter to 11_2, and the decoder output, Y_3, goes low, halting the counter. The status information or the interval count, now zero, may then be used to indicate a time period of greater than 655.35 milliseconds.

This work was done by James I. Clemmons, Jr., of **Langley Research Center.** *No further documentation is available.*

Inquiries concerning rights for the commercial use of this invention should be addressed to the Patent Counsel, Langley Research Center [see page A5]. Refer to LAR-12530.

Window Comparator for Voltages

A simple circuit determines when an input voltage lies within a narrow range.

Dryden Flight Research Center, Edwards, California

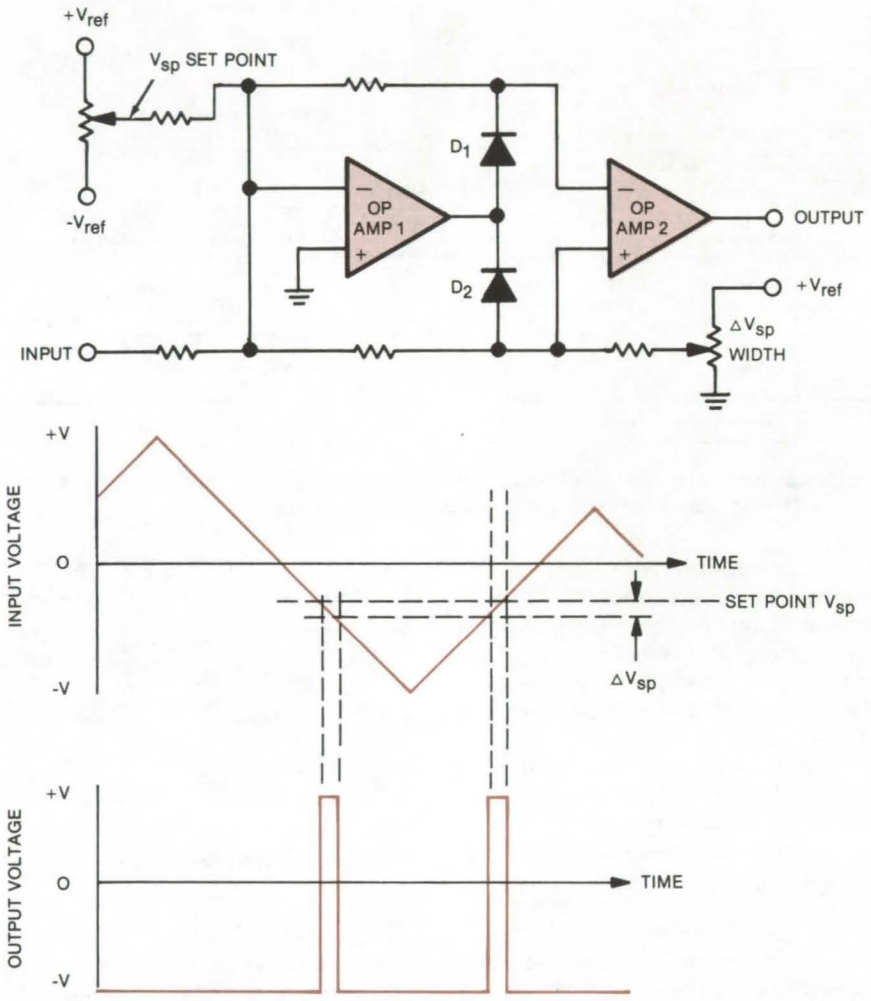
A window comparator circuit determines whether a voltage is within a preselected range of voltage levels. A new circuit requires fewer components than previous window comparators and is less susceptible to errors from reference voltage drift.

Instead of using two simple comparators in parallel — one for the upper voltage limit and the other for the lower limit as in previous circuits — the new circuit requires only two operational amplifiers and two switching diodes. One op amp subtracts the input signal from a set-point voltage. The other op amp subtracts the difference output of the first op amp from the preselected window-width voltage.

The new window comparator is useful in process-control circuitry, measuring instruments, and checkout equipment. For example, the window comparator can check the feedback signal of a servomechanism to determine whether the servo is set within a given tolerance.

In the new window comparator (see figure), the window level and the window widths are adjusted independently. The set-point voltage is adjusted so that the output of the first operational amplifier changes polarity when the algebraic difference between the input signal and the set-point voltage changes polarity. Positive or negative feedback occurs through steering diode D_1 or D_2 to maintain the negative input terminal of op amp 1 at or near ground potential. The circuit is self compensating for temperature effects upon the forward diode voltage drop.

The second op amp determines whether the output of the first op amp has changed polarity and exceeded the window-width setting. When the input is more positive than the set point, a negative output of op amp 1 controls op amp 2 through steering diode D_2 to cause the output of op amp 2 to be negative. When the polarity change occurs, op amp 2 switches its output level from negative to positive. Op amp 2 remains positive until the output of op amp 1, through the steering diode D_1, exceeds the window-width setting. Op amp 2 then reverts to its negative value.



New **Window Comparator Circuit** allows the set-point voltage V_{sp} and the window width ΔV_{sp} to be adjusted independently. The output from op amp 2 is high when the input voltage is within the voltage window and is low when the input is outside the window.

In window comparators that consist of two simple level comparators, two reference voltages are required. These voltages can drift in opposite directions, making the window too large or too small (or nonexistent). When a narrow window is required (for example, 10 millivolts in a 10-volt range), the upper and lower reference voltages must be stable to 1 part in 10,000. For the single window-width voltage in the new circuit, however, a stability of 1 part in 10 is adequate.

This work was done by James M. Black of **Dryden Flight Research Center.** *For further information, Circle 1 on the TSP Request Card.*

This invention has been patented by NASA [U.S. Patent No. 4,055,777]. Inquiries concerning nonexclusive or exclusive license for its commercial development should be addressed to the Patent Counsel, Dryden Flight Research Center [see page A5]. Refer to FRC-10090.

Low-EMI Solid-State Relay

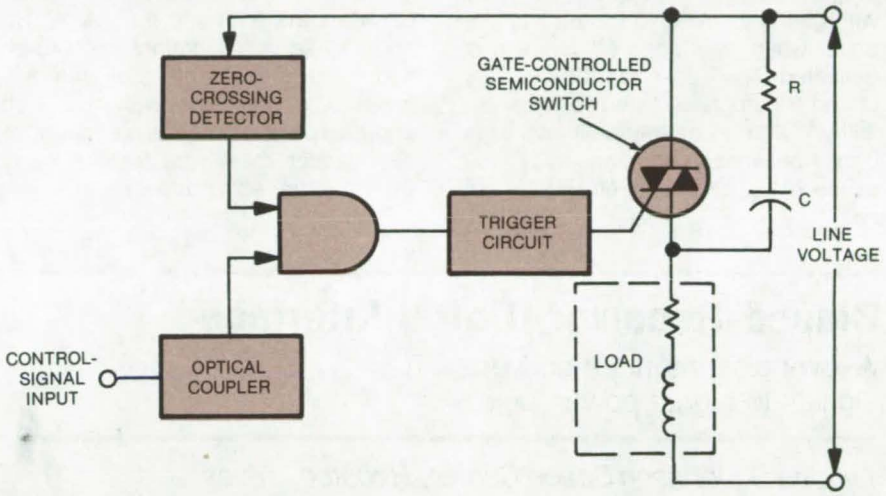
Control circuit switches on at zero voltage and off at zero current.

Lyndon B. Johnson Space Center, Houston, Texas

The proposed solid-state relay shown in the figure reduces electromagnetic interference (EMI) generated when switching ac power to a load. It could find uses in circuits that are particularly susceptible to electrical noise or contain sensitive components.

As shown, the control-signal input is coupled to the relay through a light-emitting diode (LED)/phototransistor combination, which isolates the input from the output. A zero-voltage-crossing detector, composed of a diode bridge and transistor, senses when the line ac voltage crosses zero. When a control signal is applied, the AND gate allows the signal to pass only if a zero-crossing indication is received simultaneously.

The control-signal input turns on a trigger circuit. The trigger fires a gate-controlled semiconductor switch, which switches current to the load. Since the load is turned on at zero line voltage, and the semiconductor switch turns off at nearly zero current, little or no electromagnetic radiation is generated when power is switched.



The Control Signal Is Optically Coupled to this low-EMI solid-state relay. The resistor and capacitor across the semiconductor switch reduce rate-dependent effects.

This work was done by William D. Muska of United Aircraft Corp. for **Johnson Space Center.** *For further information, Circle 2 on the TSP Request Card.*
MSC-12698

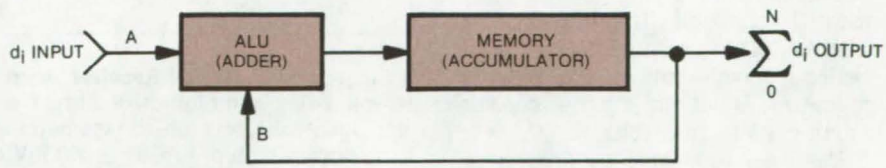
Real-Time Digital Integrator

Logic circuit processes data while accepting a new input.

NASA's Jet Propulsion Laboratory, Pasadena, California

A field-programable logic array (FPLA) has been used to make the 3-bit arithmetic logic unit (ALU) for a large integrator that can be read and cleared while a new datum, d_j, is added to begin a new integral. The integrator achieves high speed by exploiting, in the ALU, all 50 of the FPLA AND gates in a gate-sharing arrangement affording full carry/lookahead compatibility with minimum gate delays.

The form of the integrator is shown in the figure; it consists of an ALU adder and a memory (accumulator). To read (and discard) an integral while simultaneously starting a new integral, the ALU must be capable of adding two numbers or "passing" only one of them. Because circuit-board space was at a premium and no commercially available ALU in 0.3-inch (0.76-cm) pin spacing met all the circuit requirements, an FPLA was programed to do the job.



Digital Circuit Can Integrate and Dump without losing data or clock cycles. The 48-bit carry/lookahead adder uses 16 logic arrays, each programed as a 3-bit adder.

The field-programable logic array is an integrated-circuit chip with internal connections that can be arranged by the user after manufacture. The chip

(continued on next page)

contains 50 AND gates, each of which may be programed to AND any of 12 input variables. Any combination of the AND-gate outputs can be connected to any of six OR gates on the chip; the output from the chip consists of the outputs of the OR gates (which can be inverted, if desired).

For this application, the FPLA is programed as a 3-bit adder (A + B) with gating to make B be zero to the adder when the "pass A" function is activated. The adder has the auxiliary $\overline{G}$ and $\overline{P}$ outputs required for compatibility with commercially-available carry/lookahead components, such as the 74182 chip. Sixteen FPLA's are combined with 74182's in a standard carry/lookahead connection to create a 48-bit adder having only five gate delays.

Because the 50 gates available in the FPLA are insufficient to make a 4-bit lookahead adder, an alternative mechanization was considered. In that mechanization, each FPLA is programed to provide two 2-bit ripple-carry adders affording the "A + B" and "pass A" functions. A 48-bit adder using this 4-bit approach has fewer IC's than one with the 3-bit approach, but is much slower because each adder must wait for the carry from the preceding adder.

Pending commercial availability of a 74S381-like device designed to have a "pass A" function in its repertoire, the 3-bit-adder arrangement will meet real-time data integrate-and-dump requirements without either holding up the data stream for one clock cycle or using external gating to clear the integrator, or losing a datum while the integrator is cleared on a given clock cycle.

This work was done by Arthur L. Rubin, Herbert Taylor, and David E. Wallis of Caltech for **NASA's Jet Propulsion Laboratory.** *For further information, Circle 3 on the TSP Request Card.*
NPO-14530

Biased-Receiver Digital Interface

A low-noise interface converts TTL signals to higher power logic.

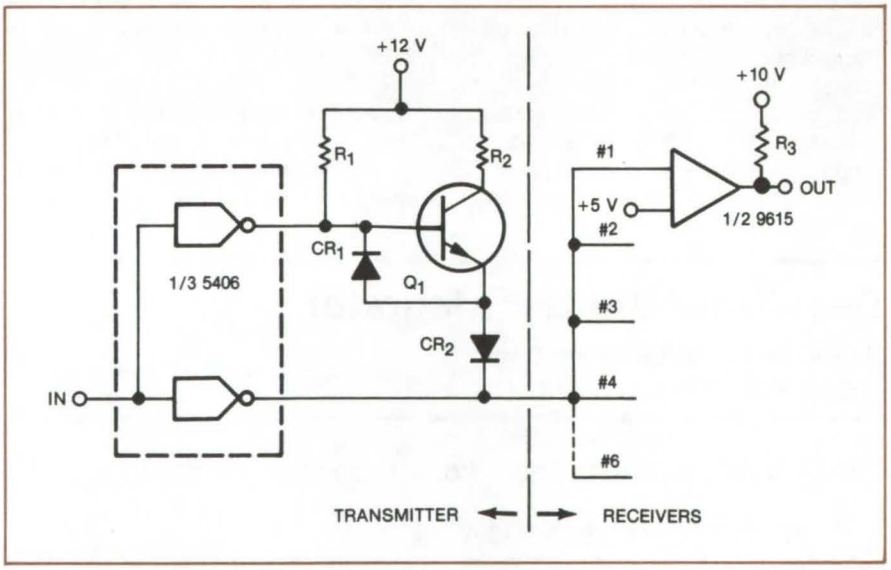
Lyndon B. Johnson Space Center, Houston, Texas

The coupling circuit shown in the figure converts TTL signals to higher voltage, higher current logic with good noise rejection. Depending on the selected components, the circuit may also be adapted to low-power applications.

The circuit is a modified version of the "totem-pole" topological circuit structure. The transmitter end of the interface amplifies a TTL signal to drive several receivers; the receivers are high-current differential line receivers with one input biased near the center of the required transmitter output-signal swing. The output logic "1" in the circuit shown is 10 V.

When the circuit input is low, both inverter outputs are open and transistor Q_1 conducts. This turns on the receiver, pulling its output to 10 V. If the input is high, both inverter outputs go low, Q_1 is cut off, and the receiver output goes to zero volts.

This work was done by Fredric C. Fitzgerald of IBM Corp. for **Johnson Space Center.** *No further documentation is available.*
MSC-14968



A **Single-Ended Biased-Receiver Interface** converts TTL signals to logic with a 10-volt swing and high-drive-current capability. The 5406 is a hex inverter/buffer with open-collector high-voltage outputs; the 9615 is a dual differential line receiver that triggers high or low on ±500 mV of differential data at its inputs.

Sensor/Amplifier for Weak Light Sources

Microvolt signals from a pyroelectric sensor are amplified to millivolt levels while noise is rejected.

Marshall Space Flight Center, Alabama

A light-sensor amplifier circuit can detect weak light and convert it into a strong electrical signal in an electrically noisy environment. Developed for astronomical measurements, the circuit is also useful in such applications as fire detection and photographic processing. Unlike previous low-level-light detectors, the new circuit is relatively simple and uses inexpensive, readily available components.

The sensor is a pyroelectric crystal, a device that develops an electric charge when it is heated unevenly. The sensor is sensitive to the heat created by light levels as low as 3×10^{-10} watt per square centimeter, for which it produces a signal of 0.1 microvolt.

The circuit amplifies this weak signal to useful voltage levels, rejecting background noise. In fact, the circuit functions without electrical shielding in a room with fluorescent lights, which generate large amounts of electrical interference. The light to the sensor is modulated at a fixed frequency by passing it through slots in a rotating disk. At the same time, the frequency response of the amplifier is restricted to a small passband around the chopping frequency. Thus, noise at frequencies outside the passband is eliminated.

Light from the source is chopped at a frequency of 107 hertz by a three-bladed mechanical chopper driven by a synchronous motor (Figure 1). The chopper also interrupts a beam from a light-emitting diode (LED), producing a square-wave reference signal at the output of a photodiode. The reference signal is adjusted mechanically (i.e., by rotation of the LED and photodiode about the axis of the chopper) so that it is in phase with the pulses from the light source to be measured. The reference signal is amplified and applied to the reference-signal input of the amplifier (Figure 2).

The chopped light from the source is sensed by the triglycerin sulfate pyroelectric crystal. The output voltage is amplified and is passed through a demodulator circuit driven by the reference signal. During the low phase of the pulsed reference signal, a complementary metal-oxide-semiconductor (CMOS) switch is off, so the 12-kilohm resistor acts as the input resistor for the second operational amplifier in the demodulator. During the high phase of the reference signal, the CMOS switch in on, and the sensor signal passes through both op amps. The resistor values are chosen so that the gain is 5 in either case, but the signal inversion in the extra amplifiers allows the output to have constant polarity if the sensor signal

(continued on next page)

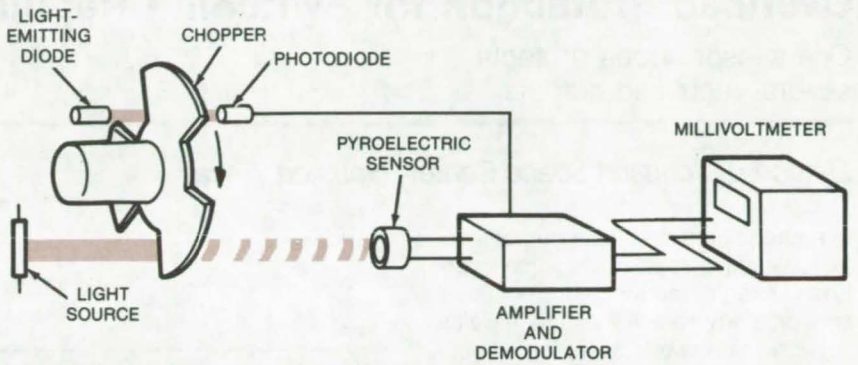


Figure 1. A **Mechanical Chopper** converts two steady light beams into pulses. The phases of the two pluse streams are compared in a demodulator to eliminate electrical noise from the sensor signal.

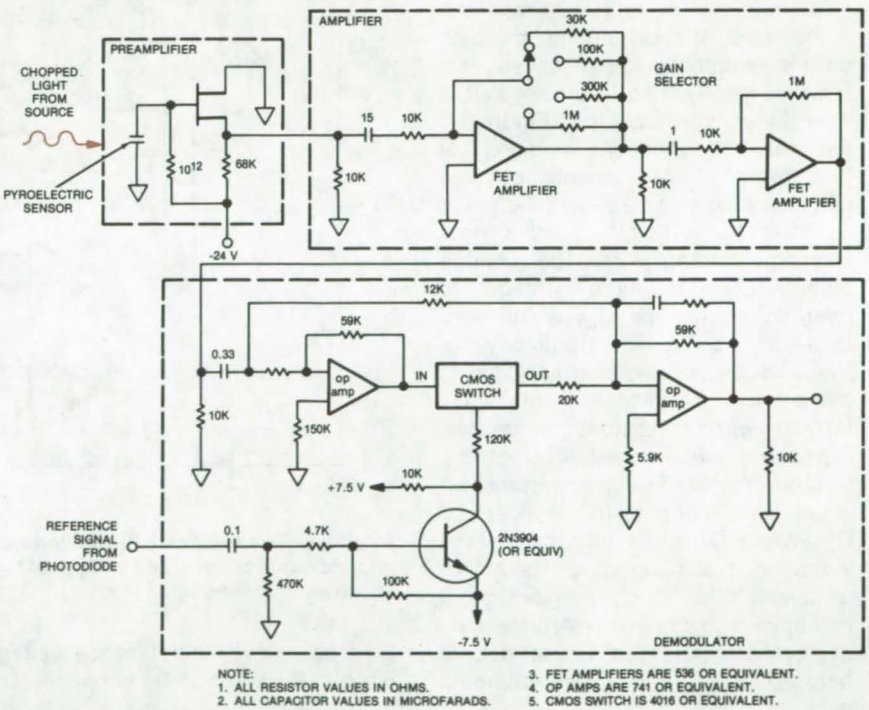


Figure 2. The **Sensor/Amplifier Compares Two Signals** — one from a reference light source and one from the light source. When the two signals are in phase, the dc voltage at the output is virtually-noise-free and is proportional to the intensity of the sensed light source.

and reference signal are in phase. Hence a dc voltage, proportional to the sensor signal, appears at the demodulator output. For frequencies other than the chopping frequency, however, the signal phase relative to the chopper phase varies rapidly, so no net dc voltage is produced.

This work was done by Donald J. DeSmet, Andrew J. Jason, and Albert C. Parr of the University of Alabama for **Marshall Space Flight Center.**

No further documentation is available.

Inquiries concerning rights for the commercial use of this invention should be addressed to the Patent Counsel, Marshall Space Flight Center [see page A5]. Refer to MFS-25025.

Overload Protection for Switching Regulators

One sensor circuit protects several regulated outputs.

Lyndon B. Johnson Space Center, Houston, Texas

A circuit protects all the output lines of a switching regulator against overloads without requiring current sensors on every line. It includes a delay network to inhibit operation during startup, when the regulator output voltage is low and surge current is high. The circuit compares the voltage drop in a current-sensing winding to a reference voltage, and if an overload is indicated, it short-circuits the bias on the switching transistor so that power is rapidly cut off from the loads.

In the voltage regulator (Figure 1), the three secondary windings of transformer T are closely coupled magnetically, so a load change modifies the output of the sensor winding (winding 6-7). The change thus alters the input voltage to operational amplifier U_2, which controls the switching frequency of transistor Q_1 and the energy stored in the primary (winding 1-2) of T. Q_1 turns on when the output voltage falls below a predetermined level at the voltage divider R_4-R_5 and turns off when its current rises to a level set by R_3. When Q_1 turns off, the energy stored in T is supplied to its output windings. If this action charges C_5 to a higher voltage than the reference level at comparator U_3, a pause occurs before the start of the next charging cycle.

The overload protector part of the circuit consists of capacitor C_2, resistors R_1, R_7, and R_8, diodes CR_4 and CR_5, and comparator U_4. Normally, the voltage at pin 2 of U_4 is higher than that at pin 3; but if one (or both) of the outputs becomes overloaded, the voltage on the sensor winding drops, and the voltage on pin 2 drops below the reference voltage on pin 3. When this happens, the output of U_4 (at pin 1) becomes low and short-circuits the noninverted input of U_1. Q_1 then cannot switch power, and the outputs to the loads drop to zero. This condition prevails until the voltage imbalance at U_4 is reversed.

C_2, R_1, R_8, and CR_5 form a delay network that keeps the bias at pin 2 of U_4 higher than that at pin 3 during startup.

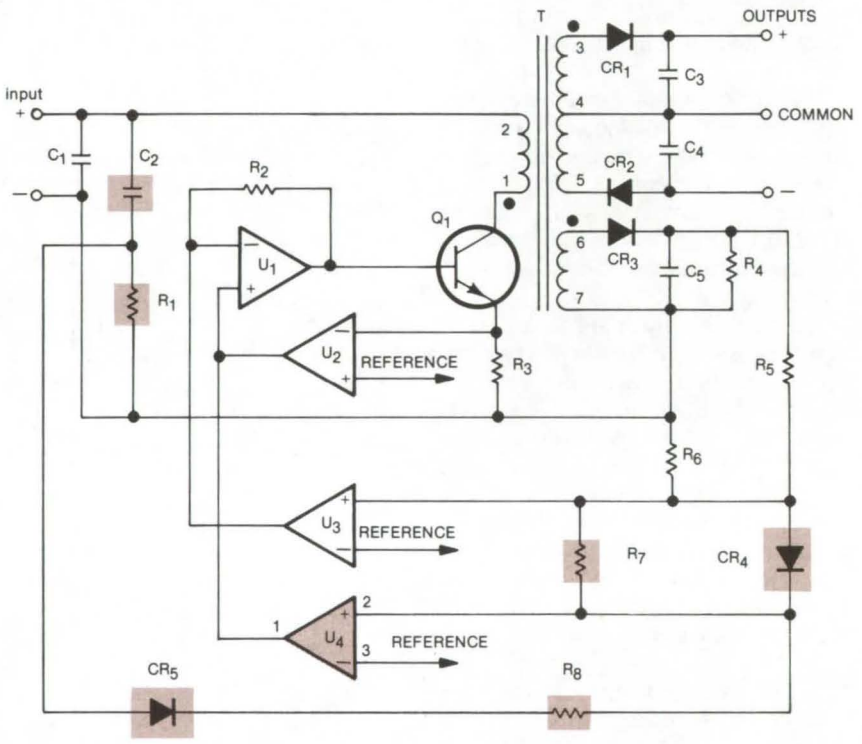


Figure 1. The Overload Protection part of this switching regulator consists of the shaded components. The voltage at C_5 is used for both the control of switching rate and overload sensing.

Although the components in the circuit of Figure 1 are inexpensive, even greater economy can be realized if many of the components are combined in a single intergrated circuit. Thus, in the circuit of Figure 2, integrated circuit U_1 performs the control functions of the discrete circuit, including the generation of control pulses for switching transistors. U_1 also produces the reference voltage. U_2 is the overload-protection comparator; and C_1, R_1, R_{14}, and

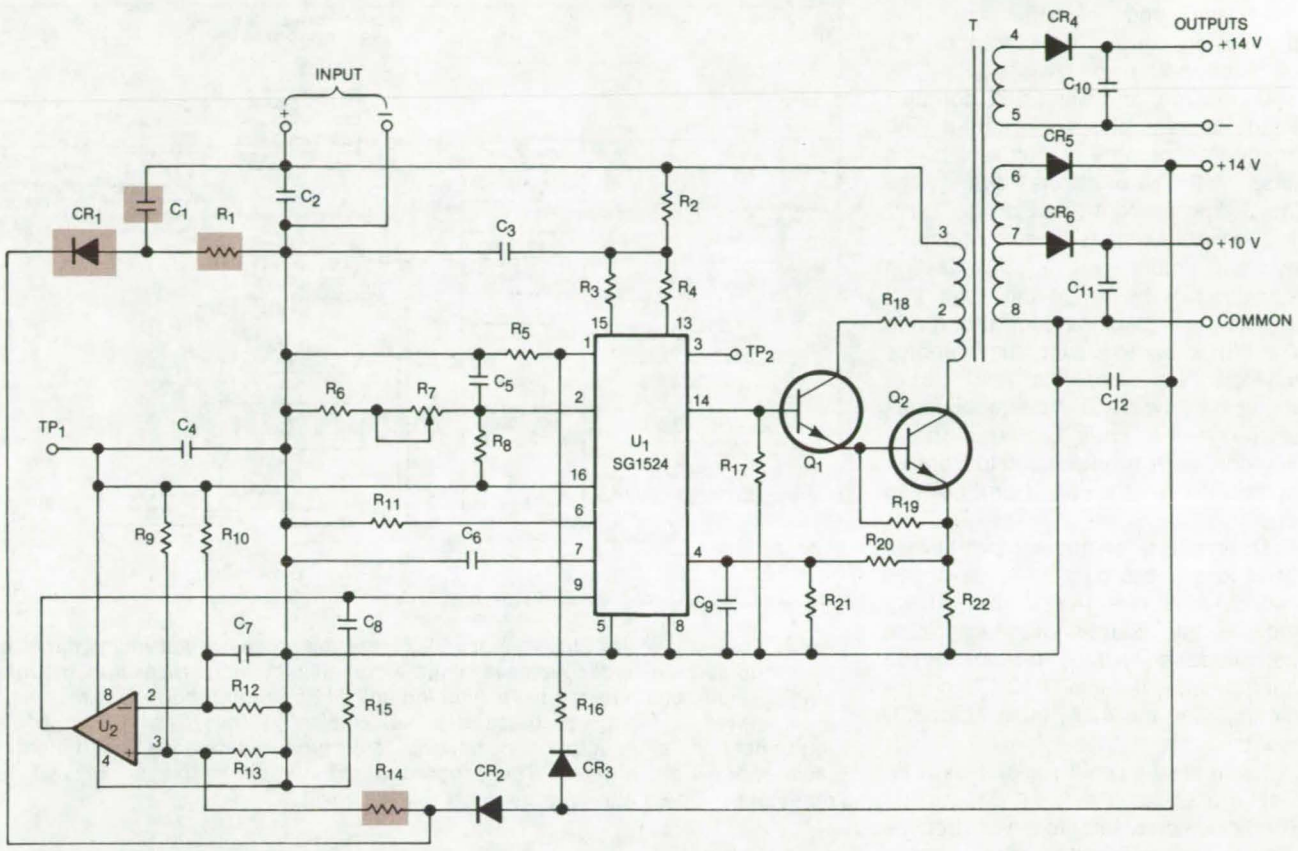


Figure 2. In **A More Complex Regulator** having more varied outputs, integrated circuit U_1 performs the control functions. As in Figure 1, the shaded components are for overload protection.

CR_1 form the startup delay network.

This work was done by Eugene Lachocki of RCA Corp. for **Johnson Space Center.** *No further documentation is available.*
MSC-18513

Azimuth Correlator Design for IC Chip

A compact, low-power circuit for real-time processing of synthetic-aperture radar signals

NASA's Jet Propulsion Laboratory, Pasadena, California

A newly-proposed azimuth correlator circuit for a synthetic-aperture radar (SAR) was designed for a single integrated-circuit (IC) chip. A set of such chips constitutes a complete azimuth correlator module, and a number of these modules could make real-time signal processing possible. Of course, the chips would be smaller and use less power than conventional circuitry.

Each azimuth correlator chip would contain all required memory, buffers, control, timing, multiplexing, and output circuitry. The SAR processor would require 1,020 chips (255 to a correlator module), to perform an azimuth correlation of data from the SEASAT satellite to produce 20-km-swath imagery with 25-m resolution, four looks. Each correlator module computes a single look of the SAR image.

Each azimuth correlator chip receives data from the range correlator via an input sample bus (see figure) as a contiguous sequence of "range lines." Each range line comprises 5,120 complex data samples accompanied by several sync signals. During a range-line processing cycle the azimuth correlator selects the appropriate set of 1,152 complex data samples from each range line, multiplies each data sample by the appropriate complex azimuth reference-function (ARF) coefficients, and adds this product via a complex adder to the appropriate cell in the accumulator register.

(continued on next page)

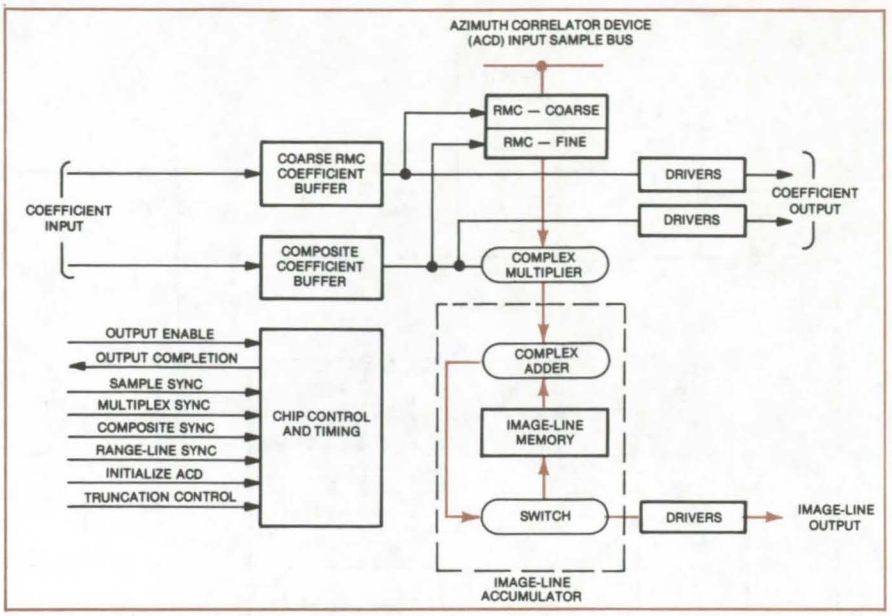
At the end of an image-line processing cycle, the output of the complex adder is switched to the output driver, and the 1,152 complex image-line samples are read out. The image-line memory, a shift register, is filled with zero levels during the image-line readout process.

The input samples are accompanied by a number of synchronization signals: (a) the range-line sync that denotes the beginning of the range line, (b) a sample sync that denotes when a data sample is valid, (c) a multiplex sync that delineates subsets of range-line samples, and (d) a composite sync that is used to transfer composite coefficients from chip to chip.

Three sets of coefficient formats are used to process data samples corresponding to one range line. These include the coarse range-migration compensation (RMC) format (1,152 coefficients), the fine RMC (72 coefficients), and the ARF, (also 72 coefficients).

There are two shift-register buffers. One is used for a set of 4,608 coarse RMC coefficients sufficient to process 4 range lines; the other stores a set of 288 coefficients.

Control and timing circuitry includes: (a) supply of clock signals to all elements, (b) control of data input and sample selection, (c) control of coefficient buffer capacity and coefficient routing, (d) control of output image-line pixels, and (e) control of selection of most significant or least significant portion of the complex image-line sample.



An **Azimuth Correlator Chip** proposed for real-time processing of image data from a synthetic-aperture radar replaces a more-complex bulkier processing module. A single IC chip contains the basic working unit of an azimuth correlator module that incorporates an array of these devices. Basically, the IC performs complex multiplication and addition, applying appropriate reference coefficients to radar-image data signals. The processed signals are displayed in real time, depicting the area surveyed by the radar system.

This work was done by Vance C. Tyree and Chialin Wu of Caltech for **NASA's Jet Propulsion Laboratory.** *For further information, Circle 4 on the TSP Request Card.*
NPO-14614

Rise-Time Control in Saturated Amplifiers

Inductive control of current rise and fall times in a saturated amplifier

Lyndon B. Johnson Space Center, Houston, Texas

An inductor in the transistor emitter circuit controls the output rise time of a saturated amplifier. Rise-time control is important in some applications to reduce radiated noise and distortion in subsequent circuits. In addition, it improves current balancing in push/pull transformer circuits. The resulting circuits are self-compensating for temperature.

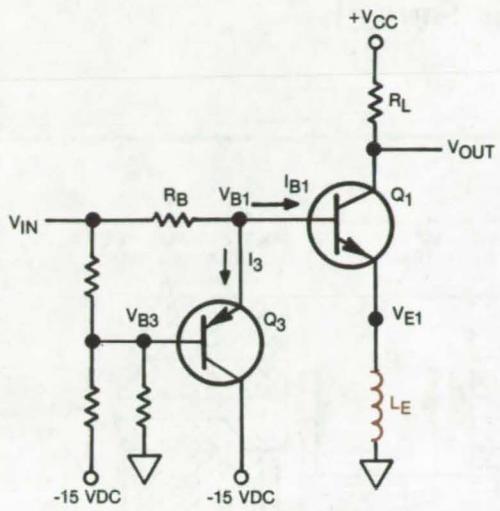
Figure 1 shows two circuits for which inductors L_E control the current rise time in the output current loop. Because current rate of change, di/dt, is expressed in terms of voltage, V, and inductance, L, as

$$di/dt = V/L$$

a constant voltage V_{E1} applied across choke inductances, L_E, for the rise duration will cause transistors Q_1 and Q_2 to have a predictable linear current rise.

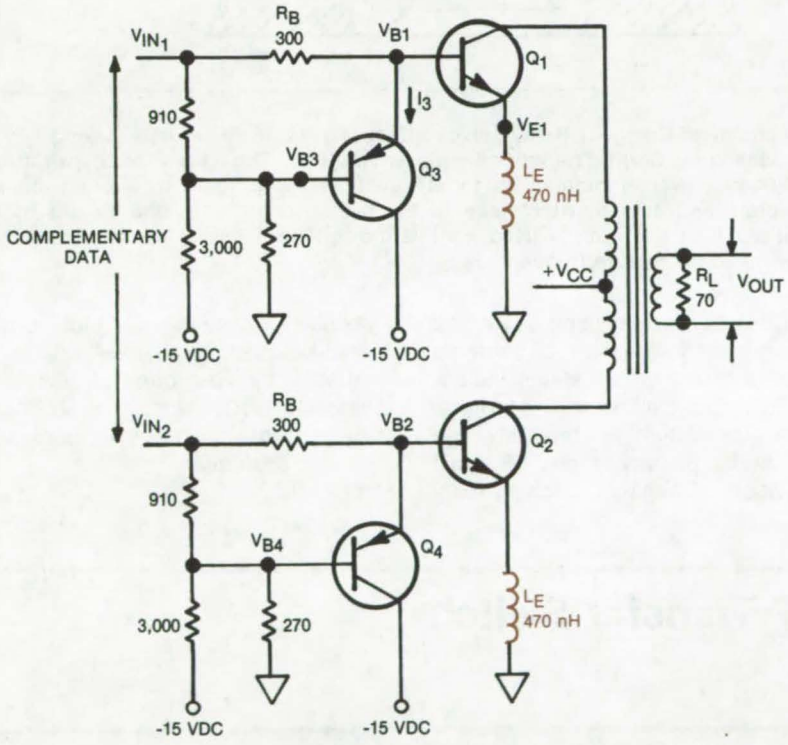
Referring to the single-ended-amplifier circuit diagram, the following typical square-wave input (V_{in}) and Q_3 base voltages (V_{B3}) produce ± 1-V transient peaks (V_{E1}) across inductor L_E for the rise- and fall-time durations (t).

	High	Low
V_{in}	+9 V	-1 V
V_{B3}	+1 V	-1 V



SINGLE-ENDED STAGE

NOTE: ALL RESISTANCES ARE IN OHMS.



PUSH/PULL STAGES

Figure 1. The **Inductor L_E Controls the Current Rise and Fall Times** in these saturated transistor amplifiers.

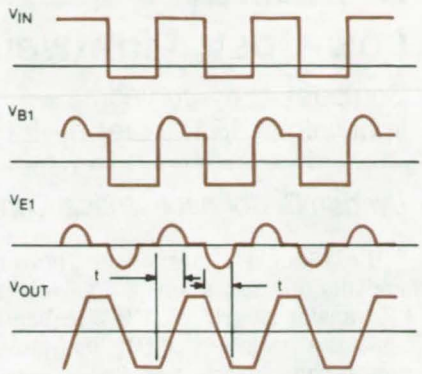


Figure 2. The **Voltage Waveforms** illustrate the single-ended-amplifier circuit response to a square-wave input.

Thus, for transistor Q_1 to turn on, V_{in} = 9 V and V_{B3} = 1 V. The transistor current is initially zero due to L_E. When the base resistor R_B conducts 25 mA through Q_3, V_{E1} = 1 V. Because of the constant voltage applied from V_{B3} through to V_{E1}, the current rise through inductor L_E is linear. Finally, as current in transistor Q_1 approaches saturation, voltage V_{E1} decreases and currents i_3 and i_{b1} decrease and increase, respectively, until all of the R_B current flows into transistor Q_1. At saturation, current through Q_1 is limited by voltage V_{cc} and the reflected impedance of R_L.

For transistor Q_1 to turn off, voltages V_{in} = -1 V and V_{B3} = -1 V. The Q_1 collector current is still at maximum because of current flow through the inductor L_E. At that point, current I_3 resumes a high value to conduct excess stored base charge from transistor Q_1. V_{E1} is held constant during the fall time of current through Q_1, and the current fall is linear.

Figure 2 shows the circuit waveforms. The circuits have been successfully tested over the temperature range from -55° to 100° C.

This work was done by C. Earle Theall of The Singer Co. for **Johnson Space Center.** *No further documentation is available.*
MSC-14934

Low-Cost, Lightweight RF Transfer Switch

Compact relay serves as a lightweight RF transfer switch.

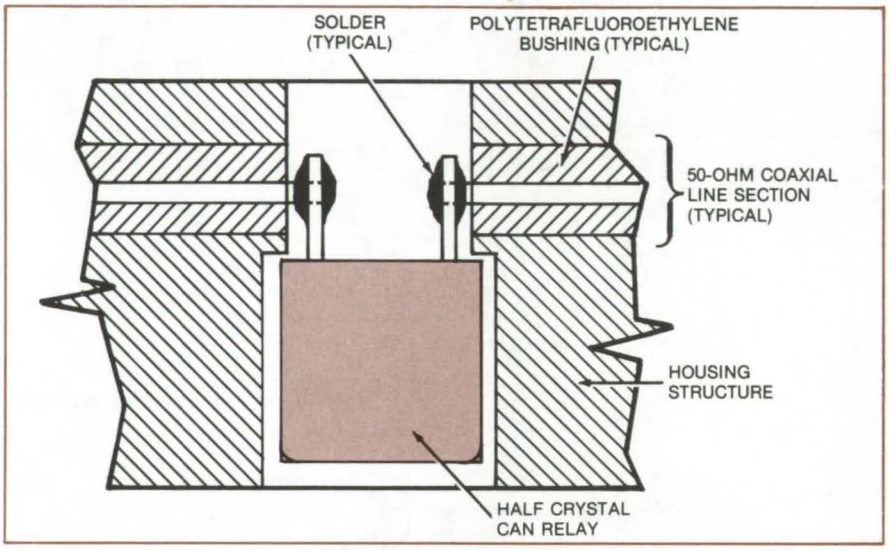
Lyndon B. Johnson Space Center, Houston, Texas

The Shuttle transponder power amplifier required a small, lightweight RF transfer switch for 1.0-W S-band signals. A miniature DPDT "half-size-crystal-can" relay (see figure) was selected after examining numerous conventional coaxial relay configurations. Coaxial relays were too large, and their RF electrical interface required a minimum of three coaxial cables and the associated connectors between the unit and the relay. Even having minimum bend radii and connectors would have taken up too much space.

While this relay was not originally designed for RF transfer, it is constructed with favorably-distributed parasitic inductances. In addition, its small size minimizes the electrical length of leads within the relay.

RF performance tests show that the relay is satisfactory if its external leads are kept short and capacitively compensated to reduce the effective inductance at the relay pin. In practice, the mounting enclosure gives the necessary capacitive compensation.

The advantages of using this relay are as follows: Connectors and cables are avoided, permitting a direct electrical interface. Packaging area and/or volume required are essentially those of the relay itself. An added bonus is the additional set of contacts that are used for relay status indication, allowing the command/control system to determine remotely the relay state at any time. (In this application, a magnetic latching relay was used, although a nonlatching type could be used equally well.)



An **Economical Compact Relay** serves effectively as an RF switch, saving weight and space in the Shuttle transponder power amplifier. The relay used to switch 1-W RF S-band power eliminates costly RF switches that come with bulky coaxial connectors and cables, which add to the overall cost, size, and weight of the amplifier. This switch can be used in miniature communication equipment operating at the vhf-to-microwave frequencies.

This work was done by David L. Olsson of TRW, Inc., for **Johnson Space Center.** *No further documentation is available.*
MSC-16907

A Reliable Solid-State RF Transfer Switch

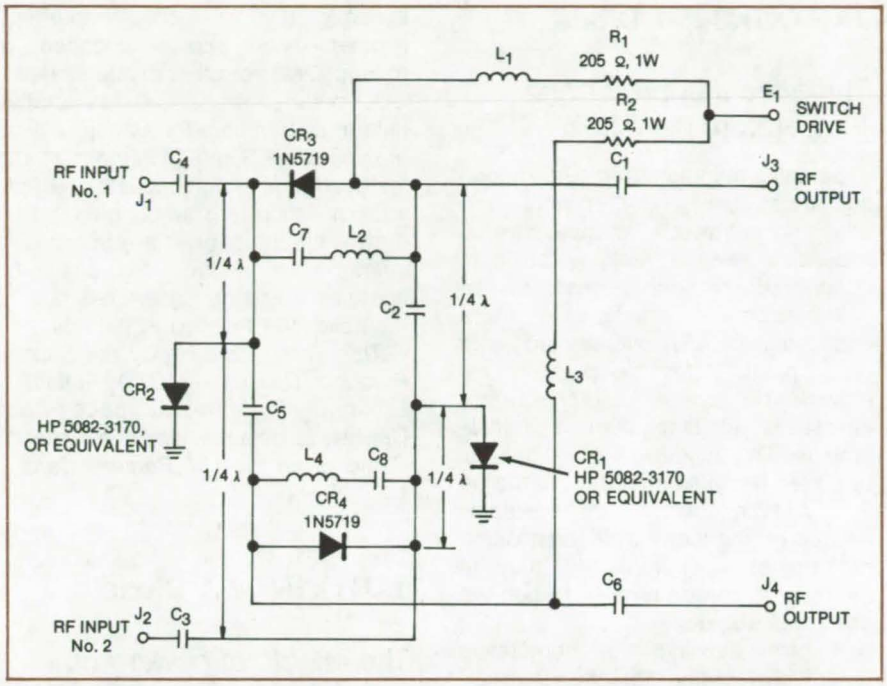
A solid-state switch replaces less-reliable mechanical switching.

Lyndon B. Johnson Space Center, Houston, Texas

A highly-reliable lightweight solid-state RF (radio-frequency) transfer switch has been developed to handle medium power for the Space Shuttle S-band power amplifier. This switch replaces the less-reliable conventional mechanical transfer switch.

The switch uses standard parts of proved reliability. It has two positions: one requiring bias [(J_1-J_3) and (J_2-J_4)] (see figure) while the other, no bias [(J_1-J_4) and (J_2-J_3)]. The switch handles 3 W, although it can be modified to handle considerably higher power levels. Hot switching is not a problem due to the solid-state design that switches in less than 1 ms.

This configuration has 23 dB of isolation while maintaining a 1.2:1 VSWR (voltage standing-wave ratio). The isolation in the unbiased mode is obtained from the series diodes CR_3 and CR_4; in the biased mode, isolation is via shunts diodes CR_1 and CR_2 spaced $\lambda/4$ away from the signal posts (λ is the wavelength of the applied signal). Additional isolation is easily obtained for narrow bandwidths by increasing the number of diodes in $1/4\lambda$ increments and shunting out the



A **Highly-Reliable RF Transfer Switch** uses solid-state components, replacing the conventional less-reliable electromechanical switches. One of its two positions [(J_1-J_4) and (J_2-J_3)] requires no bias (power), thus enhancing its reliability. Diodes CR_3 and CR_4 and shunt diode spaced 1/4λ away from the signal post yield 23 dB isolation while maintaining 1.2:1 VSWR.

stray capacitance of diodes CR_3 and CR_4.

The switch features more-reliable solid-state technology with good isolation capable of high switching speeds. Reliability is further improved because bias (power) is applied for only one of the switch positions. The switch can be used in any communication system that requires a narrow-band transfer switch with medium isolation.

This work was done by Robert W. Dodd of Watkins-Johnson Co. for **Johnson Space Center.** *No further documentation is available.*
MSC-16890

Books and Reports

These reports, studies, and handbooks are available from NASA as Technical Support Packages (TSP's) when a Request Card number is cited; otherwise they are available from the National Technical Information Service.

Semiconductor Step-Stress Testing

An extensive test program documents the behavior of discrete diodes and transistors under power and temperature overstress.

The behavior of discrete semiconductor components under temperature and power stress above the manufacturer's ratings is the subject of an extensive test program now underway for Marshall Space Flight Center. Documented in the series of reports described below, the program covers bipolar transistors, diodes, and field-effect transistors (FET's). Beyond its original intent — to characterize the NASA standard list of discretes recommended for aerospace applications — the test results should interest users of these components in other critical applications. Much of the material could also assist engineers and others in setting up similar test programs.

The initial series of reports covers 39 devices — 22 diodes and 17 transistors. The first 20 of these reports are described in this issue of *NASA Tech Briefs*. The remaining 19 will be described in Vol. 5, No. 1. Among the transistors are one FET and four dual-element packages. The diodes include switching units and Zeners. All are designed to meet MIL-spec performance standards.

In broad outline, the test procedures are the same for all components. They differ in particulars, such as electrical parameters measured, for the different kinds of devices tested. For the power-stress tests, a sample population is stressed at levels that increase in steps from half maximum rated power (MRP) to 1.75 MRP. Each power-stress step is held for 500 hours at constant ambient temperature of 25° C. Following each step, key electrical parameters are measured, and a tally of any failed units is recorded. Failed units include those for which the electrical checks fall out of MIL limits by 50 percent or more, those for which leakage current exceeds the maximum limit by 100 times or more, and shorted or open-circuit units.

The temperature-stress measurements are carried out in two groups. In the first group, the measurements are made in 160-hour steps starting at 75°C and increasing in 25° C increments to 300° C. In the other group, the steps are for 16 hours duration each, commencing at 150° C and increasing in 25° C intervals to 300° C. In both groups, the components are held at their maximum-rated

(continued on next page)

power during each step, and they are tested for electrical behavior following each step. The combination of applied power and increasing case temperature causes the device junction temperature to rise above the manufacturer's rating, typically 175° to 200° C, in all of these tests. A tally of failed units is kept, as in the power-stress measurements.

The standard procedure for each component is to take 48 samples from each of two manufacturers, to divide each sample into three groups of 16 units each, and to apply power stress to a group of 16 from each manufacturer; temperature stress is similarly applied to two groups of 16 from each manufacturer. Two units from each manufacturer are used as control samples.

For all units, data are presented as graphs showing cumulative failures (in percent) for the temperature-stress group and as tables showing how the electrical parameters changed during each test phase. An analysis of the test results and the reasons for failures are given in the concluding sections of the reports. Throughout the reports, and in the following articles, the power-stress sample population is referred to as "Group I," the first temperature-stress population is "Group II," and the second temperature-stress population is "Group III."

This work was done by Howard B. Meeks and Felminio Villella of **Marshall Space Flight Center.** *Each of the reports described below, titled "Transistor Step Stress Testing Program," presents the test procedures, results, and conclusions for one tested device. Persons wishing information about a particular unit can order the report for that device by circling the appropriate number on the TSP Request Card at the back of this issue of NASA Tech Briefs.*

[These reports were prepared to document work supported by the United States government. They are intended solely as a vehicle for the presentation of test results and are not to be construed as an endorsement or a criticism of the companies mentioned or of their products.]
MFS-25329

JANTX1N645-1 Diode

The effects of power and temperature overstress

Samples manufactured by Semtech and Micro Semiconductor were tested. The Semtech group showed excessive reverse leakage currents during each of the three test phases.

The Semtech diodes are glass encapsulated and overpainted with black paint. After the paint is removed, the reverse leakage current decreases to less than 1 microampere. This suggests that the failures occurred because of static charge on the surface of the encapsulant, caused by the thermal decomposition of the paint. Most or all of the harmful decomposition was removed when the paint was stripped.

A plot showing the cumulative failure distribution for the thermal-stress tests was drawn for the Semtech diodes. From the temperature-stress data, an activation energy of 1.36 eV was calculated for the Semtech sample lot.

This work was done by the Special Products Division of DCA Reliability Laboratory for **Marshall Space Flight Center.** *To obtain a copy of the report, Circle 5 on the TSP Request Card.*
MFS-25243

JANTX1N649-1 Diode

The effects of power and temperature overstress

Samples manufactured by Semtech and Micro Semiconductor were tested. Both lots did quite well in the tests. Semtech has one failure in Group I testing and three in Group II. Micro Semiconductor had two failures in Group II. Because of the small number of failures, only one Group II diode from each manufacturer was submitted for failure analysis.

The Semtech diode exhibits surface leakage, which developed due to the migration of impurities at the silicon/glass interface during the severe conditions of the temperature step-stress test. The Micro Semiconductor diode exhibits leakage due to degradation of the semiconductor junction by the migration of mobile impurities. Neither diode shows evidence of microplasmas or other crystal defects.

A plot showing the cumulative failure distribution for Group II was drawn for the Semtech sample lot and for the Micro Semiconductor sample lot, but Group III graphs could not be drawn because of the absence of catastrophic failures. No activation energies could be calculated due to the absence of Group III failures.

This work was done by the Special Products Division of DCA Reliability Laboratory for **Marshall Space Flight Center.** *To obtain a copy of the report, Circle 6 on the TSP Request Card.*
MFS-25244

JANTX1N746A Diode

The effects of power and temperature overstress

Samples manufactured by Siemens and Motorola were tested. Both lots held up well in the Group I testing, with one diode from each manufacturer experiencing catastrophic failure. Both groups completed the entire Group III testing, with eight failures in the Siemens sample lot and two in the Motorola lot.

Because of an apparent excess reverse-leakage-current failure mode, failure analysis was done for the Group II testing. Testing of both sample lots had to be stopped because more than 50 percent of the devices in each failed before the end of the test.

Many of the Siemens samples exhibited metal flow away from the die and up the internal lead. For many of the Motorola diodes, metal climbed partially up the internal lead, depleting the top metal connection of the die. Both diode groups failed because of the effects of high temperature, which melted the internal die metal. Over many hours, the molten metal alloyed into the silicon dice and shorted them out.

This work was done by the Special Products Division of DCA Reliability Laboratory for **Marshall Space Flight Center.** *To obtain a copy of the report, Circle 7 on the TSP Request Card.*
MFS-25245

JANTX1N759A Voltage-Regulating Diode

The effects of power and temperature overstress

Diodes manufactured by Texas Instruments and Siemens performed well in Group I testing. The Texas Instruments group had no catastrophic failures; the Siemens group had three. All three Siemens failures showed damaged junctions. The exact stress at which damage occurs is a function of the junction size, the heat-sink capability of the die, and the crystal perfection.

A failure analysis shows that Group II testing is the most detrimental to both sample lots, and the same failure mode can be clearly seen in Group III testing. The failure mode seems to be excessive I_R leakage. The Texas Instruments and Siemens diodes failed due to catastrophic junction damage induced by excessive die temperature while under power. It is almost certain that the actual failure mode involved microalloying of the metal across the semiconductor junction.

The metal between the internal wire lead and the die on some of the Siemens parts shows evidence of overheating and dewetting. The dice overhang their mountings on all of the Siemens diodes. Many of the Texas Instruments diode samples show cracked glass.

This work was done by the Special Products Division of DCA Reliability Laboratory for **Marshall Space Flight Center**. *To obtain a copy of the report, Circle 8 on the TSP Request Card.*
MFS-25246

JANTX1N937B Zener Diode

The effects of power and temperature overstress

Zener diodes manufactured by Motorola and Siemens were tested. The apparent failure mode in all three stress groups was the B_V (Zener-breakdown-voltage) minimum failure. Both manufacturers had approximately the same amount of failures in each testing, although the Motorola failures came at a later point in the testings.

The diodes of both manufacturers are constructed with two anode dice forward biased and one cathode die reverse biased. When failure analysis was performed, one anode die was operational, and the reverse-biased dice on many of the failures exhibited soft resistive curves. This indicates damage to the junctions due to microplasmas induced by the thermal and electrical stress of the burn-in.

This work was done by the Special Products Division of DCA Reliability Laboratory for **Marshall Space Flight Center**. *To obtain a copy of the report, Circle 9 on the TSP Request Card.*
MFS-25247

JANTX1N972B Zener Diode

The effects of power and temperature overstress

The tested Zeners were manufactured by Siemens and Motorola. The only step stress that did any notable damage to both manufacturers was in the Group II testing. Many of the Siemens devices failed, possibly because the thermal expansion of the center contact rods is greater than that of the glass body. This would increase the force exerted against the die at high temperature, causing the silicon to crack.

The dice of the Motorola parts were electrically damaged due to alloying with molten metal during the long test periods at high temperatures, which exceeded the designed capability of the devices.

This work was done by the Special Products Division of DCA Reliability Laboratory for **Marshall Space Flight Center**. *To obtain a copy of the report, Circle 10 on the TSP Request Card.*
MFS-25248

JANTX1N981B Zener Diode

The effects of power and temperature overstress

The tested diodes were manufactured by Motorola and Siemens. Both sample lots performed well in Group I and Group III testings. The Group II testing was the most detrimental of the three groups. The Motorola diodes completed the testing with 10 catastrophic failures; the Siemens sample lot was stopped 160 hours before the completion of Group II testing, with a total of 9 catastrophic failures.

Extreme heat was a big factor in the failure mode. The majority of the failures did not occur until the +275° C temperature step. At that point the devices experienced junction temperatures above +500° C. Apparently the devices failed due to electrical/thermal overstress, damaging the internal diode junctions. This conclusion is supported by the presence of low breakdown with soft and resistive curve traces and by the absence of surface leakage.

This work was done by the Special Products Division of DCA Reliability Laboratory for **Marshall Space Flight Center**. *To obtain a copy of the report, Circle 11 on the TSP Request Card.*
MFS-25249

JANTX1N1202A Switching Diode

The effects of power and temperature overstress

General Electric and International Rectifier switching diodes were tested. The Group II testing proved to be the most damaging to both sample lots. The International Rectifier sample lot also showed signs of weakness in the power-stress (Group I) testing. The diodes apparently failed due to heat generated by the excess power. The failure modes included metal melting, which disconnected and shorted internal die connections, and alloying of the metal with the silicon.

In Group II testing, many visual failures were seen in samples from both manufacturers. These visual failures suggest that both lots failed because they were unable to withstand the high temperature developed by the thermal-stress test. There was universal failure of the seal between the tubulation and glass. The GE diodes were weak at the point where the internal wire lead is attached to the active cell.

This work was done by the Special Products Division of DCA Reliability Laboratory for **Marshall Space Flight Center**. *To obtain a copy of the report, Circle 12 on the TSP Request Card.*
MFS-25250

JANTX1N3893 Diode

The effects of power and temperature overstress

Diodes manufactured by Siemens and Motorola were tested. Testing of the Motorola diodes was stopped in all three groups because the 50-percent-failures limit was reached. The Siemens lot endured 25 more hours of Group I testing and 480 more hours of Group II testing before being stopped, and the Siemens lot completed the entire Group III testing with one catastrophic failure.

Because of an apparent failure mode, failure analysis was performed on the Group II testing. The majority of the devices were visual catastrophic failures due to the stress. Most of the Siemens failures were caused by the anode lead detaching due to the stress. In the Motorola lot, the cup-to-stud detached, and the device came apart. Failure analysis also revealed a loss of the glass seal tubulation and wire lead on the Siemens devices.

This work was done by the Special Products Division of DCA Reliability Laboratory for **Marshall Space Flight Center**. *To obtain a copy of the report, Circle 13 on the TSP Request Card.*
MFS-25266

JANTX1N4570A Zener Diode

The effects of power and temperature overstress

Siemens and Motorola were the manufacturers of these diodes. Of the three stress groups, Group II proved to be the most detrimental to both sample lots. Many of the Siemens diodes had hard breakdowns that did not change when measured at any current between 1 microampere and 1 milliampere. The fact that they were within their breakdown limits at earlier measurement points suggests that there were originally junction defects present, which caused the devices to operate at a lower voltage. These atomic-level defects were "burned out" of the dice, thus allowing the true breakdowns to appear.

The Motorola samples each contain two dice in series, possibly as a means of tailoring the breakdown voltage to the desired value. When measured at low and high currents (1.0 μA and 1.0 mA), two distinct breakdowns can be seen. As with the Siemens devices, the change to higher breakdowns after some hundreds of hours of stress can be explained by the burning out of diffusion spikes from the junction, again allowing the true breakdowns to appear.

This work was done by the Special Products Division of DCA Reliability Laboratory for **Marshall Space Flight Center**. *To obtain a copy of the report, Circle 14 on the TSP Request Card.*
MFS-25268

JANTX1N5415 Diode

The effects of power and temperature overstress

The tested diodes were manufactured by Semtech and Micro Semiconductor. The Micro Semiconductor diodes experienced no failures in Group II and Group III testing and had only four failures in Group I.

There were two types of failures throughout all three stress tests for both manufacturers. One was a visual catastrophic reject. The failures were still within the electrical limits of the test when they became visual failures due to a loss of an external lead.

The second type of failure was reverse-bias leakage. The main cause of this failure was the conductive external paint on the diodes. When the continuity of the paint was disturbed, the reverse leakage fell to acceptable levels.

This work was done by the Special Products Division of DCA Reliability Laboratory for **Marshall Space Flight Center**. *To obtain a copy of the report, Circle 15 on the TSP Request Card.*
MFS-25270

JANTX1N5417 Diode

The effects of power and temperature overstress

The tested diodes were manufactured by Micro Semiconductor and Semtech. The only stress test that did significant damage was Group I (power-stress) testing. The majority of the Micro Semiconductor device failures occurred because of detached leads.

Excessive I_R leakage was the major cause of failure among the Semtech lot. The diodes of both manufacturers failed due to thermal effects caused by the excess power of the stress test.

This work was done by the Special Products Division of DCA Reliability Laboratory for **Marshall Space Flight Center**. *To obtain a copy of the report, Circle 16 on the TSP Request Card.*
MFS-25271

JANTX1N5420 Diode

The effects of power and temperature overstress

The testing of sample lots from Unitrode and Micro Semiconductor had to be stopped in Group I (power-stress), because the 50-percent-failures limit was reached. The Micro Semiconductor lot continued processing 500 hours further into the testing than the Unitrode lot, and the Micro Semiconductor diodes completed the entire Group II and Group III testing without a catastrophic failure.

Failure analysis was performed only on Group II testing because of an apparent failure mode. Most catastrophic failures of the Unitrode diodes were due to detaching of the anode lead.

The Micro Semiconductor diode has a shaped junction edge, a feature lacking in the Unitrode part. Junction shaping causes the breakdown stress to be shifted into the bulk of the semiconductor and away from the leakage on the surface. This approach is often successful in significantly increasing breakdown voltages and reducing leakage.

This work was done by the Special Products Division of DCA Reliability Laboratory for **Marshall Space Flight Center**. *To obtain a copy of the report, Circle 17 on the TSP Request Card.*
MFS-25272

JANTX1N5550 Switching Diode

The effects of power and temperature overstress

For this unit, the tested devices were manufactured by Semtech and Micro Semiconductor. The failure rate of the Semtech diodes exceeded 50

percent in all three stress tests at the first sequence point. For one device, the failure was directly attributed to a crack in the die, assumed to be caused from a poor die attach during assembly and subsequent operation. Another device was cross-sectioned at two different angles, and no visible anomalies were noted. The failure modes could not be precisely determined, although unseen microcracks across the junction are a suspected possible cause.

In both of the temperature-stress tests, the Semtech devices exhibited leakage because of conductive external paint, which bridged between the anode and cathode leads, and because of hygroscopic glass (which is protected from moisture as long as the paint is undamaged).

Arcing was clearly visible in the paint when one device was placed under reverse bias of several hundred volts. The paint of one device was chemically removed, after which the leakage could be varied at will over a large range by changing the device ambient atmosphere. A dry gas stream played over the diode at room temperature produced low leakage. Free air produced instability and high leakage. A 1-minute hydrofluoric acid etch was used to remove any possible invisible conductive residue of the paint. After this treatment, the glass was still hygroscopic.

This work was done by the Special Products Division of DCA Reliability Laboratory for **Marshall Space Flight Center**. *To obtain a copy of the report, Circle 18 on the TSP Request Card.*
MFS-25273

JANTX1N5552 Switching Diode

The effects of power and temperature overstress

The tested switching diodes were manufactured by Micro Semiconductor and Semtech. The testing of both lots was stopped in Group I. In Group II and Group III there were no Micro Semiconductor catastrophic failures. Therefore, only Group I was submitted for failure analysis.

In the case of the one analyzed Semtech sample and all of the analyzed Micro Semiconductor samples, the silicon die was still within acceptable electrical limits when the external lead became detached due to melting of the connecting metal. The curve-tracer pattern of the remaining analyzed Semtech diodes indicates that these devices failed due to a combination of junction damage and surface contamination, with the junction damage predominating.

This work was done by the Special Products Division of DCA Reliability Laboratory for **Marshall Space Flight Center**. *To obtain a copy of the report, Circle 19 on the TSP Request Card.*
MFS-25274

JANTX1N5554 Switching Diode

The effects of power and temperature overstress

Micro Semiconductor and Semtech diodes were tested. In Group I, the Micro Semiconductor lot was stopped 250 hours before the end of the process, but all eight failures occurred in the 175-percent MRP step. The six Semtech failures occurred in lower MRP steps.

Failure analysis was performed on Group I and Group II because of an apparent failure mode. Almost all of the Semtech failures and many of the Micro Semiconductor failures were due to excessive I_R leakage. In addition, the remaining Micro Semiconductor devices that failed were still within the electrical limits of the test when they became visual failures due to the loss of their anode leads. This suggests that these structural failures were caused by exceeding the thermal design limits.

In the case of the Semtech parts, the curve trace at peak inverse voltage indicates a condition of surface instability due to contamination. This contamination can move under the influence of temperature and bias. The analyzed samples were I_R rejects because their breakdowns drifted below 1,000 volts. The hard, stable breakdown of these samples indicates that there is no junction damage. The most probable cause of the lowered breakdown voltage is a change in the concentration of surface impurities on the pn junction.

When there is a slight concentration of impurities of the same polarity as the high-resistivity side of the junction (not sufficient to cause inversion), then that resistivity will be raised. This in turn will raise the breakdown voltage. Upon the migration of these protective charges away from the vicinity of the junction, the resistivity and the breakdown will fall. The hard breakdown curves of these samples, taken together with their acceptable leakage levels at 1,000 volts bias during earlier tests, suggests that the surface-charge migration mechanism as described above was the cause of the failures.

This work was done by the Special Products Division of DCA Reliability Laboratory for **Marshall Space Flight Center**. *To obtain a copy of the report, Circle 20 on the TSP Request Card.*
MFS-25275

JANTX1N5614 Switching Diode

The effects of power and temperature overstress

Semtech and Micro Semiconductor were the manufacturers. The Micro Semiconductor sample lot experienced catastrophic failures in Group I testing. The main failure mode was surface inversions, which were caused by the leakage of atmospheric moisture or other contaminants through the cracks in the glass.

Most of the Micro Semiconductor failures in Groups II and III were visual and were due to an external lead detaching. The high temperatures of these tests were sufficient to crack the glass in a number of cases.

This work was done by the Special Products Division of DCA Reliability Laboratory for **Marshall Space Flight Center**. *To obtain a copy of the report, Circle 21 on the TSP Request Card.*
MFS-25276

JANTX1N5615 Switching Diode

The effects of power and temperature overstress

Diodes manufactured by Semtech and Micro Semiconductor were tested. Each of the stress tests was detrimental to both sample lots. Both manufacturers exceeded the 50-percent failure rate in all three groups. However, the Micro Semiconductor lots were processed about 100 hours longer than the Semtech lots in each case.

(continued on next page)

The Semtech failures were all due to excess reverse leakage current. Failure analysis of Groups I and II revealed that these failures were caused by conductive external paint. When a band of paint was removed from each diode to interrupt the electrical conductivity, the diodes performed within acceptable test limits.

The failure mode for the Micro Semiconductor lots was mainly visual, but there were some I_R failures also. The Group I diodes failed due to glass and silicon breakage caused by exposure to excessive power-generated heat. The three diodes submitted to failure analysis from the Group III sample lot exhibited significant drift in breakdown voltage and leakage during the curve-tracer tests. The parts seemed to be affected by surface contamination. The source of the contamination is unknown; in fact, one diode had the voltage-drift problem and was still hermetically sealed.

This work was done by the Special Products Division of DCA Reliability Laboratory for **Marshall Space Flight Center**. *To obtain a copy of the report, Circle 22 on the TSP Request Card.*
MFS-25277

JANTX1N5618

Switching Diode

The effects of power and temperature overstress

The diodes tested were manufactured by Semtech and Micro Semiconductor. The Semtech sample lots successfully completed all three testings with only one catastrophic failure. All three Micro Semiconductor groups had several failures. They were therefore submitted to failure analysis.

One major failure mode was melting of the connecting metal, causing the external lead to open. The analyzed dice were still within acceptable test limits, but their reliability had been impaired by cracked glass. The other failure mode was excessive I_R leakage. Failure analysis revealed that the die and its glass were fractured due to the high junction temperatures reached in the testing.

This work was done by the Special Products Division of DCA Reliability Laboratory for **Marshall Space Flight Center**. *To obtain a copy of the report, Circle 23 on the TSP Request Card.*
MFS-25278

JANTX1N5619 Diode

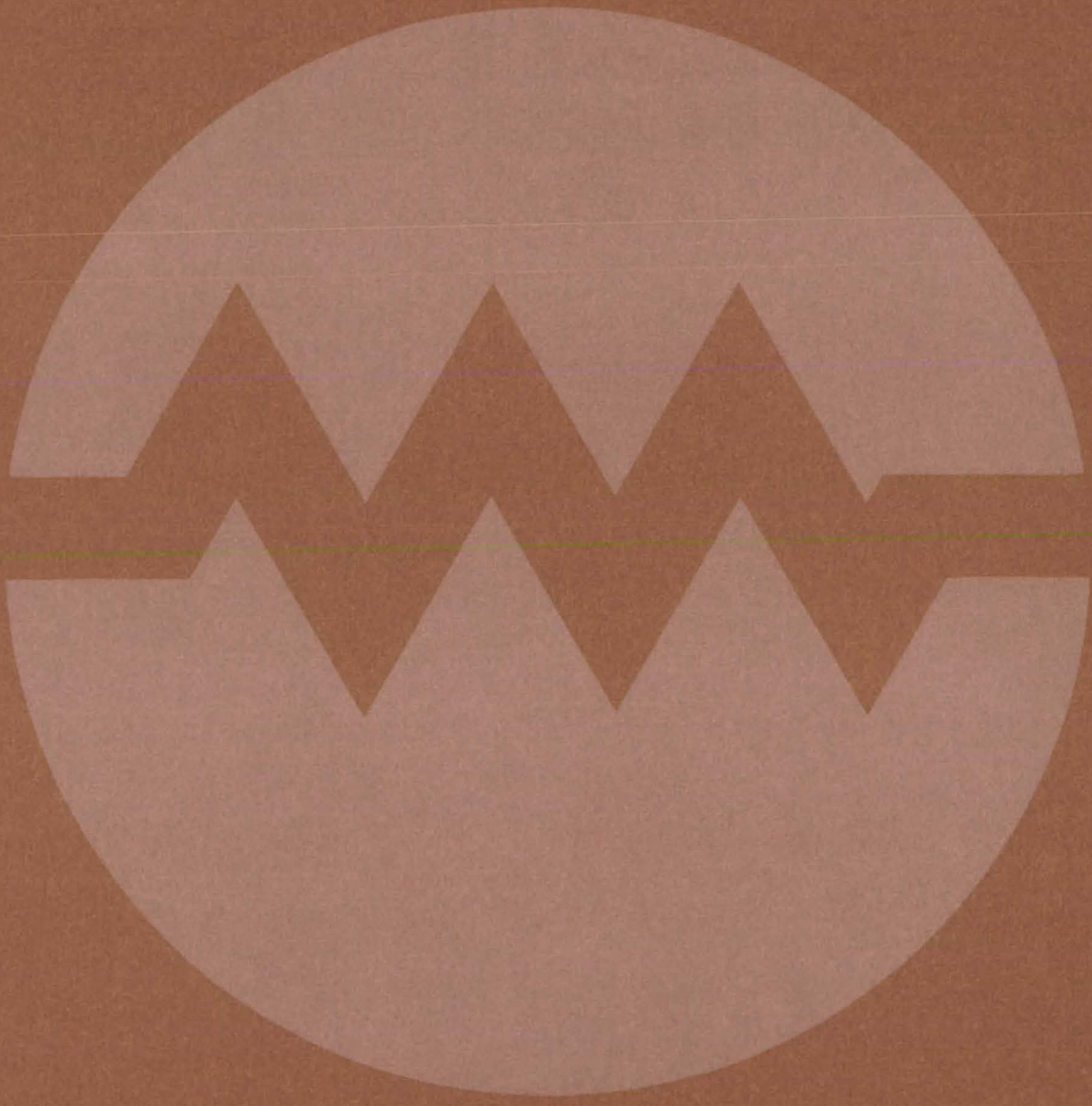
The effects of power and temperature overstress

These units were manufactured by Semtech and Micro Semiconductor. The Micro Semiconductor lot experienced catastrophic failures in Group I testing. The testing was stopped because external leads of nine of the devices detached from the internal heat sink.

In Group II testing, which was detrimental to both sample lots, the failed parameter was I_R. Retesting these devices on the curve tracer shows that the trace is free of leakage until approximately 350 volts; from there to approximately 500 volts, the curve is rounded; and then a final, hard breakdown occurred. This suggests that the stress test caused bulk silicon damage. Cracked and chipped-out metal is seen at the external anode wire attachment.

This work was done by the Special Products Division of DCA Reliability Laboratory for **Marshall Space Flight Center**. *To obtain a copy of the report, Circle 24 on the TSP Request Card.*
MFS-25279

Electronic Systems



Hardware, Techniques, and Processes

481 Variable-Resolution Facsimile System

482 Conserving Power in Computer Memories

482 Digital Generation of Command-Encoder Waveforms

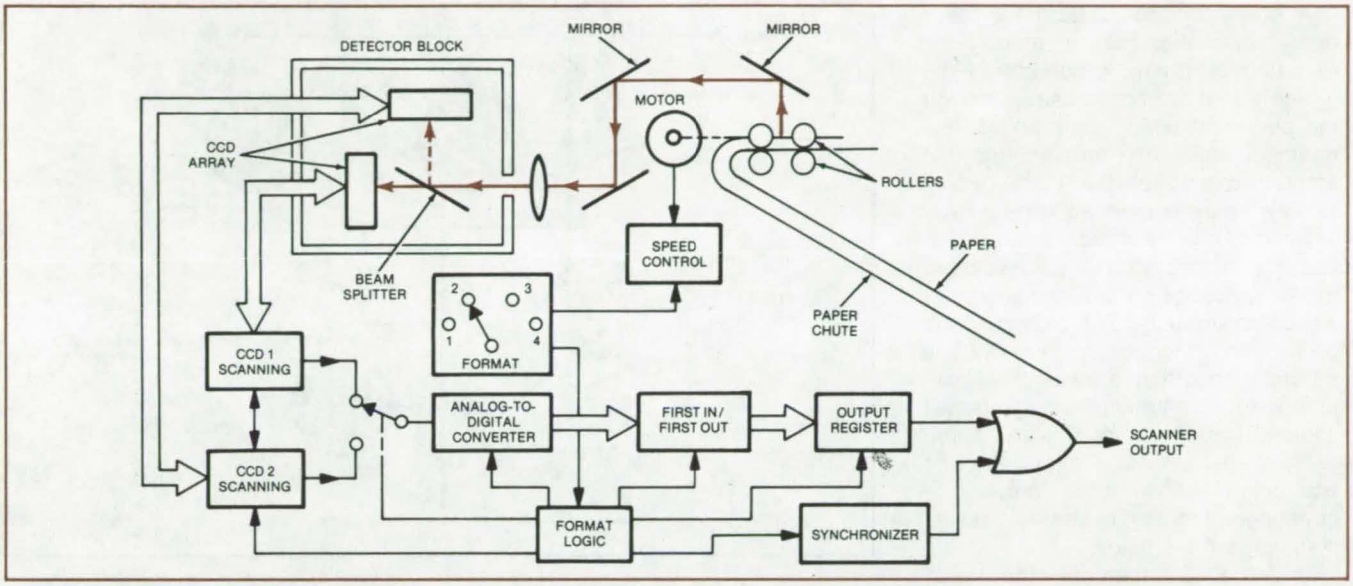
483 Binary Synchronous Simulator

484 Switching Reduces Computer Power Requirement

Variable-Resolution Facsimile System

Variable-element scanner allows resolution to be adjusted to document-transmission requirements.

Lyndon B. Johnson Space Center, Houston, Texas



This **Scanner for Variable-Resolution Facsimile** has a format selector switch that controls the paper speed and the number of elements used in the charge-coupled-device (CCD) sensor arrays. Formats 1, 2, 3, and 4 correspond to text, maps, drawings, and photographs.

A radio system for transmitting facsimiles of text, graphics, and photographs can be adjusted to produce the quality required in the final image. Thus, when high resolution is not needed, the transmission time can be greatly reduced; for example, a page of text requires only 1 minute for transmission, whereas a photograph requires 17 minutes. The system was developed for conveying maps, diagrams, text, and photographs to the crew onboard the Space Shuttle.

In the ground-to-spacecraft application, a sheet of paper or a photograph is fed into the ground-based scanner. An image area of 8-1/2 by 10 in. (21.4 by 25.4 cm) is scanned, sampled, digitized, and converted to a pulse-code-modulated (PCM) bit stream at 128 kilobits per second. The bit stream is multiplexed with two digital voice channels, a command channel, and synchronization data, forming a data stream having a bit rate of 216 kb/s. The combined data are transmitted to the Space Shuttle orbiter via a Ku-band radio link.

On the orbiter the data are demultiplexed, and the image data are supplied to a copier. Synchronized with the ground scanner, the copier converts the digitized data to an analog signal. This signal modulates a single-line-scan cathode-ray tube, which exposes a sheet of photosensitive paper. After automatic developing, the paper is a full-size copy of the original page or photograph.

The ground-based scanner employs two straight-line arrays of charge-coupled devices (CCD's), each having 1,728 light-sensing elements, for a total of 3,456 resolution elements on a single line. For maximum resolution when photographs are scanned, the system uses every element and senses 64 distinct gray levels (6-bit quantization). When less resolution is acceptable but gray tones are still needed, the system uses every other scanning element with 6-bit quantization. For high-resolution line drawings, the system uses all elements but only bilevel quantization. For text, the system uses every other element with bilevel quantization. A roller mechanism pulls the paper over a line aperture. The CCD line arrays view the paper through the aperture via a lens and mirrors (see figure).

The onboard copier weighs only 60 lb (27 kg) and consumes 100 watts. The faceplate of the cathode-ray tube is composed of high-quality optical fibers. Phosphors are deposited directly on the fiber ends so that the 1-mil (0.03-mm) light spot generated by the electron beam is carried by a fiber directly to the photographic paper without spreading.

Usually the level of resolution is selected at the transmitting end. However, an operator at the receiving end has the option of expanding light or dark areas to reveal details.

This work was done by Phillip C. Lipoma of Lockheed Electronics Co., Inc., for **Johnson Space Center.** *Further information may be found in the copyrighted article "Shuttle Orbiter Uplink Text and Graphics System" from the 1978 National Telecommunications Conference Record, copyright IEEE. To obtain a copy of the article, Circle 25 on the TSP Request Card.*
MSC-18516

Conserving Power in Computer Memories

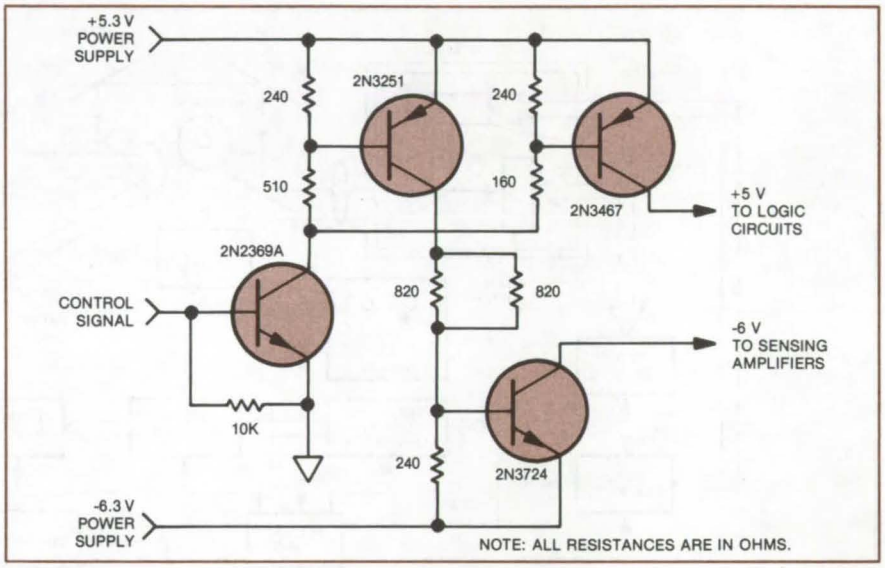
Control system switches power to memory circuits only when it is needed.

Langley Research Center, Hampton, Virginia

A power control system for electronic memories saves energy by switching off power to portions of the memory that are not in use. Although the power-off period lasts only a few microseconds or milliseconds, it amounts to a sizable part of the overall read/write cycle time; so large energy savings can be realized.

The control system was developed for the guidance control and sequencing computer (GCSC) for deep-space probes, in which every microwatt is carefully apportioned because of size and weight limitations on the power source. The control principle is applicable also to remote data-gathering equipment with limited power — oceanographic and meteorological stations, for example.

In the GCSC memory, the read/write operation lasts 1.5 microseconds, but the minimum time between consecutive read/wite operations is 3.47 microseconds. In the GCSC data-storage memory, the read/write operation lasts 1.5 microseconds, but the period between such operations is 1.5 milliseconds. The power control system cuts off power to memory logic circuits during the part of the cycle when they are not actively involved in reading and writing. For the computer memory, this inactive, power-off period is 1.97 microseconds; and for the data-storage memory, it is 1,498.5 microseconds. The only parts of the memory system that remain energized during these inactive periods are low-power logic, for addressing memory locations and for transmitting input/output data, and a minimal amount of standard logic, for receiving read and write commands to initiate a memory cycle.



This Power Switch, controlled by a master timing circuit, turns on voltages to logic circuits and amplifiers only during the active portions of their clocked cycles. The +5-volt line powers positive logic circuits; the -6-volt line is for sense amplifiers.

Power to the various parts of the memory system is turned on and off by logic power switches that are transistors controlled by standard transistor-transistor-logic (TTL) integrated circuits. The figure shows the transistorized power switch used to gate logic power to the sense amplifiers used in the read operation. The +5-volt switch shown is typical of the switches used to switch positive logic power; variations are made as necessary to meet the power requirements of the loads. The -6-volt power switch is used only to supply sense-amplifier power.

This work was done by Honeywell Inc. for **Langley Research Center.** *For further information, Circle 26 on the TSP Request Card.*
LAR-11952

Digital Generation of Command-Encoder Waveforms

Circuit produces sinusoidal command signals by purely digital means.

Goddard Space Flight Center, Greenbelt, Maryland

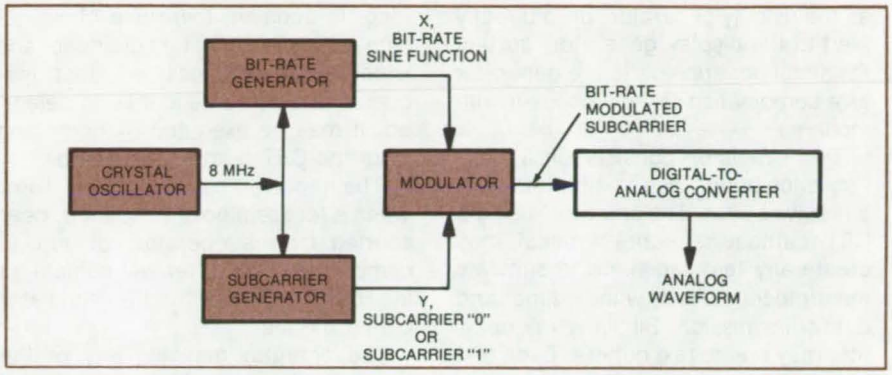
A command encoder for a command data system produces sinusoidal signals by purely digital means. The encoder produces two phase-coherent sinusoidal subcarriers — one at 8 kilohertz representing a binary "0," the other at 12 kilohertz representing a binary "1" — at a bit rate of 800 hertz.

The frequencies are programable to within ± 0.002 percent over the full range of frequencies used for encoded spacecraft commands. In addition, the phase angle at which the bit transitions take place is settable to within 0.7° of any angle between 0° and 360°. The modulation index is programable in 225 steps over the range 0.30 to 1.00.

Ordinarily, this kind of encoder would be made from analog components: a frequency synthesizer, to generate the subcarriers, and a sinusoidal oscillator and analog multiplier, to produce the output waveform. The digital version was developed to avoid the problems of drifting outputs and the difficulty of adjustment and calibration common to analog circuitry. Moreover, the digital nature of the new encoder makes it easy to change the five waveform parameters (frequency of subcarrier for "1," frequency of subcarrier for "0," bit rate, modulation index, and bit-change angle).

The encoder (see figure) consists basically of a bit-rate sine-function generator, a subcarrier generator, and a modulator. These elements are composed of digital integrated circuits, such as adders, multipliers, and programable read-only memories (PROM's).

In the bit-rate generator, the 8-MHz output of a crystal oscillator is converted to a stream of bits representing the function $X = \text{Bias} + 30 \sin \omega_b t$, which defines the bit rate, modulation index, and the angle at which a bit changes from "1" to "0" or vice versa. All these parameters can be selected by controls on the circuit.



Digital Signals representing the bit rate and the subcarriers are combined to form a modulated digital signal, which is finally converted to analog form.

In the subcarrier generator, the 8-MHz output of the same crystal oscillator is converted to a bit stream representing $Y = 127 \sin \omega_{sc} t$, which defines the subcarrier for a "1" or a "0," depending on whether a multiplexer directs a "1" or a "0" command into the subcarrier generator. The frequencies of the "1" and "0" subcarriers (ω_{sc} in the equation) are selectable.

The modulator combines X and Y, producing a bit stream of digital data representing the subcarriers modulated at the bit rate. Finally, a digital-to-analog converter changes the digital signal into sine waves.

This work was done by W. S. Ataras of General Electric Co. for **Goddard Space Flight Center.** *For further information, Circle 27 on the TSP Request Card.*
GSC-12203

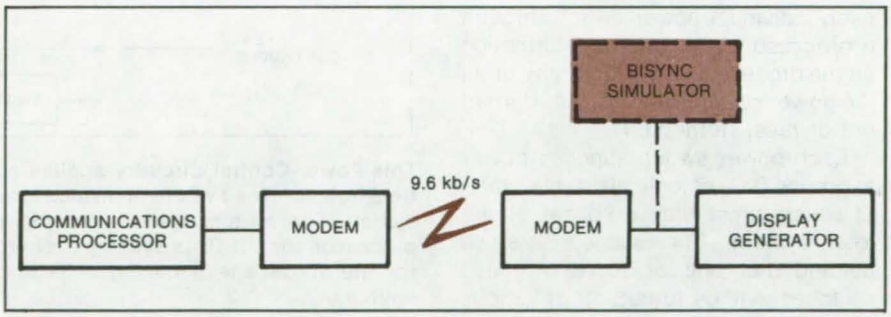
Binary Synchronous Simulator

A simulator for troubleshooting a data communications system

John F. Kennedy Space Center, Florida

A flexible simulator for troubleshooting a data transmission system (see figure) uses a binary synchronous communications protocol. The protocol produces error-free transmission of data between two points. It follows a five-step sequence: (1) a signal from the transmitting device requesting permission from the receiving device to send data; (2) a response from the receiving device; (3) data transmission to the receiving device; (4) a check by the receiving device on whether the data are correct and an acknowledgment response to the transmitter; and (5) if the data are correct, the transmitter response with an end-of-transmission signal.

Problems such as an abnormal data sequence or system failures are difficult to troubleshoot by conventional methods. Oscilloscopes and logic analyzers take a long time to set up, and the operator has no control over the data sequence. The new binary synchronous (bisync) simulator connects directly into the system and generates fully-controllable data sequences for quick troubleshooting.



A **Typical Data Transmission System** is shown that uses a binary synchronous communication protocol. A newly-developed bisync simulator is connected directly into this system, replacing either the combination of processor and modems or the display generator. The simulator generates controllable data sequences for quick troubleshooting of the transmission system.

The simulator is connected either to replace the display generator, so that the simulator appears to the processor

(continued on next page)

as the display generator, or to directly feed to the display generator, so that the simulator appears to the generator as a combination of the processor with modems.

The simulator consists of a test-sequence buffer, two text buffers, and a receive buffer. The operator, using a CRT (cathode-ray-tube) terminal, may create any test sequence to simulate the protocol signals, waiting time, and data transmission. Similarly the operator may create text buffers. Each text buffer may be up to 255 characters long. In addition, there is a choice of nine predefined text sequences and twenty-three predesigned test sequences. Once a sequence is selected, it may be executed by command from the CRT terminal keyboard.

The receiver buffer may be listed when a test sequence has failed, been aborted by the operator, or run to completion. The buffer will contain all the data received by the simulator during the test.

The operator may list any of the simulator buffers. Also a keyboard command is available to calculate cyclic redundancy-check characters for both text buffers. These characters can also be verified for the receive text buffer.

This work was done by Jacob R. Rogers III of **Kennedy Space Center.** *For further information, Circle 28 on the TSP Request Card.*

Inquiries concerning rights for the commercial use of this invention should be addressed to the Patent Counsel, Kennedy Space Center [see page A5]. Refer to KSC-11096.

Switching Reduces Computer Power Requirement

Network of switches conserves power by feeding it only to selected circuits.

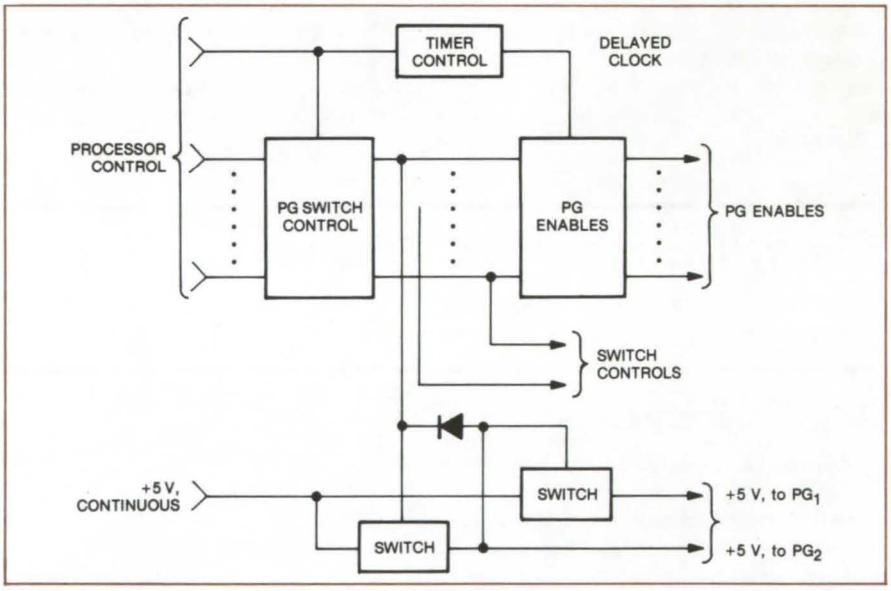
Langley Research Center, Hampton, Virginia

A system of power switches developed for the Viking Guidance Control and Sequencing Computer (GCSC) activates only selected TTL circuits necessary for that particular time interval. Power that was fed to inactive circuits and dissipated is no longer applied. Because of this, the system can use a much lighter, smaller power source — an important weight-saving factor, particularly in aircraft and spacecraft electronics.

Power switching (see figure) is implemented via a power-control register operating from a continuous +5-V supply. The register controls each individual power switch through a processor. With proper information on the processor output bus, any or all the power switches may be set (turned on) or reset (turned off).

Each power switch supplies power to groups (PG) of logic elements, each of which constitutes a subset of the total system. The subsets are so defined that one or more of these switches may be turned off at various times without affecting the intended operation of the system. The total number of subsets depends largely on the complexity of the system (i.e., the number of different operating modes) and on how well the logic is partitioned. Sometimes it becomes necessary to add redundant circuitry to avoid overlapping of these subsets.

Transients, the main problem in power switching, are not eliminated. Instead the output signal associated with the power group being switched is gated. Only those outputs interfacing with circuits in another power group are of concern. The power-group enable associated with the group being switched is used to inhibit the propagation of these transients into other power-group logic during power up and down. Very often this gating can be incorporated into the existing logic.



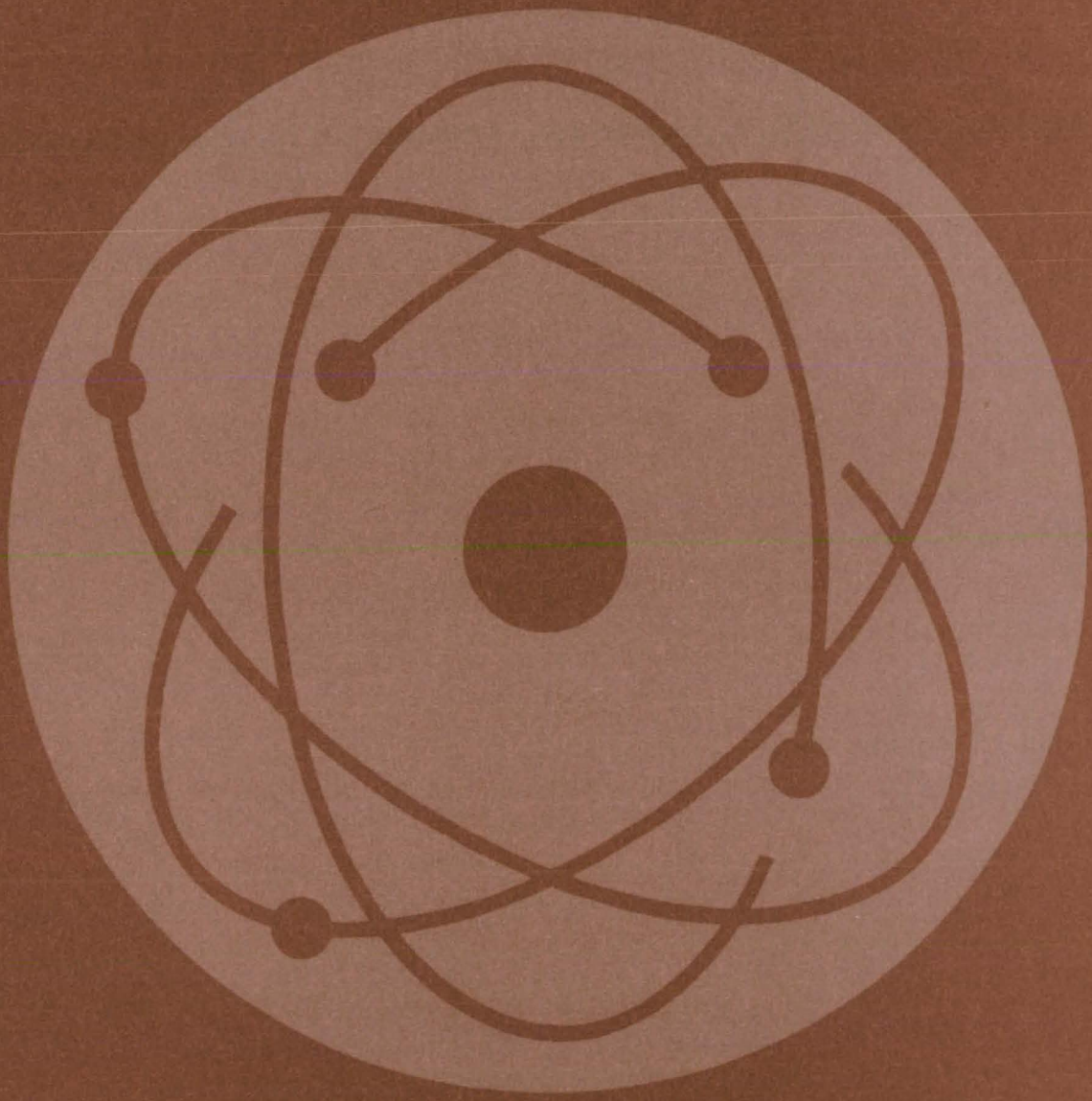
This Power-Control Circuitry applies power only to circuits being used at a given time interval. The system is divided into power groups (PG); each is controlled by a switch. The switches are turned on or off depending on the output from the processor control. This scheme deenergizes inactive circuits and draws power only for the active ones, making it possible to use smaller, lighter, system power sources.

The other area requiring transient suppression was the system interface. Significant power savings were also achieved in this area by power-switching the interface elements.

This work was done by Honeywell Inc. for **Langley Research Center.** *For further information, Circle 29 on the TSP Request Card.*

LAR-11958

Physical Sciences



Hardware, Techniques, and Processes

487 Nuclear Electro-optic Power
488 Proposed Josephson Voltage Standard
489 High-Efficiency Wind Turbine
490 Increased Fuel-Cell Cross-Pressure Limit
490 Measuring Transmissivity of Solar-Cell Covers
491 Improved Degradation Resistance of (AlGa)As Lasers
492 Improved Vapor-Growth Technique for III-V Compound Lasers
492 Germanium-on-InP heterojunction-Structure LED
493 Improved Thermal-Conducting and Current-Confining Film
494 Ohmic Contact to p-Type Indium Phosphide
494 CdSInP Semiconductor Alloy
495 Sealed High-Pressure X-Ray Detector
496 Automatically Classifying Earth Features From Orbit
497 FEP Plug Protects H_2 Masers

Books and Reports

497 Programable Solar-Energy Controller
498 Weathering of a Liquid Solar Collector
498 Testing of a Solar Collector With Concentrating Mirrors
498 Installation Package — Home Solar Heater

Computer Programs

499 Monte Carlo Variance Reduction
499 Wind-Energy Storage
500 Landsat Signature Development Program

Nuclear Electro-optic Power

Nuclear battery produces sufficient power for many applications.

Langley Research Center, Hampton, Virginia

As part of a study to develop power sources for instruments used on long-term space missions, the state of development of nuclear batteries was investigated. It was determined that existing nuclear batteries, although long lived, lacked the power required for most applications. Thus, a new approach was tried, involving the intermediate conversion of particle kinetic energy into optical energy. This has been named a tertiary-nuclear battery according to the following classification of ways of converting the kinetic energy of particle radiation into electrical energy:

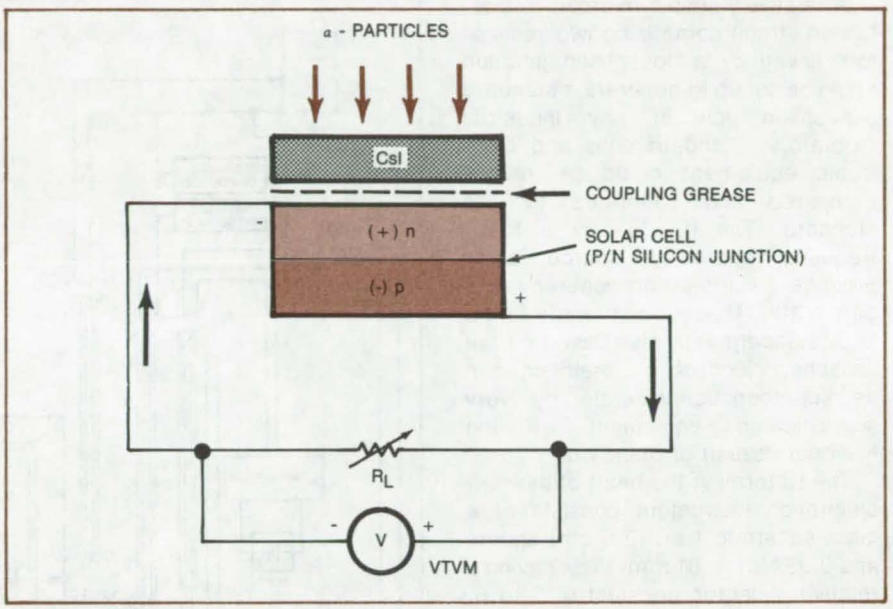
Primary: Charged particle emissions from a radiosotope placed on one electrode are collected on the second electrode. When there is an electrostatic field between electrodes, the particles constitute moving charges in the field.

Secondary: Particle kinetic energy produces electron-hole pairs near pn junctions in semiconductors or in a gaseous medium between two dissimilar metals. [Radioisotope thermal generators (RTG's), where particle kinetic energy is converted into thermal energy for further conversion into electricity also belong in this category].

Tertiary: Particle kinetic energy is converted to light pulses in phosphors such as CsI, NaI, or ZnS. The light pulses are used to activate solar cells.

Thermal nuclear batteries have been developed the most, mainly due to the powerful momentum built up by the early SNAP work. However, other nuclear batteries have thus far been little more than laboratory curiosities, because of their low-power output.

In the tertiary-nuclear battery developed, nuclear radiations produce scintillations in a phosphor. These scintillations, when allowed to fall on solar cells, produce a current through an external circuit in much the same manner as Sunlight. Since the solar cell is not directly exposed to the nuclear radiation, it does not suffer radiation damage. Efficiency is necessarily less than for a solar cell alone, since only about 15 percent of the incident particle energy can be converted to light pulses inside the phosphor.



Tertiary-Nuclear Power Cell utilizes an alpha source from which radiated particles strike a phosphor. The phosphor emits photons that are converted to electricity by a solar cell.

Choice of an appropriate phosphor and a radionuclide such as Am^{241} can improve efficiency somewhat.

Experimental results indicate that Am^{241} alpha sources are superior to beta sources because of their higher alpha specific ionization and the simultaneous production of low-energy photons (which are easily converted into photoelectrons for additional power). Measurements on pn junction silicon cells show that these units are capable of delivering several hundred microwatts per curie of Am^{241} alpha source, indicating their usefulness for a number of electronic applications, especially where reliability and long life are important.

This work was done by Jag J. Singh of **Langley Reserach Center.** *Further information may be found in NASA TM-78789 [N78-33538/NSP], "Nuclear Electric Power Sources" [$4.00]. A copy may be purchased [prepayment required] from the National Technical Information Service, Springfield, Virginia 22161.*

Inquiries concerning rights for the commercial use of this invention should be addressed to the Patent Counsel, Langley Research Center [see page A5]. Refer to LAR-12496.

Proposed Josephson Voltage Standard

Proposed microwave IC makes a readily-available Josephson voltage standard.

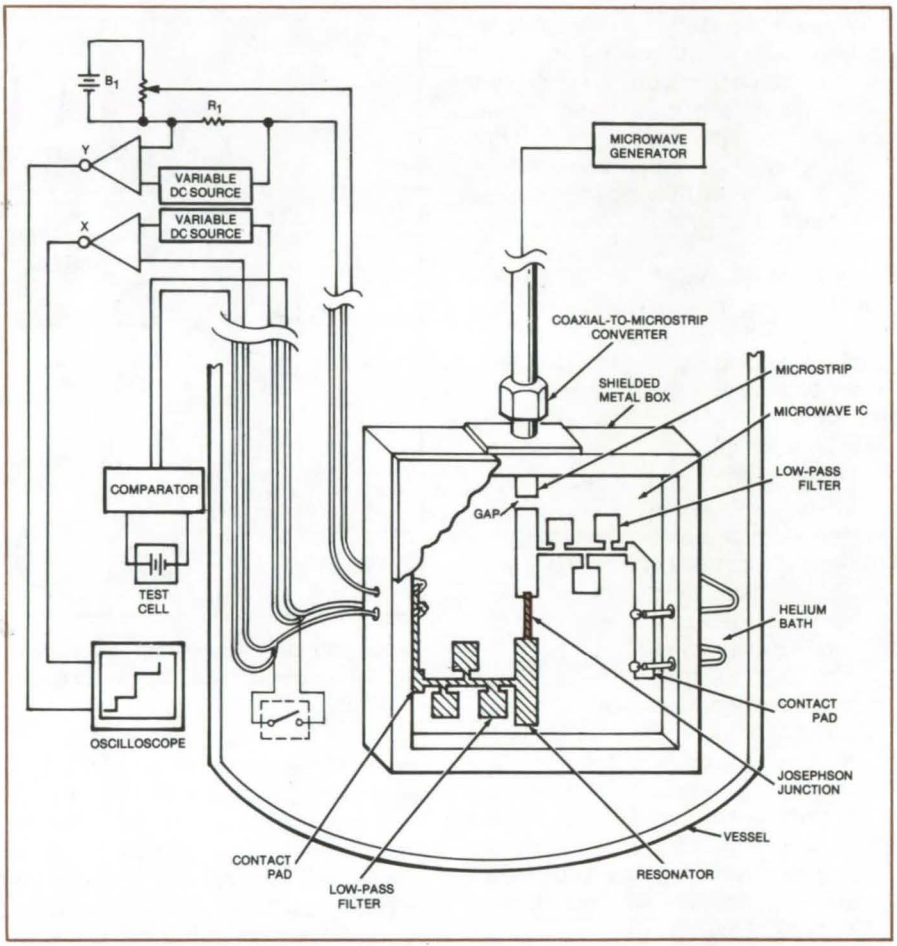
Marshall Space Flight Center, Alabama

A relatively-simple microwave integrated circuit comprising two resonators linked by a Josephson junction could be set up to generate a standard Josephson volt in any industrial laboratory. Standard cells and electronic equipment could be readily compared and calibrated to this standard. The IC, fed by a fixed-frequency microwave source, could produce 1 volt with an accuracy of 1 part in 10^6. That is comparable to the U.S. standard volt, also based on the Josephson junction but maintained in its superconducting state by very sophisticated equipment at the National Bureau of Standards.

The IC forming the heart of the new calibration instrument consists of a glass substrate 1 in. (2.5 cm) square and 0.032 in. (0.81 mm) thick having a relative dielectric constant of 5 to 6. Two lead-film circuit patterns, each defining a resonator, are vacuum-deposited on its surface in a three-step process: One film is deposited to define one resonator; it is oxidized to form an oxide layer, and a second film is deposited to form the second resonator. The deposition is through carefully-designed stencil masks. The area of overlap consisting of lead/lead oxide/lead forms the Josephson junction [the two lead layers forming the superconductor separated by a lead oxide (weak-link) layer]. An aluminum plate with a thin anodized layer secured to the back of the substrate serves as the circuit ground plane.

The IC is mounted in an RF (radio-frequency) shielded metal box (see figure) and immersed in a liquid-helium bath (4 K temperature) to bring the film to the superconductive state.

The components external to the bath connected to the IC include a bias supply, a comparator, an oscilloscope, and a microwave power generator. The microwave power (e.g., 8.99376 GHz, 50 mV) is fed to the IC via a coaxial-to-microstrip converter. The energy is transferred to the resonator via a gap acting as a capacitive coupling between the input microstrip line and the resonator.



Proposed **Josephson Voltage Standard** could be used in any industrial laboratory. The instrument utilizes a microwave IC that incorporates a Josephson junction. The device inserted into a helium bath reaches a superconductive state and produces voltage precisely proportional to the microwave frequency input. This voltage together with an input dc bias current is monitored on the oscilloscope, giving a Josephson step signal current-voltage characteristics. The established standard voltage is fed to a comparator to check the calibration of the standard Weston cells.

Direct-current bias-current input to the Josephson junction is fed by a battery B_1 through low-pass filters of each resonator circuit. The current through the junction is proportional to the potential drop across resistor R_1, which is amplified and monitored by an oscilloscope.

This voltage output is fed to the comparator connected to a Weston standard cell. A predetermined reading on the comparator indicates whether the cell is calibrated.

This work was done by C. C. Chang, Louis B. Holderman, and Jaan Toots of the U. S. Department of Commerce for **Marshall Space Flight Center.** *For further information, Circle 30 on the TSP Request Card.*

This invention is owned by NASA, and a patent application has been filed. Inquiries concerning nonexclusive or exclusive license for its commercial development should be addressed to the Patent Counsel, Marshall Space Flight Center [see page A5]. *Refer to MFS-23845.*

High-Efficiency Wind Turbine

A vertical-axis turbine combined with airflow directors extracts more energy from the wind.

Marshall Space Flight Center, Alabama

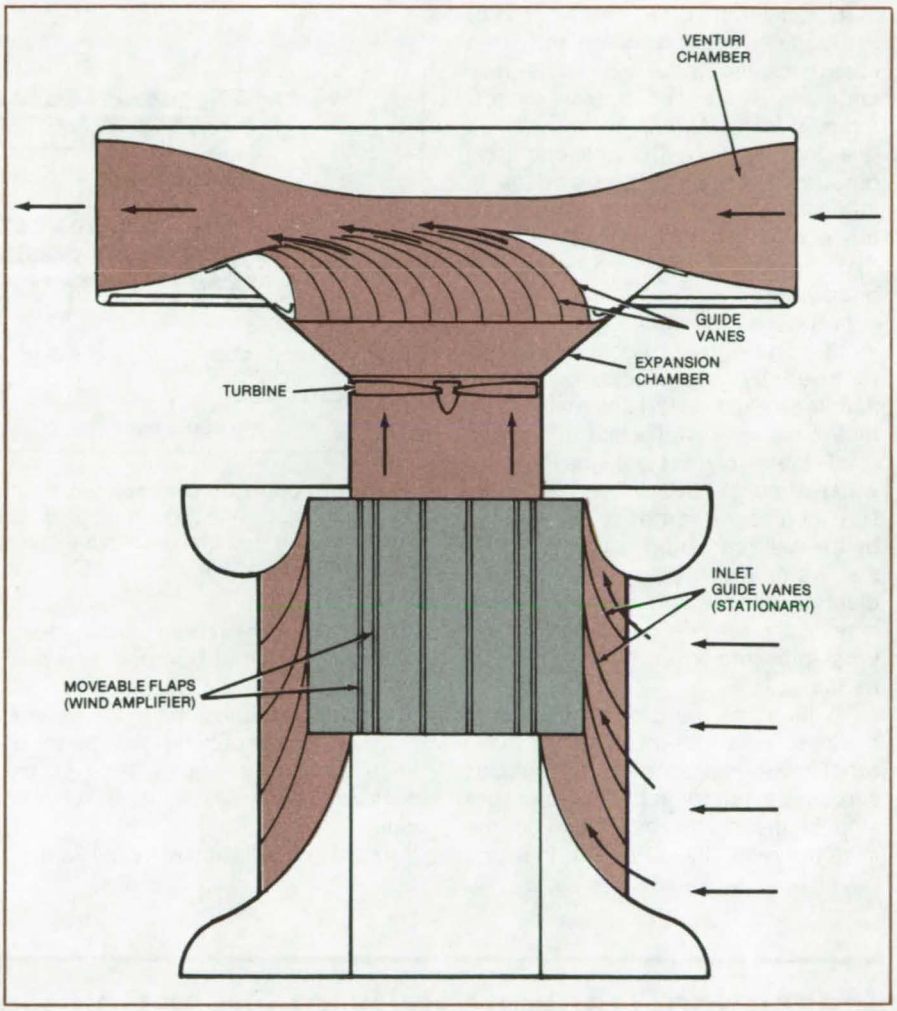
A new wind turbine, the components of which are undergoing preliminary laboratory tests, would be about 20 percent more efficient than conventional propeller-driven units. The new turbine, which has anti-"pinch-off" and wind-amplification features starts delivering energy at windspeeds of less than 13 miles per hour (6 kilometers per hour), which is considerably lower than for conventional designs.

As seen in the figure, the vertical-axis turbine is mounted in an enclosure having a horizontal inlet that is open to the wind in all directions. Between the inlet and the turbine is the wind amplifier, which directs the air into a spiral pattern as it increases the wind velocity and introduces turbulence. With greater turbulence, it is found that the air boundary layer follows the turbine blade contours over a longer distance before separating. The air thus transfers more energy to the blades with lower blade drag.

The turbine exhausts into an expansion chamber, from which the airflow emanates through guide vanes into a venturi cavity. The venturi cavity is oriented by a servomechanism into the wind. With the wind flowing through it, it acts as an aspirator, drawing air from the turbine into the windstream. The guide vanes and cavity eliminate a common problem with vertical exhaust tubes such as chimneys — that is, the back pressure, or "pinch-off" effect exterted by the wind, particularly at low windspeeds.

Several wind amplifiers have been considered, including various funnels and venturi shapes, toroids, with or without movable flaps, and Archimedic spirals. In tests, a long-necked venturi gave good performance with the least "spillover." It roughly doubled the windspeed for a reduction in flow area by a factor of 6.

In periods of no wind, it is possible that the vertical-axis wind turbine can be used in combination with an array of hot-air solar collectors. Since such arrays create their own draft as the Sun heats the air in their plenums, their air supply can be routed through the turbine. The combination of wind turbine and solar collectors can thus furnish electric power and heat. Another alternative is to pass hot gas from a chimney through the turbine to derive electric power from flue gases that would ordinarily be vented into the atmosphere.



A **Venturi-like Aspirator** prevents wind flowing over the turbine vertical exhaust from creating a back pressure. The turbine therefore turns even at low windspeeds.

This work was done by Leopold A. Hein and William N. Myers of **Marshall Space Flight Center.** *For further information, Circle 31 on the TSP Request Card.*

Inquiries concerning rights for the commercial use of this invention should be addressed to the Patent Counsel, Marshall Space Flight Center [see page A5]. Refer to MFS-23830.

Increased Fuel-Cell Cross-Pressure Limit

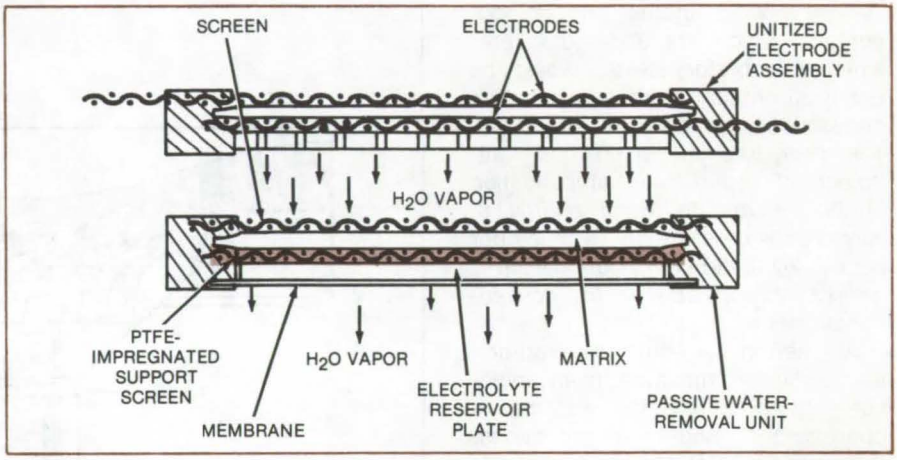
A special support screen increases cross pressure in fuel-cell water-removal units.

Marshall Space Flight Center, Alabama

A polytetrafluoroethylene (PTFE) impregnated support screen increases cross pressure on an electrolyte-filled matrix in a fuel-cell passive water-removal unit. Although the method does not increase the cell operating pressure, a major design goal in improving the cell performance, it ups the operating-pressure limit, leaving more room to develop a higher pressure cell.

In the fuel-cell configuration shown in the figure, the product water is removed by a pressure differential across an electrolyte-filled matrix. The matrix passes water while preventing the leakage of reactant gas into the water-removal cavity. The total pressure across the matrix is determined by the cell reactant-gas pressure and the water-vapor pressure over the electrolyte. Thus, the operating pressure of the fuel cell is limited by the cross-pressure characteristic of the matrix.

To increase the cross pressure at the matrix, a 100-mesh polytetrafluoroethylene-impregnated support screen is inserted on the low-pressure side of the matrix as shown in the sketch. Tests have shown that the addition of this screen substantially increases the matrix cross pressure and correspondingly increases the cell operating-pressure limit. This is one step toward improving the performance and life characteristics of the passive water-removal type of fuel cell.



A PTFE Support Screen inserted on the low-pressure side of an electrolyte-filled matrix increases the matrix cross pressure. This increases the cell operating-pressure limit that may improve the performance and life characteristics of passive water-removal-type fuel cells.

This work was done by William F. Bell and Nunziato J. Maio of United Technologies Corp. for **Marshall Space Flight Center.** *No further documentation is available.*

Inquiries concerning rights for the commercial use of this invention should be addressed to the Patent Counsel, Marshall Space Flight Center [see page A5]. *Refer to MFS-25196.*

Measuring Transmissivity of Solar-Cell Covers

The cover-material transmissivity is compared to that of a reference material.

NASA's Jet Propulsion Laboratory, Pasadena, California

A new apparatus determines the ratio of the transmissivity of a solar-cell cover material to that of a standard reference specimen. The measurement of this quantity is very important in the development of efficient solar cells. Because protective solar-cell covers deteriorate during prolonged exposure to the environment, the transmissivity drops correspondingly, decreaseing the cell efficiency.

The apparatus (see figure) uses a simulated solar point source refracted by a condensing lens. The resulting converging concentrated beam is split with one-half directed toward a reference material and the other toward the sample.

The reference material rests on a standardized solar cell, the output of which is applied to a 0.2-ohm load. Voltage at that load is fed to an operational amplifier through a normalizing potentiometer. The amplifier output serves as one input to a ratiometer. An identical setup with sample material forms a second ratiometer input.

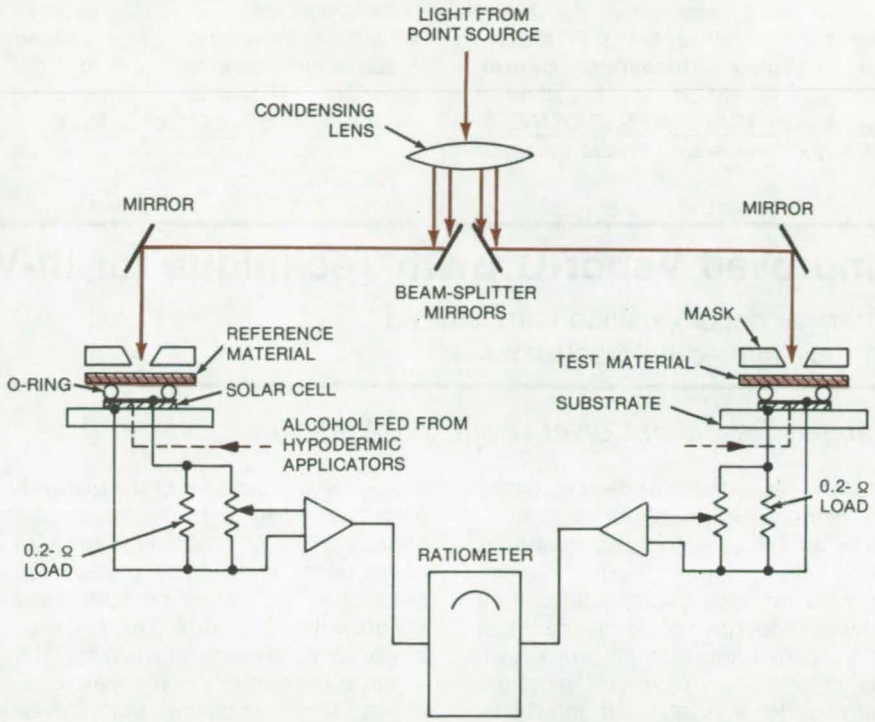
Before the test, the cell outputs are checked with covers removed and the potentiometers adjusted for unity

reading on the ratiometer output. After the system is normalized, the test and reference materials are placed on their respective cells to establish the transmissivity ratio.

An airgap (not present in fabricated cells) between the cell and the cover is filled with isopropyl alcohol. Leakage is prevented by clamping (clamps not shown) the covers to O-rings resting on the respective cell substrates. The alcohol is introduced via hypodermic applicators through tubes feeding into each substrate. This procedure eliminates about 4 percent of transmissivity loss due to reflection at the airgap.

The apparatus measures transmissivity ratios accurately to three decimal places. A standard digital voltmeter may also be used instead of the ratiometer. In this case, the voltmeter internal reference is disconnected and connected to the reference solar-cell detector, while the voltmeter input is connected to the second cell.

This work was done by Eric G. Laue of Caltech for **NASA's Jet Propulsion Laboratory.** *For further information, Circle 32 on the TSP Request Card.*
NPO-14638



Solar-Cell Cover Transmissivity is determined by comparing test material transmissivity with that of a reference material. The outputs of two solar cells without test covers are amplified to make them equal. Then the reference and test materials are put into place and compared. Isopropyl alcohol fills the airgaps between the cells and the covers to provide optical coupling between encapsulant and solar cell.

Improved Degradation Resistance of [AlGa]As Lasers

Simultaneous doping with Ge and Zn increases life of short-wave lasers.

Langley Research Center, Hampton, Virginia

Short-wavelength (AlGa)As lasers can be made to lase CW at room temperature to wavelengths approaching 7,000 Å. However, the life of these devices is much shorter than that of similar devices operating at longer wavelengths. The preferred p dopant is zinc because high doping levels cannot be achieved using germanium in aluminum-rich layers without seriously affecting the structural and optical properties of the device. However, tests indicate that simultaneous doping with Ge and Zn improves the resistance to degradation, thus opening up prospects for greatly increased reliability in lasers and LED's operating at 7,500 Å and below.

A possible contributing factor to the degradation of short-wavelength lasers could be the generation of point defects in the p-type confining layer by the energy released in nonradiative recombination. Once the point defect is generated, its movement into the recombination zone and interference with radiative recombination may be accelerated by the relatively high stress occurring in the material. The Ge could be effective in preventing point defect generation. This may be the result of a local interaction, Zn and Ge occupying different lattice sites, which reduces the probability of atomic displacement. Both dopants are p type in (AlGa)As, but they occupy different sites: the Ge fills As sites, the Zn fills Ga sites. Also, if dislocations exist, the presence of Ge and Zn as impurities could prevent their motion.

The preferred method of double-doping with Zn and Ge is to incorporate equal quantities of each. The benefits of the improved reliability are derived when the dopants are simultaneously introduced into the bounding p-type (AlGa)As layer of the heterojunction structure. It is believed that the formation of vacancies produced by the electron-hole recombination within that layer, vacancies that would normally diffuse into the recombination region and reduce the life of the device, is minimized.

(continued on next page)

This work was done by Henry Kressel and Ivan Ladany of RCA Corp. for **Langley Research Center.** *Further information may be found in NASA CR-3045 [N78-32405/NSP], "1.1 Micrometer and Visible Emission Semi-Conductor Diode Lasers" [$6.50]. A copy may be purchased [prepayment required] from the National Technical Information Service, Springfield, Virginia 22161.*

Title to this invention has been waived under the provisions of the National Aeronautics and Space Act [42 U.S.C. 2457(f)], to the RCA Corporation, Princeton, NJ 08540. LAR-12242

Improved Vapor-Growth Technique for III-V Compound Lasers

Thermal decomposition is minimized in multilayered heterostructures.

Langley Research Center, Hampton, Virginia

Many semiconductor devices based on elements in groups III, IV, and V, such as transmission photocathodes and heterojunction lasers, depend strongly on high quality, defect-free interfaces for good performance. Most of such heterojunction lasers grown via vapor epitaxy have suffered from thermal decomposition at interfacial regions. The vapor growth of multilayered group III-V heterostructures generally involves preheating the previously grown layer to the same temperature used for growth, typically 700° C, before growth commences. This technique leads to thermal decomposition, which produces many dislocation loops, which in turn degrade minority-carrier properties.

When a group III-V compound is heated, the group V element often has a higher partial vapor pressure than the group III element, resulting in a preferential loss of the group V species and in globules of the group III elements being left on the crystal surface. This is particularly true of compounds containing phosphorus because of high vapor pressure near the growth temperature. This behavior has been observed even when a group V gas is present in the preheat zone. However, a method has been developed by which thermal decomposition is minimized.

The new vapor-growth technique as outlined below reduces thermal decomposition and improves performance. In addition, it allows the fabrication of InGaP/GaAsP/InGaP, visible, CW lasers, which could not be made previously because of thermal decomposition.

1. The sample should be preheated to 650°±10° C.
2. The group V elements of the topmost layer should be present as a gaseous atmosphere in the preheat zone and wherever else the sample is subjected to elevated temperatures.
3. The sample should be rotated at approximately 10 r/min during preheat and growth to ensure a uniform temperature all across the wafer, a better thickness, and compositional uniformity.

This work was done by Charles J. Buiocchi, Gregory H. Olsen, and Thomas J. Zamerowski of RCA Corp. for **Langley Research Center.** *For further information, Circle 33 on the TSP Request Card.*

Title to this invention, covered by U.S. Patent No. 4,116,733, has been waived under the provisions of the National Aeronautics and Space Act [42 U.S.C. 2457(f)], to the RCA Corporation, Princeton, NJ 08540. LAR-12255

Germanium-on-InP Heterojunction-Structure LED

Germanium-on-indium phosphide approach is applicable to both LED's and transistors.

Langley Research Center, Hampton, Virginia

A new Ge-on-InP heterojunction-structure LED has been developed wherein a Ge film is evaporated onto an InP substrate. A commercially-available InP substrate may be used. Its surface is prepared by lapping and chemically etching to a polish, and the Ge film is evaporated to a predetermined thickness. After evaporation, both the Ge and InP surfaces are metalized for electrical contacts with electrodeless nickel followed by gold. The InP substrate is p-type, either zinc or cadmium doped, and the Ge film is n-type, as shown in Figure 1. A die is formed by cleaving or dicing and is subsequently mounted on a suitable heat sink.

The forward bias of the device is approximately 1 volt, and it emits light

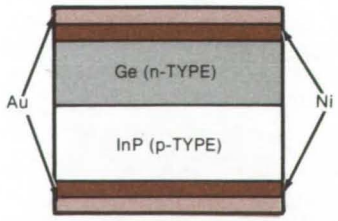


Figure 1. **Heterojunction LED** is made by evaporating a Ge film onto an InP substrate.

in the region of 9,800 Å. This technique permits easy and inexpensive fabrication of an LED for application at this wavelength. The technique can also be tailored to yield a transistor as shown in Figure 2.

This work was done by Frank Z. Hawrylo of RCA Corp. for **Langley Research Center.** *For further information, Circle 34 on the TSP Request Card.*

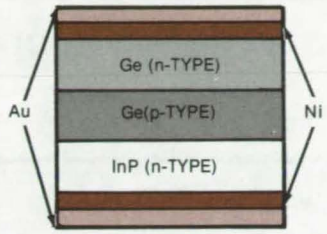


Figure 2. **Ge-on-InP Transistor**

Title to this invention, covered by U.S. Patent No. 4,158,849, has been waived under the provisions of the National Aeronautics and Space Act [42 U.S.C. 2457(f)], to the RCA Corporation, Princeton, NJ 08540. LAR-12349

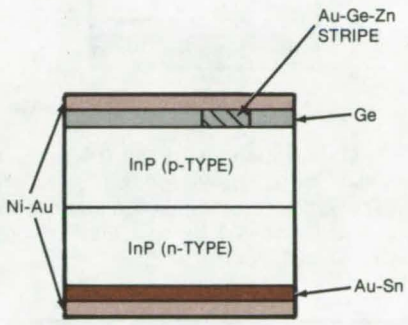
Improved Thermal-Conducting and Current-Confining Film

Germanium film replaces SiO_2 coating.

Langley Research Center, Hampton, Virginia

A common method of fabricating stripe-geometry room-temperature CW laser diodes has been to use an SiO_2 coating on the p-type surface of the device. The process then involves opening a stripe in the SiO_2 film of some predetermined width, generally around 0.5 mils; contact metalizing of the entire surface of both sides of the pn junction wafer; forming device dies; and mounting with the SiO_2 surface down onto the bulk heat sink. The SiO_2 glass which is used for current isolation and planar processing, also acts as a thermal barrier for the device. Thus, the bulk of the heat generated by the device is retained within the structure, and this adversely affects its operation.

Better heat dissipation is achieved by replacing the SiO_2 glass with an evaporated Ge film. The Ge film is polycrystalline and n-type, forming a reverse bias junction in series with the active pn laser junction when biased for lasing. The Ge film is as effective a current-confining medium as is the SiO_2 glass. However, the Ge film is a better thermal conductor than SiO_2, and it forms a thermal path for the heat generated by the device while in operation. The device is fabricated using the following procedure:



InP Laser Device uses a Ge film in place of an SiO_2 coating to improve heat dissipation.

1. The p surface of the wafer is coated with approximately 700 Å of SiO_2.
2. A stripe of predetermined width, generally 0.5 mil, is opened in the SiO_2, exposing the p surface.
3. Au-Ge-Zn (85, 13, and 2 percent) eutectic alloy is evaporated onto the striped surface.
4. Au-Sn (80 and 20 percent) eutectic alloy is evaporated onto the opposite n surface.
5. The entire wafer is sintered at 380° C for approximately 3 minutes in ambient H_2.
6. Both surfaces are plated with Ni and Au.
7. The SiO_2 glass is removed in buffered HF.
8. Ge is evaporated onto the entire p-stripe surface.
9. The entire wafer is again plated with Ni and Au.

The structure of the device is shown in the diagram.

Currently, the Ge film is being used for InP lasers. It should also be useful for (AlGa)As CW lasers. Ge is not only an improved thermal conductor but its coefficient of expansion closely matches that of GaAs, which may lessen certain unwanted strain parameters and increase the lifetime of the device.

This work was done by Frank Z. Hawrylo of RCA Corp. for **Langley Research Center.** *For further information, Circle 35 on the TSP Request Card.*

Title to this invention has been waived under the provisions of the National Aeronautics and Space Act [42 U.S.C. 2457(f)], to the RCA Corporation, Princeton, NJ 08540. LAR-12350

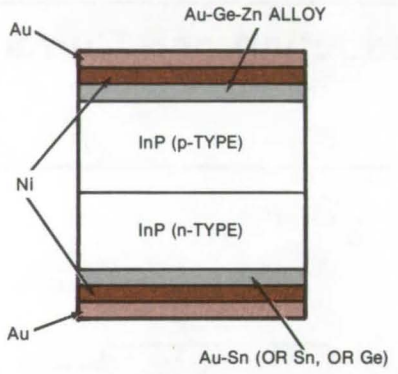
Ohmic Contact to p-Type Indium Phosphide

Low series resistance in achieved with Au-Ge-Zn eutectic alloy.

Langley Research Center, Hampton, Virginia

Room-temperature CW operation of laser devices utilizing InP should have a total series resistance of about 1 Ω. The needed low-series-resistance ohmic contact to p-type InP semiconductor material is difficult to achieve because of the low saturation solubility (approximately 5×10^{18} cm^{-3}) of the accepter dopant, usually Zn or Cd. Many metals otherwise suitable for the metalization of InP do not result in an ohmic contact. Normally a Au-Zn alloy is evaporated or sputtered onto the p surface of the InP, producing an ohmic contact but tending toward a higher resistance.

The new technique utilizes a Au-Ge-Zn eutectic alloy (Au 84.28, Ge 13.72, and Zn 2.00 percent). This alloy sets and adheres well to the semiconductor surface because of its Ge content. In addition, a higher percentage of Zn is retained during deposition, resulting in a higher accepter concentration at the metal semiconductor interface. The Au-Ge-Zn proportions allow evaporation at lower temperatures, more effectively retaining the more volatile constituents. A Au-Sn alloy (Au 80 and Sn 20 percent), or Sn alone, or Ge alone, is evaporated onto the n-type InP surface. After the evaporations onto both surfaces, the entire wafer is sintered at 380° C for about 3 minutes in ambient H_2. Both surfaces are then plated with Ni and Au using electrodeless plating solutions. The structure of the device is shown in the figure.



InP Metalization With Au-Ge-Zn has proved satisfactory for pn junction LED's and lasers. Series resistances in devices fabricated by this method are lower than 1 ohm.

This work was done by Frank Z. Hawrylo of RCA Corp. for **Langley Research Center.** *For further information, Circle 36 on the TSP Request Card.*

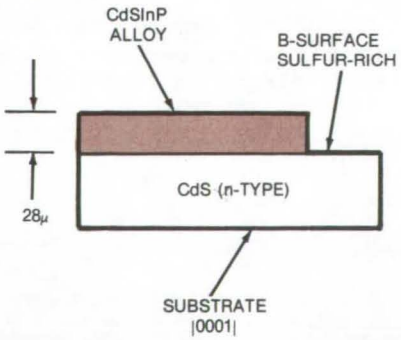
Title to this invention has been waived under the provisions of the National Aeronautics and Space Act [42 U.S.C. 2457(f)], to the RCA Corporation, Princeton, NJ 08540. LAR-12351

CdSInP Semiconductor Alloy

Inclusion of cadmium sulfide could increase laser life and improve operation.

Langley Research Center, Hampton, Virginia

A semiconductor alloy of CdSInP has been deposited onto a CdS substrate using liquid-phase epitaxy (LPE) employing an In solvent. The CdS substrate was n type and oriented |0001| basal plane perpendicular to the C-axis. The alloy was grown on a sulfur-rich Cds surface designated the B-surface as shown in the figure. The solution used contained approximately 2 g In, 1 g Cd, 1 mg Zn, 3 mg InP, and 4 mg CdS. Growth temperature was approximately 610° C. The thickness of the semiconductor layer was approximately 28μ. X-ray diffractometry tests showed that both the substrate and the alloy layer had single-crystaling hexagonal-wurtzite structures, indicating that the layer consists of a single-phase alloy.



CdSInP Alloy Device is prepared by liquid-phase epitaxy onto a CdS substrate. Continuous-wave lasers made with such devices are expected to have lower current densities and longer lives.

The CdSInP alloy system may find application as a replacement for the currently-used InP n- and p-type heterojunction layers contained in InGaAsP laser devices such as those being researched for fiber-optic communications. The difference in band gap between the InP walls and the InGaAsP recombination region is small. The addition of CdS to these walls should increase the electron-volt differential at the electro-optic confining-wall interface. This increased differential, in turn, should aid in lowering the current density of the laser device and enhance its longevity and CW operation at room temperature.

This work was done by Frank Z. Hawrylo of RCA Corp. for **Langley Research Center.** *For further information, Circle 37 on the TSP Request Card.*

Title to this invention has been waived under the provisions of the National Aeronautics and Space Act [42 U.S.C. 2457(f)], to the RCA Corporation, Princeton, NJ 08540. LAR-12405

Sealed High-Pressure X-Ray Detector

A sealed imaging proportional counter is simpler than many previous designs.

Goddard Space Flight Center, Greenbelt, Maryland

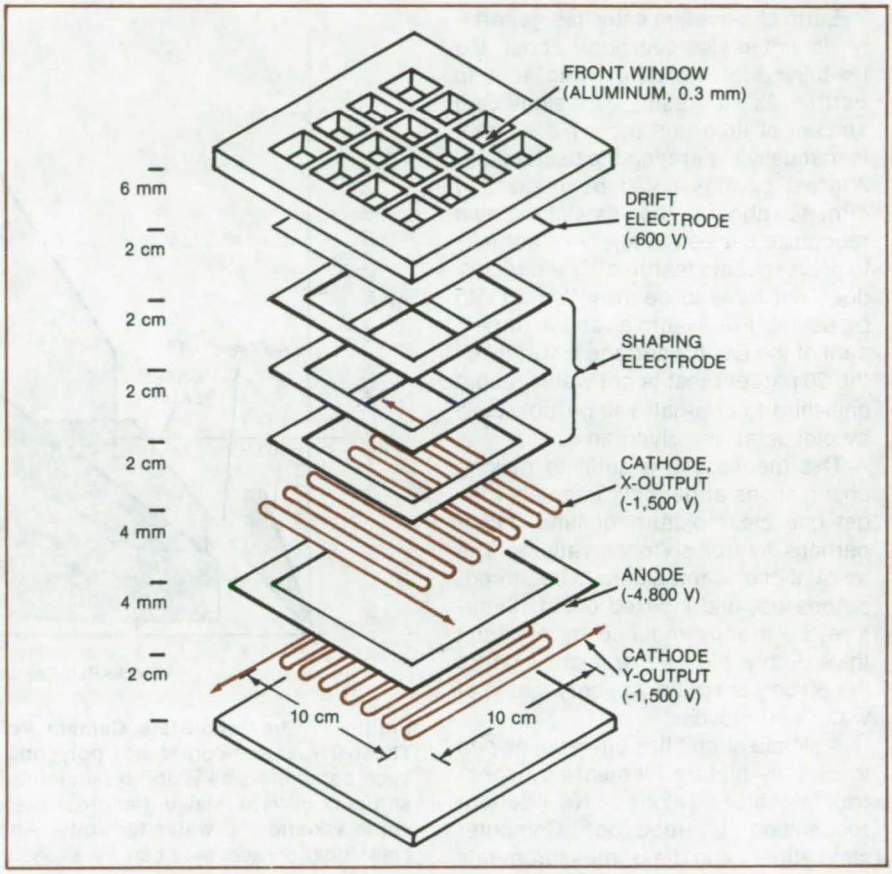
In contrast to conventional designs, which require continuous gas flow to sweep out contaminants, a new imaging hard X-ray detector operates for long periods on a single filling. Originally intended for use in space where the complexity of flowing systems would have been impractical, the new sealed detector also has potential applications in nuclear medicine for imaging the heart and circulatory system (made visible with radioactive tracers). It could also be used for X-ray or gamma-ray astronomy.

The new detector is filled to a pressure of 2 atmospheres with a mixture of 95 percent xenon and 5 percent methane for recording hard X-ray (50- to 100-keV) images with a spatial resolution of about a millimeter. Being sealed, the detector requires no gas purification or replenishment after the initial fill.

The detector electrode configuration is illustrated in the figure. It reads the coordinates by the Borkowski/Kopp differential time measurement of induced cathode signals. Thus, all information on position in two dimensions and energy comes through only four feedthrough connections, two per cathode.

The comparatively-large drift region of the detector (24 atm-cm or more) requires that the gas be free of contaminants that would recombine with the primary electrons before the electrons reach the anode. The major contaminants are oxygen and water vapor, which can diffuse into the sensitive volume through leaks or can outgas from materials that are inside the detector.

The problem of contamination in a sealed housing is solved by extended vacuum baking of selected parts prior to assembly and by the addition of passive, internal "getters." The passive getters work without power, following an initial activation period. Unlike getters that utilize heated filaments, they do not remove methane. (They do remove carbon dioxide, however, so CO_2 is not a possible quench gas.)



This **Sealed Imaging X-Ray Detector** is effective for energies up to about 100 keV. Contaminants are eliminated by passive getters and by extended vacuum baking. Only four electrode feedthroughs are needed, reducing the opportunity for leaks to develop.

To drive off adsorbed atmospheric contamination, all of the counter parts are vacuum baked. The grids are baked for 2 weeks at 150° C, during which considerable gas is evolved. None of the internal parts are exposed to the atmosphere after the vacuum baking. The assembled counter is then pumped out and filled with research-grade xenon and methane.

For hard X-ray or soft gamma-ray astronomy, the detector is used in conjunction with a coded aperture, such as a multiple pinhole or multiple slot array, to form an X-ray camera. The camera has a broad field-of-view and an angular resolution of about a few arc minutes.

An established diagnostic technique for the heart and circulatory system is the imaging of certain radioactive pharmaceutical agents. When the preferred radiopharmaceutical emits gamma rays below 80 keV, the sealed detector should produce a better image than many detectors in current use. Such pharmaceuticals are sometimes preferred for biological reasons.

This work was done by Paul Gorenstein of Smithsonian Astrophysical Observatory for **Goddard Space Flight Center.** *For further information, Circle 38 on the TSP Request Card.*

GSC-12519

Automatically Classifying Earth Features From Orbit

Solid-state imaging devices are used to identify vegetation, bare land, water, and clouds or snow.

Langley Research Center, Hampton, Virginia

Earth observation satellites generally do not make decisions about the usefulness of the data being sent to Earth. As a result, a significant amount of time and money are spent in manually separating the useful data. A great savings could be realized if circuits aboard the satellite could recognize useless imagery or actually look for specific features. The circuitry does not have to be very "smart" to be useful. For example, about 70 percent of the Earth's surface is water. Of the 30 percent that is not water, about one-third to one-half will be obscured by clouds at any given time.

This means that a satellite making observations at periodic intervals may get one clear picture of land out of perhaps five or six observations. The amount of unwanted data to be stored, processed, and indexed could, therefore, be greatly reduced by a circuit that simply blocked transmission of the 80 percent of the imagery that is of water and clouds.

A simple circuit has been developed to classify picture elements by spectral signature alone. No pattern recognition is required. Computer simulations and field measurements have confirmed that the four basic feature types — vegetation, bare land, water, and clouds or snow — can be separated by radiance measurements at two discrete wavelengths: 650 and 850 nanometers.

Green vegetation is dark at 650 nm due to the chlorophyll absorption band; but vegetation is characteristically very bright in the near-infrared around 850 nm. Water is just the opposite; it reflects red light reasonably well but absorbs nearly all near-infrared radiation. Bare land, clouds, and snow are between these extremes. They appear somewhat brighter at 650 nm than at 850 nm, but the radiance ratio is much smaller than for water. Furthermore, clouds and snow are much brighter than most bare-land forms at 650 nm. The relative spectral radiances for the different feature classes are illustrated in Figure 1.

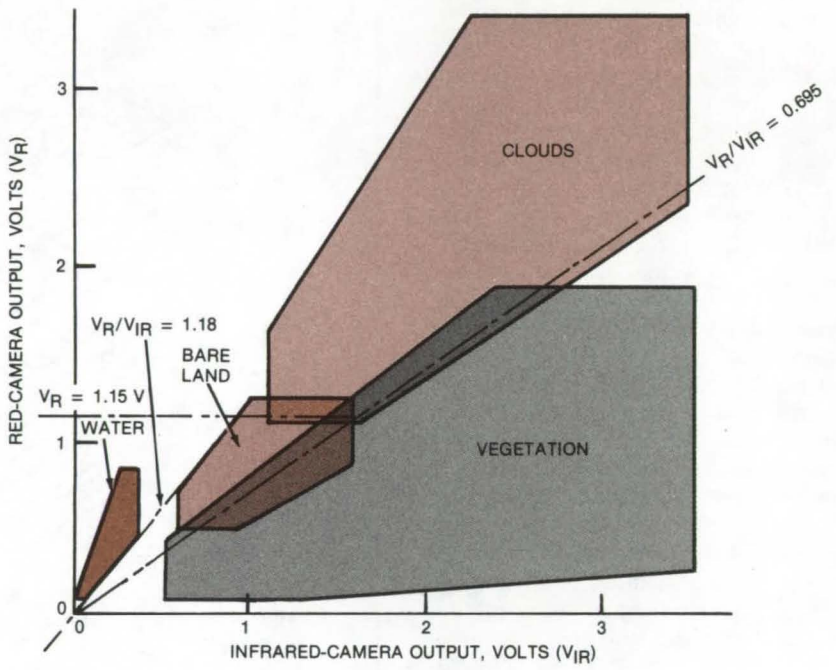


Figure 1. The **Solid-State Camera Voltage Ratios** provide feature classification. These 99-percent-confidence polygons are based on a computer model considering such parameters as visibility, illumination angle, sensor noise, pixel nonuniformity and dark current, viewing angle, variations in vegetation and bare-land types, and some variation in water turbidity. Analyses indicate that better than 95 percent classification accuracy can be expected for pure signatures under typical viewing conditions.

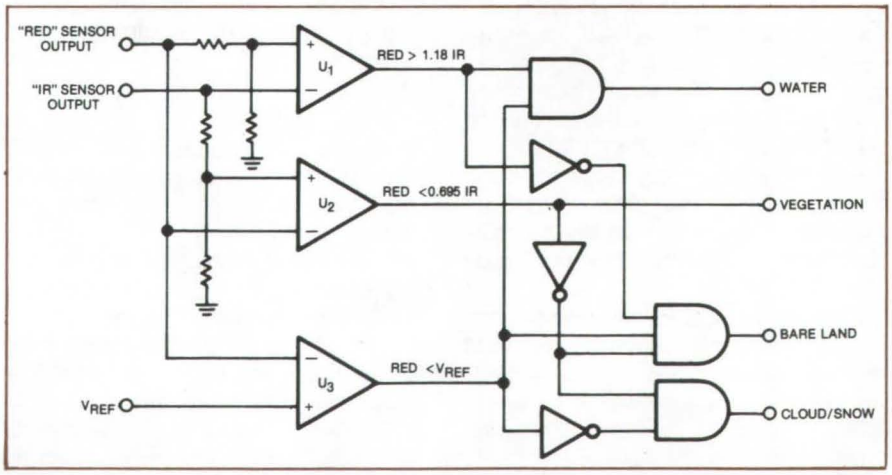


Figure 2. In the **Picture-Element Classification Circuit,** the output voltage of the red and infrared (CCD or CID) sensors is divided and goes to comparators, with one comparator receiving a reference voltage. Comparator outputs are logically combined, producing gating signals to route clock pulses to pixel counters corresponding to the four Earth features.

which shows output voltages for two solid-state cameras, one observing a mixed-feature scene at 850 nm and the other at 650 nm.

Figure 2 is a schematic diagram of a circuit that uses the information in Figure 1 to perform a real-time analysis of the output of two sensors operating at these wavelengths. These cameras could be the primary science sensors of the satellite or could be specially provided for the scene analysis. Comparator U_1 checks for a high ratio of red to infrared radiance, which would indicate water. U_2 checks for a high ratio of infrared to red radiance, which would indicate vegetation. U_3 compares the red sensor output with a reference voltage.

The logic circuitry following the comparators combines the outputs of U_1, U_2, and U_3 to divide the red/IR plane into regions approximating the polygons of Figure 1. One, and only one, of the logic outputs will be high for any sensor-output voltage pair. Typically, these logic signals would gate pixel-rate clock pulses to counters so that, at the end of the scanning period, the counters would contain counts of the total number of pixels that were classified in each of the four categories. A little added logic could then inhibit the transmission of data if the cloud and/or water pixel counts exceeded a selected value.

Two modifications to the circuit in Figure 2 are required for a practical circuit. The comparator outputs should be latched so that the logic outputs will not be changing during a clock pulse; and the threshold voltage should be varied as a function of local Sun angle, since the threshold separating clouds from bare lands is a function of scene illumination. Great precision is not required in the reference voltage. For example, where the orbit "beta" angle is small (0°±15°), two fixed levels are adequate to handle two-thirds of the Sunlit half of the orbit, since clouds have much higher reflectance than most bare-land types.

The classification technique is part of the Feature Identification and Location Experiment (FILE) hardware under development and is scheduled for flight tests on the Shuttle orbiter.

This work was done by Roland L. Hulstrom, Roger T. Schappell, and John C. Tietz of Martin Marietta Corp. for **Langley Research Center.** *Further information may be found in NASA CR-158997 [N79-16339/NSP], "Experimental and Simulation Study Results for Video Landmark Acquisition and Tracking Technology" [$6]. A copy may be purchased [prepayment required] from the National Technical Information Service, Springfield, Virginia 22161.*

Inquiries concerning rights for the commercial use of this invention should be addressed to the Patent Counsel, Langley Research Center [see page A5]. Refer to LAR-12589.

FEP Plug Protects H_2 Masers

A thick plug of fluorinated ethylene-propylene polymer increases the lifetime of hydrogen-maser storage bulbs.

Goddard Space Flight Center, Greenbelt, Maryland

A simple design modification protects the polytetrafluoroethylene coating on the inside of hydrogen-maser storage bulbs. Although quartz maser bulbs are normally coated with a thin FEP layer, the coating tends to wear on the surface opposite the entrance stem because of bombardment by energetic atoms and ultraviolet light generated by hydrogen dissociation.

The problem is solved by putting a hole in the storage bulb at a point opposite the entrance stem and placing a thick FEP plug in the hole. (The plug is inserted after the interior of the bulb has been coated with the usual FEP layer.) Although heavy atoms and ultraviolet light strike the plug and coating with the same intensity, the plug lasts longer than the coating because it is hundreds of times thicker.

The FEP plug replaces a beam-stop plate at either the hydrogen dissociator or the state-selecting magnet. The beam stop was unsatisfactory because it reduced the flow of state-selected hydrogen in the same proporton as it reduced the amount of heavy atoms and ultraviolet light.

This work was done by John J. DeLuca and Victor S. Reinhardt of **Goddard Space Flight Center.** *No further documentation is available.*
GSC-12552

Books and Reports

These reports, studies, and handbooks are available from NASA as Technical Support Packages (TSP's) when a Request Card number is cited; otherwise they are available from the National Technical Information Service.

Programable Solar-Energy Controller

Performance, design, and other data used in evaluating solar-energy controller

A report characterizes a commercially-developed solar-energy-control IPECH (integrated programable electronic controller and hydronic) subsystem, giving all the information used in evaluating its performance. The report is divided into the following sections: performance specification,

(continued on next page)

design and data brochure, installation drawing, assembly drawing, and qualificaton and acceptance test procedures.

The subsystem incorporates a power panel with programable microprocessor, a hydronic solar-collection pumping unit, and a hydronic-heating hot-water pumping unit. It may be programed to control the solar-energy collector based on the user's need according to solar insolation, the date, the time of day, outdoor ambient conditions, and other related inputs. Additional programing is available to control the distribution of solar heat to various zones according to thermostat settings inside the user's facility or to store solar energy in the facility storage tanks. The program may be modified to readjust the sequence of system operation, set points, and priorities without system reversing.

The performance specification section describes the subsystem operating environment: 40° to 100° F (4° to 38° C) temperature; 5 to 95 percent relative humidity; and 60-Hz, 117±10-percent-Vac, single-phase 30-A service. The other specifications characterize the solar-collector circulation system, zone water system, collector-panel manifold-valve module, and zone manifold-valve modules. The subsystem has a design life of 20 years; is 32 in. (0.81 m) deep, 6 ft (1.8 m) high, and 4 ft (1.2 m) wide; and weighs 400 lb (182 kg). There are other specifications for analog inputs, switch inputs, digital outputs, voltages, overvoltage protection, and interface, real-time clock, and programability data.

The design data brochure specifies parts used in the subsystem. It defines piping, fittings, control valves, constant-flow control devices, valves, strainers, pressure gages, pumps, hangers, structural frame, and insulation. Two drawings are given depicting the subsystem installation and assembly.

The final section describes qualification and acceptance test procedures fully outlining a comprehensive test program. This section outlines test details and equipment and parameters used in conducting such tests. Sample data sheets are included and a test setup is given.

This work was done by the Sunkeeper Control Corp. for **Marshall Space Flight Center.** *To obtain a copy of the report, "Design Package for Programmable Controller and Hydronic Subsystem," Circle 39 on the TSP Request Card.*
MFS-25189

Weathering of a Liquid Solar Collector

Ten-month weathering produced only slight degradation in performance.

A report presents the results of long-term weathering on a commercial solar collector. The flat-plate collector uses water as the heat-transfer medium and has a single glass cover plate. It measures 38 in. (97 cm) in width, 240 in. (610 cm) in length, and 3-7/8 in. (9.8 cm) in thickness. The solar aperture area is 53.34 ft^2 (4.9 m^2).

After initial thermal-performance measurements, the collector was exposed to natural weather conditions for about 10 months. Following the exposure, the collector performance was measured again. The before and after measurements were made outdoors according to standard test procedures.

A visual inspection just before the postexposure measurements revealed that rainwater had leaked through the cover seal, leaving watermarks on the absorber plate, although no other defects were apparent. The measurements indicated a slight increase in heat loss and a slight decrease in either the absorptivity of the absorber plate or the transmissivity of the cover glass.

Collector efficiency was calculated and plotted from measurements of the fluid temperature and flow rate, the ambient temperature, and the solar flux. Windspeed and wind direction were also measured during the tests.

This work was done by the Solar Energy Systems Division of Wyle Laboratories for **Marshall Space Flight Center.** *To obtain a copy of the report, "Long-Term" Weathering Effects on the Thermal Performance of the Solargenics [Liquid] Solar Collector at Outdoor Conditions," Circle 40 on the TSP Request Card.*
MFS-25300

Testing of a Solar Collector With Concentrating Mirrors

A commercial unit is tested for the effects of weathering.

A commercial flat-plate solar collector with concentrating mirrors has been tested for thermal performance, structural behavior under static load, and the effects of long-term exposure to natural weathering. The test results are documented in a report that is now available.

The collector uses water as the working fluid. It weights about 137 pounds (62.3 kilograms) and measures 35 by 77 by 6.75 in. (88.9 by 195.6 by 17.l cm). Collector efficiency was measured (using a solar simulator) before and after weathering and plotted against a parameter $U = (T_i - T_a)/I$ (where T_i and T_a are the inlet and ambient temperatures, respectively, and I is the incident flux).

Although the slope of the efficiency curve did not change appreciably, the postweathering intercept with the U axis was lowered, indicating a significant loss of efficiency. Since there was no noticeable change in the transmissivity of the glass cover plates, it is concluded that the absorptivity was degraded by the weathering. In fact, a deterioration of the absorber-plate coating was obvious during the weather exposure.

This work was done by the Solar Energy Systems Division of Wyle Laboratories for **Marshall Space Flight Center.** *To obtain a copy of the report, "Indoor Test and Long-Term Weathering Effects on the Thermal Performance of the Solar Energy System [Liquid] Solar Collector," Circle 41on the TSP Request Card.*
MFS-25310

Installation Package — Home Solar Heater

Collectors supplant roofing or siding in a residential structure.

The installation of a commercial solar-heating system at a site in New Hampshire is described in a 68-page report that is now available. The

system collectors are an integral part of the building; they are fastened directly to the roof or wall framing on 24-inch (61-centimeter) centers, forming a weathertight assembly that replaces conventional roofing or siding. [This system is described in "Solar-Heating System Design Package" (MFS-25226) on page 360 of *NASA Tech Briefs*, Vol. 4, No. 3.]

The solar heater is part of a "residential solar laboratory" — actually a two-story, three-bedroom house — at the New Hampshire Vocational Technical College in Manchester. Besides warm-air panel collectors, the heating system includes ductwork, a buried rock bin for heat storage, a high-efficiency centrifugal fan, motor-driven air valves in a single "universal switching unit," a logical control unit, and an oil-fired auxiliary heater. Depending on the air temperatures in the collector and the storage bin, the system supplies heat to the house from the collectors, from storage, from the auxiliary heater and storage, or from the auxiliary heater alone.

The report contains installation drawings for the New Hampshire site and a manual on installation, operation, and maintenance. Users of the same or comparable systems and users of systems in locations with similar climate should find the documentation quite useful.

Also included in the report are a general description of the system and its operation and guidelines and references on building insulation, orientation of the building, and roof angle. Instructions for determining the collector area required for a given building size and heating load are also included.

This work was done by Contemporary Systems, Inc., for **Marshall Space Flight Center.** *To obtain a copy of the report, "System Installation Package for the New Hampshire Vocational Technical College, Manchester, N.H.," Circle 42 on the TSP Request Card.*
MFS-25338

Computer Programs

These programs may be obtained at very reasonable cost from COSMIC, a facility sponsored by NASA to make new programs available to the public. For information on program price, size, and availability, circle the reference letter on the COSMIC Request Card in this issue.

Monte Carlo Variance Reduction

Determination of radiation environment within a complex system

Because of the harmful effects that nuclear radiation has on both organic systems and inorganic systems, it is important to determine the radiation environment in all systems that are exposed to any significant amount of radiation. The determination of the nuclear radiation environment at specific points within a complex system can be a difficult and costly task. For a large class of radiation transport problems, the only method proved to be effective is the Monte Carlo method. While other methods are usually restricted to two-dimensional problems, the Monte Carlo method can be used to solve complex three-dimensional, time-dependent problems.

However, the Monte Carlo approach suffers from the disadvantage that as a probabilistic method, considerable amounts of computer time are required to obtain statistically meaningful results. This computer program was developed to incorporate a new technique called the iterative forward-adjoint Monte Carlo method. In this technique, the adjoint Monte Carlo method is used to reduce the variance of the forward Monte Carlo method for a given amount of computer time.

The technique utilizes the fact that the adjoint fluence determined in an adjoint Monte Carlo calculation can be used to calculate altered sampling distributions (for source parameters, path length, and past-collision parameters), which can then be used in the forward calculation. Random sampling from these altered distributions, instead of the natural distributions, results in a reduced variance of the effects of interest because the most important part of the distribution is sampled most often. The forward fluence determined in the forward Monte Carlo calculation can likewise be used to alter the distribution function of the adjoint calculation.

By iteratively performing both the forward and the adjoint calculations and updating the altered sampling distributions between each calculation, the variance can be reduced in a relatively small number of iterations. The fluence estimates approach the actual value with each iteration, thus improving the altered distribution functions and improving the effect-of-interest estimates.

This computer program is written in FORTRAN IV for batch execution and has been implemented on the UNIVAC 1108 with a central memory requirement of approximately 64K of 36-bit words. The program was developed in 1975.

This program was written by N. Ricky Byrn of Science Applications, Inc., for **Marshall Space Flight Center.** *For further information, Circle A on the COSMIC Request Card.*
MFS-23645

Wind-Energy Storage

SIMWEST models five storage systems for wind energy.

A comprehensive computer program has been developed for modeling wind-energy storage systems. Designated SIMWEST (Simulation Model for Wind Energy Storage), the program can model systems using any combination of five types of storage: pumped hydro, battery, thermal, flywheel, and pneumatic. SIMWEST can be used as a tool to aid in the design of an optimal wind-energy storage system for a given application and to allow the resulting system to be evaluated and verified through realistic simulation.

Energy storage is often necessary in power systems having an intermittent power source (e.g., those systems which rely on the wind or the Sun). The type and size of storage needed

(continued on next page)

for a particular application must be determined. For wind-energy storage systems, SIMWEST can be used to evaluate the general performance and economic feasibility of specific designs. SIMWEST may also be modified by the addition of the proper subroutine, to other levels of detail, or to analyze other solar-energy storage systems (e.g., thermal, heating and cooling, and photovoltaic).

Other computer programs exist for the simulation of wind systems and various forms of energy storage. However, SIMWEST is capable of simulating total wind systems containing any one or combination of the above types of storage and at the same time has the flexibility and depth required to perform thorough parametric studies.

The SIMWEST program runs on the UNIVAC 1100 series of computers. SIMWEST consists of two basic programs and library of system, environmental, and load components. The first program — the Model Generation Program — is a precompiler that generates computer models (in FORTRAN) of complex wind-energy generator, storage, and application systems, from user specifications using SIMWEST library components. The second program — the Simulation Program — exercises the resulting computer model to perform cost and potential utilization analysis. It handles input, output, and integration of system dynamics and iterates to obtain convergence of variables involved in implicit loops. The combination of these two programs is a powerful tool for analyzing alternate storage-system designs.

The SIMWEST library comprises five types of component: physical, environmental, load, logical, and utility. Physical components model actual physical hardware that might be used in a wind-energy system and encompass such things as motors, generators, transmissions, and flywheels. Environmental components are those that simulate environment conditions (e.g., windspeed and ambient temperature) and are generally used as inputs to physical components. The load components in the SIMWEST library simulate various types of power demand, monitor how well the system meets the simulated demand, and compute the value of the energy delivered by the wind-energy system to the load. The logical components of the library determine how power is divided or distributed within a specified load and storage system and thus provide an idealized way to model the control function, which in practice might be performed by a control-room operator or minicomputer. Finally, the utility components include the tape read, the histogram, and the cost monitor that all serve to help the program user run the simulation and analyze its results.

The program was written in FORTRAN IV, for use on a UNIVAC 1100 computer.

This program was written by L. H. Gordon of **Lewis Research Center** *and Y. K. Chan, R. W. Edsinger, and A. W. Warren of The Boeing Co. Further information may be found in:*

NASA CR-135283 [N78-20802/NSP], "A Simulation Model for Wind Energy Storage Systems" Volume I: Technical Report [$6.50];
NASA CR-135284 [N78-20803/NSP], "A Simulation Model for Wind Energy Storage Systems" Volume II: Operation Manual [$13.25]; and
NASA CR-135285 [N78-20804/NSP], "A Simulation Model for Wind Energy Storage Systems" Volume III: Program Description [$9.50].

Copies of these reports may be purchased [prepayment required] from the National Technical Information Service, Springfield, Virginia 22161. For further information, Circle B on the COSMIC Request Card.
LEW-13097

Landsat Signature Development Program

Classification of Landsat data requires little knowledge of computer techniques.

Interest in the use of Landsat digital image data is becoming more widespread, particularly among small-scale users. Most of the available digital image-analysis software systems require computer expertise and remote-sensing knowledge that is not usually available to the small-scale user. The Landsat Signature Development Program (LSDP) automatically produces an unsupervised classification of a scene from a Landsat data tape. Use of the LSDP requires only a basic understanding of computer and remote-sensing procedures. The program is effective enough to be useful to the sophisticated remote-sensing analyst, yet is simple enough to be utilized in the initial training of students in remote-sensing techniques. The LSDP should be very useful to the investigator who is more familiar with the ground truth of the area to be analyzed than with image processing.

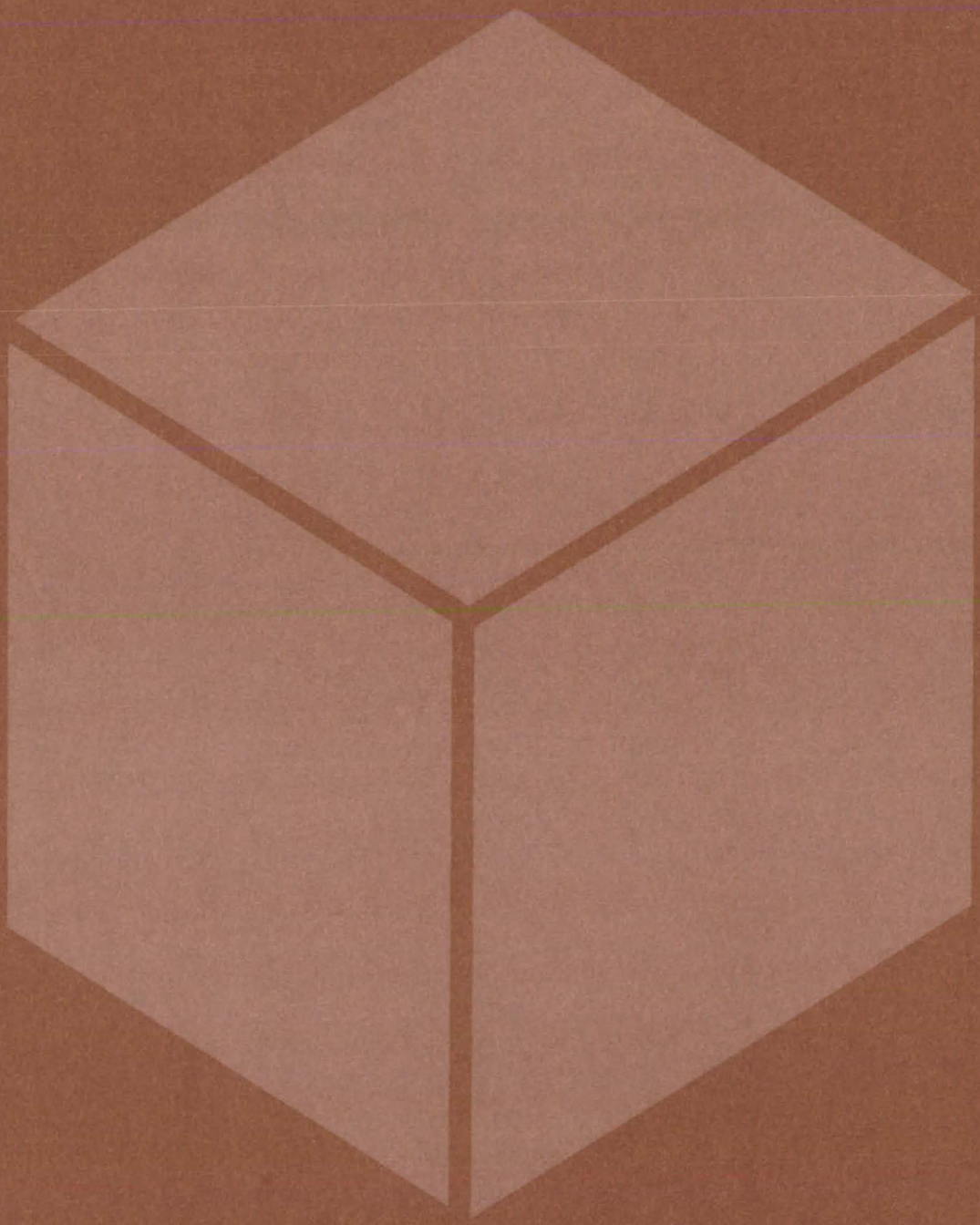
The LSDP classification scheme is based on the clustering tendencies of the multispectral scanner data within Landsat scenes. A rotation matrix, computed from the matrix of eigenvectors, is used to realine the data to improve the overall effectiveness of the band-by-band classification approach. Once transformed, the covariant terms are assumed to be zero. Pixels that occur less than a specified number of times are removed from the data before transformation. Each cluster is formed by examining all pixels within a fixed distance of a seed pixel and then accepting only pixels that do not change the variance by more than a chi-square distribution would permit.

Cluster pairs with a mean separation within a certain hyperellipsoidal region are merged. When all of the clusters have been reduced to a stable group, they are inspected for overlaps in the three standard-deviation ranges. Overlaps are resolved by the maximum-likelihood rule, using the mean frequencies as the a priori factors. The result of the processing is a set of nonoverlapping regions in the data space. Pixels that fall within these regions are assigned unique characters and mapped from that data set. The LSDP generates a line-printer map of the scene with each unique character representing a unique spectral signature. The program also generates tables describing the spectral properties of each signature, certain interclass relationships,dent statistics, and processing infomation.

This program is written in FORTRAN and has been implemented on an HIS-635 computer with a core memory requirement of approximately 27K of 36-bit words using the overlay feature. The LSDP was developed in 1978.

This program was written by Roy A. Bland of **Kennedy Space Center** *and Royce Hall of Computer Sciences Corp. For further information, Circle C on the COSMIC Request Card.*
KSC-11113

Materials



Hardware, Techniques, and Processes

503 Simultaneous Stack-Gas Scrubbing and Wastewater Treatment
504 Low Cost Disposal of MMH
505 A Low-Cost Molecular-Leak Valve
506 Improved Synthesis of Polyformals
506 Separating Liquid and Gaseous Solutions
507 Self-Curing Polyimide Foam
508 Composites of Immiscible Metals
509 Vacuum-Bonded Covering Withstands Low Temperatures
509 Longer Shelf Life for Ceramic Slurries

Books and Reports

510 Shear Strength of Aluminum Fillet Welds
510 Engineering Properties of Incoloy-903 and CTX-1

Computer Programs

511 Unresolved Mossbauer Hyperfine Spectra
511 Single-, Two-, and Three-Phase Binary-Alloy Systems

Simultaneous Stack-Gas Scrubbing and Wastewater Treatment

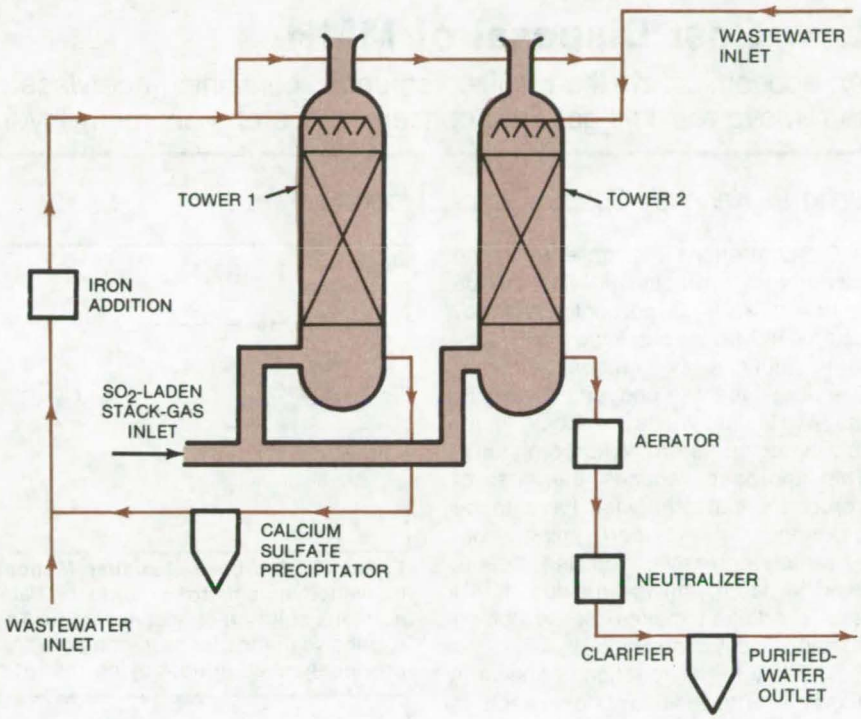
Acidified, iron-enriched effluent from stack-gas purification is used in water physical/chemical treatment.

Lyndon B. Johnson Space Center, Houston, Texas

Two normally-independent purification treatments — sulfur dioxide scrubbing from stack gas and wastewater purification — could be combined in a single two-stage process, making both treatments more efficient and more economical. According to the results of preliminary tests, the acidic solution generated by the scrubbing cycle could be used to reduce the bacterial content of wastewater. Both processes would also benefit by sharing small concentrations of iron as a catalyzing, accelerating, and flocculating agent.

SO_2 scrubbing by aqueous solutions to form sulfurous acid has been previously investigated. Without catalytic enhancement, SO_2 absorption by water is limited to less than 8 pounds (3.6 kg) per 1,000 gal (3,780 l). However, under certain conditions, the sulfite radical can be oxidized to sulfate, which allows more SO_2 to be absorbed. This conversion depends on the rate of oxygen absorption by water. In this process the sulfite conversion to sulfate is enhanced by the addition of 600 to 1,200 parts per million (ppm) of iron in the scrubbing solution and by maintaining the water temperature at about 140° F (60° C).

Sulfate precipitation is prevented while SO_2 absorption is continued by maintaining the scrubbing solution at or near a pH of 2.0. This pH level also reduces wastewater coliform to acceptable levels. After the iron concentration and pH are adjusted from 50 to 100 ppm and from 6.5 to 7.2, respectively, complex iron hydroxides form, which provide coagulation and precipitation of wastewater particulate impurities. Thus, the acidic nature of stack gas and the iron catalysts in the scrubbing process could serve as a wastewater disinfectant and colloid destabilizer. If all steps are carried out under the right conditions and time sequence, stack-gas scrubbing and wastewater purification could proceed simultaneously.



The Simultaneous Treatment of Wastewater and SO_2-Laden Stack Gas proceeds in this two-cycle system. Most of the SO_2 scrubbing and some disinfection occur in tower 1; the tower 2 facility houses most of the disinfection and some scrubbing. Aeration and neutralization of the tower 2 output encourage coagulation and precipitation in the clarifier.

As shown in the figure, the proposed system consists of two scrubbing towers: Tower 1 is a partial catalytic recycle loop; tower 2 is an open-loop "once-through" facility. Wastewater enters the cycle at two points. The SO_2-laden stack gas is fed to both towers from a common manifold. Packing material in both towers promotes excellent water/gas contact for effective scrubbing of the gas.

Wastewater enters the flow loop for tower 1 and passes through the iron-addition stage where the iron content is maintained at from 600 to 1,200 ppm. After passing through tower 1, the pH is readjusted (if necessary) to about 2.0 with lime in the calcium sulfate precipitator. Thus, continuous scrubbing of SO_2 and wastewater disinfection proceed in tower 1.

A portion of the acidified iron-enriched wastewater is withdrawn near the tower 1 inlet and is passed to tower 2. Additional wastewater is added to the slipstream from tower 1 to reduce the iron content from 50 to 100 ppm. After passing through tower 2, the waterflow passes through an aerator and is then neutralized with lime to a pH of from 6.5 to 7.2. The water is flocced and settled in a clarifier and is then discharged.

This work was done by Jerry C. Poradek of **Johnson Space Center** *and Dwight D. Collins of Chemsoil Corp. Further information may be*

(continued on next page)

found in NASA CR-160280 [N80-12620/NSP], "A Study of Simultaneous Stack Gas Scrubbing and Wastewater Purification" [$8]. A copy may be purchased [prepayment required] from the National Technical Information Service, Springfield, Virginia 22161.

This invention is owned by NASA, and a patent application has been filed. Inquiries concerning nonexclusive or exclusive license for its commercial development should be addressed to the Patent Counsel, Johnson Space Center [see page A5]. Refer to MSC-16258.

Low Cost Disposal of MMH

An economical method utilizes scrubber containing acetylacetone solution to remove residual gaseous concentrations of monomethylhydrazine.

John F. Kennedy Space Center, Florida

Concentrations of gaseous toxic monomethylhydrazine (MMH) can be removed at 99.9 percent efficiency using scrubbers containing acetylacetone solutions as scrubbing liquors. The acetylacetone converts the residual MMH in the waste scrubbing liquor to a nontoxic heterocyclic compound. This approach reduces the cost of scrubbers that otherwise have to be protected by an inert lining from extremely-corrosive oxidizing agents used in destroying the residual MMH and in addition makes the scrubbing solution easily disposable.

The key to the reaction is shown in Figure 1. The residual MMH reacts in aqueous solutions with acetylacetone to form 1,3,5-trimethylpyrazole (1,3,5-TMP). Although there are no published toxicity data for 1,3,5-TMP, sufficient data are available about the toxicity of its parent compound pyrazole. Pyrazole is known to be relatively nontoxic at high concentrations. Preliminary results with the waste scrubber liquor containing 1,3,5-TMP concentrations of 500 ppm (parts per million) have shown it to be nontoxic to water hyacinths, algae, and small frogs.

Figure 2 shows the results obtained by scrubbing with 13 percent, pH 7.0 acetylacetone solution. Although the scrubber inlet concentrations of MMH vary between 600 to 1,200 ppm, at no point does its scrubber effluent concentration rise above the detectable 1 ppm. The pH of the waste scrubber liquor rises slowly, but the MMH content does not rise at all for the duration of 100 min. Both acetylacetone and 1,3,5-TPM are noncorrosive and nontoxic and the scrubbing is highly efficient.

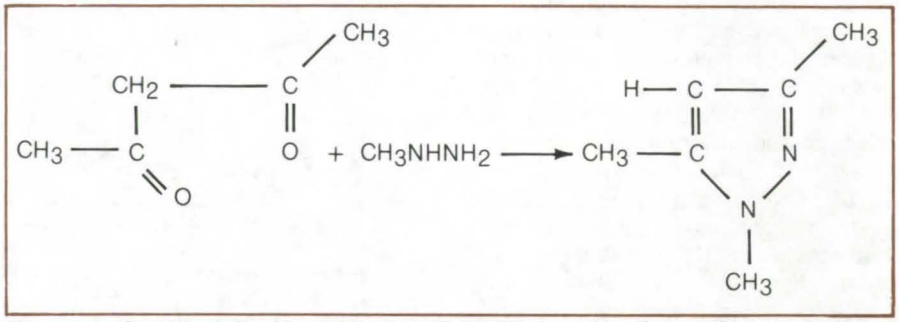


Figure 1. **Scrubbed Residual Monomethylhydrazine** (the Space Shuttle fuel) is converted in situ to a nontoxic heterocyclic compound upon reaction with an aqueous solution of acetylacetone. The resulting product is easily disposable, and expensive linings for protecting the scrubber from strong oxidizing agents that were previously used in destroying the residual MMH are not needed.

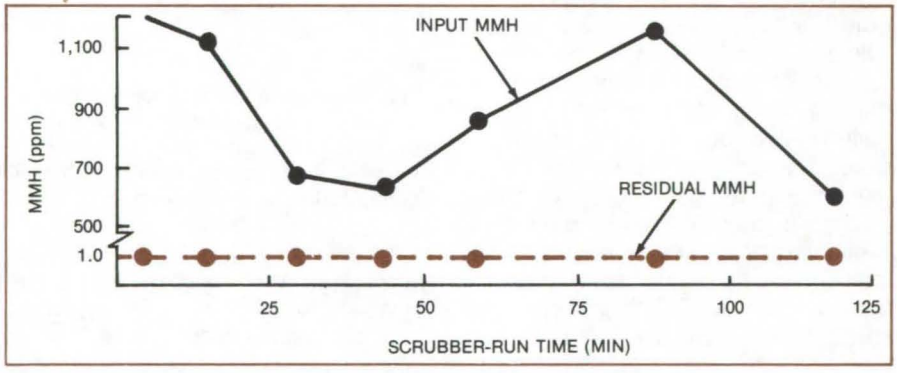


Figure 2. The **Effectiveness of Detoxifying the MMH** with a 13-percent aqueous acetylacetone scrubber solution is shown. This experiment was conducted in a model laboratory scrubber.

This work was done by John J. Thomas and Thomas French of the Florida Institute of Technology for **Kennedy Space Center.** *For further information, Circle 43 on the TSP Request Card.*

Inquiries concerning rights for the commercial use of this invention should be addressed to the Patent Counsel, Kennedy Space Center [see page A5]. Refer to KSC-11135.

A Low-Cost Molecular-Leak Valve

A simple reliable device for mass-spectrometer ion sources

Langley Research Center, Hampton, Virginia

A solenoid-operated molecular-leak and shutoff valve was developed for a small, portable, automated mass spectrometer used to measure trace constituents in air or other gases. The valve costs much less to produce than a precision needle-in-foil type. Yet its performance closely matches that version.

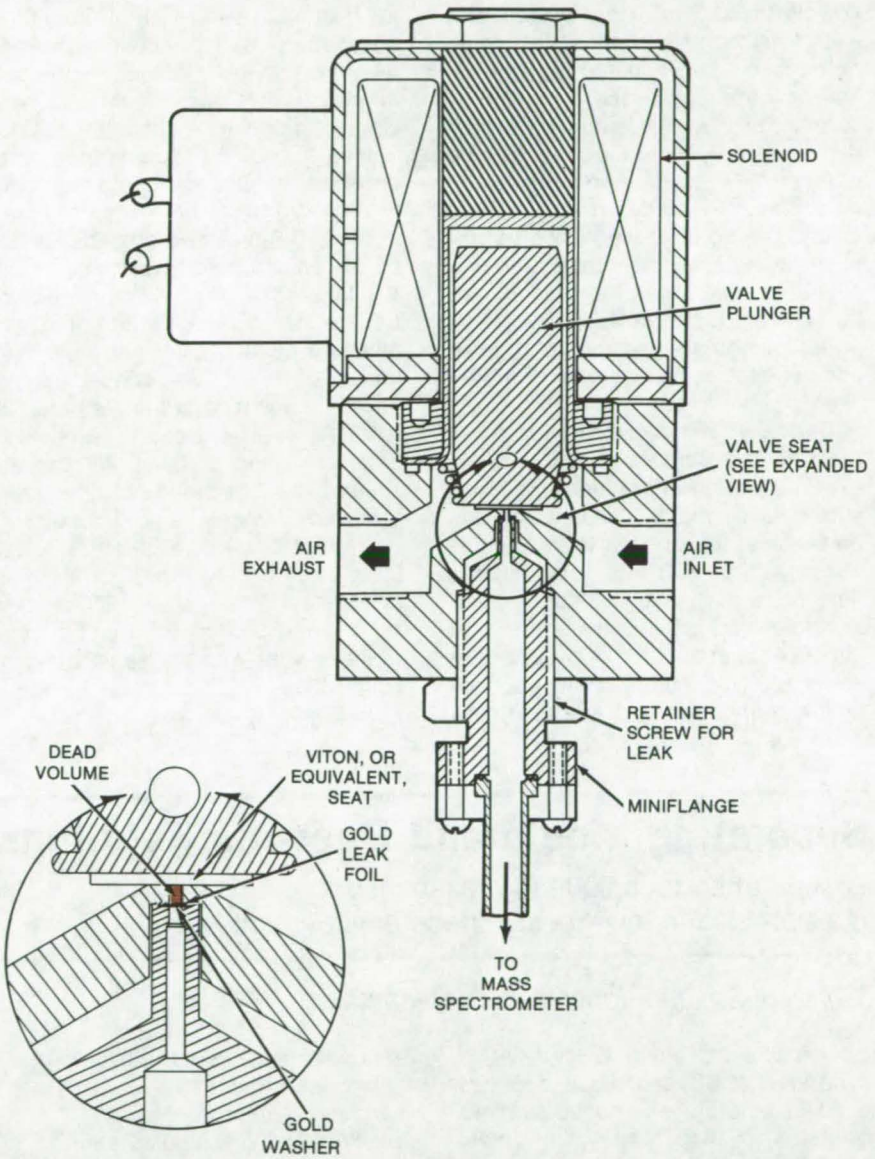
A very small trapped volume eliminates pressure rise in the mass-spectrometer vacuum envelope during the loss of power. Mechanical vacuum pumps used on conventional leak valves to reduce the pressure of molecular leak are not necessary. A gold leak foil admits gases at a slow fixed-rate, permitting the device to be used at up to 1 atmosphere without affecting the vacuum environment.

A solenoid-activated plunger (see figure) admits the gas samples. The samples enter a 0.15-μl dead volume (most commercial valves have a 20-μl dead volume) between the valve seat and the gold leak foil. From there they are slowly passed through the foil into the spectrometer.

The foil is held under compression against the bottom surface of the valve seat by a retainer screw that also serves as an exit tube for the gases. A gold friction washer prevents the foil from distoring as the retaining screw is torqued down to constrain the foil.

The valve was successfully tested. In the closed position, its leakage rate of less than 2×10^{-11} cm^3/s was measured by a helium-leak detector. Such a low leakage level is very important during the loss of power when the valve remains shut.

This work was done by Charles M. Judson, James L. Lawrence, Jr., and Frederick P. Pickett of Analog Technology Corp. for **Langley Research Center.** *For further information, Circle 44 on the TSP Request Card.*
LAR-12249



A **Low-Cost Molecular-Leak Valve** utilizes a gold leak foil to admit sample gases at constant rates. The valve has a very small 0.15-μl dead volume. An insignificant amount of gas trapped in that volume prevents any pressure buildup in the spectrometer vacuum envelope during a power shutdown. Conventional molecular-leak valves with a larger dead volume of about 20 μl require a mechanical pump to prevent that problem.

Improved Synthesis of Polyformals

Synthesis time reduced from hours to minutes

Ames Research Center, Moffett Field, California

Formals of $CH_2OH(CHOH)_nCH_2OH$ polyols (n = 2 to 4) are prepared in less than 15 min as opposed to hours or days by conventional processes. The new approach uses a mixture of sorbitol, or mannitol, and paraformaldehyde rapidly heated in the presence of an acidic catalyst. The process can be carried in stages using almost stoichiometric quantities of paraformaldehyde without any change in the overall heating time. The product can be converted into ethylenically unsaturated monomers and into aphrogenic and pyrostatic phosphorylated derivatives and the like.

Basically, a powdered mixture of the selected compound and a slight excess of paraformaldehyde are stirred and rapidly heated in the presence of the catalyst to a temperature of about 125° C. Total heating time lasts from about 5 to 15 min. During this period, the solids first turn into a paste at about 70° C, liquefy at about 100° C, and are finally converted into a dry powder at a temperature between 115° and 125° C. The acidic catalyst must be present in quantities between 0.1 to 1.0 mole-percent and may include hydrochloric acid, sulfuric acid, methanesulfonic acid, and zinc chloride with hydrochloric acid.

Five successful experiments were carried out. One used a mixture of 18.2 g of sorbitol, 9.5 g of paraformaldehyde, 0.5 g of zinc chloride, and 4 ml of concentrated hydrochloric acid. A total of 20.1 g (95 percent yield) of fine white powder was produced having a melting point between 214° and 216° C. (1,3:2,4:5,6-trimethylenesorbitol is reported to melt at 212° to 216° C.) A similar result was obtained using 5 g of 40 percent sulfuric acid instead of the zinc chloride/hydrochloric acid catalyst.

A third two-stage process using 9.1 g of sorbitol, 3.1 g of paraformaldehyde, and 1.3 g of 25 percent sulfuric acid produced 9.1 g of the fine white powder with the same melting-point range.

In the fourth experiment, the same mixture was used as in the first except sorbitol was substituted with 18.2 g mannitol. A combined total of 20.4 g (94 percent total yield) of white powder was produced that had a melting point between 229° and 230° C. (1,3:2,5:4,6-trimethylene-mannitol is reported to melt at 232° to 233° C.)

A two stage process also using mannitol instead of sorbitol produced 9.1 g of mannitol triformal with a melting-point range of 230° to 231° C.

This work was done by Algirdas C. Poshkus of **Ames Research Center.** *For further information, Circle 45 on the TSP Request Card.*

This invention is owned by NASA, and a patent application has been filed. Inquiries concerning nonexclusive or exclusive license for its commercial development should be addressed to the Patent Counsel, Ames Research Center [see page A5]. *Refer to ARC-11244.*

Separating Liquid and Gaseous Solutions

A separation technique is reexamined for possible use in low-gravity space environment.

Marshall Space Flight Center, Alabama

A well-established Clusius-Dickel separation (CDS) technique currently used in laboratory-scale separations of certain isotopes may find more effective applications in low-gravity space environments. The technique couples thermal diffusion and countercurrent natural convective flow to separate liquids and gases in solutions. The reasons for its decline included large power requirements, costly equipment, and small processing volumes. The materials separable by this technique include:

- aqueous biological solutions,
- isotopes in both gas and liquid states,
- aqueous solutions of both ionized and un-ionized materials,
- organic solutions,
- liquid metallic solutions, and
- ortho- and para-hydrogen mixtures.

Following a critical reexamination of its features, it was concluded that the technique may find few applications by utilizing modified cell designs or by combining it with other separative techniques or such principles as electrophoresis, field-flow fractionation, adsorption, and chemical reactions, particularly in space environments. Some potential applications on the ground include solar water desalination, energy conversion devices, and the utilization of waste heat.

The advantages to be realized in low-gravity space environments are based on the following considerations:

- Reduced convective-flow velocities in low-g environments will allow larger cell-wall spacings, allowing in turn larger throughputs and avoiding "parasitic" remixing.
- Power requirements will be supplied "free" via solar heating and radiation cooling.
- Larger allowable cell-wall spacings will reduce equipment construction costs.

- The lack of gravity-induced mechanical stresses will allow longer cell lengths to be utilized, thereby increasing throughput.
- A possibility of conducting CDS with free-floating liquid spheres.

The present evaluation also investigates the possibility of improving efficiencies of the CDS technique by altering convective-flow patterns. The question of whether multicellular flow or turbulence can introduce a new separation mechanism that would boost separation efficiencies at least an order of magnitude was considered briefly. The results indicate that certain multicellular-flow patterns probably can increase separation efficiencies. However, that has not been verified experimentally, primarily because of the difficulties in defining required boundary conditions for a given multicellular-flow pattern.

The findings also indicate the technique may be promising in the areas of biological and polymer separations. Biological and polymer solutes generally have high thermal-diffusion factors and so can be readily separated with low power consumption. Furthermore, the ability of the technique to separate solute molecules on the basis of shape differences alone should present very exciting possibilities for the separations of such complicated biological materials, as DNA (deoxyribonucleic acid) molecules, viruses, and "B" and "T" lymphocytes. The possibility of combining the technique with other techniques, especially with the field-flow fractionation technique, may produce some positive results.

The thermal diffusion (Soret effect) can generate potential gradients in electrolytic solutions. Nonconvective liquid thermocells, therefore, can convert heat into electricity. It has been reported by others that such a cell utilizing lead electrodes and sulfuric acid can attain an efficiency of 6.16 percent, comparable to 10 percent for the best thermoelectric generators currently used.

This work was done by J. W. Benefield and P. Grodzka of Lockheed Aircraft Corp. for **Marshall Space Flight Center.** *For further information, Circle 46 on the TSP Request Card.*
MFS-23368

Self-Curing Polyimide Foam

Heat of reaction polymerizes mixture and forms cellular structure.

Ames Research Center, Moffett Field, California

A new chemical formulation produces foamed polyimide plastic without external heat. Polyimide foams can thus be formed "onsite" in limited-access locations where the application of heat is difficult or impossible.

The new foam is less dense than conventional polyimide foams and also is far more flame-resistant (see table). In a standard fire test, a sample of the new foam showed no deterioration after exposure to a jet-fuel flame, whereas a sample of conventional foam material became cracked and distorted and quickly burned through. Potential applications include pillows, padding, and foamed-in-place thermal insulation.

Foam Type	Density (g/cm^3)	Burnthrough Time (s)	Comments
Prior-Art Foam	0.048	474	Fissures, Shrinkage Distortion, Burnthrough
Sample 1	0.016	405*	Stable: No Burnthrough
Sample 2	0.008	191*	Stable: No Burnthrough

*Test terminated: no obvious deterioration

The Excellent Flame Resistance of the self-curing foam is all the more remarkable because of its low density.

The formulation consists of an aromatic dianhydride and an aromatic polyisocyanate combined with an inorganic acid and a lower-molecular-weight alcohol (for example, dilute sulfuric or phosphoric acid and furfuryl alcohol). The acid and alcohol react to produce the heat necessary for the other reactants to foam and polymerize. Unlike conventional processes for making polyimide foams, the new process requires no external heating to produce a light, stable, uniform cellular plastic. Moreover, unlike previous formulations for internally heated foams, the new mixture is not readily charred by the acid.

This work was done by Salvatore R. Riccitiello and Paul M. Sawko of **Ames Research Center** *and Charles L. Hamermesh of Rockwell International Corp. For further informaton, Circle 47 on the TSP Request Card.*

This invention is owned by NASA, and a patent application has been filed. Inquiries concerning nonexclusive or exclusive license for its commercial development should be addressed to the Patent Counsel, Ames Research Center [see page A5]. *Refer to ARC-11170.*

Composites of Immiscible Metals

A process prepares composites of previously incompatible metals.

Marshall Space Flight Center, Alabama

Composites of metals that are immiscible in the liquid phase are made with the aid of a new process. Alined, uniformly dispersed spheres or rods (see Figure 1) of bismuth in aluminum, lead in aluminum, bismuth in zinc, and other systems are prepared by using specific dopants and growth procedures.

The new process makes it possible to select the dispersed metal for a property such as superconductivity, lubricity, catalytic activity, or nuclear or electronic activity. The matrix metal is independently selected for its structural strength, resistance to wear or corrosion, or other characteristics.

In the process, a melt composed of the composite components plus a small amount of dopant is solidified under controlled conditions so that the liquid/solid boundary proceeds in only one direction. The dopant breaks the boundary down in a cellular pattern, thereby alining the minor-component particles in the major-component matrix.

For aluminum-based alloys, a transition element such as iron, nickel, or cobalt is an effective dopant. For zinc-based alloys, iron is a good choice. From 0.1 to 0.6 percent dopant by weight is required. The temperature gradient and the speed with which the solid/liquid boundary advances are controlled to produce minor-component particles of the required shape, size, and distance from one another.

The new process is carried out in a chamber containing a furnace at the top and a quench block at the bottom. The metal components of the alloy are held in a vertical alumina-rod crucible that passes through the center of the chamber. The rod remains stationary while the chamber is moved upward at a controlled rate. Water flowing through the quench block removes heat from the molten alloy and solidifies it. Thus, as the chamber moves upward, the liquid/solid boundary moves upward too.

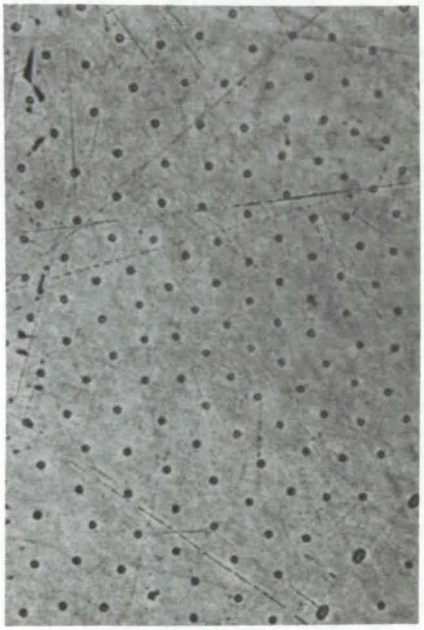


Figure 1. **Lead Rods in an Aluminum Matrix** were formed by directional solidification under dopant-induced breakdown. In this photomicrograph, taken at 100X magnification, the rods appear in cross section. The alloy composition is 4 percent lead and 0.2 percent iron dopant in aluminum.

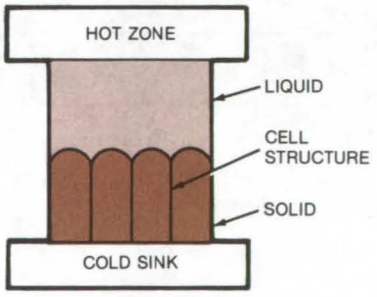


Figure 2. The **Solid Melt Liquid Interface** is believed to break down into a cellular structure under the proper conditions of dopant concentration, growth rate, and temperature difference. The vertical cells encourage solidification of alined spheres or rods of the mirror alloy component.

The shape of the boundary is determined by the concentration of dopant in the melt, by the growth rate R (the rate of movement of the crucible), and by the temperature gradient G (the temperature difference between the furnace and the quench block). When the values of the three variables are adjusted properly, the cellular solidification pattern shown in Figure 2 results, instead of the usual dendritic pattern. A temperature gradient between 150° and 600°/cm and a growth rate between 0.6 and 22 cm/h are appropriate for iron-doped aluminum/bismuth and aluminum/lead melts.

The spacing of the particles varies with the product of G and R. At lower values of G, the minor component of the alloy takes the form of continuous rods; and at higher G values, discrete spheres result. In the alloy Al/3.4 percent Bi/0.2 percent Fe, for example, spheres are formed at growth rates above 1 cm/h. The size of the spheres varies according to $(RG)^{1/4}$.

This work was done by Mary H. Johnston, John C. McClure, and Richard A. Parr of **Marshall Space Flight Center.** *For further information, Circle 48 on the TSP Request Card.*

This invention is owned by NASA, and a patent application has been filed. Inquiries concerning nonexclusive or exclusive license for its commercial development should be addressed to the Patent Counsel, Marshall Space Flight Center [see page A5]. *Refer to MFS-23816.*

Vacuum-Bonded Covering Withstands Low Temperatures

A composite material for wrapping pipes withstands liquid oxygen and liquid air.

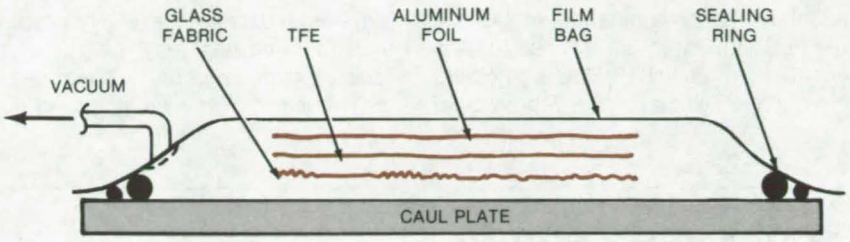
Lyndon B. Johnson Space Center, Houston, Texas

Aluminum foil, tetrafluoroethylene (TFE), and glass fabric can be vacuum-bonded together to make a composite covering material that is flexible and easy to handle. It was developed to cover the insulation on hydraulic lines and ducts in an environment of liquid-oxygen leakage and liquid-air formation around cryogenic components. Ordinary adhesives could not hold aluminum to glass fabric in this environment, but the TFE vacuum bond is unaffected by the cold liquids.

In the bonding process, a TFE film 1 mil (0.025 millimeter) thick is placed between a glass fabric and 1 mil aluminum foil. The materials are laid on a caul plate and covered with a vacuum bag (see figure). The composite is cured at 550° F (288° C) for 3 hours under full vacuum.

The resulting material is easy to handle and can be sewn by machine or by hand. It can be wrapped around odd-shaped objects and can be bent sharply without breaking the fibers. Tetrafluoroethylene (Teflon, or equivalent) was selected as the layer-bonding material because, unlike conventional adhesives, it can withstand cryogenic liquids.

The aluminum/TFE/glass-fabric composite replaces 1 mil stainless-steel foil originally used to cover the pipe insulation. The stainless steel was difficult to wrap and was hard to handle because of its razor-sharp edges.



The **Three Component Layers** of the insulation cover are bonded together by baking under vacuum in a film bag. The composite is strong, flexible, and can be sewn by hand or by machine.

This work was done by Guillermo Lerma and Zenon Siminski of Rockwell International Corp. for **Johnson Space Center.** *No further documentation is available.*
MSC-16235

Longer Shelf Life for Ceramic Slurries

A simple additive stabilizes the viscosity of water-based glass-frit slurries.

Lyndon B. Johnson Space Center, Houston, Texas

Coating Slurry	Viscosity, Ford Cup (Seconds)		
	As Prepared	After Storage	
		1 Week	2 Months
Treated	23.3	22.7	23.1
Untreated	17.0	12.0*	

*Unsatisfactory coating slurry application (occurs after 1 day storage)

The **Viscosity of an Untreated Slurry** quickly deteriorates, and the slurry becomes unusable. A slurry treated with ammonium hydroxide, in contrast, retains its viscosity for at least 2 months.

The viscosity of ceramic-coating slurries containing an organic acrylate viscosity-control agent can be stabilized by the addition of ammonium hydroxide. With the additive, slurries can be stored for over 2 months without significant change in viscosity, whereas without the additive they become unacceptably thin in only 1 day (see table).

The ammonium hydroxide treatment was developed for glass-frit water-base slurries that form high-temperature ceramic coatings for the Space Shuttle. The treatment could benefit other ceramic-coating slurries

(continued on next page)

as well. Since treated slurries can be stored, frequent mixing of fresh batches is unnecessary; and, conceivably, less pure (and therefore less expensive) materials could be used in the slurry mix.

The glass-frit water-base slurry in the Shuttle formulation contains an organic acrylate as a viscosity-control agent. Iron contamination in the frit reacts with ammonia ions in the acrylate (as do ions of other metallic elements). When it is deprived of ammonia, the acrylate becomes insoluble in the water base, and the slurry viscosity decreases. Even an iron content of less than 0.02 percent of frit weight sharply lowers the slurry viscosity.

The addition of ammonium hydroxide to the mix gives the metal-ion contaminants an alternative source of ammonia. During the slurry preparation, 2.5 percent (by weight of the glass frit) of 29 percent concentrated ammonium hydroxide is added. The slurry is otherwise unchanged, consisting of the glass frit in water with 5.5 percent (by weight of glass frit) of acrylate. The ammonium hydroxide additive does not affect the firing of the ceramic coating.

This work was done by Y. D. Izu and T. M. Tanabe of Lockheed Missiles & Space Co., Inc., for **Johnson Space Center.** *No further documentation is available.*
MSC-18543

Books and Reports

These reports, studies, and handbooks are available from NASA as Technical Support Packages (TSP's) when a Request Card number is cited; otherwise they are available from the National Technical Information Service.

Shear Strength of Aluminum Fillet Welds

Results of a study on 2219 alloy.

Shear-strength tests on aluminum fillet welds are documented in a 20-page report. The tests were made on aluminum alloy 2219 to aid designers in specifying the sizes and lengths of the fillet welds necessary to sustain the expected loads in this material.

The shear ultimate strength was found to be linearly related to the number of internal defects in the welds. The test specimens were made from web and plate members. The automatic tungsten-inert-gas (TIG) weld process was used to join the two members in a tee panel with a fillet weld on each side of the web member. Defects were introduced intentionally by contaminating the fusion faces of the base materials or by contaminating the deposited fillet material after the first weld pass. After radiographic inspection, the specimens were subjected to shear testing.

The report discusses fillet-weld size and geometry, including root penetration and surface contour (convexity or concavity). The results of radiographic weld inspection are compared with those of optical-comparator inspection of the shear fracture plane. The wide disparity between the two inspection methods (radiographic inspection always reveals a smaller quantity of defects per area) is explained. Tabular comparisons of the two methods are presented.

Transverse stress as a function of weld quality is discussed. The design-allowable shear stress is determined by statistical ratio analysis. The design shear ultimate stress allowable for as-welded fillet is found to be 20 ksi (138×10^6 N/m^2) and that for aged fillet welds is found to be 22 ksi (152×10^6 N/m^2). These values correspond to 57 percent of the "A" allowable for butt welds. The report presents fillet-weld stress values associated with a probability/confidence level.

This work was done by Charles V. Lovoy of **Marshall Space Flight Center.** *Further information may be found in NASA TM-78168 [N78-21495/NSP], "Shear Strength of Fillet Welds in Aluminum Alloy 2219" [$4.50]. A copy may be purchased [prepayment required] from the National Technical Information Service, Springfield, Virginia 22161.*
MFS-23946

Engineering Properties of Incoloy-903 and CTX-1

A report characterizing the two high-strength superalloys

A comprehensive 125-page report characterizes the engineering properties of Incoloy-903 sheet and of a CTX-1 (a high-strength austenitic Fe-Ni-Co alloy) bar. The Incoloy was tested in the annealed and precipitation heat-treated conditions; the CTX-1, under nonrecrystallized and recrystallized heat treatments.

The Incoloy underwent tension, notched tension, compression, density, thermal conductivity, and thermal expansion tests over the temperature range 20 through 1,033 K. Fracture toughness tests were performed at room temperature. Creep and rupture tests were conducted at 811, 922, and 1,033 K. Transverse unnotched and notched fatigue tests were performed at room temperature and 922 K.

The effects of welding were also evaluated utilizing tension, notched tension, fracture toughness, as well as unnotched and notched fatigue specimens. The elevated-temperature stability of the Incoloy was investigated by exposing unstressed tension, notched tension (welded and nonwelded), and plane stress fracture-toughness (welded and nonwelded)

specimens at 922 K for 10 hours in air. After exposure, specimens were tested at various temperatures.

The CTX-1 alloy underwent tension, Charpy V-notch impact, density, thermal conductivity, and thermal expansion tests conducted over the temperature range 20 through 1,033 K. Poisson's ratio was determined at room temperature and at 811, 922, and 1,033 K. Notched tension and compression tests were performed at 20 K, room temperature, and 922 K. In addition, plane strain fracture-toughness tests were conducted at room temperature and at 77 and 20 K. Creep and rupture tests were performed at 811, 922, and 1,033 K. Longitudinal unnotched and notched fatigue tests at R = 0.1 were conducted at room temperature and 922 K.

The elevated-temperature stability of CTX-1 was investigated by exposing unstressed tension, notched tension, Charpy V-notch, and fracture toughness specimens at 922 K for 10 hours in air. After exposure, the specimens were tested at various temperatures.

The report includes tables and plots of test data and photographs of the microstructures of the samples used. Two appendixes include specimen configurations and data collected from an industrial survey.

This work was done by Paul E. Ruff of Battelle Memorial Institute for **Marshall Space Flight Center.** *To obtain a copy of the report, "Determination of Structural Engineering Properties of Incoloy 903 and CTX-1 Alloys," Circle 49 on the TSP Request Card.*
MFS-23359

Computer Programs

These programs may be obtained at very reasonable cost from COSMIC, a facility sponsored by NASA to make new programs available to the public. For information on program price, size, and availability, circle the reference letter on the COSMIC Request Card in this issue.

Unresolved Mossbauer Hyperfine Spectra

Effects of impurity atoms on spectra

The MOSS-2 computer program analyzes unresolved Mossbauer hyperfine spectra resulting from the existence of several local environments in dilute binary iron alloys. This program has proved useful in studying the effects of impurity atoms on iron Mossbauer spectra. In such an investigation, it is desirable to resolve the composite iron-alloy spectrum into single-configuration spectra so that the effects of impurity atoms in various configurations can be separated. Such an analysis allows a determination of the most important impurity sites that affect critical Mossbauer parameters. The MOSS-2 program can separate individual unresolved composite peaks into constituent Lorentzian peaks and has been extensively applied to the study of FeAl alloys.

The MOSS-2 analysis treats each hyperfine peak as a composite of the Lorentzian peaks with a component for each of the distinct atomic configurations affecting the Mossbauer spectrum. The analysis is greatly simplified if the baseline parabola is eliminated and good initial estimates of the amplitudes, positions, and half-widths are available. These parameters can be obtained from the spectra using various curve-fitting techniques.

For low-impurity concentrations, it can be shown that only near-neighbor impurity populations in a few atomic shells have significant effect on the Mossbauer spectrum of the alloy. Using only those significant impurity-atom configurations, it is assumed that each experimental peak in the hyperfine spectra is composed of a Lorentzian peak for each configuration. The intensity of each Lorentzian peak is determined by the probability for the corresponding configuration. A least-squares differential correction method is applied to estimate the optimal value of the constituent parameters. The program has shown good agreement with reported values for FeAl alloys that contain as much as 2 atomic percent aluminum.

This program is written in FORTRAN IV for batch execution and has been implemented on a CDC CYBER 70-series machine with a central memory requirement of approximately 31K (octal) of 60-bit words. The MOSS-2 computer program was developed in 1978.

This program was written by James R. Schiess and Jag J. Singh of **Langley Research Center.** *For further information, Circle D on the COSMIC Request Card.*
LAR-12439

Single-, Two-, and Three-Phase Binary-Alloy Systems

Numerical analyses for treating diffusion

A series of three computer programs solves one-dimensional transient diffusion problems in single- and multiple-phase binary-alloy systems. An accurate understanding of the diffusion process in binary-alloy systems is important for the development of metal matrix composites, coatings for elevated-temperature oxidation protection, and for thin-film technology. Previous solutions of the diffusion equations have generally been restricted to one geometry, applicable only to infinite or semi-infinite systems, or require that the diffusion coefficient (D) be constant.

The finite-difference solutions developed for this package are applicable for planar, cylindrical, and spherical geometries with any diffusion-zone size and any continuous variation of the diffusion coefficient with concentration. Special techniques were included to account for differences in molal volumes, initiation and growth of an intermediate phase, disappearance of a phase, and the presence of an initial composition profile in the specimen. In each analysis, an effort was made to achieve good accuracy while minimizing computation time.

(continued on next page)

The solutions to the diffusion equations for single-, two-, and three-phase binary-alloy systems are calculated numerically by the three programs NAD1, NAD2, and NAD3. NAD1 treats the diffusion between pure metals or alloys that belong to a single-phase system. Diffusion in this system is described by a one-dimensional Fick's second law and will result in a continuous composition variation. For computational purposes, Fick's second law is expressed as an explicit second-order finite-difference equation. Finite-difference calculations are made by choosing the grid spacing small enough to give convergent solutions of acceptable accuracy.

NAD2 treats diffusion between pure metals or alloys that form a two-phase system. Diffusion in the two-phase system is described by two partial differential equations (a Fick's second law for each phase) and an interface-flux-balance equation that describes the location of the interface. Actual interface motion is obtained by a mass conservation procedure. To account for changes in the thicknesses of the two phases as diffusion progresses, a variable-grid technique developed by Murray and Landis is employed. These equations are expressed in finite-difference form and solved numerically.

Program NAD3 treats diffusion between pure metals or alloys that form a two-phase system with an intermediate third phase. Diffusion in the three-phase system is described by three partial differential expressions of Frick's second law and two interface-flux-balance equations. As with the two-phase case, a variable-grid finite difference is used to solve the diffusion equations numerically. Computation time is minimized without sacrificing solution accuracy by treating the three-phase problem as a two-phase problem when the thickness of the intermediate phase is less than a preset value. Comparisons between these programs and other solutions have shown excellent agreement.

The programs are written in FORTRAN IV for batch execution on the CDC 6600 with a central memory requirement of approximately 51K (octal) 60-bit words.

This program was written by D. R. Tenney of **Langley Research Center** *and J. Unnam of Virginia Polytechnic Institute and State University. For further information, Circle E on the COSMIC Request Card.*
LAR-12381

Life Sciences



Hardware, Techniques, and Processes

515 Indirect Microbial Detection

516 Extracting Trace Substances From Biological Fluids

517 Monitoring Fetal pH by Telemetry

517 Trifunctional Transducer for Myocardial Monitoring

Indirect Microbial Detection

Barrier that prevents cell migration allows a simplified experimental setup for noncontact monitoring of cell growth.

Langley Research Center, Hampton, Virginia

In microbiology, the indirect or remote monitoring of cell growth is desirable when test conditions prohibit direct contact of the probe or sensor with the organisms or preclude physical manipulation of the spatial relationship of the cellular elements. This requirement is especially evident when handling highly infectious organisms or in critical biochemical studies. A new indirect method for the detection of microbial growth utilizes the flow of charged particles across a barrier that physically separates the growing cells from the electrodes and measures the resulting difference in potential between two platinum electrodes.

Conventional indirect methods include a microcalorimetric technique that measures the amount of heat generated during cell growth, a chromatographic method that measures the amounts and types of gases evolved during metabolism, and a radiometric technique that measures tagged CO_2 evolved from the cellular breakdown of tagged C^{14} glucose. All of these require sophisticated instrumentation and highly trained operators. Optical methods are also used to measure absorbed or reflected light, but these techniques fail to differentiate between living and dead cells. Total gas pressure can be measured with pressure transducers, but the requirement for a gastight system is a handicap.

In the setup shown in Figure 1, two arms of a parabiotic chamber are separated by a sterile 0.22-μm membrane filter. This filter prevents microbial movement from the left arm to the right arm, but permits the movement of charged particles from the inoculated side to the uninoculated right arm. Sterile nutrient broth was added to both arms and the left arm inoculated with bacteria: *Escherichia coli* and *Staphylococcus aureus* were used in the tests. Two sterile platinum electrodes, with surface area ratios of 4:1, were placed in the uninoculated right arm and connected to a strip-chart recorder. The parabiotic chamber was placed in a 35° C incubator and the strip-chart recorder activated.

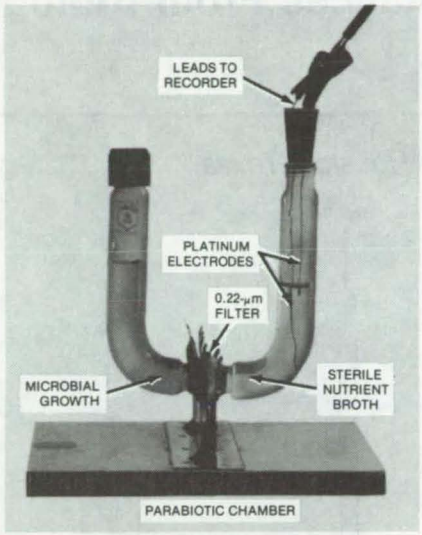


Figure 1. **Parabiotic Chamber** separates microbe-containing solution from electrolyte with a filter that passes charged particles but not bacteria. The length of time between inoculation of the left arm and a voltage rise between electrodes is proportional to the number of cells added.

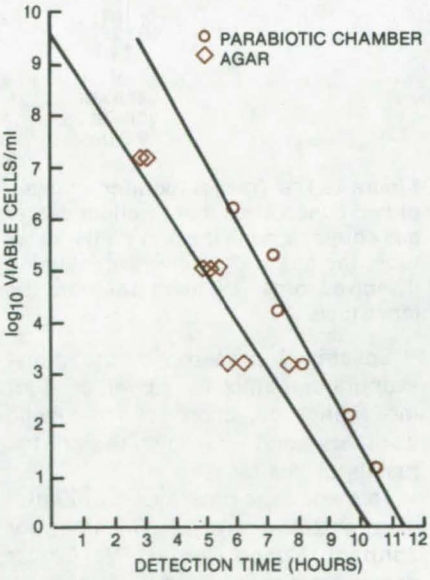


Figure 2. **Dose Response Relationship** for E. coli shows that cell concentration is a linear function of detection (voltage-rise) time.

A typical strip-chart recording consists of a flat baseline followed by an increase in voltage. The length of time between inoculation of the left arm and the increase in voltage in the uninoculated right arm is a function of the number of cells added at zero time. The dose response relationship for *E. coli* is linear and is shown in Figure 2. Although similar responses were noted for the *Staphylococcus aureus*, which represents the other major group of bacteria, the gram-positive organisms, they were weaker and not as consistent as with *E. coli*.

In a second experimental setup, the bottom portion of a petri dish was drilled on opposite sides to accept two platinum-wire electrodes that extended across the diameter of the dish. Sterile 1.0 percent agar (without nutrients) was added to the dish and acted as the cell migration barrier. Bacteria were added to nutrient broth containing melted and cooled 0.5 percent agar. Multiplication of the bacteria was restricted as the 1.0 percent agar does not support growth of the organism. The flow of charged particles, however, is not restricted by the 1.0 percent agar. The petri dish was placed in a 35° C incubator and the leads from the strip-chart recorder connected to the electrodes. The response curves obtained were essentially similar to those observed in the parabiotic studies.

One of the main advantages of this technique over previous ones is its simplicity. The only operational requirement is the existence of a barrier that prevents cell migration but permits the flow of charged particles. Any number of semipermeable membranes are available that could function as suitable barriers, or sterile agar may be used. Another advantage of this method is the ability to detect

(continued on next page)

microbial growth on agar, the most widely used substrate in microbiology for the detection and isolation of micro-organisms. This technique has potential application in diagnostic laboratories and in the remote monitoring of pollution in water.

This work was done by Judd R. Wilkins of **Langley Research Center.** *No further documentation is available.*

Inquiries concerning rights for the commercial use of this invention should be addressed to the Patent Counsel, Langley Research Center [see page A5]. Refer to LAR-12520.

Extracting Trace Substances From Biological Fluids

A "transevaporator" aids in the extraction of volatile organics.

Lyndon B. Johnson Space Center, Houston, Texas

Trace amounts of volatile organics can be extracted from biological fluids with the aid of a new apparatus. Called a "transevaporator," the apparatus makes it possible to prepare the volatile fraction for analysis by high-resolution gas chromatography.

The transevaporator consists of two concentric glass tubes (see Figure 1). The outer tube has an arm attached to it through which a gas can be introduced. To extract the volatile fraction about 10 to 500 microliters of the biological fluid (such as urine, serum, milk, saliva, or amniotic fluid) is injected by syringe into a silica filter column in a conical-tip centrifuge tube (Figure 2). An elution solvent such as pentane is added to the centrifuge tube.

Next, a supply of helium gas is connected to the arm of the transevaporator and is passed through the filter column, carrying the solvent and dissolved volatile organic substance with it. The silica column retains most of the water and high-molecular-weight material.

The helium carrier gas flows through the center tube of the transevaporator into a tube containing an adsorbent, such as glass beads, which collects the organic fraction.

Heating the tube containing the adsorbent drives off the volatile fraction, which is condensed in a small column cooled by liquid nitrogen. The cryogenic column concentrates the volatile fraction into a narrow band that can be injected directly into the capillary column of a gas chromatograph or gas chromatographic/mass spectrometer for component identification.

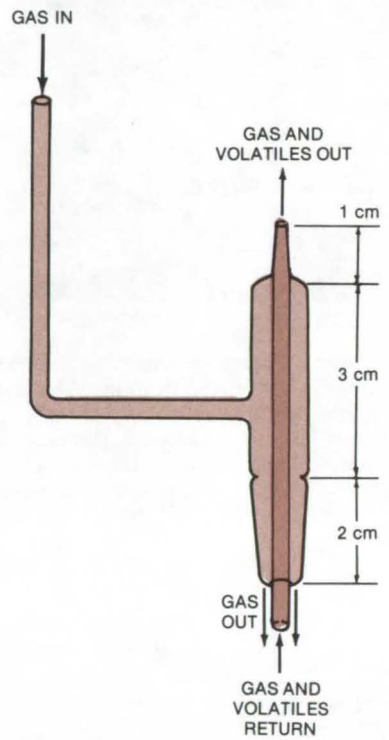


Figure 1. The **Transevaporator** consists of two concentric tubes. Helium carrier gas enters through the arm on the outer tube; the gas and a solvent containing dissolved organics leave through the inner tube.

Specimens prepared by the transevaporator method have been used for the early detection of metabolic disorders and for monitoring the results of treatment.

This work was done by Albert Zlatkis of the University of Houston for **Johnson Space Center.** *No further documentation is available.*
MSC-18522

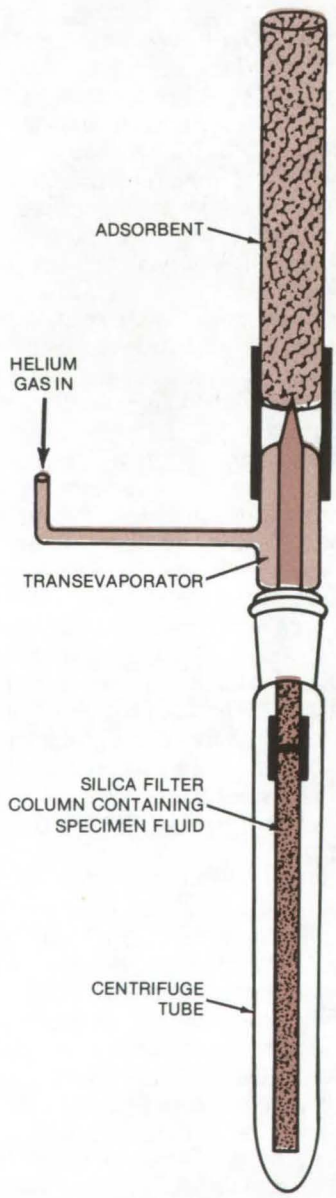


Figure 2. The **Transevaporator is Attached** to a filter column containing a biological fluid; it supports an upper tube containing an adsorbent, which collects the volatile organic substances in the fluid.

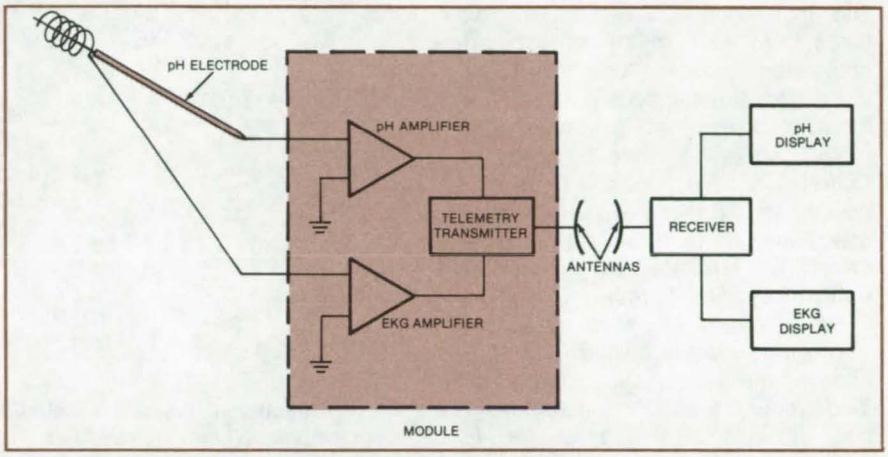
Monitoring Fetal pH by Telemetry

Data on pH and EKG are continuously radioed to instrument console as a delivery-room aid.

Goddard Space Flight Center, Greenbelt, Maryland

A telemetry unit has been developed for possible use in measuring the scalp-tissue pH and heart rate of an unborn infant. It radios the data to a receiver as much as 50 feet (15 meters) away. It is being considered for use during the hours just before childbirth, to give a warning of problems that might require cesarean delivery. The telemetry unit eliminates problems encountered in the direct wire connection from the fetus and mother to an instrument console, now used for taking a fetal electrocardiogram (EKG). Moreover, because the radio unit monitors continuously, it eliminates intermittent pH measurements made by periodically scratching the fetal scalp to obtain a small blood sample and carrying the sample to a pH-analyzing machine.

The new instrument was devised at the request of obstetricians, but to date has been tested only on laboratory animals. The pH probe, which would be inserted into the vagina and hooked into the scalp of the fetus, connects by wire to a small electronic module strapped to the mother's thigh. The module contains pH sensors, EKG amplifiers, and a telemetry transmitter (see figure) in a 3- by 3- by 1-inch (7.5- by 7.5- by 2.5-centimeter) package. The transmitted pH signal accurately reflects tissue pH fluctuations, varying at approximately 0.6 volt per pH unit. The receiver displays both the voltage and the pH value.



A **Small Electronic Module** worn on the mother's thigh transmits data on fetal-tissue acidity/alkalinity and heart rate to indicating instruments.

The telemetry unit can be made still smaller by combining the transmitter components in a single integrated circuit and by mounting the pH sensors and EKG amplifiers — also in integrated-circuit form — directly on the probe.

This work was done by Albert Blum, Theresa Donahoe, Murzban D. Jhabvala, and William Ryan of **Goddard Space Flight Center.** *No further documentation is available.*
GSC-12507

Trifunctional Transducer for Myocardial Monitoring

Transducer simultaneously measures force, displacement, and thickness of the heart muscle.

NASA's Jet Propulsion Laboratory, Pasadena, California

In heart research, the assessment of myocardial mechanics relies on electromechanical transducers to record dynamic activity. Typical transducers separately measure the internal force, the displacement, and the thickness of the heart muscle fiber. However, because of size limitations, most transducers do not simultaneously measure these parameters in the same area of muscle tissue.

A prototype myocardial transducer (see figure) simultaneously monitors these three quantities in a localized area of the heart muscle. In laboratory tests, oscillograms generated by the new transducer implanted in the heart of a dog, recorded the variations in the force, displacement, and thickness of the muscle fiber.

Referring to the figure, the transducer is retained in the heart by the indentations in tines A and B. These have low compliance compared to the muscle fiber so that the force in the fiber applies stress to the point where the arms are joined. A piezoelectric sensor measures the stress at that point.

A high-compliance elliptical circlet is attached to tine A. The lower part of the circlet is free to slide along the tine, and the bottom surface presses against the muscle fiber. Any change in thickness of the muscle shortens the minor axis of the circlet. This change is measured by a piezoelectric element on the circlet.

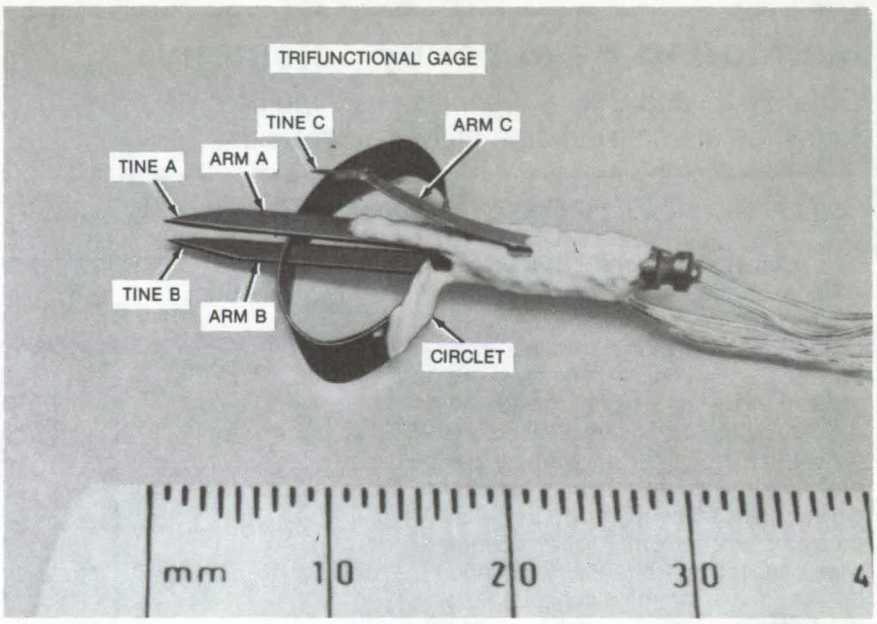
(continued on next page)

Rigidly attached to tine B is a high-compliance arm (arm C) that also terminates in a tine. Any linear displacement of the muscle fiber between tines B and C is measured by the piezoelectric sensor attached to the high-compliance arm.

The trifunctional transducer can be placed in a muscle fiber in an area less than about 1.5 by 4 mm. Two leads from each of the sensors are connected to conventional instrumentation for simultaneously measuring force, thickness, and displacement.

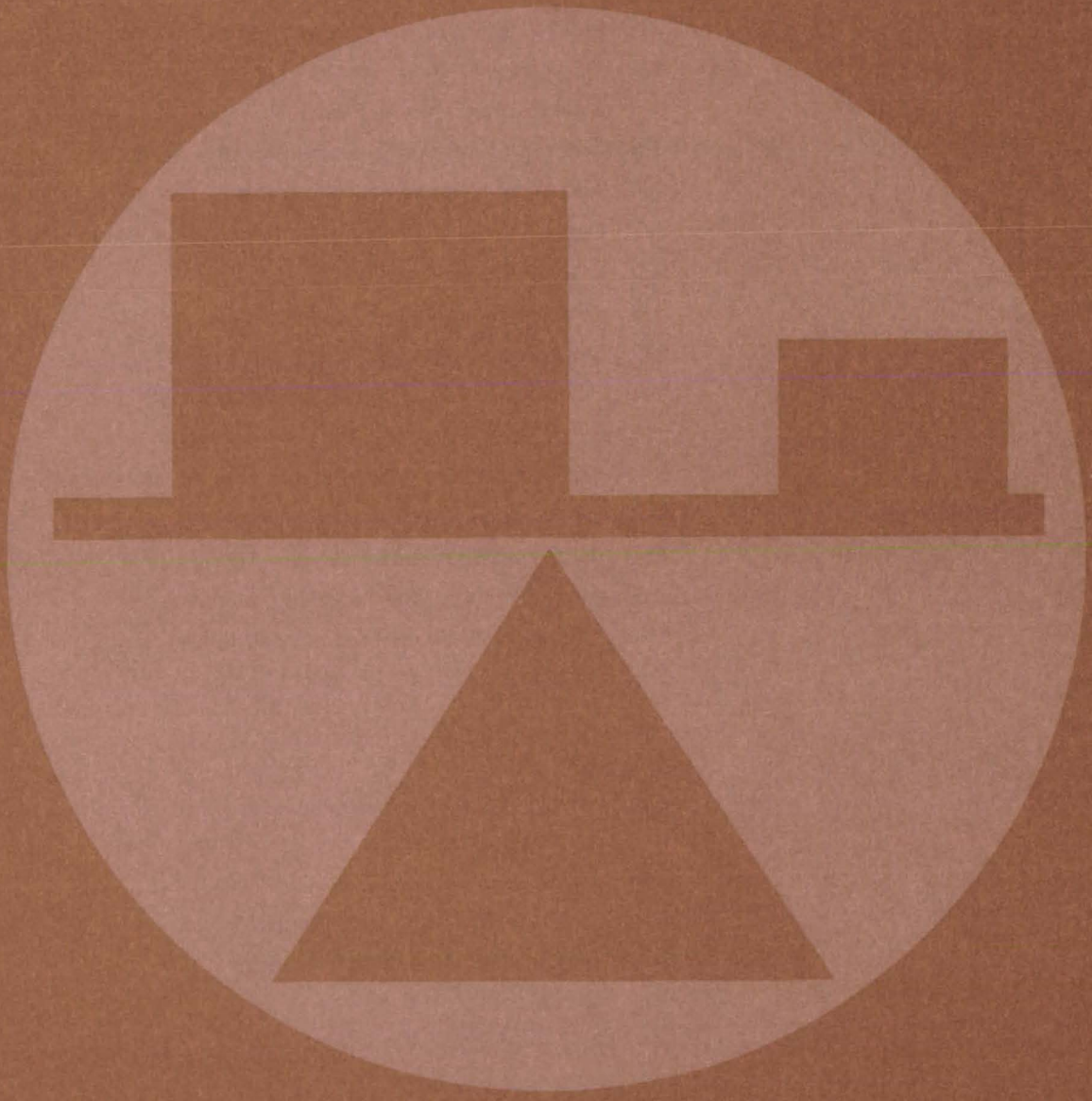
This work was done by Virgil H. Culler, Cyril Feldstein, and Gilbert W. Lewis of Caltech and Samuel Meerbaum of Cedars Sinai Medical Center for **NASA's Jet Propulsion Laboratory.** *For further information, Circle 51 on the TSP Request Card.*

This invention is owned by NASA, and a patent application has been filed. Inquiries concerning nonexclusive or exclusive license for its commercial development should be addressed to the Patent Counsel, NASA Resident Legal Office-JPL [see page A5]. Refer to NPO-14329.



This **Trifunctional Transducer** simultaneously measures force, thickness, and displacement in heart muscle fiber. Arms A and B are made of stainless-steel rod for low resiliency; arm C is flexible stainless-steel shim stock.

Mechanics



Hardware, Techniques, and Processes

521 Triple-Exposure Holography for Materials Tests
522 Resonant-Fatigue Cracking Apparatus
523 Measuring Acoustic Properties of Materials and Jet Nozzles
524 Tire-Pressure Measuring Concept
525 Synthetic Seawater as Stress-Corrosion Test Medium
526 Detecting Insulation Defects in Metal/Plastic Films
526 Acoustical Measurement Separates Core Noise and Jet Noise
527 Onsite Testing of Pressure-Sampling Valves
528 Graphite/Epoxy-Tape Test Specimens
529 "Three-Dimensional" Vibration Fixture
529 Rapid Testing of Pulse Transformers
530 Detector Verifier for Circuit Analyzers
531 Rugged Fast-Response Temperature Probe
532 High-Temperature High-Pressure Magnetic Pickup
533 Controlling Subsynchronous Whirl in Turbopumps
534 Mechanical-Load Indicator
535 Adjustable Holder for Transducer Mounting
536 An Evaluation of Low-Cost Payload Carrier
536 Determining Radii of Cylindrical Segments

Computer Programs

537 Overall Loudness of Steady Sounds
537 Nonlinear Structural Analysis
538 Redundant Structures at Elevated Temperatures
538 Aerodynamic Performance of Jet-Flap Wings
539 Transonic Flow Past Swept Wings
540 Transonic Airfoil Analysis and Design
540 Helicopter Sling Loads
541 Wing and Leading-Edge Thrust
541 Spacecraft Trajectory

Triple-Exposure Holography for Materials Tests

New approach improves the analysis of holographic fringe patterns.

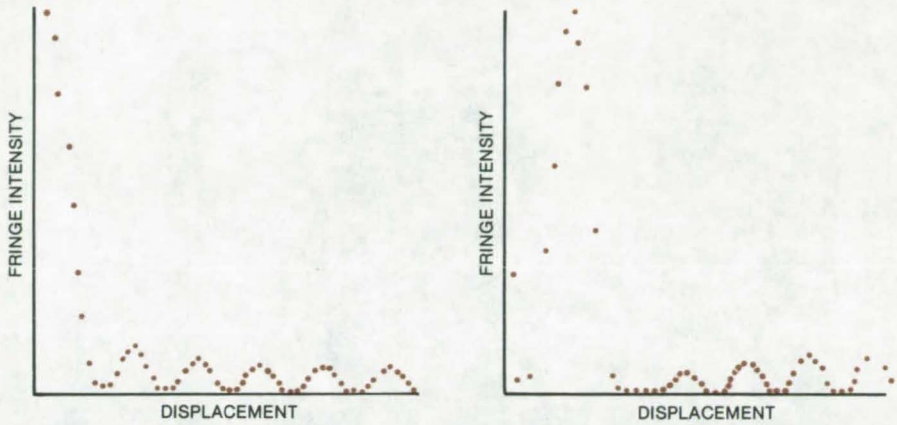
Marshall Space Flight Center, Alabama

The superposition of holographic interference patterns obtained before and after a material is stressed is a well-known technique for locating flaws and verifying the behavior of the material under load. Since flawed regions are displaced relative to the rest of the material, the flaws are evident as changes in the fringe pattern for the local regions around the defective areas.

Two analytical problems can arise when quantifying the fringe motion: First, it is not always easy to determine which are unshifted ("no-motion") fringes after the load is applied; and second, it is sometimes difficult to determine the direction of fringe motion. For example, it may be hard to ascertain whether a shifted fringe has moved a short distance to the left or a longer distance from the right.

In a new approach to holographic nondestructive testing, three interference patterns are taken of the material and superimposed: Two of the patterns are the usual "before" and "after" images of conventional testing, and the third pattern is taken by exposing the holographic plate while the load is building up to its final value. In addition, a variable phase shifter is placed in either of the arms of the laser interferometer, and selected phase shifts are introduced during the exposures of the intermediate and final images. The exposure time for the intermediate image is also controlled.

A theoretical analysis shows that significant information can be extracted from the triple-exposure holographic image. For example, if a 180° phase shift is introduced in one arm of the interferometer when the last pattern is taken, then the no-motion fringes in the composite will be preferentially enhanced (see figure, left). If a 90° phase shift is introduced, then rather than being uniformly bright, the intensity of the fringes gradually changes in one direction or another, depending on whether they are displaced to the left or to the right (see figure, right). The first condition thus allows no-motion fringes to be easily identified, and the second condition allows the direction of fringe shift to be identified. (The direction of shift is easily related to the direction of movement of the material and thus to the nature of the flaw.)



These **Computer-Simulated Fringe Patterns** show the results of triple-exposure holography with variable phase shift. In the pattern at the left, a 180° phase shift is inroduced when exposing the final image, and a long intermediate exposure time is used. The enhancement of the zero-order or "no-motion" fringe is apparent. The figure at the right shows the effect of introducing a 90° phase shift. A relatively-short intermediate exposure time is used here. Note that the fringe amplitudes after zero-order increase in amplitude, indicating a "positive" displacement relative to a fixed axis. For a "negative" displacement, the fringe amplitudes decrease.

The new approach appears to be superior for locating flaws than simply subtracting the after-load image from that taken before the load is applied. Although the difference image should in principle isolate the flawed areas, it is usually complicated by slight misalinements between the before and after patterns. Often, an image that is just as complicated as the original images results.

This work was done by Hua-Kuang Liu of Lumin, Inc., for **Marshall Space Flight Center.** *For further information, Circle 52 on the TSP Request Card.*

MFS-25180

Resonant-Fatigue Cracking Apparatus

Controlled surface cracks are produced for structural studies.

Lewis Research Center, Cleveland, Ohio

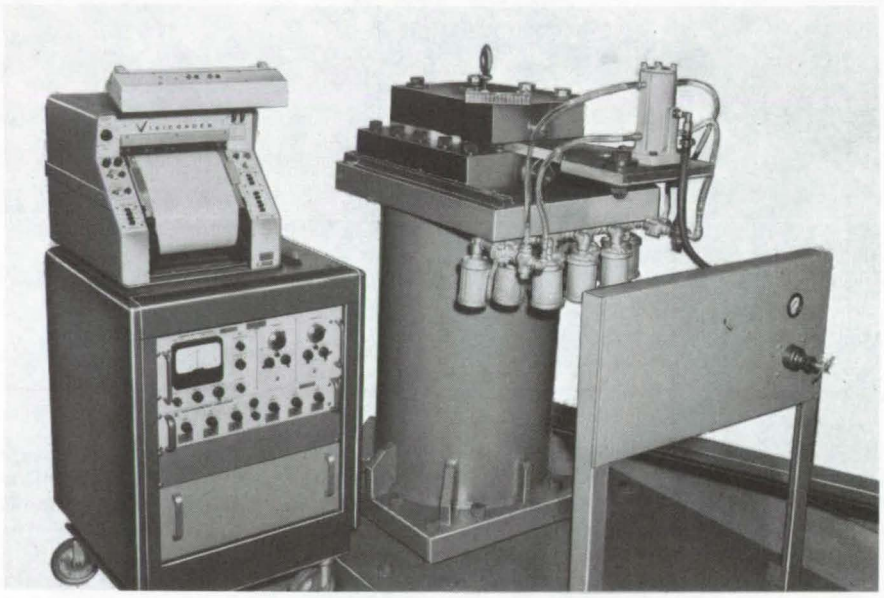


Figure 1. **Resonant-Fatigue Cracking** apparatus produces controlled surface cracks in test specimens.

Perhaps the most-commonly-observed structural defect is the surface crack. Fracture-control plans superimposed on modern structural design generally begin (and often conclude) with an assessment of performance in the presence of this type of flaw. Frequently these assessments are made empirically, based on tests using surface-cracked specimens that simulate structural service. A low-cost resonant-fatiguing apparatus has been developed that is useful in the production of surface cracks of controlled size and shape in fracture specimens. This apparatus has been used to develop fatigue cracks primarily in large (36 in. long) surface-crack tension test specimens.

The resonant-fatiguing apparatus consists of a specially-designed stand-mounted clamping fixture, a commercially-available pneumatic actuator, and suitable sound-control mufflers (Figure 1).

One end of a specimen is securely fixed to the stand-mounted clamping fixture while the other (free) end of the specimen has the pneumatic actuator attached to it. The pneumatic actuator induces movement in the free end of the specimen.

The pneumatic actuator consists of an air-driven piston moving up and down in a cylinder. The kinetic energy of the piston is transmitted to the specimen and causes the specimen to oscillate at a resonant frequency determined by the specimen material and design characteristics of the test specimen/actuator combination. The deflection or amplitude of the oscillations can be controlled by the air pressure supplied to the actuator.

Final tuning of the system is accomplished by positioning of the actuator, the addition of weights, and exhaust air throttling. As the fatigue crack grows, small changes in air pressure are required to maintain constant specimen deflection. Specimen deflection is easily monitored by use of a simple handmade paper deflection wedge, or gage, that is taped to the oscillating end of the test specimen.

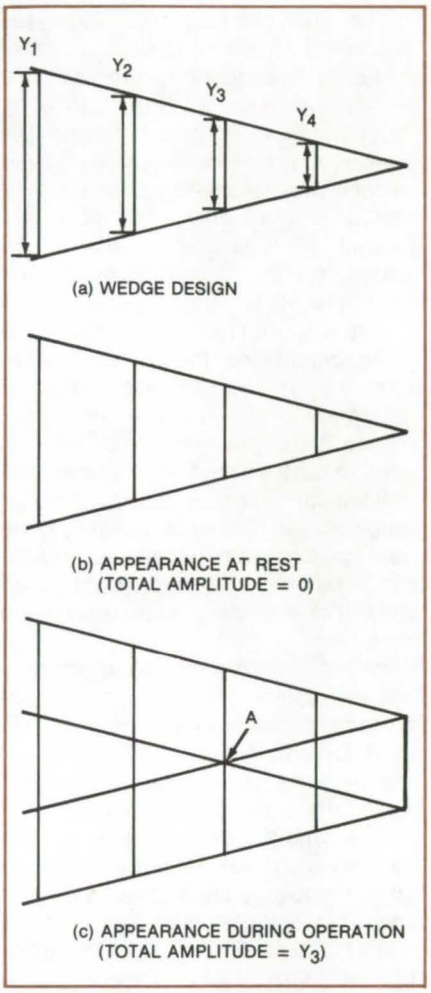


Figure 2. Paper **Deflection Wedge** is used to monitor the deflection of a test specimen. The wedge is made of a convenient length and marked with segments Y_1, Y_2, . . . (**a** above). When attached to an oscillating specimen, the wedge appears to have a pair of lines intersecting at the graduation representing the amplitude of oscillation.

Figure 2 shows the design and working appearance of the deflection wedge. The base of the wedge is made larger than the expected total end deflection of the specimen. Any number of "Y" segments can be added, and any convenient wedge

length can be used. Figure 2 (b) shows the wedge at rest, while Figure 2 (c) shows the appearance of the wedge during testing. (This example shows the wedge oscillating with an amplitude of Y_3.) As the amplitude is increased or decreased, the apparent wedge intersection (A) moves to the left or right, respectively.

Fatiguing frequency and accumulated cycles are measured using a magnetic pickup mounted on the apparatus at the specimen rest plane in close proximity to a steel exciter attached to the specimen. Two pulses/cycle are generated and fed to frequency and cycle counters as double values.

This work was done by John P. Dorner, William S. Pierce, and John L. Shannon, Jr., of **Lewis Research Center.** *No further documentation is available.*
LEW-13037

Measuring Acoustic Properties of Materials and Jet Nozzles

Test time and complication are reduced.

Lewis Research Center, Cleveland, Ohio

A method has been developed for measuring the acoustic properties of sound-absorbent materials and of a jet-nozzle system. The method, which uses a high-voltage spark discharge as a pulse source of sound, is based upon the fact that such a sound pulse has a broadband spectral content and is capable of being analyzed by a fast Fourier-transform (FFT) digital processor.

The pulse of sound generated by the spark discharge passes across the pressure transducer (Figure 1) and is partially reflected from the absorbent surface. The transducer "sees" the incident and reflected pulses separated in time. Each pulse time history is fed into a dual-channel fast Fourier-transform (FFT) analyzer for computation of the transfer function at all frequencies. The transfer function is then used to compute the reflection coefficient and acoustic impedance coefficient as a function of frequency.

For the jet-nozzle situation (Figure 2) the acoustic pulse passes through the nozzle and is measured by a far-field microphone. The transmission coefficient for each polar angle, Θ, is computed from the transfer function between the far-field transmitted pulse and the incident in-duct pulse by using the dual-channel FFT analyzer in the same processing procedure as described for acoustic material evaluation.

The advantages of the impulse method over other methods are: (1) test time is dramatically reduced since one pulse covers the entire frequency

(continued on next page)

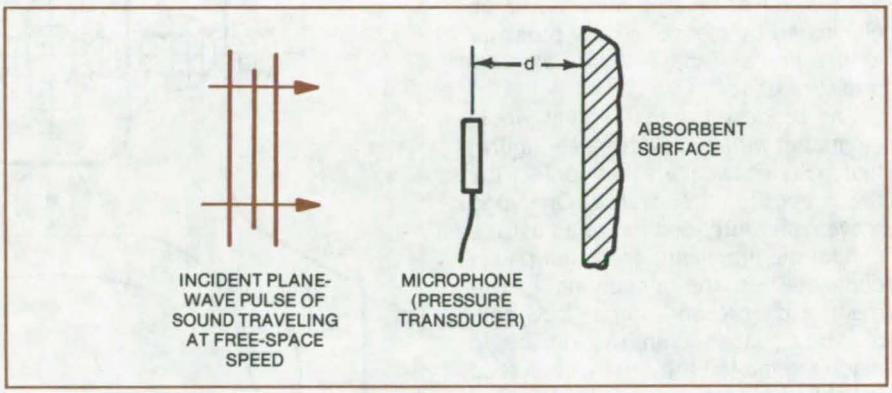


Figure 1. **Generalized Free-Field Measurement** of acoustic properties utilizes the test setup shown above. A spark-generated sound pulse is detected as it passes the microphone heading toward the test surface, and the reflected wave is detected as it returns past the microphone.

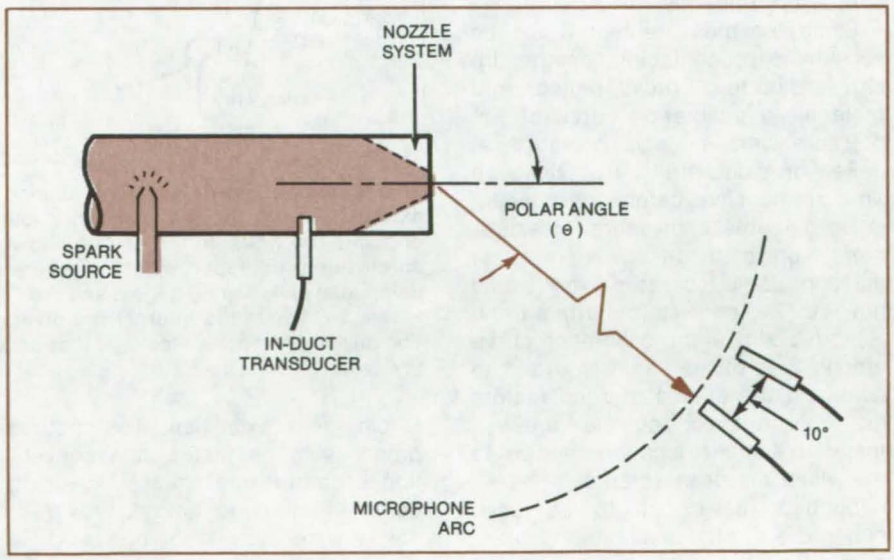


Figure 2. **Jet-Nozzle Measurement** requires a spark-generated sound pulse that passes through the nozzle. The deflected pulse is detected by a microphone at the required polar angles. An additional transducer within the duct detects the undeflected pulse.

range, (2) the complication of environmental reflections is eliminated, and (3) the source is compact and simple.

The results obtained from the impulse method have been compared with those from existing methods, both experimental and theoretical, and show excellent agreement.

This work was done by P. D. Dean, H. E. Plumblee, and M. Salikuddin of Lockheed Aircraft Corp. for **Lewis Research Center.** *For further information, Circle 53 on the TSP Request Card.*
LEW-13265

Tire-Pressure Measuring Concept

A proposal for measuring tire pressure without air loss

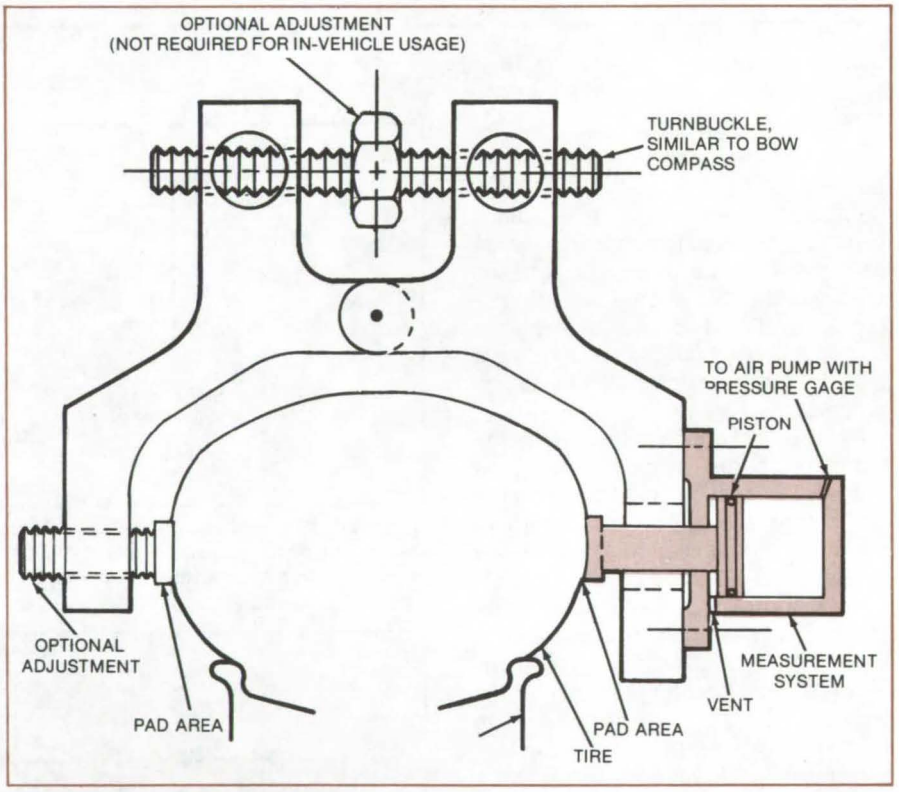
Lyndon B. Johnson Space Center, Houston, Texas

Conventional tire-pressure measurement or monitoring always results in some air-pressure loss when a gage or similar instrument is inserted into the tire valve. This problem could be eliminated by measuring the pressure at the tire surface with an external pressure gage.

The proposed measurement would be made with a device (see figure) that includes two pads that contact the two opposite tire walls. One pad moves on a threaded rod to adjust the unit for the tire width. The other pad is connected to the measuring instrument; e.g., pressure gage, load cell, or strain gage. With the device in place around the tire, an external load is applied to that pad until the tire wall deflects. At that point, the externally applied pressure is approximately equal to the internal tire pressure and is measured directly.

Since the measurement would be sensitive to such factors as the tire size, design (e.g., radial, belted), and material, a calibration curve of tire pressure versus gage pressure at deflection would first be obtained on an equivalent tire before the concept is used to make pressure measurements on a field-installed tire. In addition, some laboratory work would have to be done to determine the reproducibility of the calibration curve among tires of the same type and to ascertain the effects of such factors as the hardness of the tire-wall material and the location relative to the wheel rim or tread area.

Such a device might be used onboard aircraft for monitoring pressure during the wheel well storage. It could be easily removed during landing-gear extension. The method promises to be faster than conventional tire-pressure checks, speeding up the turnaround time for aircraft. The device can also be used to measure tire pressures on land vehicles.



This **External Tire-Pressure Measuring Concept** involves a device that applies external load to the tire wall to measure its internal pressure. Two pads grip the opposite tire walls. In the version shown, load is applied to the pad on the right by an air pump equipped with a pressure gage. Alternately, the load can be applied using load cells, strain gages, and the like. As the tire deflects, the equilibrium point is reached where the internal tire pressure is equal to the measured external load. The device prevents air leakage that occurs when pressure is measured through the tire valve.

This work was done by Lloyd O. Ashmore of Rockwell International Corp. for **Johnson Space Center.** *No further documentation is available.*
MSC-18490

Synthetic Seawater as Stress-Corrosion Test Medium

Seawater minimizes pitting corrosion of aluminum-alloy test samples.

Marshall Space Flight Center, Alabama

Stress-corrosion-cracking (SCC) resistance of aluminum alloys and of other metals is determined by an accelerated method of alternately immersing the strained test specimens in a 3.5-percent saltwater solution. A problem with this procedure is that the saltwater accelerates pitting corrosion of aluminum alloys containing copper, making it difficult to evaluate the tests. A new approach is to use synthetic seawater to minimize the pitting corrosion.

Of the three corrosion-inhibiting methods evaluated using (a) chromate inhibitors in the saltwater, (b) surface treating the samples via anodizing or alodine treatment, and (c) synthetic seawater, synthetic seawater was found to be the most effective test medium. Synthetic seawater is prepared according to the formulation shown in the table. It is more uniform than fresh seawater; the latter may be diluted or contaminated and would be difficult to transport to inland laboratories.

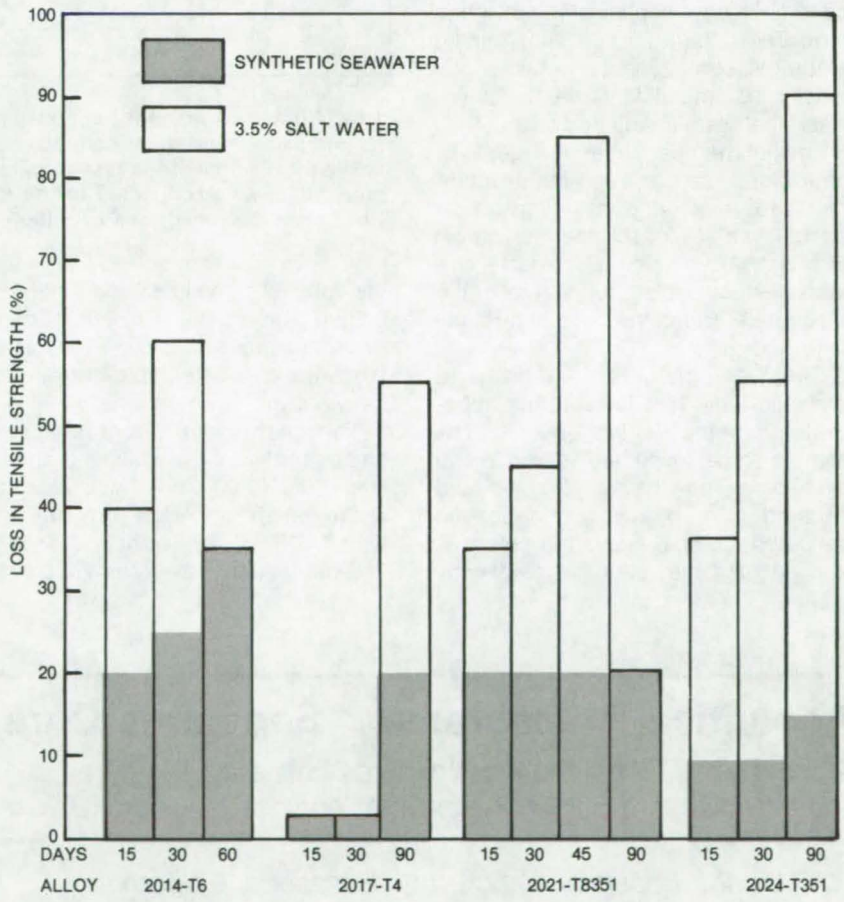
The illustration compares pitting corrosion of aluminum samples immersed in saltwater and prepared seawater. For example, loss in tensile strength of unstressed T351 specimens immersed in saltwater ranged from 35 percent in 15 days to 90 percent in 90 days, while the strength loss in seawater was only 15 percent in 90 days. In many cases the losses in saltwater exceeded 25 percent after 15 days and 25 percent after 30 days. In seawater the losses did not exceed 20 percent after 90 days except for the 2014-T6 alloy.

This work was done by T. S. Humphries and E. E. Nelson of **Marshall Space Flight Center.** *For a copy of the report, NASA TM-X-64733 [N73-22062/NSP], "Synthetic Sea Water — An Improved Stress Corrosion Test Medium for Aluminum Alloys," Circle 54 on the TSP Request Card.*

MFS-22706

NaCl	2.453	$NaHCO_3$	0.0201
$MgCl_2$	0.520	KBr	0.0101
Na_2SO_4	0.409	H_3BO_3	0.0027
$CaCl_2$	0.116	$SrCl_2$	0.0025
KCl	0.069	NaF	0.0003

Chemical Composition of synthetic seawater in weight percent



Loss in Tensile Properties of unstressed SCC specimens is significantly reduced using synthetic seawater as a test medium.

Detecting Insulation Defects in Metal/Plastic Films

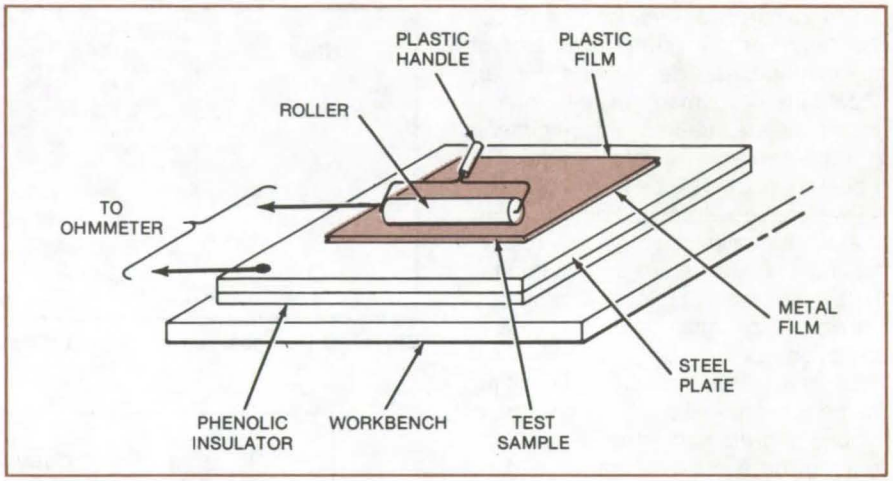
A simple apparatus checks the insulation between plastic and metal surfaces.

Marshall Space Flight Center, Alabama

Plastic surfaces of metal-clad plastic-film laminates must be completely insulated from the underlying metal film. The insulation is important when the laminates are used in electrical applications. During the fabrication, conductive particles may reach the plastic surface and later cause shorts between the surface and the metal film. The surface breaks may be microscopic and remain undetected by visual inspection.

Film can be inspected more accurately by a simple apparatus developed to inspect copper-clad polyimide film. The apparatus can spot minute electrical contaminants between the plastic and metal films. A flat stainless-steel plate connected to a 200-V, 80-megohm-impedance Megger, or equivalent, set (a high-range ohmmeter for measuring insulation resistances) serves as one electrical terminal. A precision-machined stainless-steel roller also connected to the Megger set forms the second terminal (see figure).

The steel plate is secured to a phenolic base that isolates the apparatus from the working bench. The sample to be inspected is laid metal side down on the steel plate and secured to it by two spring-loaded insulated clamps. Next, the power is applied, and the roller is grasped by the phenolic handle and manually guided over the entire plastic surface. Any conductive breaks in the plastic surface cause detectable current flow between the roller and the plate.



This Simple Apparatus spots insulation defects on metal-clad plastic-film laminates. A steel roller connected to a high-range ohmmeter is guided over the entire plastic area of the test sample. The metal-film side of the sample rests on a steel plate, also connected to the test instrument. The ohmmeter detects current flow when the roller rides over the conductive break in the plastic surface.

The roller is 8 in. (20 cm) long and has a polished finish making a contact line 1-mil (0.03 mm) thick along its entire length. It weighs 2 lb (0.9 kg), which effectively translate into a 250-psi (1.76×10^6-N/m^2) contact pressure at the plastic surface sufficient to locate microscopic defects.

This work was done by Richard N. Buggle of Honeywell, Inc., for **Marshall Space Flight Center.** *For further information, Circle 55 on the TSP Request Card.*

Inquiries concerning rights for the commercial use of this invention should be addressed to the Patent Counsel, Marshall Space Flight Center [*see page A5*]. *Refer to MFS-25127.*

Acoustical Measurement Separates Core Noise and Jet Noise

A measuring technique discriminates between the jet noise and core noise of a jet engine.

NASA's Jet Propulsion Laboratory, Pasadena, California

Signals from microphones at widely separated angles in the far field of a jet can be cross-correlated to separate and measure core and jet noise. Earlier correlations of transducer signals at the source and in the far field were inaccurate because of temperature and flow fluctuations.

In tests, core noise is coherent throughout the far field because its sources and the observer are nearly at rest with respect to the engine (e.g., in static-engine and wind-tunnel tests). However; jet-noise sources are in motion and the noise undergoes large Doppler shifts, resulting in negligible coherence over widely separated directions. Thus the cross-correlation of sound pressures between wide angle essentially represents the autocorrelation of core noise radiated to the far field.

If the microphones are located on an arc of a circle in the far field, the

maximums of all correlations occur at time, $\tau = 0$. There are symmetric autocorreations for each angle, and the cross-correlation is symmetric because it represents an autocorrelation (the core noise in this case). In general, if the jet noise contribution is not negligible, the cross-correlation may be made symmetric about $\tau = 0$. Such a procedure will remove any residual contribution from jet noise, which at large angular separations is essentially asymmetric about $\tau = 0$.

Experiments have been performed in which nitrogen gas at ambient temperature flowed at several jet velocities through a nozzle. Internal turbulence and noise were present in the plenum because of abrupt changes in the flow directions at the entrance. Noise data measured by a rectangular array of eight microphones in the far field were recorded and processed.

The results confirmed that core noise and jet noise can be separated by examining the cross-correlation of far-field microphone signals and that the crossover point between core noise and jet noise moves toward higher velocities at higher angles with respect to the jet axis. The method can be extended to separate the spectral components and to determine the effects of a surrounding flow simulating forward motion.

This work was done by Shakkottai P. Parthasarathy of Caltech for **NASA's Jet Propulsion Laboratory.** *For further information, Circle 56 on the TSP Request Card.*
NPO-14698

Onsite Testing of Pressure-Sampling Valves

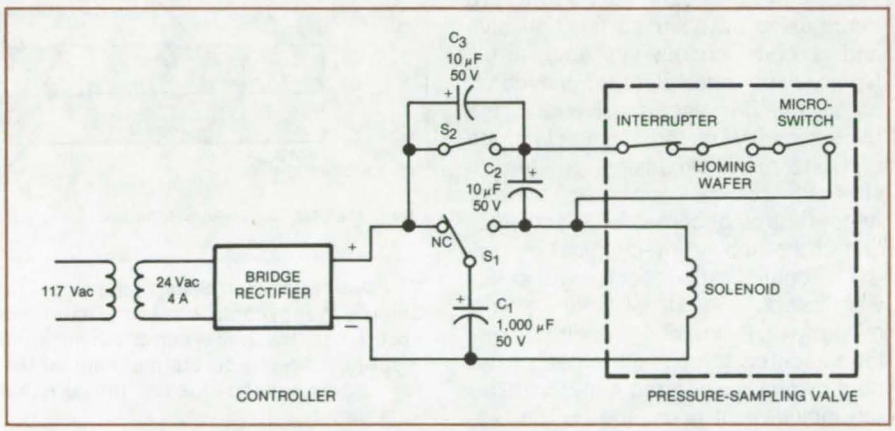
Portable instrument is used in wind tunnels.

Langley Research Center, Hampton, Virginia

The testing of pressure-sampling valves, which are installed in wind tunnels and models to acquire aerodynamic research data, requires the use of such equipment as a solenoid stepper, BCD decoder, regulated power supply, and digitial voltmeter. These are troublesome to transport and often are not available at all test sites. Also, the use of a facility data-acquisition system may be required when it could otherwise be used for gathering data on other research tests or calibrating other devices. It is also necessary to have two or three technicians working through an intercom system to perform the sampling-valve test, making the completion of alinement and leak checks very difficult.

A portable test instrument was devised containing a controller, pressure port identification, a 5-V power source for transducer excitation, and a digital voltmeter to test pressure-sampling valves completely, including the leak and plug check before, during, or after installation in any location or environment. The controller comprises a 117/24-Vac 100-watt transformer, a bridge rectifier, a capacitive-discharge stepper, and a constant voltage source for homing the sampling valve. It also includes a 5-V regulated power supply and a bipolar digital voltmeter having a 10-μV resolution.

The 5-V power supply and the digital voltmeter are used to excite and measure the output of the strain-gage pressure transducer used with the pressure-sampling valve. The 5-V power supply may also be used as the logic-supply voltage for the port-identification decoder, which can be BCD to seven-segment display or similar, depending on the type of port-identification transmitter used.



Controller Connection to Sampling Valve includes a stepping switch (S_1) and a homing switch (S_2). Capacitor C_1 acts as a filter during the homing operation and provides a stepping pulse by discharging through the solenoid during the stepping operation. Both S_1 and S_2 are momentary switches; C_2 is used as an arc suppressor for the sampling valve, and C_3 provides the same protection for the homing switch.

This work was done by Randy Mallory of Wyle Laboratories for **Langley Research Center.** *For further information, Circle 57 on the TSP Request Card.*

Inquiries concerning rights for the commercial use of this invention should be addressed to the Patent Counsel, Langley Research Center [see page A5]. Refer to LAR-12428.

Graphite/Epoxy-Tape Test Specimens

Better-constructed tensile-test specimens produce accurate results.

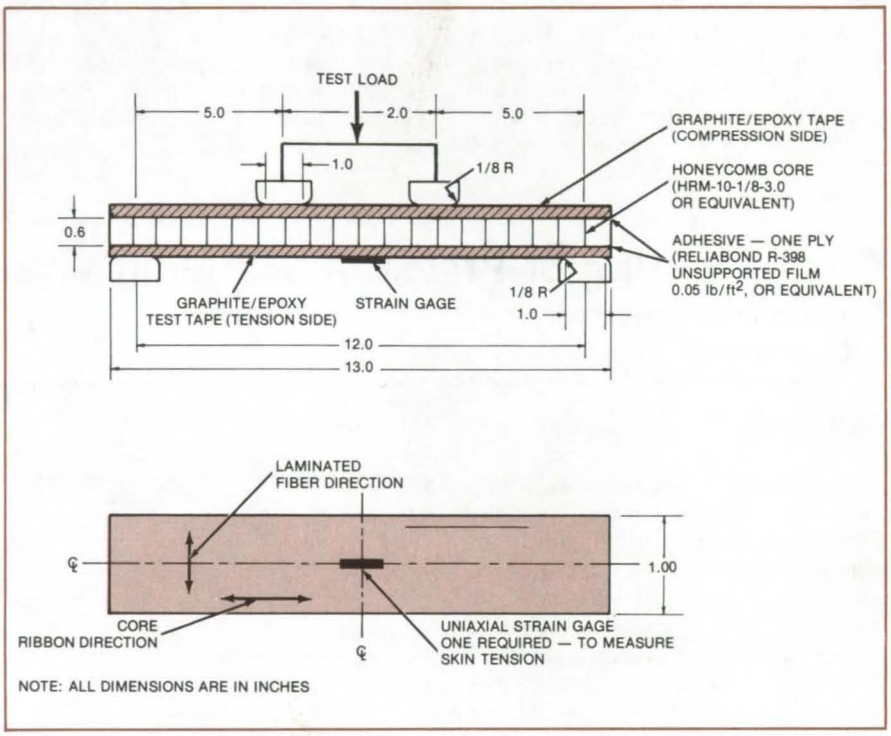
Lyndon B. Johnson Space Center, Houston, Texas

Newly constructed specimens for transverse tensile testing of unidirectional graphite/epoxy tape can be tested more accurately than the earlier samples. Earlier samples were attached to opposite sides of an aluminum core with adhesives. Because the tests were run at temperatures ranging between -175° and 350° F (-112° and 177° C), uneven thermal expansion and contraction between the tape and the core often ruptured the tape prematurely, making it difficult to determine the actual magnitude of the applied mechanical stress.

The new specimens (see figure) are made using an unsupported adhesive and a commercially-available (e.g., Nomex, or equivalent) honeycomb core. The flexible adhesive and the dimensionally stable core eliminate uneven thermal expansion. The tensile strength of the tape at various temperatures becomes a direct function of the applied mechanical stress.

The configuration, basically a sandwich beam, consists of layers of 4.0 mils/ply (0.1 mm/ply) graphite/epoxy tape secured to opposite sides of the core by an unsupported adhesive. The top includes 24 plies, the bottom 20. The tape fibers are orthogonal to the specimen length.

The specimens are machined with a diamond-coated cutoff wheel, and the machined edges are hand-polished with #400-grit abrasive paper to remove nicks and any damaged area that may cause premature tape failure. A uniaxial strain gage is attached to the tension face (bottom) of the specimen. The specimen is then placed in a universal test machine and tested to failure. The strain at which the failure occurs is recorded.



Transverse Tension Specimens of parallel-laminated collimated fiber tape are made using a honeycomb structure sandwiched between two tape layers. The tape is secured to the honeycomb by an unsupported adhesive film. This configuration responds directly to the mechanical test load. Thermal expansion and contraction forces between the tape and the core that occurred on earlier samples are effectively eliminated.

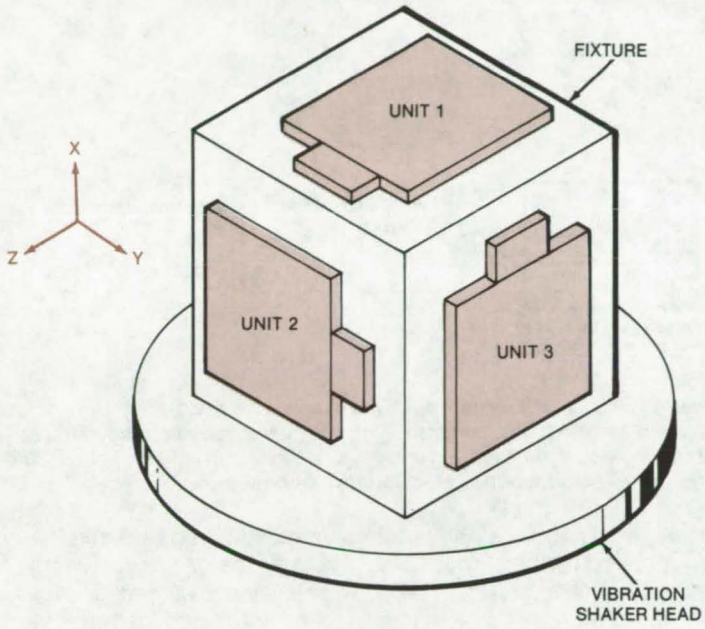
The tests are conducted at various temperature levels to determine how the tensile strength varies with temperature. Specimens using commercially available materials (e.g., Hexcel's F263 resin, or equivalent, on Thornel fibers, or equivalent) have produced strain values as high as 7,300 μin./in. (7.300 μm/mm) at room temperature and 8,600 μin./in. (8.600 μm/mm) at 350° F (177° C), which is higher than the 4,900-μin./in. (4.900-μm/mm) and 5,800-μin./in. (5.800-μm/mm) specifications, respectively, that were difficult to reach previously due to the uneven expansion.

This work was done by Jim L. Cupp and Francis S. Spears of Rockwell International Corp. for **Johnson Space Center.** *No further documentation is available.*
MSC-18495

"Three-Dimensional" Vibration Fixture

Cube-shaped fixture speeds up vibration tests threefold.

Lyndon B. Johnson Space Center, Houston, Texas



VIBRATION AXIS

	RUN 1	RUN 2	RUN 3
UNIT 1	X	Z	Y
UNIT 2	Z	Y	X
UNIT 3	Y	X	Z

A **Simple Cube-Shaped Fixture** reduces vibration-test time to one-third that required previously. Three units are supported at once. During one run each unit is tested along one of the axes. The units are repositioned on the second run for tests along different axes. Three runs complete the test as illustrated in the inset table. This fixture can be set up to test small, lightweight high-production units.

A cube-shaped fixture (see figure) developed for vibration testing of pyrotechnic initiator controllers can handle three units at once. The units are mounted on the top and two adjacent walls of the cube. The cube is attached to a vibration shaker head that vibrates in the vertical axis. When power is applied, each unit vibrates along one of the three mutually orthogonal axes. After one run the units are repositioned so that each unit is tested along another axis. After the third run, each unit has been tested in all three axes (see table) and the test is complete.

The fixture speeds up the test time threefold. It does not have to be removed from the test setup to reposition the units, and the shaker head need not be repositioned for testing along the different axes. In addition, the vibration spectrum need not be reverified and readjusted between the axes.

A conventional apparatus can test only a single unit at one time and on one axis. To test along another axis, the unit and the fixture must be removed from the shaker head, the shaker head repositioned, and the vibration spectrum rechecked.

This work was done by Cecil A. Schumacher of Martin Marietta Corp. for **Johnson Space Center.** *No further documentation is available. MSC-16305*

Rapid Testing of Pulse Transformers

Droop and rise time are determined from voltage measurements at discrete frequencies.

Lyndon B. Johnson Space Center, Houston, Texas

Quality-control testing of pulse transformers is speeded up by a new method for determining rise time and droop. Instead of using an oscilloscope and square-wave generator to measure these characteristics directly, the new method uses a voltmeter and a sine-wave generator (see figure) to measure them indirectly in about one-tenth the time.

Droop — the slope of the top of the output pulse — is determined by measuring the input and output voltages (e_i and e_o) of a pulse transformer at 1 Hz and 1 kHz sinusoidal excitation. The e_o/e_i ratio is then compared with allowable test limits previously established by correlating

(continued on next page)

low-frequency sine-wave behavior with pulse transient behavior.

Rise time — the time for the transformer output to rise from 10 percent to 90 percent of the peak amplitude of a pulse — is also measured indirectly, except that the test frequencies are 1 MHz and 4 MHz.

The correlation between direct and indirect measurement is based on transient analysis of the transformer under pulse excitation and under excitation at low and high sinusoidal frequencies. For example, the high-frequency pulse response is

$$\frac{e_o}{e_i} \approx K_R(1 - e^{-t/T}) \qquad (1)$$

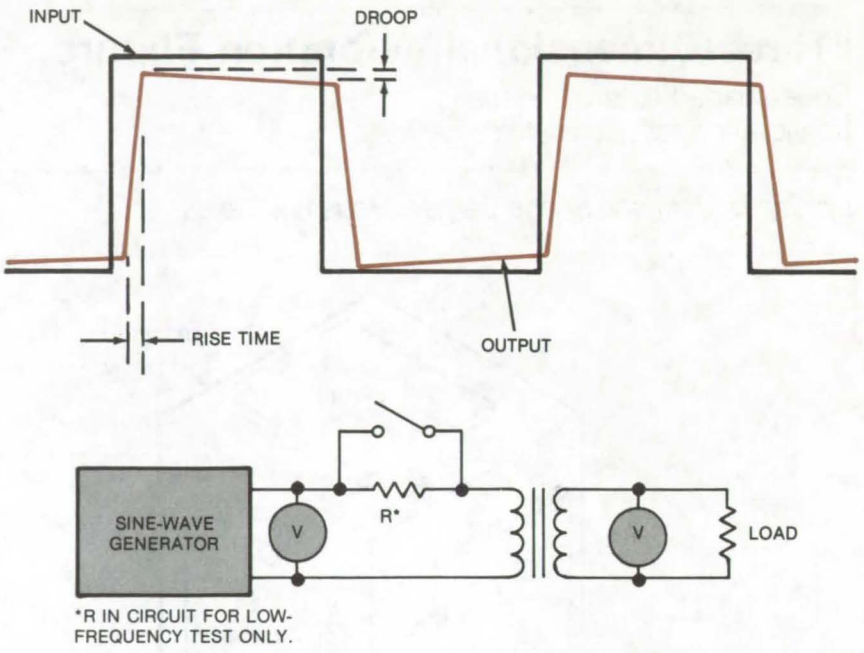
where t is time and K_R and T are constants determined by the transformer equivalent resistance and inductance. From this equation, the rise time can be plotted as a function of T. The high-frequency sinusoidal response is

$$\frac{e_o}{e_i} \approx \frac{K_R}{1 + j\omega T} \qquad (2)$$

where ω is the frequency. This equation can be used to plot e_o/e_i as a function of ω for various values of T.

A given maximum allowable value of rise time dictates a certain value of T, which can be found from equation 1. This value of T likewise dictates certain values of e_o/e_i at 1 MHz and 4 MHz, which can be found from equation 2. Thus, to find the rise time of a pulse transformer, the test operator merely verifies that the measured values of e_o/e_i at 1 MHz and 4 MHz match the calculated values.

For the droop test, the operator refers to a plot of e_o/e_i versus T at 100 Hz and 1 kHz. In this case, T is determined from a graph of allowable droop versus T, based on a low-frequency transient-pulse analysis. In a way that is similar to the rise-time calculation, allowable values of e_o/e_i are determined (at 100 Hz and 1 kHz) for comparison with experiment.



Transformer Characteristics Are Rapidly Measured by the circuit shown. Droop and rise time are determined by measuring the input/output voltage ratio at just four frequencies. Previous methods, requiring comparison of the input and output waveforms on an oscilloscope, are more time-consuming.

This work was done by Joseph Grillo of The Singer Co. for **Johnson Space Center.** *For further information, Circle 58 on the TSP Request Card.*
MSC-18202

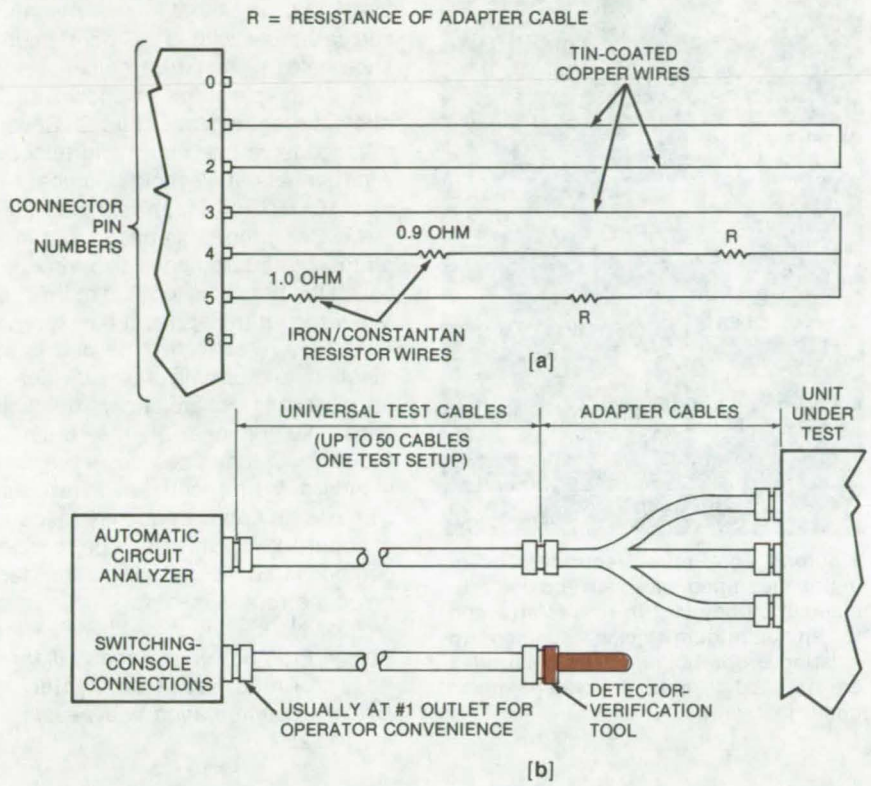
Detector Verifier for Circuit Analyzers

A test circuit verifies the operation of an automatic circuit analyzer.

Lyndon B. Johnson Space Center, Houston, Texas

An economical detector-verification tool (DVT) is used to check the operation of an automatic circuit analyzer. When testing circuits and complex harnesses for continuity or shorts, an analyzer can malfunction and indicate a nonexistent circuit fault. The DVT, connected directly to the analyzer console, can verify whether the analyzer was operating properly during the test. The DVT can be handled by one operator instead of two previously necessary to check out the analyzer with a manually-operated variable-resistor test box.

Basically the DVT is a test circuit consisting of a set of loops (see figure) where each loop incorporates an iron/constantan return wire of a selected resistance value. These wires have a temperature-stable resistance and can withstand currents of up to 2.5 A. The wires are cut to proper length and spliced into copper conductors, and the entire assembly is incorporated into a short stub feeding a standard universal connector cable.



Detector-Verification Tool is a circuit that uses a set of fixed resistance loops (see part a) to verify the operation of an automatic circuit analyzer. Each loop is addressed directly from the analyzer console by switching the internal analyzer bridge to a resistance that equals that of the connecting cables plus a specified limiting test value. The procedure verifies whether the detected faults in the circuit under test are actually due to the analyzer malfunction. Standard-length universal test cables (see part b) make it possible to shift the detector tool from cable to cable without resistance compensation.

The resistance values are selected according to the analyzer specification. Over 48 different test values can fit a standard 100-wire universal test cable. Some loops can be fixed as shorts.

The analyzer uses a set of standard-length universal cables, and the DVT construction is simplified because all the cables on a given test setup have the same resistance. Typical lengths used in work on the Space Shuttle are 30 and 80 ft (9 and 24 m). For any given test setup, identical lengths are used. The DVT is connected to the analyzer via one of these cables using a standard pin connector and is addressed by the operator at the analyzer console.

This work was done by Daniel L. Pope and Robert L. Wooters of Rockwell International Corp. for **Johnson Space Center.** *No further documentation is available.*
MSC-19669

Rugged Fast-Response Temperature Probe

Rugged probe measures very small temperature fluctuations.

Ames Research Center, Moffett Field, California

Total temperature and the fluctuations about a mean value usually are measured by using fine thermocouples, thermistors, or unheated wires in an appropriate geometrical configuration. When temperature fluctuations are as fast as 10 to 20 kHz, a fine unheated wire is usually employed. For wind-tunnel and atmospheric flight experiments, the magnitudes of temperature fluctuations can be very small, yet rugged sensors are required to survive the test environment.

In the past, rugged sensors were made from 5-μm tungsten wire about 1

(continued on next page)

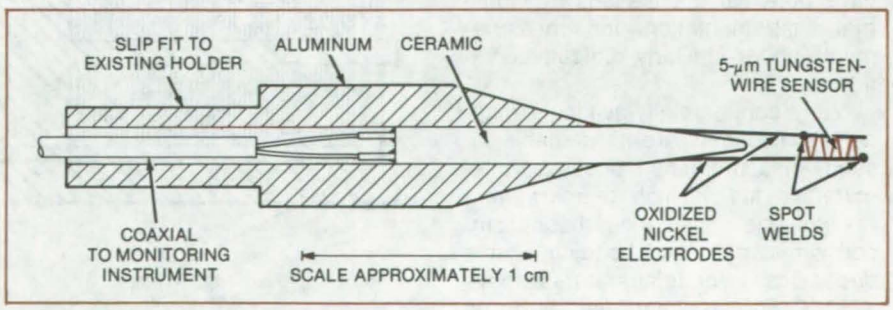


Figure 1. This **Very-Sensitive Temperature Probe** uses a 5-μm tungsten sensor wire wrapped around two notched electrodes. This design combines the ruggedness of an earlier but less sensitive probe using a very-short sensor wire with a very-sensitive but fragile version with sensor wires wrapped around nonconducting frames.

mm in length. These wires have been flown for up to 60 hours of atmospheric flight time without breakage; however, with such a short sensor length, they were insensitive to low-level temperature fluctuations. In contrast, wires wound around nonconducting frames have been demonstrated to be very sensitive to small temperature variations, but they lack the strength to survive even relatively-mild wind-tunnel situations.

The new probe shown in Figure 1 combines the wound-wire concept with a short sensor length for each turn of tungsten wire. The 5-μm sensor wire is spot-welded at the tip of one nickel electrode and then wound around the two electrodes and spot-welded at the back of the opposite electrode. Electrical contact between the sensor wire and electrodes at other than the welds is prevented by a nickel oxide coating.

The nickel electrodes are epoxied into a ceramic body that is epoxied into an aluminum jacket for adaptation to existing probe holders. A miniature coaxial cable with a 50-ohm impedance helps to minimize noise.

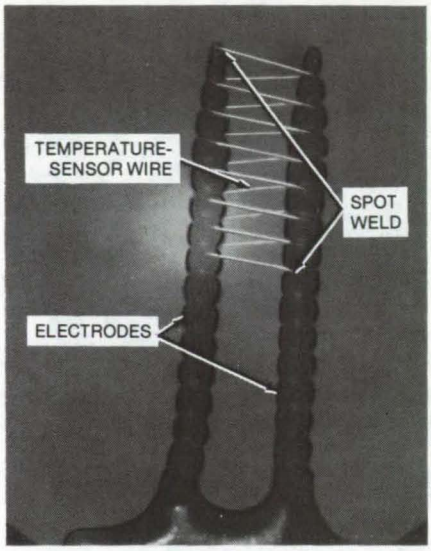


Figure 2. The **Probe Electrodes** shown in this magnified photo are epoxied into a ceramic body that in turn is attached to an aluminum jacket adapted to existing probe holders. The electrodes are notched to hold the wire in place under fast winds.

A prototype probe is shown in the photomicrograph of Figure 2. Several of these have been built and tested in wind tunnels at Reynolds numbers up to 1×10^7/m and Mach numbers up to 0.95. One probe has been used in an atmospheric turbulence experiment in which the sensor is located at the nose of a large jet transport. It has survived for 50 hours of flight time and is still functioning normally. Sensitivities of up to 10 volts/°C are easily attainable. Thus, fluctuations of the order of 0.0001° C can be observed with standard instrumentation. The 5-μm wire has an upper frequency response of about 1 kHz, which can be routinely compensated to 20 kHz for fast-response requirements.

This work was done by Pearl L. Bailey, Fred R. Lemos, and William C. Rose of **Ames Research Center.** *No further documentation is available.*
ARC-11289

High-Temperature High-Pressure Magnetic Pickup

New choices of materials raise the operating temperature to 1,100° C and the pressure limit to above 2.5 kilobars.

Lyndon B. Johnson Space Center, Houston, Texas

New magnetic-pickup transducers operate at temperatures as high as 1,100° C and pressures in excess of 2.5 kilobars (0.25×10^9 N/m^2). The transducers are being developed to obtain simulated seismic data in laboratory experiments at high temperatures and pressures. They also have potential applications in industrial instrumentation for measurements under similarly difficult conditions.

Many commercially-available magnetic transducers are not suitable for such measurements because their materials fail at high temperatures; their magnets lose their magnetism, coil wires melt, and bonding agents decompose. For temperatures above 175° C, it has been necessary to insulate and water-cool conventional transducers; however, this is difficult to do in the confines of a high-pressure vessel. Moreover, many conventional

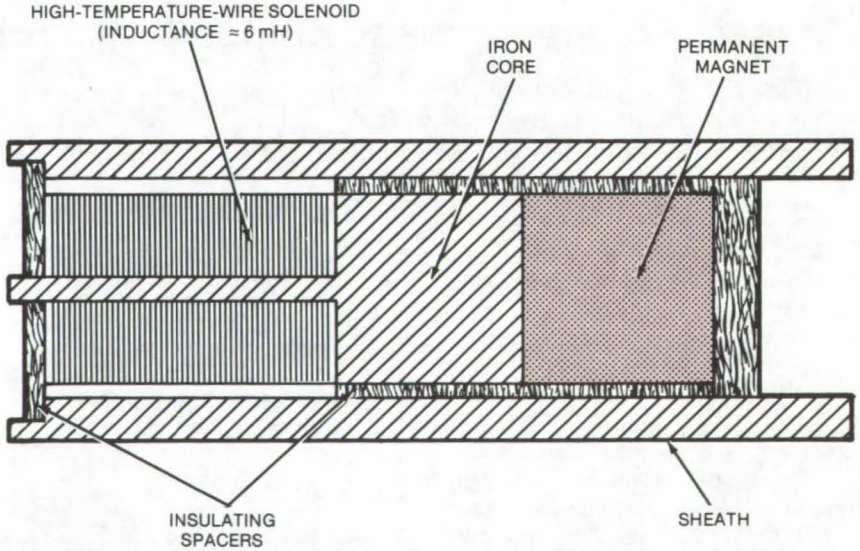


Figure 1. A **Permanent-Magnet Pickup** uses high-temperature materials for its bonding cement, windings, magnet, and other components. Operating temperatures to 600° C are possible with this construction.

transducers cease to function above about 2.5 kilobars of pressure.

The new transducers use high-temperature cement to bond the parts together and high-temperature-insulated copper or aluminum wire for the windings. One version (see Figure 1), available for temperatures up to 300° or 600° C depending on the exact choice of materials, uses high-Curie-temperature magnetic alloys for the permanent-magnet pickup. A second version (see Figure 2), with a temperature limit of 1,100° C, has a solenoid rather than a permanent-magnet pickup. The solenoid core in this version is cobalt.

The transducer in Figure 2 has two windings: Winding B carries direct current, which creates a magnetic bias in the cobalt core. Winding A, the output winding, develops an induced voltage when the motion of nearby magnetic materials changes the flux in the core. This voltage is amplified as the sensor signal.

The sensor output is enhanced and signal-to-noise ratio is improved by connecting the transducer to the superregenerative circuit shown. Signal enhancement is possible because the voltage change induced on winding A is also induced on winding B. Thus, with careful selection of resistor values, the B voltage is amplified so as to alter the bias current and augment the induced voltage in winding A. The resistor values in the bias circuit must be selected so that they bring the regenerative effect close to, but just short of, the point of oscillation.

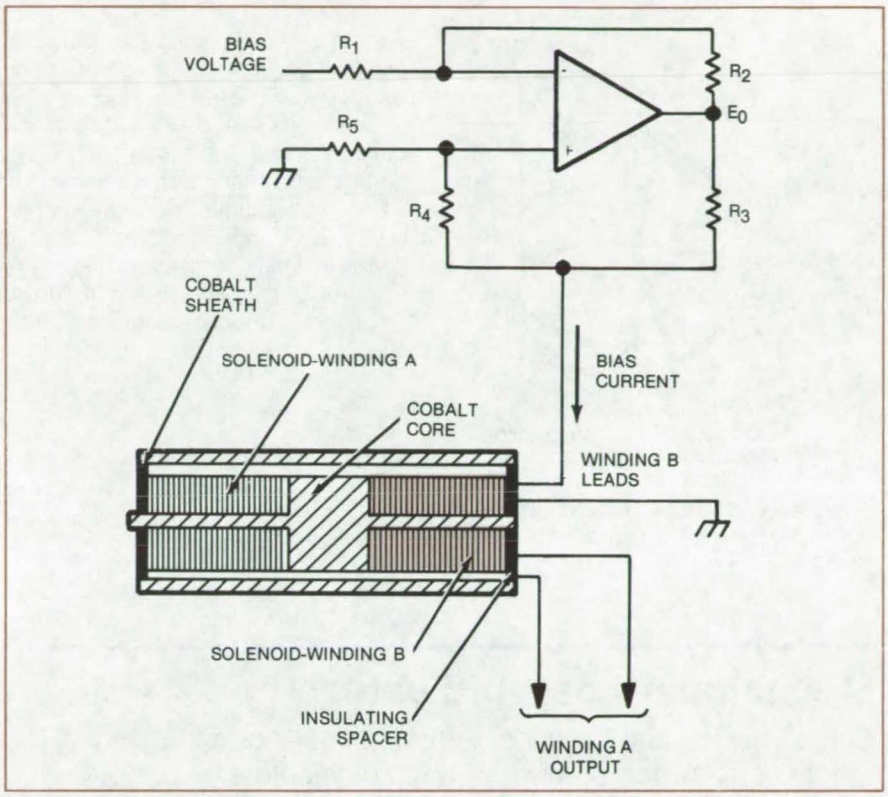


Figure 2. A **Solenoid-Magnet Pickup** with a cobalt core and sheath withstands temperatures to 1,100° C. The superregenerative circuit enhances the output signal-to-noise ratio.

This work was done by Lloyd A. Ahlberg and Bernhard R. Tittmann of Rockwell International Corp. for **Johnson Space Center.** *For further information, including details on the materials used in the new transducers, Circle 59 on the TSP Request Card.*
MSC-18389

Controlling Subsynchronous Whirl in Turbopumps

Active fluidic dampers are proposed for controlling turbopump-shaft whirl.

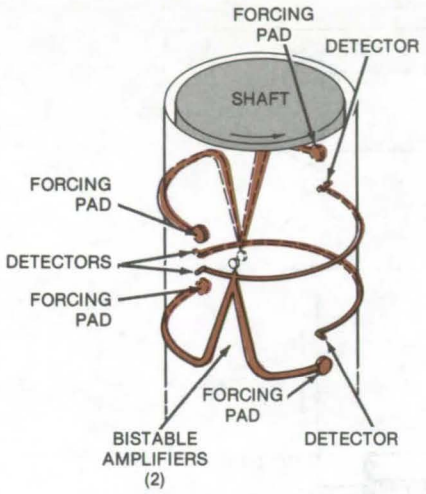
Marshall Space Flight Center, Alabama

Active fluidic dampers may be the best answer among possible alternatives for controlling subsynchronous whirl in turbopump shafts. A preliminary study indicates that a linear variable-bleed detector and a linear bistable amplifier are effective in supplying sizable controlled damping forces.

The possible detector choices investigated are: (a) hydrodynamic pressure pickoffs, (b) velocity-sensitive free-force compression pickoffs, (c) linear variable-bleed chambers, and (d) vortex variable-bleed chambers. Among these four, the linear variable-bleed detector was chosen because the others were either too complex or produced inadequate signal strength.

The possible amplifier candidates were: (a) linear bistable, (b) linear proportional, (c) vortex bistable, and (d) vortex proportional. In this case a linear bistable device was considered as the simplest and most adequate. The vortex devices had a questionable frequency response and were complex. However, these can be more compact, have no diffuser recovery losses, and have more-complete mainstream cutoff capability. In some applications, these factors may be advantageous.

(continued on next page)



The **Linear Bistable Fluidic Damper** may be effective in controlling turbopump-shaft whirl.

A possible linear bistable damping system is shown, using four detectors and four power amplifiers. In general, volume-fill times and viscous flow effects associated with the linear devices are less important as design parameters than performance and sizing; but volume, viscosity, control hysteresis, and impedance fluctuations all significantly affect the placement of detectors relative to power amplifiers. Breadboard testing of the spatial lead angles of detectors relative to power amplifiers is required to tune the system.

This work was done by M. Dean Black and Bernard F. Rowan of Rockwell International Corp. for **Marshall Space Flight Center.** *For further information, Circle 60 on the TSP Request Card.*

Inquiries concerning rights for the commercial use of this invention should be addressed to the Patent Counsel, Marshall Space Flight Center [see page A5]. *Refer to MFS-19423.*

Mechanical-Load Indicator

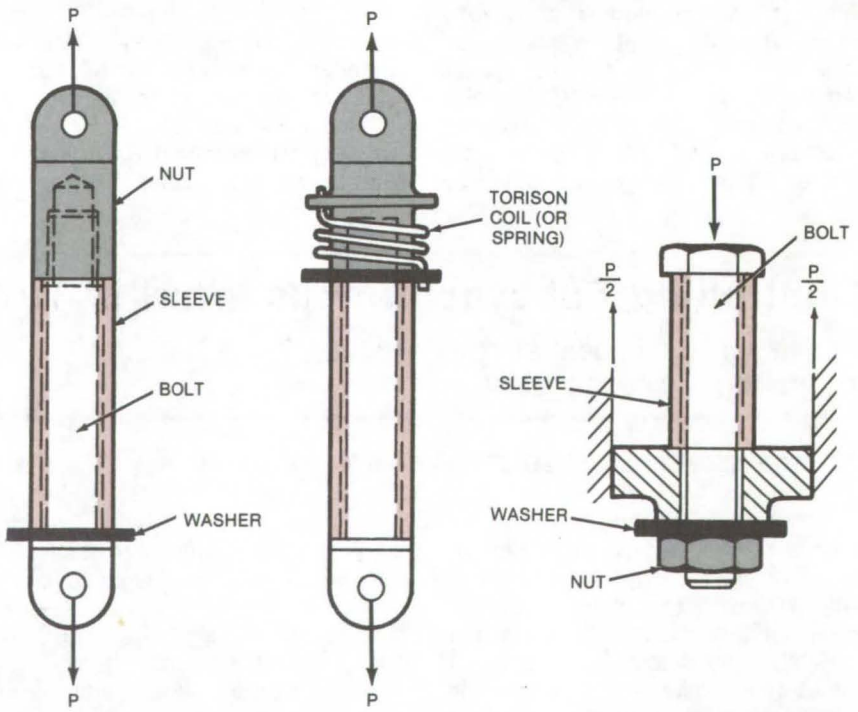
Simple device can be used as a sequencer or a mechanical switch as well as a load indicator.

Lyndon B. Johnson Space Center, Houston, Texas

By rotation of a washerlike part, a mechanical indicator shows when a predetermined compression or tension load has been reached. In its simplest form, the indicator consists of a bolt, a sleeve, a load-indicating washer, and a nut (see figure, left). The nut is part of the upper load-bearing clevis, and the bolt is part of the lower clevis. Tightening the nut produces tension in the bolt shank, thereby increasing its length; and at the same time, the nut compresses and shortens the sleeve with an equal but opposite load.

The assembly is calibrated by applying a known tension load on the bolt shank, then hand-tightening the nut. This could be done by using a tensile test machine. With the nut only loosely screwed on the bolt, a known tension load is applied. The operator then tightens the nut with one hand until the washer can no longer be rotated by the other hand.

When the load is removed, the sleeve prevents the bolt from returning to its original length. However, if tension is again placed on the assembly, the compression of the sleeve will drop to zero when the load exceeds the preset amount; and the



A **Simple Load Indicator** (left) is made from a washer, a sleeve, and two load-bearing clevises. The upper clevis is attached to a nut; a bolt is part of the lower clevis. The washer spins freely when a preset load is applied. In the version shown in the center, a torsion coil rotates the washer; a compression-monitoring version is shown at the right.

washer once more will be free to rotate. This rotation indicates that the preset load has been exceeded.

The washer can be made to spin automatically at the moment the load is exceeded by adding a torsion coil (see figure, center). To make a shorter, more-compact indicating device for light loads, the compression sleeve can be replaced by a coil spring. For measuring compression loads, the design shown at the right in the figure can be used. The accuracy of the indicator is high whether a sleeve or spring is used. The washer-release load usually matches the preset load within ±10 percent.

Besides its obvious application as a load indicator, the device has uses as a remote indicator of a mechanical action. In fact, it was originally developed to indicate to the Space Shuttle orbiter crew that sufficient tension had been applied to remote latches to open the orbiter doors.

The rotating washer can also act as a sequencer, signaling an action to begin upon attainment of a certain load. It can be used, for example, to initiate a work cycle after stored energy has been built up in hydraulic or pneumatic power equipment. It can also be used as a remote, nonelectrical switch in hazardous environments.

This work was done by Walter T. Appleberry of Rockwell International Corp. for **Johnson Space Center.** *For further information, Circle 61 on the TSP Request Card.*
MSC-19511

Adjustable Holder for Transducer Mounting

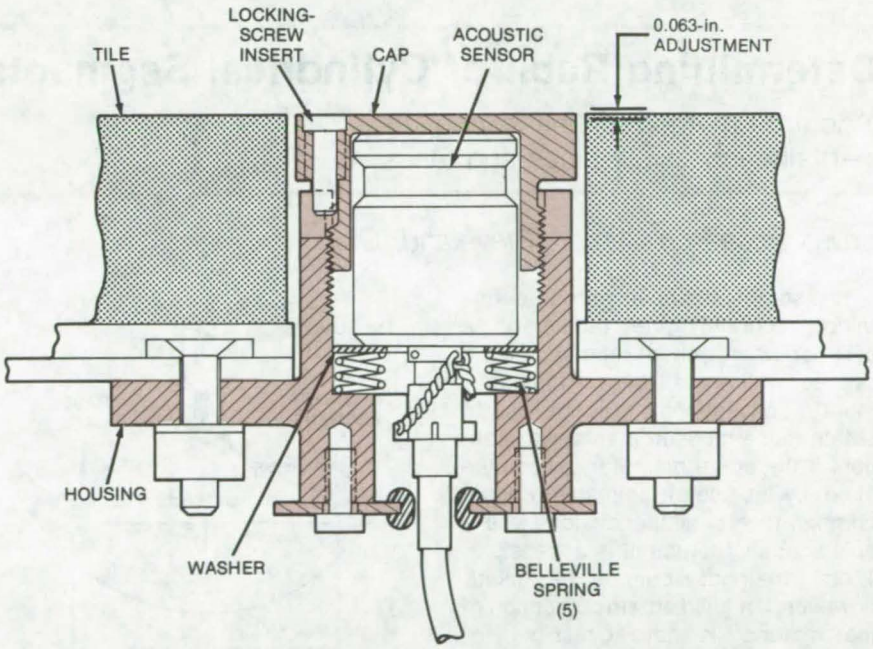
An acoustic sensor or other transducer is precisely positioned and loaded.

Lyndon B. Johnson Space Center, Houston, Texas

The positioning of an acoustic sensor, strain gage, or similar transducer is facilitated by the adjustable holder shown in the figure. Developed for installation on the Space Shuttle, it includes springs for maintaining uniform load on the transducer and an adjustable threaded cap for precisely controlling the position of the sensor with respect to the surrounding structure. This adjustment is critical on the Shuttle; the transducer must not protrude above the outer tile surface, or the aerodynamic flow will be disturbed.

As shown, the holder consists of a housing, a threaded cap, positioning springs, and a locking-screw insert. The sensor is placed on the springs in the housing, and the cap is installed and rotated until the sensor is at the desired height. An additional rotation of the cap by no more than 45° alines the locking-screw insert with one of four notches in the housing. With the notch and insert alined, the screw is threaded through the insert into the notch to lock the cap and sensor in position.

The five Belleville springs maintain uniform compressive load on the sensor as the cap is rotated. The load varies from 71 to 97 lb (316 to 431 N) over a height adjustment range of 0.063 in. (0.16 cm) for the Shuttle acoustic sensor. The cap is threaded at 20 threads/in. (8 threads/cm).



Precise Positioning of An Acoustic Sensor is made possible by this adjustable holder. This model, designed for the Space Shuttle, measures 2.0 in. (5.1 cm) in diameter by 1.5 in. (3.8 cm) in height.

This work was done by Richard C. Deotsch of Rockwell International Corp. for **Johnson Space Center.** *For further information, including engineering drawings of the holder, Circle 62 on the TSP Request Card.*
MSC-18371

An Evaluation of Low-Cost Payload Carrier

A payload-carrier concept and associated costs are evaluated in connection with experiments in space.

Marshall Space Flight Center, Alabama

A payload carrier designed for space vehicles is essentially a cargo carrier that supports, positions, and protects various equipment and materials used in conducting experiments in the weightless space environment. A payload-carrier concept has been evaluated for the Shuttle orbiter. Its details are presented in a report that evaluates the proposed design and analyzes the dimensions, weights, and costs of developing the concept.

The proposed carrier entited Materials Experiment Assembly II (MEA-II) is considered superior to previously developed models in size, weight, and cost to the user. The structure is a lightweight truss made of a stiff material with an insulated exterior. It could be custom sized to meet user needs. It consists of a series of rectangles that occupy most of the cylindrical volume of the orbiter bay. Most of these rectangles would be braced between two opposite corners to form triangles that, in turn, form a truss.

The report also includes a number of illustrations, tables, and charts giving a detailed picture of the proposed carrier.

This work was done by Vaughn H. Yost of **Marshall Space Flight Center.** *To obtain a copy of the report, "Device to Support, Position and/or Protect Equipment in the Shuttle Orbiter Bay," Circle 63 on the TSP Request Card.*

Inquiries concerning rights for the commercial use of this invention should be addressed to the Patent Counsel, Marshall Space Flight Center [see page A5]. Refer to MFS-25129.

Determining Radii of Cylindrical Segments

Accurate method for measuring partially accessible pipes and tubes

Lewis Research Center, Cleveland, Ohio

It is sometimes necessary to determine accurately the radius of a cylinder when only a segment of the cylinder wall is available for measurement. Conventional practice is to obtain these measurements with calipers if the entire diameter is accessible or by the use of templates, optical comparators, or similar devices where only a smaller segment is accessible. These methods cannot be used, however, if a full diametrical section of the material is not accessible for caliper measurement or if the size, condition, or maneuverability of the cylinder is not amenable to the use of template or comparator-type devices. A simple method has been developed by which either the inside or outside radius of a cylindrical segment may be accurately determined in these situations. This method employs a standard micrometer or depth gage with a ball-end rod and a fixed-length baseplate.

The procedure for measuring an inside radius is shown in Figure 1. The depth gage is placed on top of a rigid baseplate of known length L with the rod extending through a central hole in the plate. The ends of the plate rest on the inside wall of the cylinder, and the length of the baseplate (L) becomes a chord of the circle with a radius that is the same as the inside radius of the cylinder. The ends of the plate, being parallel, are readily alined with the longitudinal axis of the cylindrical segment. The depth gage is used in the conventional manner to measure

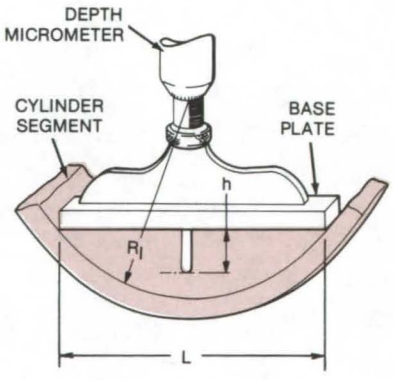


Figure 1. **Inside Radius** of a cylindrical segment is determined using a baseplate of known length and measuring the perpendicular distance from the center of the plate to the inside surface of the cylinder.

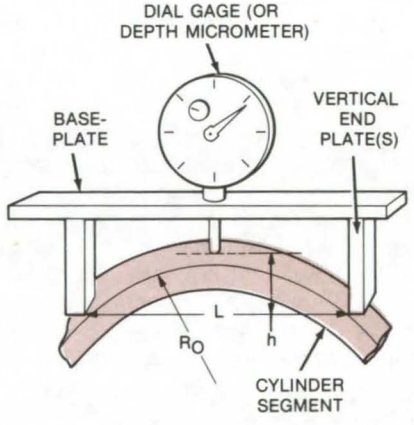


Figure 2. **Outside Radius** of a cylindrical segment is obtained using a baseplate with two identical vertical end plates separated by a known distance and measuring the distance h shown above.

the distance h between the baseplate and the cylinder wall. The inside radius of the cylinder (R_I) is then calculated by the formula

$$R_I = \frac{L^2 + 4h^2}{8h}$$

Outside radii can be determined by the same general method. Vertical end plates fastened securely to the baseplate allow it to span a convex surface, as shown in Figure 2. The points of contact of the end plates on the convex surface constitute the fixed L dimension of the formula for determining the radius. The h dimension is obtained by subtracting the depth reading obtained with the device resting on the convex surface from the zero-depth indication obtained by calibrating the device on a flat surface.

The new method is more adaptable in a variety of situations than are existing methods, and measurements can be obtained under conditions that may be difficult if not impossible using other methods. For example, this method could be used to measure accurately the radii of partially-exposed buried pipelines, or of pipes and ducts, in hazardous environments where manipulators must be used to handle tools.

This work was done by R. J. Buzzard of **Lewis Research Center.** *No further documentation is available.*
LEW-12826

Computer Programs

These programs may be obtained at very reasonable cost from COSMIC, a facility sponsored by NASA to make new programs available to the public. For information on program price, size, and availability, circle the reference letter on the COSMIC Request Card in this issue.

Overall Loudness of Steady Sounds

Loudness of vehicles, machinery, and other sources can be predicted.

The loudness (in sones) and loudness level (in phons) of any sound that is steady for a few tenths of a second can be calculated using a computer program derived from a new operational theory of loudness. The loudness theory is constructed from psychoacoustic and physiological data on mammalian (monkey) auditory systems. The computer program is valid if the sound spectrum is discrete or continuous and within the frequency range 20 to 23,000 Hz. The valid regime includes all sound pressures and bandwidths audible to humans with the possible exception of broadband (> 2,000-Hz bandwidth) white noise within 20 decibels of the loudness threshold, and sound near the pain threshold.

Generally, the only program inputs required are the mode of listening (free field or earphones) and the sound spectrum (determined analytically or from audio spectrum analysis). The bandwidths of the spectrum analyzer should be no greater than critical bandwidths for loudness, although the program applies for any bandwidth. [One-octave-bandwidth measurements of broadband sounds have yielded calculated loudness levels up to 2 phons greater than those obtained from calculations using one-third-octave data (which generally exceed critical bandwidths).] In the case of tones less than 10 Hz apart, which produce audible beats, it is necessary to specify the initial phases of the frequency components and the time following an initial time because the loudness of these steady sounds is phase and time dependent.

The operational theory from which the present loudness calculation procedure is derived takes into account the transmission characteristics of the auditory system, a squaring operation that occurs in the mechanical-to-electrical transduction in the inner ear, a channeling process (associated with critical bands for loudness), frequency interactions that result because neuron bandwidths exceed channel bandwidths, half-wave rectification in the auditory nerve, and the auditory integration time.

Among psychoacoustic phenomena accounted for by the theory are audible beats, the audibility of sounds consisting of subliminal components, critical bands for loudness, periodicity pitch, and pitch of the residue. The fundamental conceptual differences between this theory and earlier proposals are that loudness summation is replaced by power (or energy) summation and neural inhibition is replaced by discharge periodicity phenomena.

This computer program should permit prediction of the loudness of any steady sound including, for example, transportation noises, machinery noises, and other environmental noises, with possible additional applications to broadcasting, sound reproduction, establishment and enforcement of noise laws, and in fact, to any situation involving loudness.

This computer program supersedes the earlier computer program, reference LEW-11761, announced in NASA Tech Brief B72-10579.

This program was written by Walton L. Howes of **Lewis Research Center** *and Virginia R. Canright of the U.S. Army Research & Technology Labs. The theory behind this computer program is discussed in NASA RP-1001 [N79-25753/NSP], "Overall Loudness of Steady Sounds According to Theory and Experiment" [$7.25]. A copy may be purchased [prepayment required] from the National Technical Information Service, Springfield, Virginia 22161. For further information, Circle F on the COSMIC Request Card.*
LEW-12914

Nonlinear Structural Analysis

AGGIE I — A moderately-sized finite-element program

The development of computer programs for nonlinear structural analyses has progressed from special-application programs to large, generalized programs. Many of the larger general-purpose programs were

(continued on next page)

originally developed for linear structures and subsequently were extended to include a nonlinear capability.

The AGGIE I program is a moderately-sized finite-element program that was developed specifically for nonlinear structural analysis. It is based on two- and three-dimensional isoparametric solid elements. AGGIE I accounts for nonlinearities due to large displacements, large strains, and nonlinear material behavior. Material models incorporated include linear elastic, nonlinear elastic, orthotropic, nonlinear elastic incompressible, and elastic plastic.

Both static and dynamic response predictions are possible. A displacement incrementation capability is included to predict buckling and postbuckling response. Provisions are included for both conservative and nonconservative (deformation-dependent) loadings. Dynamic dimensioning allows efficient use of available high-speed memory. Problem and available-memory sizes are used to select either the in-core or out-of-core equation solver.

AGGIE I solves a set of linearized incremental equilibrium equations for each time step or load step. To ensure that equilibrium is being satisfied at each step, a modified Newton-Raphson method is used to perform the equilibrium iteration. During the iterative process, the tangent-stiffness matrix is updated periodically when convergence deteriorates; alternately, the matrix may be updated at a user-specified frequency. In dynamic analyses, a time integration procedure is invoked using either the Wilson or Newmark method.

All elements and most material models used in AGGIE I are based on a total Lagrangian formulation. Several material models using the updated Lagrangian solution are also available. Elements currently available include a three-dimensional truss element, a two-dimensional isoparametric solid element with 4 to 8 nodes, and a three-dimensional isoparametric solid element with 8 to 21 nodes. The two-dimensional element is reducible to a constant-strain triangular element, and the three-dimensional element is reducible to a constant-strain tetrahedron. Inputs consist of node, element, and control data along with loads, forces, and damping information. There are a restart capability and a rudimentary substructure option. Outputs include both tabular and plotted results.

This program is written in FORTRAN IV for batch execution and has been implemented on an IBM 360-series computer with a problem-dependent memory requirement with a minimum requirement of approximately 400K of 8-bit bytes. The program produces plotted output using standard CALCOMP plotting routines. AGGIE I was developed in 1977.

This program was written by Walter E. Haisler of Texas A&M Research Foundation for **Marshall Space Flight Center.** *For further information, Circle G on the COSMIC Request Card.*
MFS-25122

Redundant Structures at Elevated Temperatures

Inelastic analysis to determine safety under loads

In many structural systems it is desirable to perform an analysis to determine how safe the structure is when subjected to "yielding" loads. The FRAME1 computer program analyzes, in both the plastic and elastic ranges, redundant structures subjected to thermal and mechanical loads.

In the program model, as the structure strains, the various elements in each cross section behave in accordance with the assumption that plane sections remain plane. The axial bending stresses must balance the internal loads when strains are converted to stresses and integrated over the cross section. A neutral axis shift may be required to achieve this balance. Some elements of the structure may be loaded beyond their buckling capacity, limiting the stress-carry capabilities of those elements and further redistributing loads on the cross section.

A user may compute the cross-sectional load balance using either a Ramberg-Osgood stress-strain relationship or a "perfectly plastic" relationship. The load moment is balanced by iteration at each cross section in the structure.

Input data include structure description, cross-section data, material properties, mechanical loads, and temperature data. Outputs include a description of the user-defined structure, a description of the automatically-determined cutback structure and redundants, the redundant values and internal loads for each iteration, and for each cross section, a detailed look at stresses and strains for the final moment axial-load distribution.

This program is written in FORTRAN IV for batch execution and has been implemented on a CDC CYBER 70-series computer with a central memory requirement of approximately 110K (octal) of 60-bit words. FRAME1 was developed in 1977.

This program was written by Larry I. Guidry and Gerald H. Mintz of Rockwell International Corp. for **Johnson Space Center.** *For further information, Circle H on the COSMIC Request Card.*
MSC-18476

Aerodynamic Performance of Jet-Flap Wings

Vortex-lattice method of analysis

During the past few years there has been renewed interest in the aerodynamics of the high-lift blown-jet, or jet-flap, wings. Although this concept was originally proposed nearly 40 years ago, prospective new applications of the jet-flap principle to V/STOL aircraft and helicopter rotors have raised a demand for a better understanding of the jet-flap wing. A computer program has now been developed to help analyze the performance of jet-flap wings.

A fast and easy-to-use prediction technique, it generates accurate solutions for a wide range of wing geometries and trailing-edge jet momentum distributions. The analysis is based on an optimized vortex-lattice approach and has been shown to result in the rapid convergence of both the overall and distributed loadings.

This generalized approach allows treatment of swept tapered-wing planforms with nonuniform part-span blowing.

The vortex-lattice method for the analysis of lifting-surface aerodynamics has become a widely used technique during the past decade. It can be readily applied to configurations having complex geometries. Relatively simple mathematics are used for computation, and no special a priori loading-function assumptions are needed.

The analysis considers the steady, subsonic flow of an inviscid fluid over a thin jet-flap wing. The problem is treated within the framework of linearized lifting-surface theory. A swept tapered-wing planform is considered, with the wing root chord normalized to unity. Consistent with thin-wing theory, it is assumed that the thickness of the trailing jet is zero; however, the jet is assumed to have a finite distribution of momentum flux in the span direction and to support a discontinuity of pressure. It is further assumed that the momentum flux is constant along the jet in each plane of the stream direction.

The entire lifting surface, the wing plus the jet, is subdivided into a number of lattices with a swept horseshoe vortex of initially unknown strength located in each. The bound portion of the vortex is placed along the individual lattice quarter chord with the trailing vortex legs extending to downstream infinity. To solve for the unknown vortex strengths, the total upwash induced by all the horseshoe vortexes is evaluated at each control point and is used to satisfy the boundary conditions. Both the overall and distributed aerodynamic loadings on the jet-flap system can then be calculated in a straightforward manner.

These loadings consist of both a circulation component, which includes the usual circulation due to camber and angle of attack as well as the induced "supercirculation" arising from the jet, and a jet reaction component, which is equivalent to the integrated contribution of the jet from the trailing-edge to downstream infinity. The total lift coefficient, total pitching-moment coefficient, and the mean aerodynamic chord are calculated. Finally, the induced drag coefficient from the wing circulation can be evaluated.

The computer program is written in FORTRAN IV for batch execution and has been implemented on a CDC 6000-series computer with a central memory requirement of approximately 40K (octal) of 60-bit words. The program accesses the International Mathematics and Statistics Library (IMSL) to obtain numerical solutions to a set of linear equations using Gaussian elimination. The user of this program should have access to IMSL or similar routines. The program was developed in 1976.

This program was written by Gary R. Hough of Vought Corp. for **Ames Research Center.** *For further information, Circle J on the COSMIC Request Card.*
ARC-11215

Transonic Flow Past Swept Wings

Numerical analysis to predict characteristics

The FLO-22 computer program aids in the numerical analysis of the transonic potential flow past a lifting, swept wing. The development of profile shapes capable of efficient operation in the transonic regime has spurred interest in aircraft designed specifically to operate at near-sonic speeds or efficiently at high-subsonic speeds. The ability to predict accurately the aerodynamic characteristics of the complete three-dimensional wing would allow many detailed trade-off studies to be performed without recourse to wind-tunnel testing of every design variation.

FLO-22 uses a relaxation method to solve a finite-difference approximation of the full-potential equation for the transonic flow past a configuration consisting of a wing of arbitrary planform and dihedral extending from a symmetry plane or wall. Comparisons of FLO-22 calculated results with experimental data for both conventional and supercritical transport wings have shown good agreement.

The finite-difference approximation for the full-potential equation used in FLO-22 is the rotated-difference scheme introduced by Jameson. In the FLO-22 program, the flow is analyzed in coordinate planes parallel to the free-stream velocity vector with symmetry conditions applied on a single coordinate surface. The span-direction coordinate lines are alined with the wing leading edge to allow the use of a fine mesh in that sensitive region. For wings of appreciable sweep the coordinate system used becomes highly nonorthogonal, but it allows accurate representation of the finite-difference boundary conditions.

In the absence of strong shock waves, the steady, inviscid motion of a compressible fluid is accurately approximated by the standard equation for the velocity potential. The relaxation scheme used to solve the finite-difference equations simulates an artificial time-dependent process that converges to the desired solution of the steady-state equation. At each iteration step, the three-dimensional solution is obtained by solving the equations in streamwise planes by using a successive-line overrelaxation algorithm. To speed convergence, calculations can be performed on succeedingly finer grids by using interpolations of the proceeding solution as initial values.

This program is written in FORTRAN IV for batch execution and has been implemented on a CDC 6000-series machine with a central memory requirement of approximately 145K (octal) of 60-bit words. For plotted output, access to a CALCOMP plotting system is required. The FLO-22 program was developed over the period 1974-76.

This program was written by D. A. Caughey of Cornell University and Antony Jameson of New York University for **Langley Research Center.** *For further information, Circle K on the COSMIC Request Card.*
LAR-12446

Transonic Airfoil Analysis and Design

Efficient and accurate numerical data for transonic region

Recent interest in improving performance in the transonic flight regime has created the need for an effective numerical tool for the design and analysis of transonic airfoils. The TRANDES program provides the aircraft engineer with an accurate and efficient tool for the analysis of steady, irrotational, transonic flow over a specified two-dimensional airfoil in free air. The program can also be used to design airfoils having a prescribed pressure distribution, including the effects of weak viscous interaction.

The inviscid flow field is calculated by solving the full, inviscid, perturbation-potential flow equation on a Cartesian grid, which is usually alined relative to the airfoil chord line. Efficiency of the method is improved by stretching the coordinate plane so that the infinite physical plane is mapped into a finite computation plane. In this manner, boundary conditions at infinity can be applied directly. TRANDES has been found to yield accurate solutions efficiently for biconvex, conventional, and aft-cambered airfoils.

TRANDES replaces the governing second-order partial differential equation with a nonconservative system of finite-difference equations. A form of Jameson's rotated difference scheme is included at supersonic points. The difference equations are solved using a column-relaxation scheme. In order to obtain rapid convergence, it is best to apply the scheme on several different grids. In the analysis case, the difference equation is first solved on a very coarse grid. The grid is iteratively reduced using interpolated values from preceding grids as initial conditions.

In the inverse case, used for airfoil design and modification, the initial shape of the airfoil must be assumed for the specified pressure distribution. The initially assumed shape is not critical because of the rapid convergence properties of the iterative column-relaxation scheme used. After the design solution is obtained, the resultant shape is treated as a displacement surface so that the displacement thickness is subtracted to obtain the actual airfoil surface. The boundary layer characteristics are determined using the Nash-Macdonald method with smoothing. The program can include the effects of boundary layer interaction, but no correction is included for the effects of wake curvature; and an empirical approach is incorporated in the trailing-edge region.

This program is written in FORTRAN IV and has been implemented on a CDC CYBER 175 with a central memory requirement of approximately 111K (octal) of 60-bit words. TRANDES was developed in 1977.

This program was written by Leland A. Carlson of Texas A. & M. University for **Langley Research Center.** *For further information, Circle L on the COSMIC Request Card.*
LAR-12354

Helicopter Sling Loads

Simulation program for system analysis

A new computer program compares various control-system concepts for improving the handling qualities of single-rotor helicopters carrying relatively-large external sling loads. The use of a sling can add capacity and flexibility to the transport prospects of a helicopter, but it also seriously impairs the handling characteristics of the craft. Several ideas have been introduced to improve the handling characteristics of a sling-loaded helicopter: control jets at the load, a movable cable-attachment point on the helicopter, and a cable-angle feedback into the helicopter stability augmentation system.

The computer program developed to test these and other ideas helps to circumvent expensive prototyping and field testing. Comparisons between (1) computed data and flight data, (2) simulation-system values and flight-test data, and (3) pilot evaluations of simulation and actual-flight conditions have been very favorable.

The overall mathematical model used in the program consists of numerous submodules that describe various components of the total dynamic system. The atmospheric model has variable air density, winds with variable magnitude and direction, and variable-intensity turbulence. The helicopter control-system model converts the pilot's cyclic-control-stick, collective-stick, and pedal inputs into main- and tail-rotor cyclic and collective-pitch data. Nonlinear models for the main and tail rotors define thrust, drag, and side forces as well as hub and force moments representative of articulated rotors over a wide range of airspeeds.

The rotor models account for variable inflow velocity, variable rotor speed, blade twist, tip loss, blade coning, blade flapping, actuator dynamics, flapping-hinge offset, and tail-rotor flapping-hinge cant angle. The automatic flight-control system model is based on the system used by the U.S. Army CH-54 helicopter. The fuselage aerodynamics model defines nonlinear lift, drag, and side forces as well as pitching, rolling, and yawing moments in terms of a wide range of angle of attack, sideslip, rotor downwash, body angular rates, and dynamic pressure.

A similar aerodynamic model is used for the external load. The load-suspension model defines cable tension in one or more cables and the resulting forces and moments acting on the helicopter and the external load. To approximate the forces and moments acting on the load during pickup and landing, a ground-contact model is included.

A general set of nonlinear, rigid-body, equations of motion for both the helicopter and external load determines the motion of each body with respect to a flat, nonrotating Earth. A well-tested algorithm determines the trimmed helicopter-control positions, helicopter attitude, and load position and attitude. The computer program was developed for real-time flight simulation; it accepts analog-to-digital converted input and generated output for conversion to analog for use in the simulation exercise.

This program is written in CDC FORTRAN and COMPASS with an

overlay structure for real-time execution. The program has been implemented on a CDC CYBER 175 with a central memory requirement of approximately 54K (octal) of 60-bit words. For plotted output, a CALCOMP 763 30-inch plotter and CALCOMP software library are required. The program was developed in 1979.

This program was written by John D. Shaughnessy and Kenneth R. Yenni of **Langley Research Center** *and Thomas N. Deaux of Sperry Rand Corp. For further information, Circle M on the COSMIC Request Card.*
LAR-12557

Wing and Leading-Edge Thrust

Linearized wing theory is used to predict thrust at supersonic speeds.

Leading-edge thrust is an important factor in the aerodynamic performance of wings at subsonic speeds. This force results from the upwash field ahead of the wing, the high local velocities, and accompanying low pressures generated as air flows around the leading edge to the upper surface from a stagnation point on the undersurface. The high aerodynamic efficiency of wings with a large aspect ratio depends directly on the presence of leading-edge thrust to counteract the drag arising from pressure forces acting on the remainder of the airfoil.

Numerous techniques are available for predicting leading-edge thrust at subsonic speeds. Leading-edge thrust plays a reduced role at supersonic speeds. However, accurate thrust predictions are still considered very important in the analysis of wings at supersonic speeds. For low supersonic speeds and for wings with well-rounded leading edges, an appreciable amount of leading-edge thrust may be developed. Furthermore, these effects can appear with flow reattachment in an associated phenomenon, the formation of leading-edge vortex flow. A computer program was developed to predict the leading-edge thrust for wings of arbitrary planform at supersonic speeds.

The methods used in the program are based on linearized wing theory. The magnitude of the leading-edge thrust developed by a thin lifting wing is dependent on the upwash just ahead of the leading edge and on the airfoil camber surface just behind the leading edge. The influence of both of these factors is reflected in the pressure distribution in the vicinity of the leading edge. The program first calculates the lifting pressures, lift coefficients, drag coefficients, moment coefficients, and lift distributions by using an aft-element sensing technique. Next, an empirical function is used to calculate a set of adjusted pressure-coefficient locations along the leading edge. This information is then used to determine the limiting value of the singularity parameter and from this, the value of the local leading-edge thrust coefficient. The leading-edge thrust coefficient and distribution are calculated on a flat-plate as well as a cambered and twisted wing for the arbitrary planform that was specified.

This program is written in FORTRAN V for batch execution and has been implemented on a CDC CYBER 175 with a central memory requirement of approximately 74K (octal) of 60-bit words. This program was developed in 1978.

This program was written by Harry W. Carlson and Robert J. Mack of **Langley Research Center.** *For further information, Circle N on the COSMIC Request Card.*
LAR-12516

Spacecraft Trajectory

Simulation program for long-range missions

Two programs, Hiltop I and Hiltop II, generate optimum trajectory data for electric propulsion missions of interest in the exploration of the solar system. Hiltop I evaluates electric propulsion systems and may, in the hands of a skilled analyst, efficiently simulate a wide variety of interplanetary missions. It uses numerical integration of the two-body, three-dimensional equations of motion and the Euler-Lagrange equations. It contains transversality conditions that permit the rapid generation of converged maximum-payload trajectory data and allows the optimization of numerous other performance indices for which no transversality conditions are included.

In addition to optimizing the thrust direction and on/off switch times, other significant performance parameters that can be optimized are jet-exhaust speed, power level, hyperbolic excess speeds, launch-asymptote geocentric declination, flight time, and launch date. The ability to simulate constrained optimum solutions, including trajectories having specified propulsion time and constant-thrust cone angle, are also available. Performance requirements for a variety of launch vehicles may be determined.

Hiltop I may simulate missions having as many as four targets (celestial objects) along a trajectory. Various types of encounter such as rendezvous, stopover, orbital capture, and flyby can be accommodated. One target is designated as the "primary" target (which may be absent in such missions as, for example, extra-ecliptic probes). In addition, up to three "intermediate" targets are permissible, such that the intermediate targets are visited prior to the primary target. At present, intermediate targets must be relatively massless objects such as comets and asteroids, because the gravitational perturbing effect of an intermediate target on the spacecraft is not coded into the program. In addition, the spacecraft is optionally permitted to swing by the primary target and continue onward ballistically to up to five "post-swingby" targets.

Hiltop II is a more realistic propulsion-system model involving the actual ion beam current and voltage of the thruster. The power processor efficienty, ion thruster efficiency, and thruster specific impulse are modeled as variable functions of the power (solar, nuclear, or other) available to the propulsion system. The number of operating thrusters are staged, and the beam voltage is selected from a set of five (or less) constant voltages. The minimum and maximum numbers of operating thrusters, the minimum throttling ratio, and the maximum input power to an individual thruster

(continued on next page)

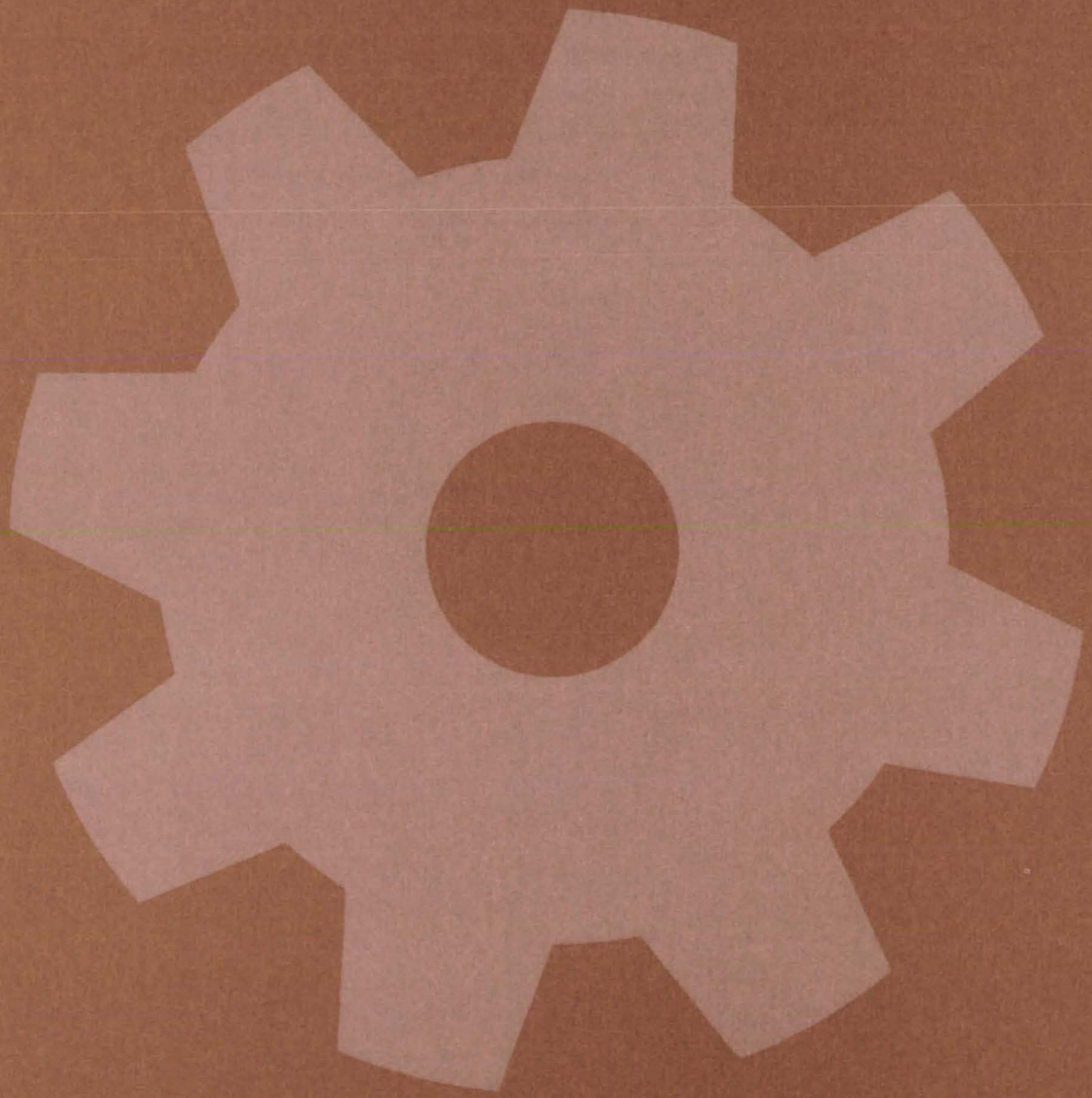
are specified as input data. The constant beam voltages may be optimized individually or collectively.

The new propulsion-system logic is activated by a single program-input key; program modifications have been designed to retain the Hiltop I program within the framework of the new logic, so that Hiltop I input data files (with no modifications required) will run the Hiltop II program version and produce identical results as before. The capability of simulating solar array degradation and the capability of simulating the new spacecraft model under the Launch Vehicle (LVI) mode are contained in Hiltop I and not in Hiltop II.

The programs are written in FORTRAN IV for use on an IBM 360 or UNIVAC 1100 computer.

This program was written by J. L. Horsewood and F. J. Mann of Business & Technological Systems, Inc., for **Lewis Research Center.** *For further information, Circle P on the COSMIC Request Card.*
LEW-13248

Machinery



Hardware, Techniques, and Processes

545 High-Acceleration Cable Deployment

546 A Simple Self-Sealing Plug

547 Miniature Motor-Driven Instrument Valve

548 Flexible Sliding Seal

549 Improved Table-Saw Guard

550 Recirculating Sprayer for Fiber-Filled Paints

550 Screw/Stud Removal Tool

551 A Tool for Installation and Removal of Cylindrical Baffles

552 Simplified Installation of Thrust Bearings

High-Acceleration Cable Deployment

A communication cable survives up to 20,000 g deployment for monitoring below-surface probes.

Ames Research Center, Moffett Field, California

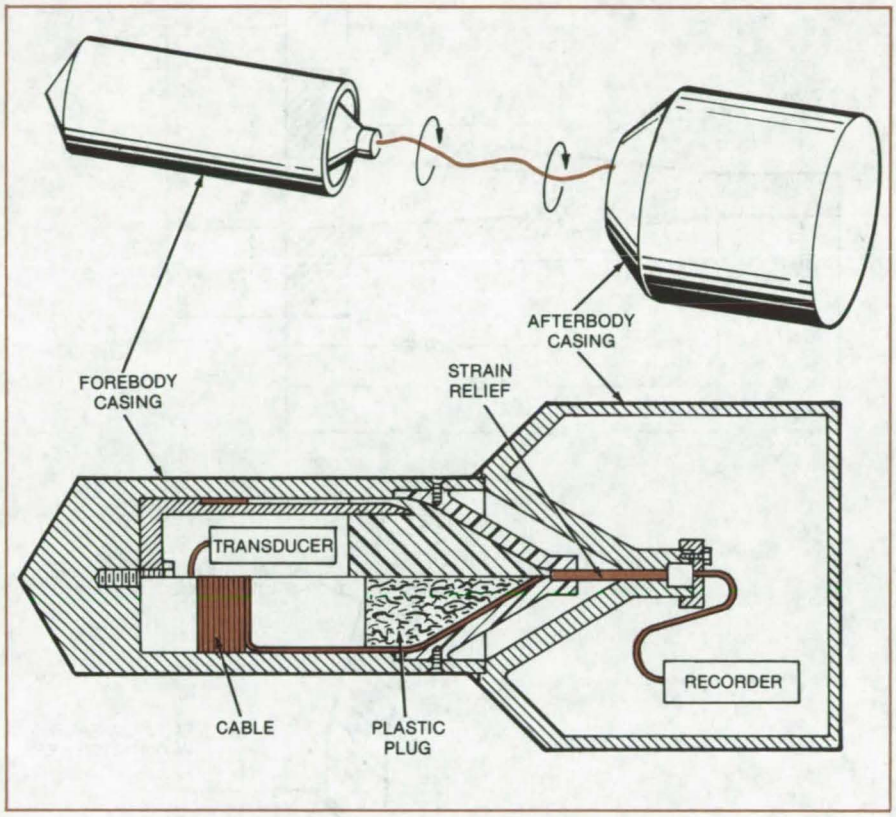
A prototype high-acceleration umbilical-cable deployment allows electrical communication between aboveground instrumentation and a ballistic projectile below the surface.

In its original application as a communications link for an instrument probe that is fired up to 40 feet (12 m) into the Martian surface, the deployment uncoils the cable without breaking at accelerations up to 20,000 g's and velocities up to 500 ft/s (150 m/s). A similar design could be used in the study of sea ice and in other surface-penetration studies.

The projectile forebody (see figure) includes a ballistic casing with a plastic drag funnel mounted over the rear opening. The cable is coiled in a single layer on a cylindrical spool within the casing. There is a slight gap between the cable and the inner wall of the casing, which allows the cable to feed along the wall and out of the hole in the center of the funnel. The interior of the funnel and a portion of the spool cavity are filled with a low-density, cellular-plastic plug that sandwiches the cable between the plug and the inner wall of the funnel. The end surface of the spool and inner surface of the funnel at its opening are curved to permit smooth acceleration and reduce bending stresses and to reduce wear on the cable as it is deployed. The cable is made of a high-tensile-strength (200,000 psi) beryllium/copper alloy with good elongation and low electrical resistance. A tough, lightweight, coating (similar to enamel) insulates the wire.

The afterbody contains a funnel with a flexible, stepped-diameter, strain relief that protects the cable at the point of greatest flexing. The cable passes through the strain relief, and the space between the cable and strain relief is filled with an adhesive.

The forebody is joined to the afterbody with a light friction fit. Alternate methods of attachment might include detents or shearpins.



The **Cable Deployment** is shown at rest and as the cable is being deployed. The plastic plug and the funnels in the forebody and afterbody absorb the cable rotational energy. Otherwise, the energy could rupture the cable.

The forebody can be separated from the afterbody by a rocket, or they can be fired as a unit at a target that stops the afterbody on impact (the forebody would continue, deploying the cable).

As the forebody moves away from the afterbody, the cable unwinds and cuts and grinds a passageway in the plastic plug. The plug and funnel thus allow the cable to yield its rotational energy to friction. (The afterbody funnel has the same effect.)

The prototype was fired at 150 m/s at an aperture in a plywood/aluminum target. The target stripped the afterbody off the forebody with a deceleration of 20,000 g's; the forebody continued until it was stopped in a plastic- and particle-board-filled box. The cable survived the 20,000-g deployment.

This work was done by Christopher E. Barns, Thomas N. Canning, Bobby Gin, Robert W. King, and James P. Murphy of **Ames Research Center.** *For further information, Circle 64 on the TSP Request Card.*

This invention is owned by NASA, and a patent application has been filed. Inquiries concerning nonexclusive or exclusive license for its commercial development should be addressed to the Patent Counsel, Ames Research Center [see page A5]. *Refer to ARC-11256.*

A Simple Self-Sealing Plug

An inexpensive self-expanding plug makes a convenient low-pressure seal.

Lyndon B. Johnson Space Center, Houston, Texas

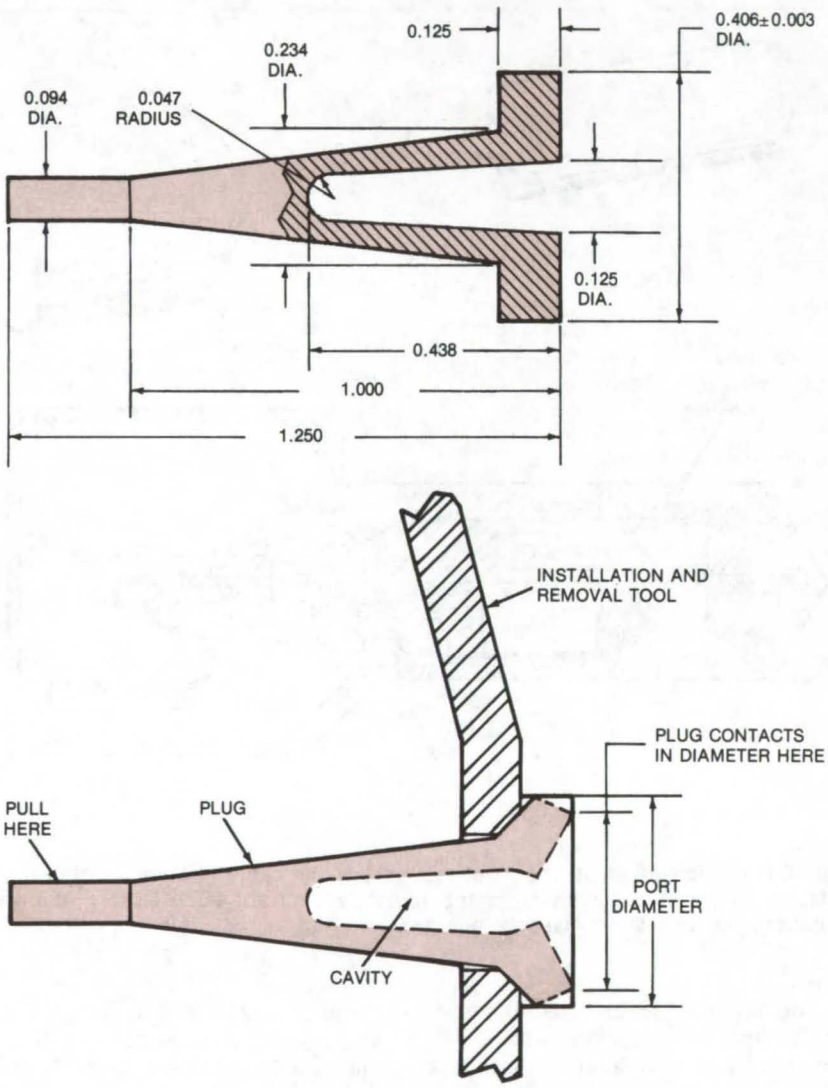


Figure 1. This **Self-Sealing Plug** has an internal cavity to accommodate contraction and expansion of the sealing edge during the installation. A plastic installation tool has a hole that fits over the plug for contracting the sealing edge to a diameter small enough to fit the port. As the tool is removed, the sealing edge expands to its original shape, sealing the port. The plug is removed using the same tool or by pulling the tab.

A simple elastomeric plug seals round ports and holes better than regular cork. The plug is inserted with a plastic tool that squeezes it to a diameter smaller than the port opening. Once the tool is removed, the plug self-expands to its original shape, exerting stronger pressure to the sealed surface than a cork. The plug is less expensive to make than screw-on or cam-expanded seals.

As shown in Figure 1, an internal cavity in the plug accommodates the contraction and expansion during the installation; a molded pull tab makes handling easier. The tool is simply a piece of transparent plastic with a hole smaller than the plug. The tool handle is angled for convenient handling.

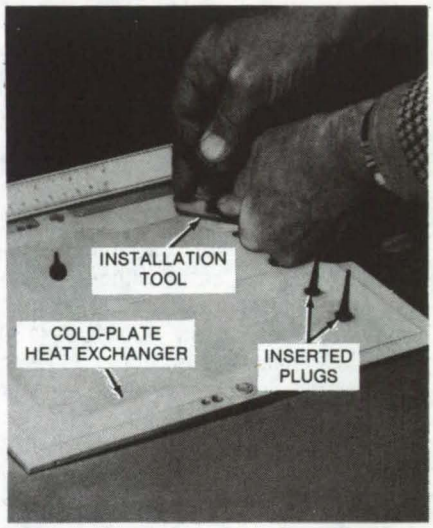


Figure 2. These **Sealing Plugs** successfully protected portholes of the Space Shuttle cold-plate heat exchangers during the manufacturing steps.

During the installation, the tab is pulled through the hole in the tool until the sealing edge tapers to a diameter smaller than the port opening. The plug is inserted into the port and the tool removed, releasing the plug to expand and seal the port. The plug is removed using the same tool or by merely pulling the tab.

The plugs were successfully used as temporary seals on ports of the Space Shuttle cold-plate heat exchanger (Figure 2). The ports were protected during the manufacturing, cleaning, and plating operations.

This work was done by Emil P. Ruppe of Rockwell International Corp. for **Johnson Space Center.** *No further documentation is available.*
MSC-19635

Miniature Motor-Driven Instrument Valve

For applications requiring pilot valves for control devices

Lewis Research Center, Cleveland, Ohio

Many pressure measurements are taken during testing in wind tunnels and engine test stands. The pressure transducers used for these measurements require frequent recalibration because the transducers are not stable for long periods of time. A valve was needed that could be operated by computer command to connect alternately the pressure transducers to known sources of pressure for calibrating purposes. It had to withstand pressures up to 600 psi, (4.2×10^6 N/m^2); commercially available valves used for this purpose withstand pressures of only 300 psi (2.1×10^6 N/m^2).

The valve, shown in Figure 1, consists of a small geared reversible motor, operated by a momentary contact closure, which drives a shaft with O-rings placed to seal selected ports. The shaft rotates and also moves axially, causing the ports to be alternately connected and disconnected. Electrical control of the valve is provided by limit switches and relays as shown in Figure 2.

The valve can be made in various configurations, such as 6-pole double throw, 12-pole single throw, etc. The valve can connect a common port to any one of many instrument transducers.

The new instrument valve design has a number of advantages over other available valves. Less precision machining of parts is required; therefore the machining operations are less expensive. Seals are made with O-rings, which are easily replaceable and inexpensive; and the valve uses less power.

This instrument valve can be used in any application requiring pilot valves for control devices.

This work was done by Herbert L. Minkin of **Lewis Research Center.** *No further documentation is available.*

Inquiries concerning rights for the commercial use of this invention should be addressed to the Patent Counsel, Lewis Research Center [see page A5]. Refer to LEW-13195.

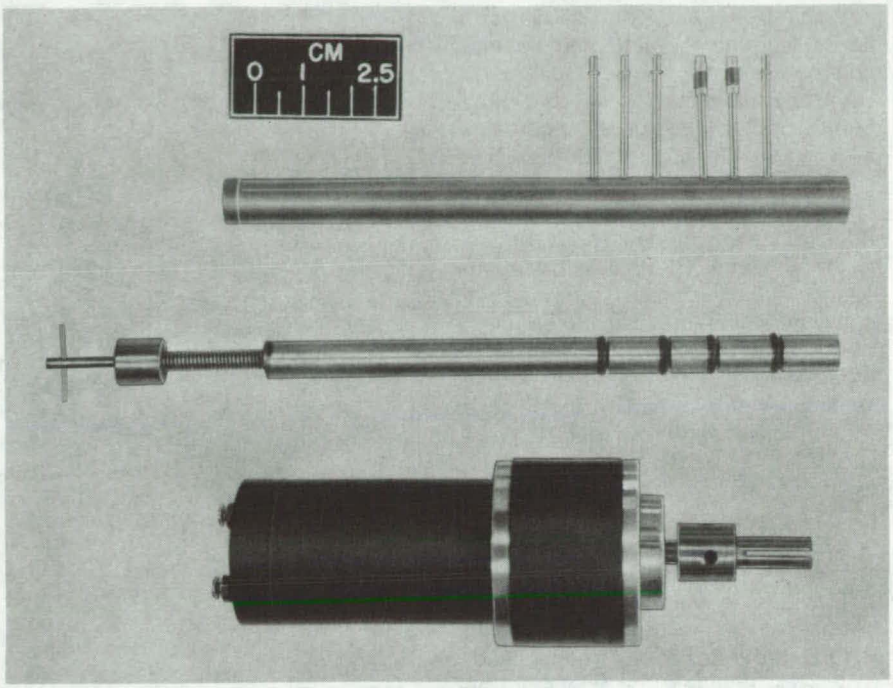


Figure 1. **Miniature Motor-Driven Instrument Valve** has been designed and built. It consumes one-tenth the power of previously-used instrument valves, withstands up to 600 psi, and can be operated by computer command.

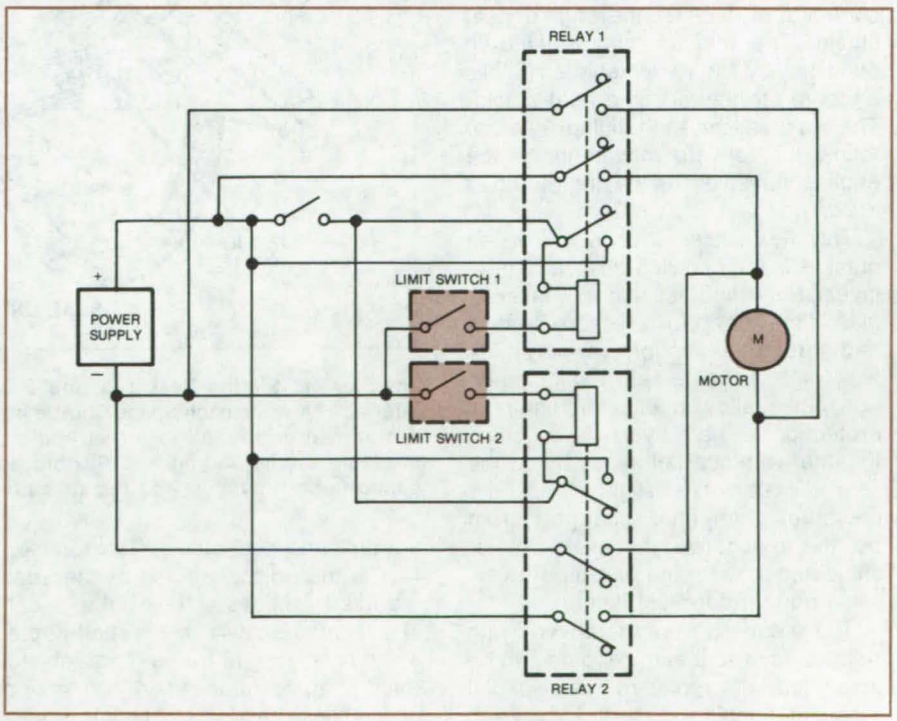


Figure 2. **Control Circuit** for the valve shown in Figure 1 consists primarily of limit switches and relays.

Flexible Sliding Seal

Composite seal withstands temperatures up to 1,600° F.

Lyndon B. Johnson Space Center, Houston, Texas

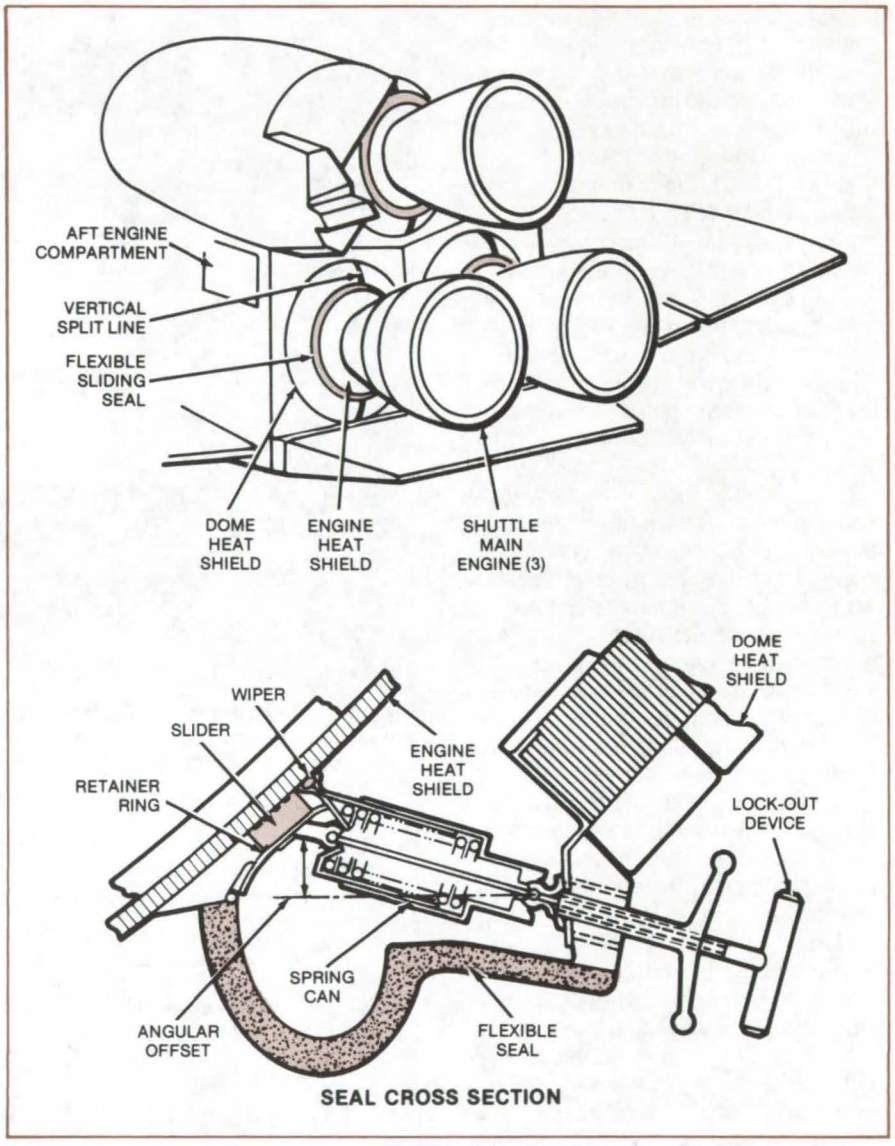
A circular seal both slides and flexes to accommodate relative motion between two sealed members. Originally developed for the Space Shuttle orbiter (see figure), it contains a sliding seal to accommodate engine gimbaling and a flexible seal that absorbs the forward motion at high thrust of the engine heat shield relative to the airframe. Other possible applications are in the support structures of heavy machinery and vehicle engines.

The seal can withstand temperatures up to 1,600° F (871° C) while sealing against moderate positive (crush) and negative (burst) pressures. It vents the interior to the exterior at a crush pressure difference of 1.32 psi (9,100 N/m^2) and a burst pressure difference of 2.65 psi (18,200 N/m^2).

The sliding seal consists of a silicone-rubber wiper coated with PTFE and a series of electrodeposited-nickel-on-graphite slider blocks. Forty-eight spring cans in a retainer ring exert pressure on the graphite block so that they slide and seal against the spherical surface of the engine heat shield. The retainer ring is held in position by four articulated links anchored to the airframe heat shield. The links allow the sliding seal to follow the forward movement of the engine heat shield as the engine thrust builds up.

The flexible seal consists of an outside layer of silica-fiber fabric, a layer of thermal insulation, a layer of glass-fiber fabric for pressure sealing and structural support, a polyimide film for a pressure-seal backup, and iron/nickel-alloy mesh for lightning protection. The layers are sewn together with quartz thread. Since the seal flexes only slightly as the pressure differential changes from positive to negative, the layers are not subjected to wrinkling or shape reversals and therefore last longer.

The seal can be removed with relative ease so that the engine can be inspected or replaced. A special "lockout" tool is inserted in each spring and turned to lock the can to the airframe heat shield. The retainer ring is then disconnected at the seal meridian splices. (Like the heat shields, the seal is in two half-circle sections.) The airframe heat shield (plus seal) is removed in two major assemblies, and the engine heat shield is removed in two halves.



The Flexible Sliding Seal is a ring about 7 feet (2.1 meters) in diameter at the interface between each Space Shuttle main engine and the engine compartment. The design can be resized for other applications. The cross-sectional view shows the structure of the sliding and flexible portions. The curvature of the flexible seal supports both positive and negative pressures without wrinkling.

This work was done by Edwin L. Wallenhorst of Rockwell International Corp. for **Johnson Space Center.** *To obtain a copy of a report describing the development of the Space Shuttle aft-heat-shield seal, Circle 65 on the TSP Request Card.*
MSC-18467

Improved Table-Saw Guard

Counterbalanced guard reduces damage in cutting fragile foam-type materials.

Lyndon B. Johnson Space Center, Houston, Texas

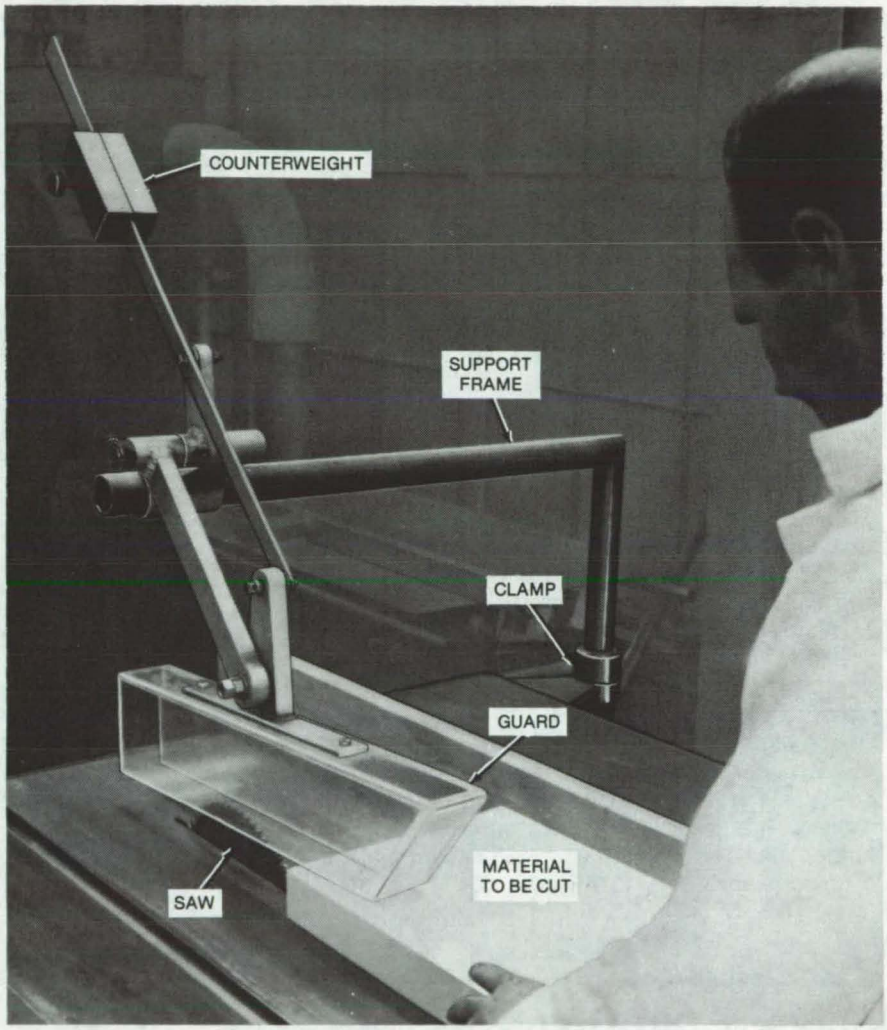
An improved table-saw guard, as shown, is held by a side support frame with a counterbalanced linkage that reduces the weight of the guard on the part being cut and permits easier operation. Slotting cuts can be made that are not possible with conventional guards supported by struts through the saw slot.

The guard is a transparent plastic enclosure held by a side-attached overhead support arm. The vertical section of the arm can be unclamped to rotate the guard off the table. The arm is combined with an adjustable-counterweight guard linkage to reduce the downward force holding the guard on the sliding material being cut. The counterweight adjustment is limited so the guard will always have adequate downward movement.

The lighter contact of the counterbalanced guard on the material being sawed reduces damage to foam and other fragile materials. This has been verified by successfully cutting fragile Space Shuttle exterior insulation. In addition, cuts are better controlled than on saws with conventional guards, making it possible to produce slot and step cuts. Thick materials are easily pushed under the guard with reduced force.

Possible modifications include building an electrical interlock so that the saw will not operate with the guard out of position. Presently, the vertical post is kept clamped in position until the interlock is developed. Another feature that could be added is "kickback" control.

This work was done by Benjamin R. Dunn and Paul P. Zebus of Rockwell International Corp. for **Johnson Space Center.** *No further documentation is available.*
MSC-19550



This **Counterbalanced Table-Saw Guard** makes a lighter contact on materials being sawed. The cuts are better controlled, and damages to fragile foam-type materials are reduced. The overhead support makes it possible to perform slot and step cuts, and thick materials are pushed under the guard with less force. The table shown uses a 12- to 14-in. tilting arbor saw.

Recirculating Sprayer for Fiber-Filled Paints

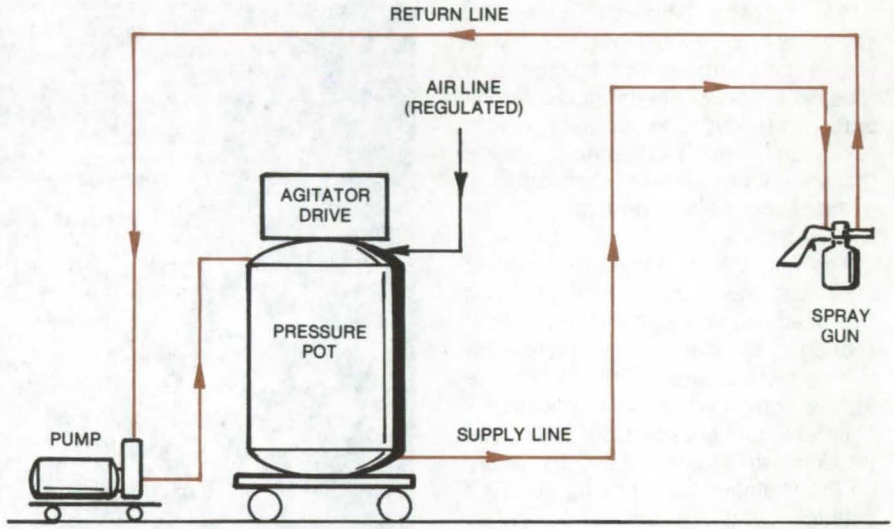
Improved equipment prevents suspended material from plugging lines and orifices.

John F. Kennedy Space Center, Florida

A new recirculating paint sprayer applies a spray of coarse filler in a highly volatile solvent. The sprayer was developed for applying an insulation material containing epoxy resin, glass fibers and inert fillers suspended in chlorinated solvents. The combination of coarse fibers and volatile solvent tended to clog lines and orifices when conventional recirculating sprayers were used. The new sprayer also resists the abrasive action of the fiberglass filler and the chemical activity of the solvent.

Like the conventional sprayers, the new equipment recirculates a portion of the fluid from the nozzle back to a pressure pot to keep the filler and glass fibers in suspension. The new sprayer, hower, uses a lobe pump instead of a piston pump and positions it in the fluid return line close to the pressure pot. The new pump and position ensure more uniform pressure at the spray gun without a back-pressure regulator, which tended to clog in the old sprayer.

A high-performance agitator in the pressure pot keeps the filler from settling. The possibility of clogging is further reduced by using a large-diameter supply line [3/4-inch (1.8-centimeter) tubing] and return line [5/8-inch (1.5-centimeter) tubing].



Anticlogging Features of coarse-suspension paint sprayer include large-diameter supply line and return line, a heavy-duty agitator in the pressure pot, and a lobe pump in the return line.

In the new equipment, fluid pressure can be accurately controlled at the spray gun, and the fluid can be circulated without adversely affecting the nozzle pressure. As a result, the paint can be applied at a uniform and controlled rate.

This work was done by R. K. Major of United Space Boosters, Inc., for **Kennedy Space Center.** *No further documentation is available.*

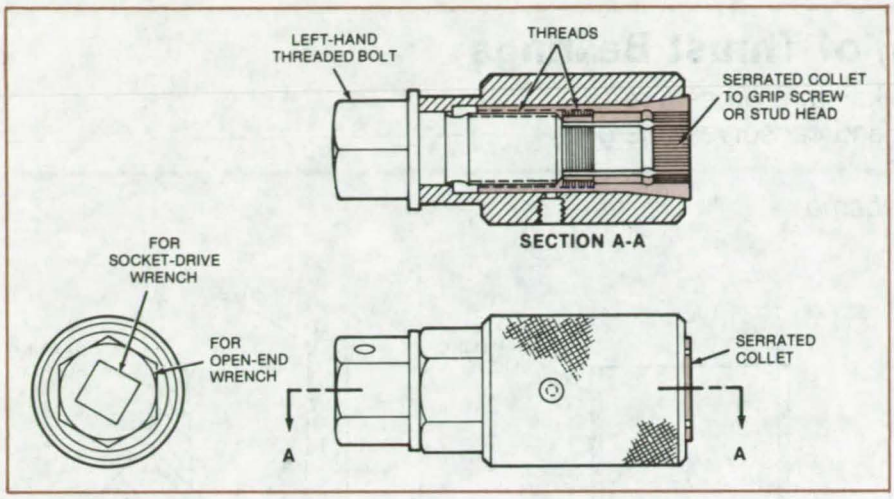
Inquiries concerning rights for the commercial use of this invention should be addressed to the Patent Counsel, Kennedy Space Center [see page A5]. Refer to KSC-11146.

Screw/Stud Removal Tool

A tool for removing high-torque screws and tight studs

Marshall Space Flight Center, Alabama

A relatively simple tool was developed for removing "stubborn" pan-headed screws or studs where conventional tools would be either too "weak" or inconvenient to use. The tool (see figure)) features a serrated collet that fits over the screwhead, gripping it around the circumference. The collet is tightened via a left-hand threaded bolt turned counterclockwise by an open-end or socket-drive wrench. A counterclockwise torque on the left-hand threaded bolt, combined with increased gripping pressure of the collet, is all that is necessary to loosen conventional right-hand threaded screws or studs without slipping. Screws with damaged heads or slots can also be removed this way.



This **Screw Removal Tool** utilizes a serrated collet to grip the screwhead around the circumference. The left-hand threaded bolt operated by an open-end or socket wrench tightens the collet over the screwhead, simultaneously loosening the screw. The collet grip, proportionately increasing with applied torque, prevents the tool from slipping.

The tool can be worked with one hand and easily fits limited-access and blind areas. It can be made in various sizes to fit different screwheads.

This work was done by K. Daniels, D. E. Herrick, and L. Rothermel of Martin Marietta Corp. for **Marshall Space Flight Center.** *No further documentation is available.*
MFS-22957

A Tool for Installation and Removal of Cylindrical Baffles

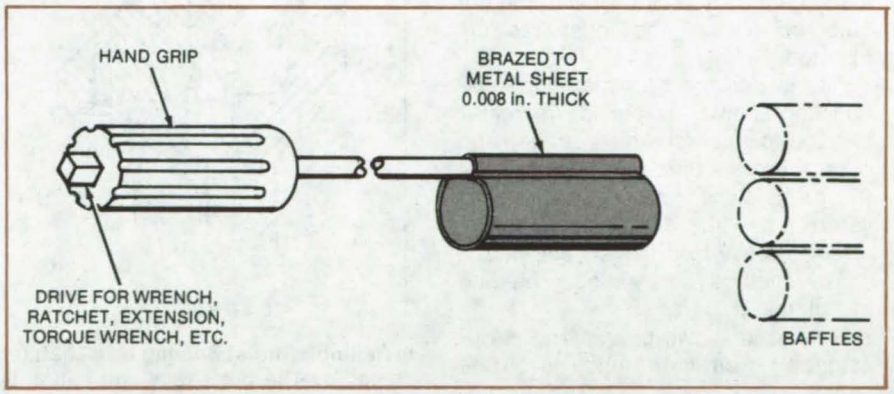
Thread-on baffles are easily tightened or loosened, using this tool.

Marshall Space Flight Center, Alabama

A simple tool based on the principle of an automobile oil wrench slips over a cylindrical thread-on baffle to install or remove it from the baffle assembly. As shown in the illustration, the tool consists of a curled metal sheet brazed onto a handgrip. The handgrip is adapted to be driven by a wrench, ratchet, extension, torque wrench, or some other convenient tool.

A clockwise twist of the handgrip, as shown, tightens the metal sheet around the baffle to advance it into the threaded joint. A counterclockwise twist loosens the sheet for repositioning or tool removal. An oppositely-oriented "mirror image" tool is used to remove the baffles.

This work was done by R. Pessin of Rockwell International Corp. for **Marshall Space Flight Center.** *No further documentation is available.*
MFS-19508



A **Tool for Installing or Removing Thread-On Baffles** consists of a curled metal sheet brazed onto a handgrip. The sheet is slipped over the baffle. A clockwise turn by a wrench applied to the handle grip grasps the baffle, advancing it into the threaded joint. A "mirror image" tool of the one shown is used to remove the baffle.

Simplified Installation of Thrust Bearings

A special handling sleeve is the key to a procedure that saves time, prevents corrosion, and conserves energy.

Marshall Space Flight Center, Alabama

A method of installing thrust bearings, developed for assembling bearings on the shaft of a low-pressure oxygen turbopump, eliminates the possibility of corrosion formation. The previous assembly method consisted of heating the entire bearing, chilling the shaft so that it contracted and could be slipped into the heat-expanded bearing, and drying the shaft/bearing assembly in a vacuum oven. This procedure was unsatisfactory because it caused corrosion in about 40 percent of the assemblies.

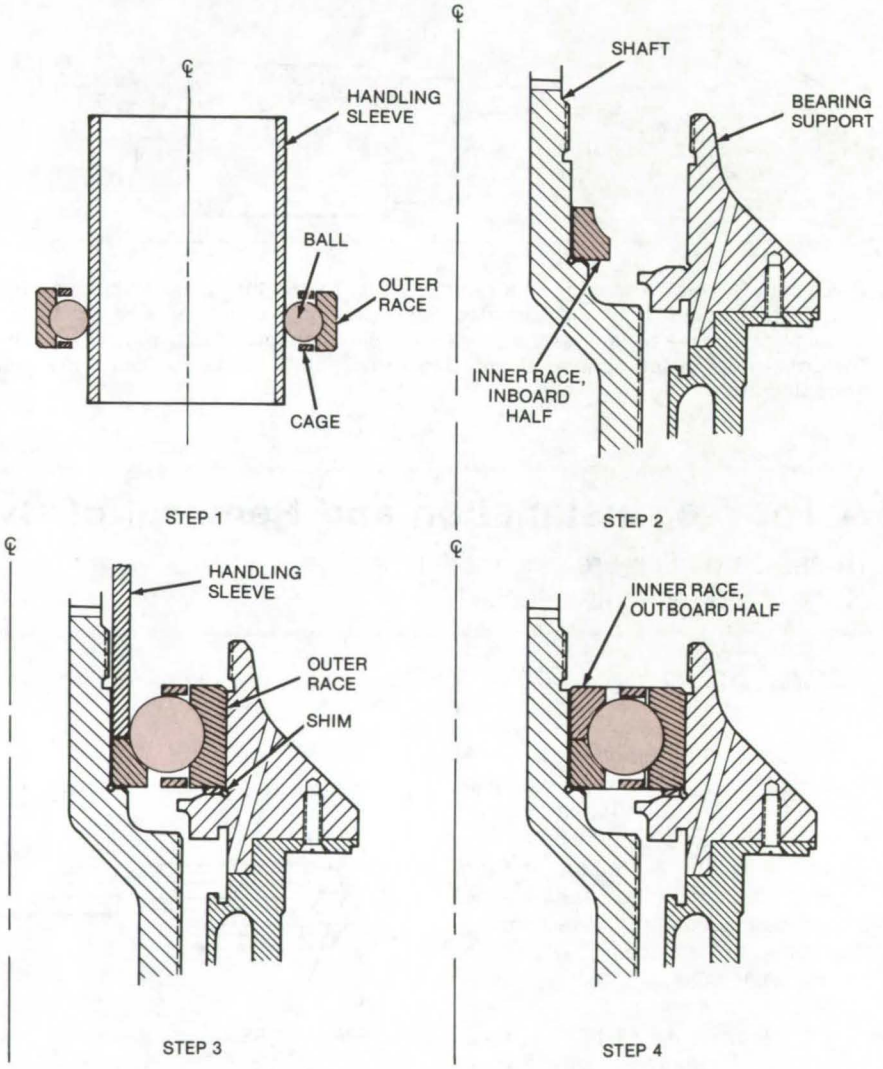
The new method eliminates the cooling and vacuum-drying steps. Only the bearing inner-race halves are heated [to about 300° F (150° C)]. First, the outer race, balls, and cage are placed on a special handling sleeve (see figure). The inboard half of the hot inner race is slipped on the shaft (which is at ambient temperature) and allowed to cool. The outer race, balls, and cage are then rolled off of the handling sleeve and nested in the bearing support. Finally, the hot outboard half of the inner race is inserted.

The key to the new method is the handling sleeve. Its outside diameter is sized to retain the balls, cage, and outer race as a unit, without danger of the balls falling out of place. At the same time, the inside diameter is sized for easy insertion on the shaft.

The method can simplify bearing installation if:

- the race is in two pieces and is designed for an interference fit on the shaft,
- the outer race can be held by a loose-to-light press fit at the time of assembly, and
- the balls are held in position by a cage.

Besides eliminating corrosion and speeding up assembly, the procedure saves energy because it requires no liquid nitrogen for cooling the shaft and no natural gas or electric power for operating the vacuum oven.

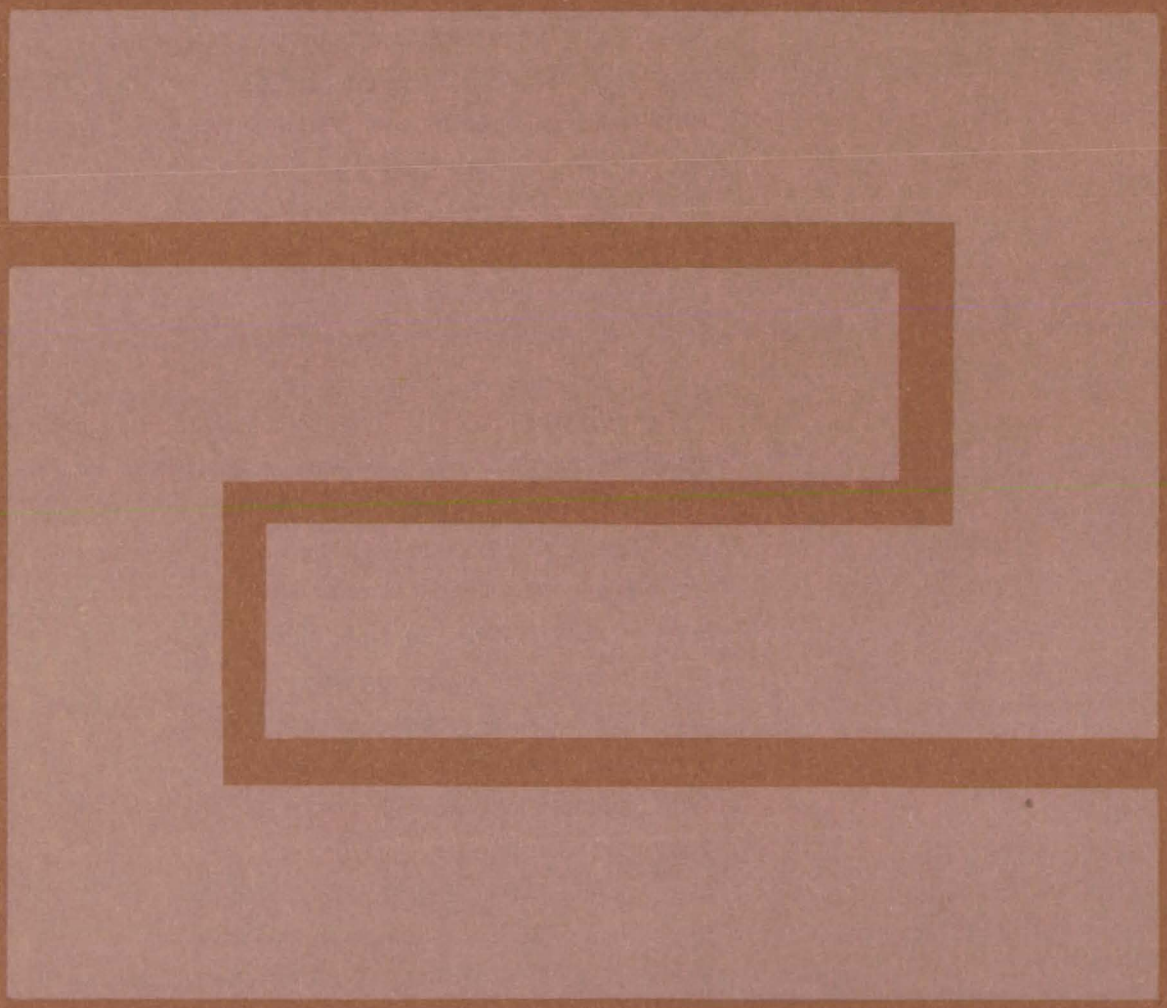


Installing a Thrust Bearing on a shaft (shown here in half cross section) requires four steps: (1) The outer race and ball subassembly are placed on a special handling sleeve, (2) the hot inner race (inboard half) is placed on the shaft, (3) the subassembly is rolled off the sleeve into the bearing support, and (4) the hot inner race (outboard half) is placed on the shaft.

This work was done by Norman D. Sensenbaugh of Rockwell International Corp. for **Marshall Space Flight Center.** *No further documentation is available.*

Inquiries concerning rights for the commercial use of this invention should be addressed to the Patent Counsel, Marshall Space Flight Center [see page A5]. Refer to MFS-19473.

Fabrication Technology



Hardware, Techniques, and Processes

555 Stress-Relieved Solder Joints
556 Repairing Flat Cables
557 Scratch Encourages Selective Doping
557 Wire Stripper Protects Cable Shielding
558 Stitch-Bond Parallel-Gap Welding for IC Circuits
559 Crimped Thermocouple Connections
560 Multilayer Metalization of MOS IC's
561 Improved Process Control for VMOS FET's
561 Securing Connector Pins to a PC Board
562 Improved Switch-Resistor Packaging
563 Precision Scriber
564 Improved Acoustic Levitation Apparatus
565 A Plasma-Sprayed Valve Coating
565 Inhibiting Oxidation of Tungsten at High Temperatures
566 Electrodeposition Process Reduces Cost of Cold Plates
567 Tube-Shape Verifier
568 Adjusting an Electron Beam for Drilling
568 Repairing Sealing Surfaces on Aluminum Castings
569 Protecting Brazing Furnaces From Air Leaks
570 An Improved Welding-Arc Starter
571 Microscope for High-Temperature Welding
571 Brazing Titanium to Stainless Steel
572 Switchbox for Welding Torches
572 Thermal Jack
573 Viewing Electron-Beam Welds in Progress
574 Welding Multiple Plies With an Electron Beam
574 Bonding Soft Rubber of Plasticized Elastomers to Metal
575 Vacuum-and-Pressure Laminating Polymer Materials
576 Evacuated-Displacement Compression Molding
577 Electromagnetic Bonding of Plastics to Aluminum
578 Structurally-Continuous Composite Corners
579 Removing Bonded Skin From a Substrate

Books and Reports

579 Arc-Termination Cracks in Inconel 718 and Incoloy 903
580 Cost Savings in LSI Fabrication

Stress-Relieved Solder Joints

Attachment method halves the stress in RF component leads.

Lyndon B. Johnson Space Center, Houston, Texas

Mechanical stress on solder joints is reduced by a procedure for soldering electronic components to circuit boards. The procedure was developed for radio-frequency (RF) strip-line circuits, for which dimensions must be carefully controlled to minimize parasitic capacitance and inductance. Because the component leads are usually quite short in RF circuits, considerable stress can build up when the leads are soldered to the strip-line circuit board.

The new procedure consists of loosening a component from its mounting after each lead is soldered so as to relieve the induced stresses before the next soldering step. Using mounting screws that allow it to "float," a component is centered on its site on the circuit board (see Figure 1). The screws are tightened, and the most-stress-susceptible lead is soldered and allowed to cool to room temperature. Then the screws are loosened so that the component is free to move, and the stress in the soldered lead relaxes.

Next, the component is refastened, and the lead on the opposite side is soldered. After the solder joint cools, the component is loosened once more and allowed to center itself so that the stress in the second lead is then shared by the two leads. The maximum stress on each lead is thus one-half that originally on the second (more lightly stressed) lead. Finally, the screws are retightened and sealed.

In a typical soldering operation, a lead is heated to about 500° F (260° C). Solder is applied, melted, and solidified at 361° F (183° C) (for a solder composition of 63 percent lead, 37 percent tin). During the solidification process, thermal stress builds up in the lead. For example, at room temperature, the stress in one RF transistor used in the Apollo S-band power amplifier has been calculated to be 4,650 lb/in.^{2} (32x10^6 N/m^2). Moreover, as the transistor heats up

(continued on next page)

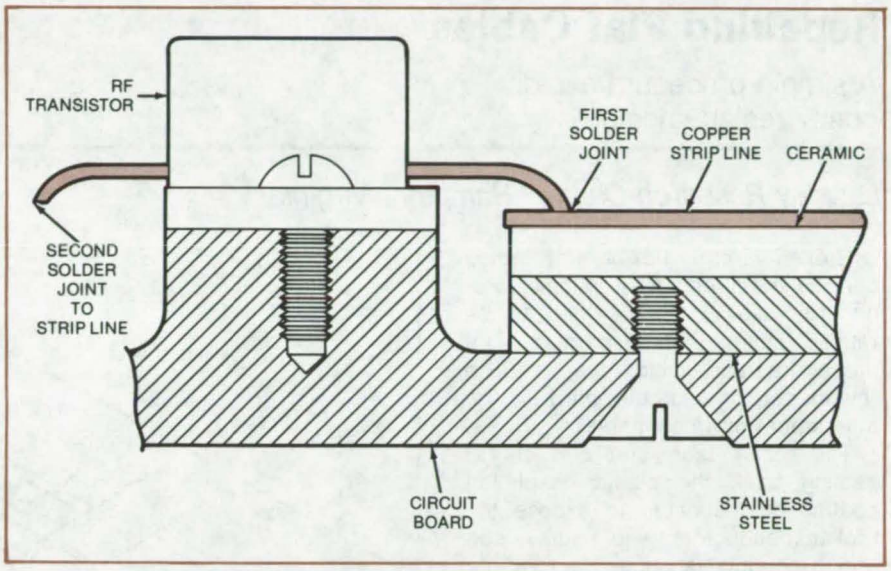


Figure 1. An **RF Transistor on a Strip-Line Circuit Board** is fastened by screws. After each lead is soldered, the screws are loosened to redistribute the stress in the leads.

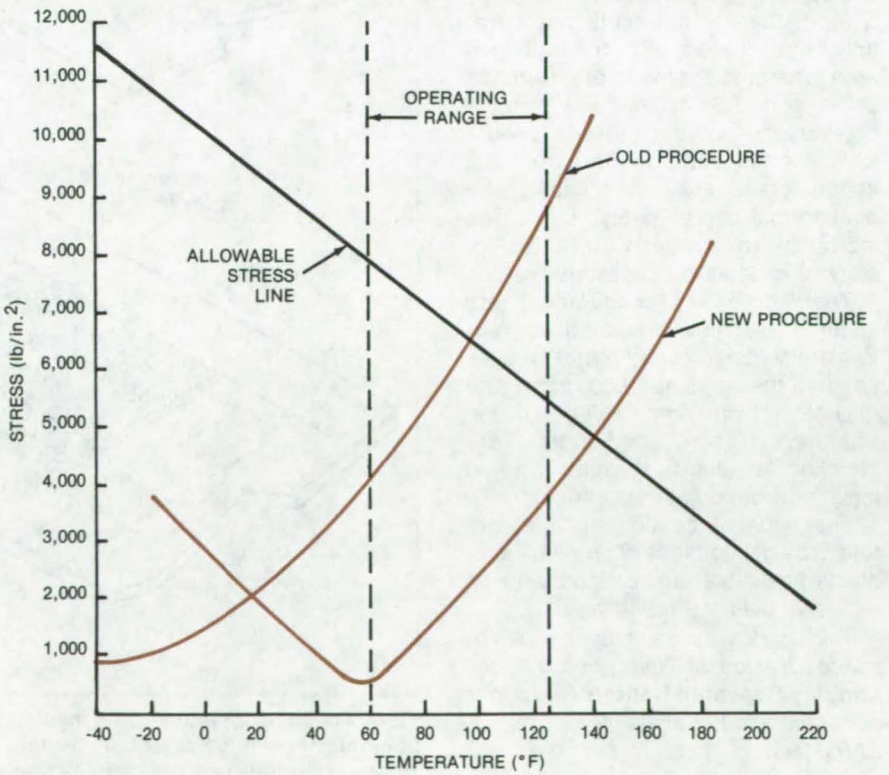


Figure 2. **Mechanical Stress Is Reduced** on a strip-line solder joint by the improved soldering procedure. The "allowable" stress line is shown for comparison. Note that, using the old procedure, the stress exceeded the allowable limit.

during operation, additional stress is superimposed on the residual room-temperature stress. At 122° F (50° C) operating temperature, the stress in the transistor lead can be 8,800 lb/in.^{2} (60.1x10^6 N/m^2), which exceeds the maximum allowable stress at that temperature. As shown in Figure 2, the stress is reduced to below 4,000 lb/in.^{2} (27.5x10^6 N/m^2) by the new procedure.

This work was done by Charles J. Zemenick of Rockwell International Corp. for **Johnson Space Center.** *No further documentation is available.*
MSC-14981

Repairing Flat Cables

A simple procedure avoids costly replacements.

Langley Research Center, Hampton, Virginia

Broken wires in flexible flat cables can be repaired by a simple procedure, allowing the cables to be reused instead of discarded. The procedure also avoids the need to rework part of a circuit board for the attachment of a new cable.

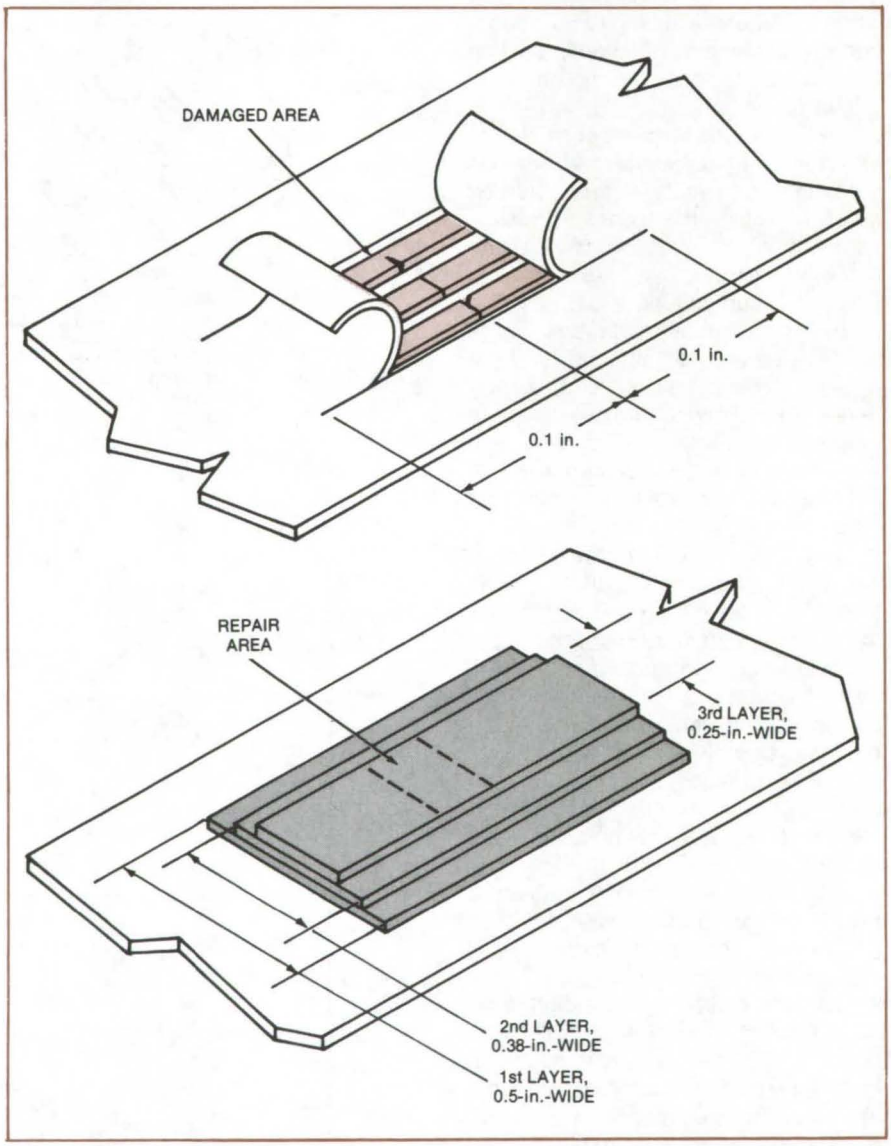
The repair technique consists of peeling back the plastic insulation coating on the cable to expose the broken conductors (see figure), soldering conductive bridges across the gap, and replacing the peeled-away insulation with an overlapping coating that allows the cable to flex without overstressing the repaired area.

First, the original coating is carefully cut at the edges of the damaged area. The cuts are made at a distance of 0.1 inch (2.54 millimeters) from the outside edge of the broken conductors. Another cut is made across the conductors to release two flaps of the coating that can be peeled back. The incisions are made with a sharp, pointed knife at low pressure.

The exposed conductors are cleaned, and new pretinned conductors are soldered over the broken ones so that they extend 0.03 inch (0.8 millimeter) on both sides of the fractures. The conductors are checked for electrical continuity and isolation from adjacent conductors.

The flaps of coating material are folded back into place. Three layers of plastic insulation are bonded with an adhesive over the repair area.

This work was done by the Aerospace Division of Honeywell Inc. for **Langley Research Center.** *No further documentation is available.*
LAR-11950



Flaps Are Cut (top) in the cable insulation and peeled back to expose the conductor fractures. Insulation layers of decreasing size (bottom) allow the cable to flex without overstressing the mended connectors.

Scratch Encourages Selective Doping

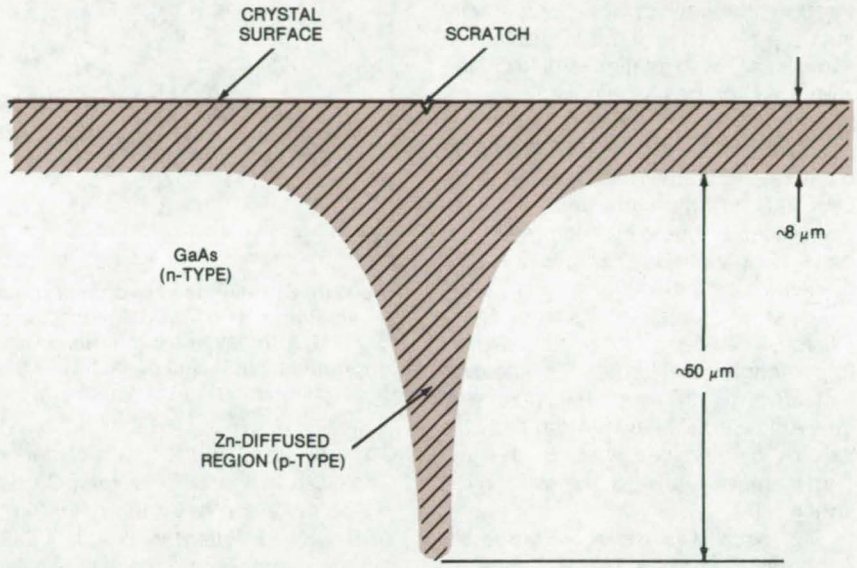
Dislocations induced by scratching produce deep narrow spikes of zinc diffused in gallium arsenide.

Langley Research Center, Hampton, Virginia

Many semiconductor devices require the selective diffusion of dopants into narrow regions of a host material. Such regions are often required with dimensions of the order of a few micrometers or less. At the same time, it is desired that the diffused dopants penetrate deeply into the crystal.

In preliminary tests, such deep narrow channels of diffused zinc in gallium arsenide (GaAs) were obtained by lightly scratching the surface of the GaAs crystal wafer. It is conjectured that the density of defects thus formed (dislocations) locally increases the zinc diffusion coefficient. (Enhancements by a factor of 6 have been observed.)

As shown in the figure, which is a sketch of typical results obtained thus far, the diffusion front is narrow and deep, as required. A layer of zinc-doped gallium arsenide, about 8 micrometers deep, is formed at the surface of the crystal. This shallow layer can be etched away. In the region that has been scratched, the spike formed by the zinc-diffused region penetrates about 50 micrometers below the shallow region.



A Controlled Spike Appears in the zinc diffusion front where the GaAs surface has been lightly scratched.

The diffusions were done at 850° C. Other temperatures, however, can be used. The technique should also work for other dopants than zinc and for other semiconductors besides GaAs.

This work was done by Frank Z. Hawrylo and Henry Kressel of RCA Corp. for **Langley Research Center.** *No further documentation is available.*
LAR-11590

Wire Stripper Protects Cable Shielding

Four-blade stripper removes insulation from end or middle of wire without damagaing the shielding.

Dryden Flight Research Center, Edwards, California

Typical wire strippers use a pair of curved blades that are closed on the wire to cut the insulation while a clamp or hand pulls the insulation off the wire. Since the shielding net can be easily damaged by closed blades pulled along it, these strippers are not readily usable for shielded wires.

A simply-constructed prototype wire stripper guards against damage to the shielding and forms accurately controlled cuts in a wire to strip the insulation. Though especially useful for stripping insulation from shielded wires, it can also be utilized on unshielded wire to strip insulation from the end or from a middle portion of the wire.

As illustrated, two pairs of jaws pivotally mounted on a body move against and away from a wire positioned between the jaws. The wire, from which insulation is to be stripped, is inserted through the hole and held in one hand while the wire stripper is held in the other hand. The thumb and forefinger depress the first set of jaws, the blades of which — extending perpendicular to the axis of the wire — penetrate the insulation.

(continued on next page)

These are the transverse blades. Circumferential cuts are made by rotating the stripper.

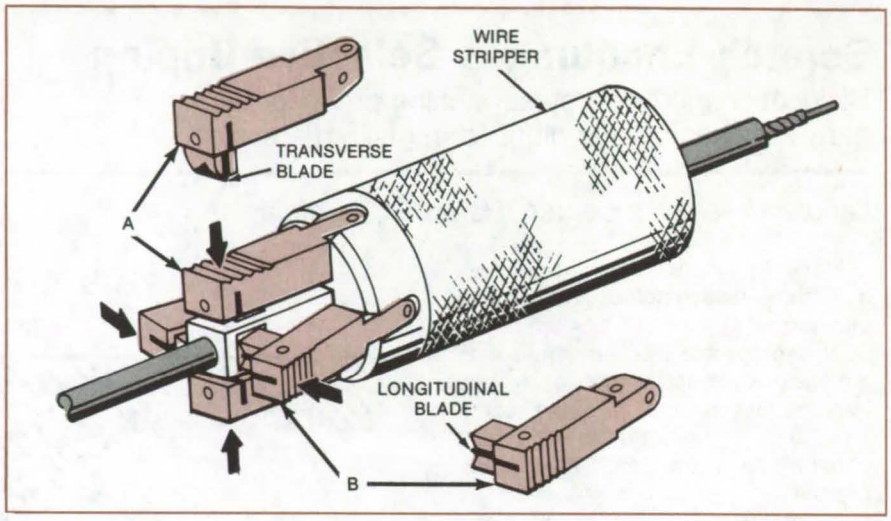
When this is done, the first pair of jaws is released, and a second pair having blade edges extending parallel to the wire (the longitudinal blades) is squeezed together to penetrate the insulation. The wire is pulled back through the device, and longitudinal cuts are formed in the insulation. The two pieces of insulation cut from the wire are then easily removed.

Each blade is located within a concave block that centers the blade on the wire and limits the depth of penetration of the blade into the wire. The blades are held by setscrews that can be loosened to reposition the blades for deeper cuts.

To strip insulation from ordinary twisted-wire pairs, the blades that form longitudinal cuts are floating instead of rigidly fixed. Each blade is guided toward and away from the wire axis by blade guide walls in the jaw and is moved toward the wire by a spring.

This work was done by Merle A. Economu of **Dryden Flight Research Center.** *For further information, Circle 66 on the TSP Request Card.*

This invention has been patented by NASA [U.S. Patent No. 4,117,749]. Inquiries concerning nonexclusive or exclusive license for its commercial development should be addressed to the Patent Counsel, Dryden Flight Research Center [see page A5]. Refer to FRC-10111.



The Wire Stripper uses two pairs of jaws for removing insulation without damaging the shielding. The first pair contains blades oriented perpendicular to the wire axis for making transverse circumferential cuts, and the second pair contains blades for longitudinal cuts. One of each type of jaw has been redrawn to show the vee grooves that aid in centering the wire.

Stitch-Bond Parallel-Gap Welding for IC Circuits

Stitch-bonded flatpacks can be superior to soldered dual-in-lines where size, weight, and reliability are important.

Lyndon B. Johnson Space Center, Houston, Texas

Flatpack integrated circuits installed by stitch-bond/parallel-gap welding can be considerably more economical for complex circuit boards than conventional solder-installed dual-in-line IC's. This is the conclusion of a study of the two approaches as applied to circuit packaging for spacecraft, where considerations of size, weight, and reliability are of paramount importance. Terrestrially, the study results should interest the designers of packaging for complex high-reliability electronics, such as that used in security systems, industrial process control, and vehicle electronics.

In considering package size, it was found that it is possible to package approximately 2-1/2 flatpacks in the area usually allotted for a single dual-in-line package. The area required for a 14-pin flatpack that is installed by stitch-bond/parallel-gap welding is 0.711 cm^2. The area required for a 14-pin dual-in-line package is about 1.9 cm^2.

The weight per flatpack, using the stitch-bond/parallel-gap method, is about 2.45 grams per IC, as compared to 3.67 grams for conventionally-mounted dual-in-line packages. Thus, when printed-circuit boards having a complexity of hundreds of IC's and thousands of stitch welds are involved, the weight savings can be substantial.

In considering the ease of manufacture, the assembly time for one flatpack using the stitch-bond/parallel-gap process is 10 to 15 percent less than the assembly time using conventional processes. Moreover, there is a 20- to 30-percent improvement in the ease of performing rework and a reduction of over 40 percent in the engineering design/package effort.

This work was done by Paul Chvostal, Jay Tuttle, and Richard Vanderpool of Odetics, Inc. for **Johnson Space Center.** *No further documentation is available.*
MSC-16459

Crimped Thermocouple Connections

When proper procedures are followed, a hand crimping tool makes reliable, low-cost thermocouple connections.

Lyndon B. Johnson Space Center, Houston, Texas

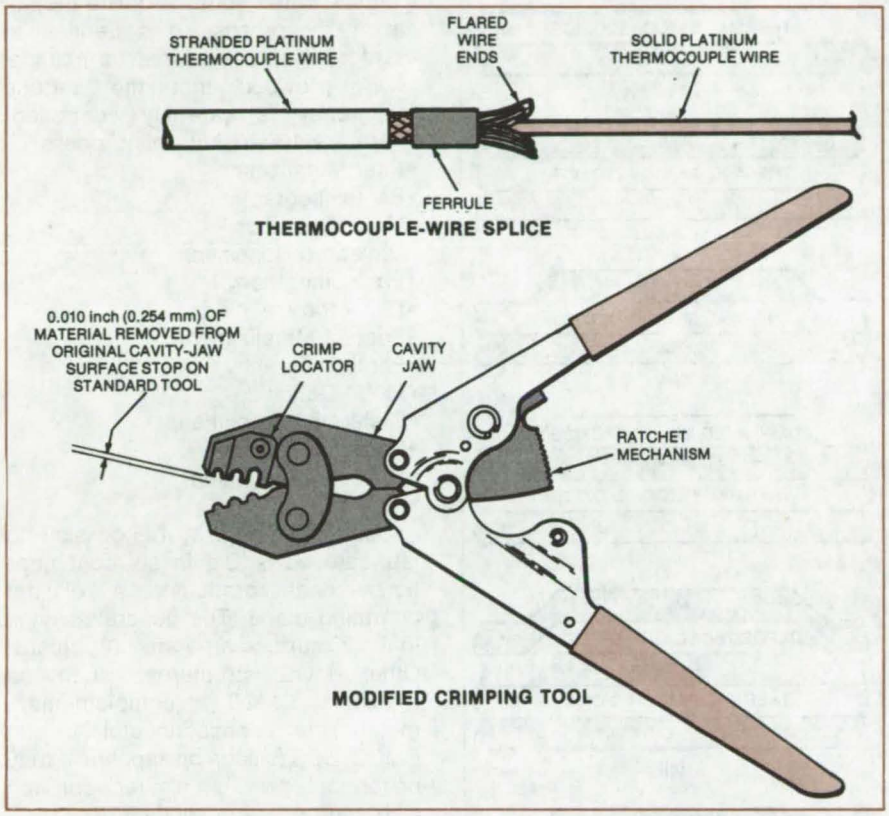


Figure 1. **Solid Thermocouple Wire** is inserted into the flared end of the stranded wire, and the ferrule is slid to the end of the strands. The crimping tool then compresses the ferrule to complete the splice.

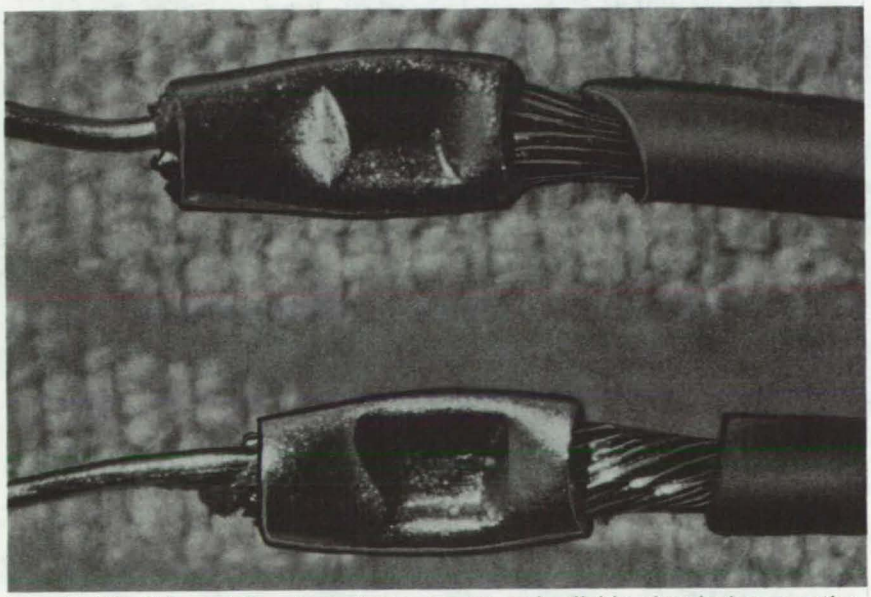


Figure 2. The **Crimped Ferrule** makes a secure and reliable electrical connection between solid and stranded platinum thermocouple wires (magnified 17X).

A simple crimping procedure reduces the time and expense of splicing solid and stranded platinum thermocouple wires. Using a slightly-modified commercial crimping tool, reliable attachments are made more economically than by resistance welding, the method previously used.

The technique was developed for connecting measuring instruments to thermocouple junctions embedded in spacecraft heat shields. It is used for connections between thin solid platinum wire [0.010 inch (0.25 millimeter) in diameter] and 30 AWG stranded insulated platinum wire. The basic approach should be adaptable to wires of other sizes and materials.

To make a splice, the insulation is first stripped off the stranded wire for a distance of 0.30 inch (0.076 millimeter). A nickel ferrule is slipped over the stranded wire and pushed back to the insulation (see Figure 1). The strands are flared, and the solid thermocouple wire is inserted into the flare. The ferrule is slid back to the end of the strands, and the crimping tool is used to press an indentation into the ferrule. The completed connection is shown in Figure 2. The crimping tool is a standard commercial model, modified by the removal of 0.01 in. (0.025 cm) of thickness of material from the original cavity jaw surface.

This work was done by Kennard L. Billington and Harry S. May of Rockwell International Corp. for **Johnson Space Center.** *No further documentation is available.*
MSC-18489

Multilayer Metalization of MOS IC's

A modified ion-bombardment technique interconnects MOS circuit elements without affecting the circuit parameters.

Marshall Space Flight Center, Alabama

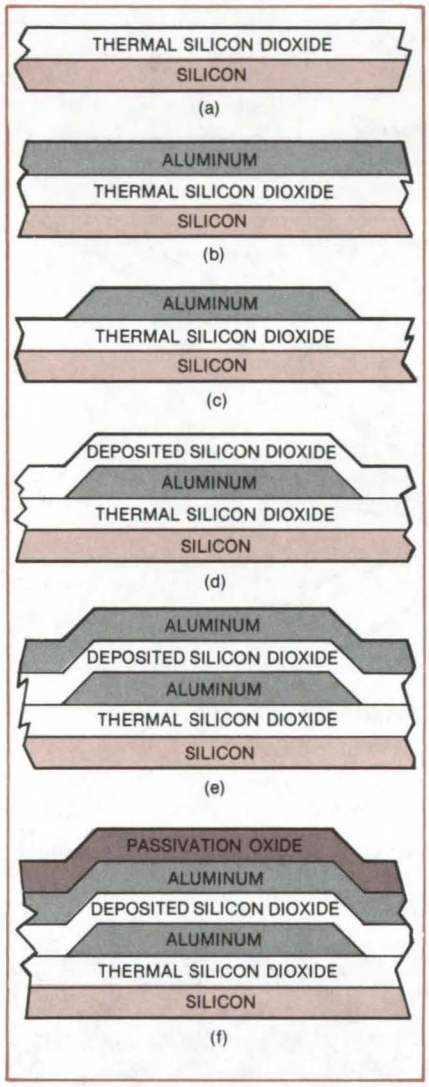
An ion-bombardment multilevel metalization technique successfully used in fabricating bipolar large-scale integrated (LSI) circuits could not be adapted to MOS (metal-oxide semiconductor) IC's (integrated circuits). This method using electron-gun, RF (radio-frequency), or dc sputtering induces large amounts of charge in the MOS gate oxide, seriously affecting the MOS electrical parameters. Another well-tried method incorporating a diffused conductor for multilevel interconnection resulted in a compromise between the slow circuit-response time and low packing density. Metalization employing polysilicon, a widely-used intermediate conductive material, had a similar problem.

A newly-developed multilayer metalization process applies metalization steps after the gate oxide is grown. The process is keyed to a modified ion-bombardment technique using either **E x B** or a magnetron sputtering system producing low radiation levels at the MOS substrate surface that can be easily removed by annealing. The approach is similar to a dc sputtering technique. In the new process, however, no bias is applied to the substrate, and the majority of secondary electrons generated during the ionization collision is prevented from reaching the substrate surface by a specially-designed anode collector. This circular conical collector forces the secondary electrons close to the anode surface where they are captured. Only low-level positive radiation reaches the substrate.

A two-level metalization process for a p-channel MOS is shown as an example in the figure. Prior to metalization, the processing is identical to that for a single-layer metal p-channel MOS, provided that the surface topography is carefully controlled. There are 13 steps in this process:

- First Metalization
- Photolithography
- Metal Definition
- Dielectric Deposition
- Photolithography
- Dielectric Definition
- Second Metalization
- Photolithography
- Metal Definition
- Dielectric Deposition
- Photolithography
- Dielectric Definition
- Sintering

Using this process, it is possible to fabricate MOS IC's in six configurations, each producing a distinct operating mode. The general savings in the IC surface area are 50 percent. Other MOS structures, such as n-MOS, CMOS (complementary metal-oxide semiconductor), and CMOS/SOS (silicon on sapphire), may be fabricated using a similar approach with appropriate modifications.



Multilevel Metalization of p-MOS IC device involves (a) surface treatment prior to metalization, (b) first metalization, (c) metal pattern definition and photoresist removal, (d) dielectric deposition, (e) second metalization, and (f) final dielectric deposition. This procedure, using only two metalization layers, reduces the circuit area by 50 percent. Six types of p-MOS devices may be constructed this way, each with a different operating mode.

This work was done by David L. Bouldin, William R. Feltner, Ben R. Hollis, Jr., and Donald E. Routh of **Marshall Space Flight Center.** *For further information, Circle 67 on the TSP Request Card.*

This invention has been patented by NASA [U.S. Patent No. 4,111,775]. Inquiries concerning nonexclusive or exclusive license for its commercial development should be addressed to the Patent Counsel, Marshall Space Flight Center *[see page A5]*. *Refer to MFS-23541.*

Improved Process Control for VMOS FET's

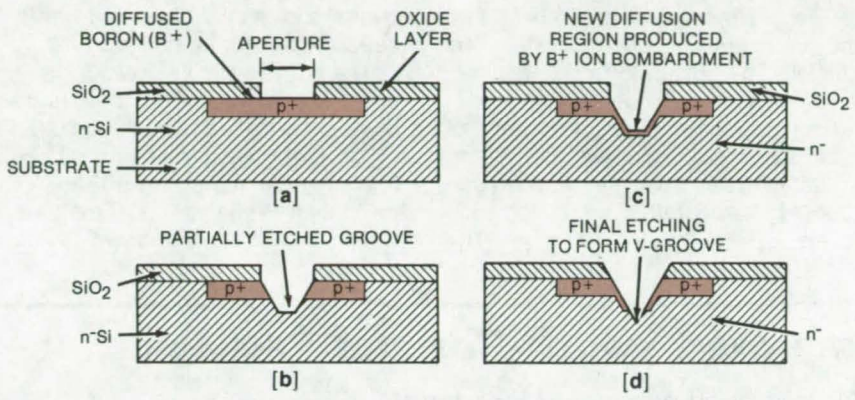
Forming precise channel region in VMOS FET's

Goddard Space Flight Center, Greenbelt, Maryland

Very short channels between the source and the drain in VMOS FET's have been formed using anisotropic etches. For example, N_2H_4 and KOH etchants have been used to dissolve the ⟨100⟩ silicon crystal planes more rapidly than the ⟨111⟩ planes. These etchants applied through an appropriate mask are used to form the VMOS channels. The process, however, is only moderately accurate, making the channel length dependent upon the mask opening and the diffusion depth. A more accurate approach using ion implantation eliminates the diffusion depth factor, making it possible to control channel lengths with high precision.

The modification is introduced in the middle of the VMOS manufacturing process (see figure). After the n⁻Si substrate surface is oxidized, the p^+ region formed, and the V-groove mask made, KOH is applied to the exposed ⟨100⟩ surface of the substrate. Instead of letting the self-stopping etching be completed, it is allowed to run only part of the way by rinsing the wafer in the water bath after 10 minutes.

A partially formed V-groove that results penetrates the p^+ region, dividing it into two parts that will become the source and drain regions of the field-effect transistor. Boron ions are then implanted into the region by bombarding the lower portion of the groove at 52 keV, using an ion concentration of 10^{13} B^+ ions/cm^2. The implantation process very accurately defines the crucial geometry of the diffusion.



An **Improved Method of Making VMOS FET's** is applied in the middle of the fabrication process: (a) After the mask region is formed, the diffused-boron region is etched. (b) The etching is left incomplete for ion implantation. (c) Boron ions are implanted into the region to define accurately the crucial geometry of the V-groove. (d) The groove is then etched to completion, forming two well-defined diffusion regions that will serve as the source and drain of the transistor. The remaining processing is conventional.

The wafer is dipped in HF for approximately 10 seconds and rinsed to bevel the edge of the SiO_2 layer. The KOH is reapplied for about 6 minutes so that the V-groove etch is completed as shown in d.

The finished V-groove completely penetrates the diffusion region, thereby assuring that no shorts will occur due to diffusion spikes produced in the earlier process. The remaining processing steps are conventional.

This work was done by Murzban D. Jhabvala of **Goddard Space Flight Center.** *For further information, Circle 68 on the TSP Request Card.*

This invention is owned by NASA, and a patent application has been filed. Inquiries concerning nonexclusive or exclusive license for its commercial development should be addressed to the Patent Counsel, Goddard Space Flight Center [see page A5]. *Refer to GSC-12515.*

Securing Connector Pins to a PC Board

Solder preforms hold pins firmly to withstand repeated insertion and removal of circuit cards.

Lyndon B. Johnson Space Center, Houston, Texas

A new method speeds up soldering wire-wrap pins to the multilayer printed-circuit (PC) mother board of an electronic chassis. The mother board couples circuits of several PC cards among each other and to the input and output plugs on the chassis. It is equipped with many wire-wrap connectors arranged in a predetermined pattern. The pins have to be firmly secured to withstand the longitudinal forces of repeated insertion and removal of PC cards.

A special fixture is used to solder the pins. It consists of a flat sheet of plastic or other suitable material (such as a fiber-reinforced phenolic) 0.093 in. (2.36 mm) thick and having length and width dimensions correspondng to

(continued on next page)

the board. Drilled in the fixture are holes in the same pattern as the board. The holes are slightly larger than the wire-wrap pins and are countersunk on one side to receive a solder preform (a small solder ring). The preforms have an internal diameter slightly larger than the wire-wrap pins to fit freely over them.

The preforms are assembled into the countersinks of the fixture by placing the fixture on a resilient surface, with the countersunk holes facing up. Then a large excess of preforms is sprinkled over the fixture surface. The tip of an electric vibration tool (e.g., a vibratory engraving tool) is applied to the fixture edge. The vibrations cause the preforms to fall into and fill most (typically 95 percent of 1,565) of the countersunk holes in about 1 minute. The remaining holes are filled using tweezers.

The wire-wrap pins on the mother board are alined and fully inserted through the preform-filled fixture holes. The entire assembly is turned over, and the fixture is carefully separated from the board.

The board with the solder preform assembly is immersed in a preheat bath for 1 to 1-1/2 min at about 300° F (150° C) to avoid any thermal shock and is then immersed in a reflow bath for about 1 min at 400° to 450° F (205° to 230° C) to reflow the solder preforms into the interstices between the board holes and the pin surfaces. It is then allowed to cool at room temperature, after rinsing in trichloroethylene and hot water.

The reinforced pins can easily withstand the card plug insertion and removal. An additional advantage of this method is excellent electrical continuity between the board circuits and the pins.

This work was done by Dean Graham, Raymond Wilkes, and James Zorns of Sperry Rand Corp. for **Johnson Space Center.** *No further documentation is available.*
MSC-16059

Improved Switch-Resistor Packaging

An improved packaging technique for multiswitch resistor arrays.

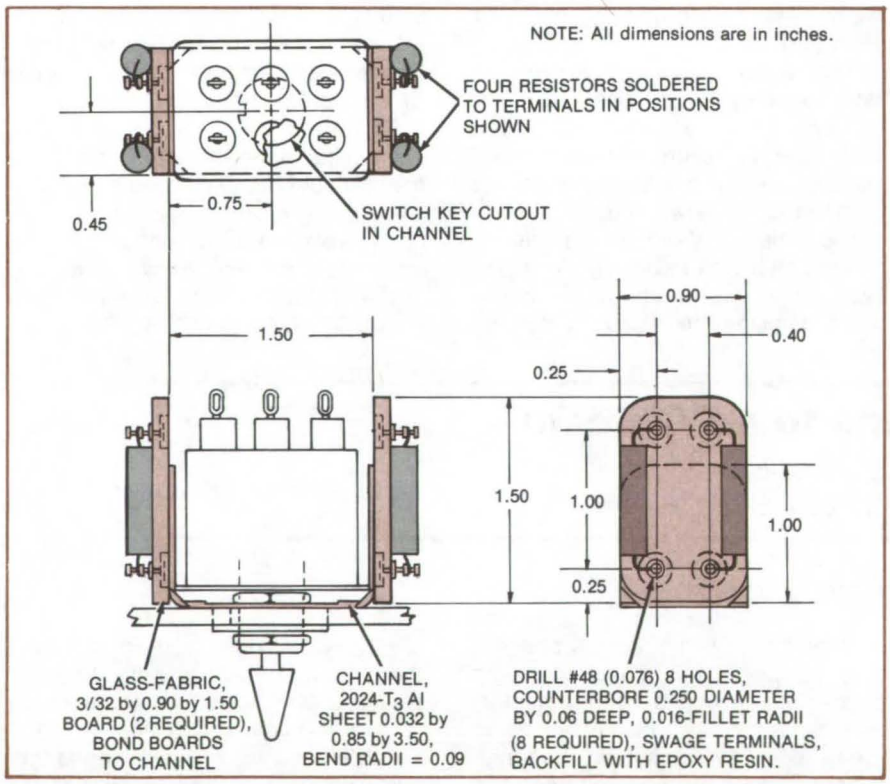
Lyndon B. Johnson Space Center, Houston, Texas

The switch-scan and current-limiter resistor board assembly, originally proposed for all display and control panels for the Space Shuttle orbiter, was difficult to troubleshoot because the resistors for all switches were installed on a single board. Failures could not be easily isolated and repaired because the one-board arrangement made it difficult to associate a particular failed resistor with its corresponding switch circuit.

A new packaging approach, shown in the figure, has made the resistors more accessible and easily identified with specific switches. Failures are repaired more quickly because of the improved accessibility. The resistors are mounted on a bracket attached to the switch. A typical board includes one resistor that acts as a circuit breaker, and the others are positioned so that their values can be easily measured when the switch is operated. Failures are rapidly located because each resistor is identified with a particular switch.

This approach simplifies the board assembly and wiring and incorporates the same materials and devices that were used previously. In addition it saves weight by using less wire and saves valuable panel space.

This work was done by Robert E. Redmerski of Rockwell International Corp. for **Johnson Space Center.** *No further documentation is available.*
MSC-19531



This **Packaging Configuration** makes resistors more accessible to troubleshooting than single-board packaging. The packaging method is utilized on Space Shuttle display and control panels.

Precision Scriber

Attachment to toolmaker's microscope requires no alteration of equipment.

Lewis Research Center, Cleveland, Ohio

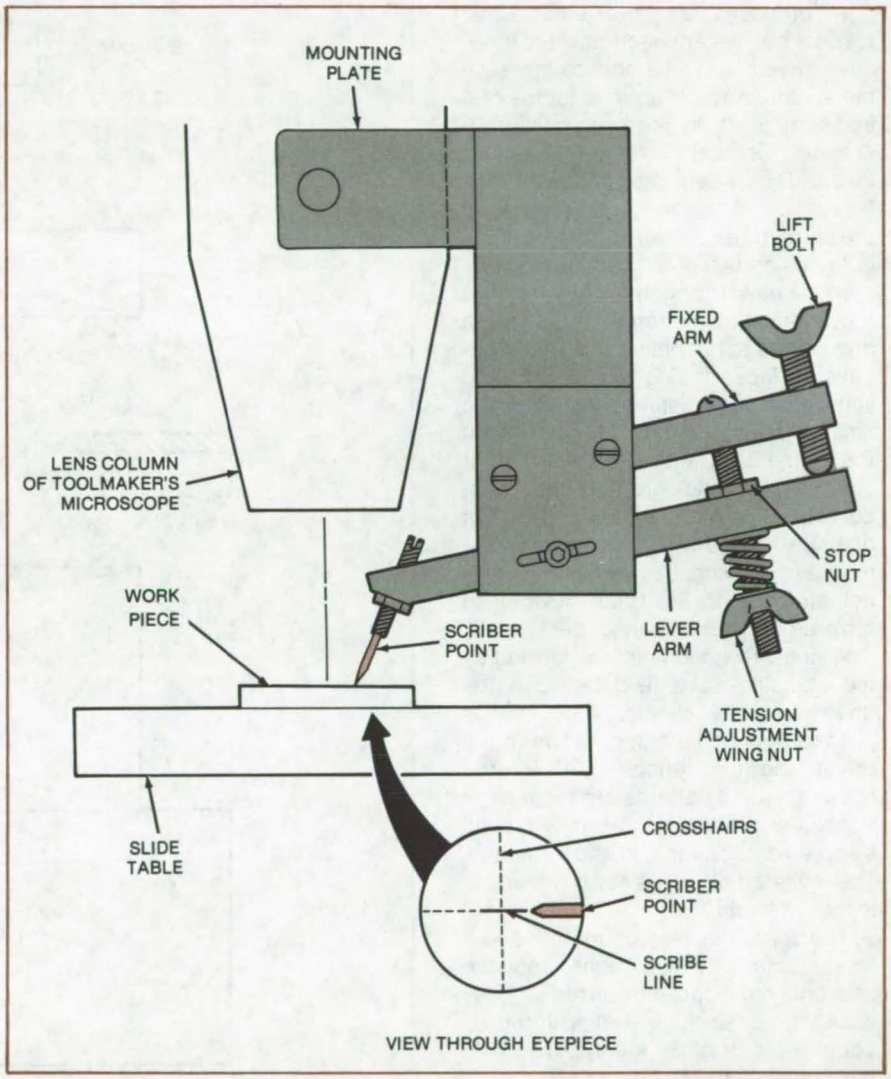
A new device will scribe fine lines to precise tolerances on flat or round surfaces. This scriber is used in conjunction with a toolmaker's microscope and will scribe metal or nonmetallic surfaces.

This new scriber was originally designed to scribe gage marks on specimens used in a materials-testing program. It draws fine, straight parallel lines with a high degree of accuracy. The device (see figure) is installed by means of a mounting plate screwed or clamped onto the lens-holding column of a toolmaker's microscope. No alteration to the microscope is required. The scriber is manually adjusted so that the marking point coincides with the vertical crosshair of the eyepiece.

To operate the scriber, the point is first lowered to the working surface at the desired position. Movement of the microscope slide table by use of the micrometer feed causes the scriber point to traverse and mark the material in a predetermined manner. The resulting scribe line will coincide with the vertical centerline crosshair of the eyepiece.

The depth and width of the scribe line are adjustable by regulating the spring tension on the lever arm to which the scriber point is attached. Points of various types may be used, including steel, carbide, and diamonds.

Parallel scribed lines can be spaced to close tolerances by using the microscope spacer block and/or micrometer screw to translate the slide table horizontally. Precise angles may also be scribed by using the slide-table azimuth ring. It is also possible to scribe round stock by supporting the stock in centering points mounted on the slide table.



Precision Scriber is attached to the column of a toolmaker's microscope with a mounting plate. The scriber is adjusted manually to line up with the vertical crosshair of the microscope.

When not in use, the scriber can easily be retracted or swung out of the way so the microscope can be used for other purposes.

This work was done by Robert J. Buzzard of **Lewis Research Center.** *No further documentation is available. LEW-12976*

Improved Acoustic Levitation Apparatus

Concave surfaces enhance and shape acoustic forces to lift heavier objects.

Marshall Space Flight Center, Alabama

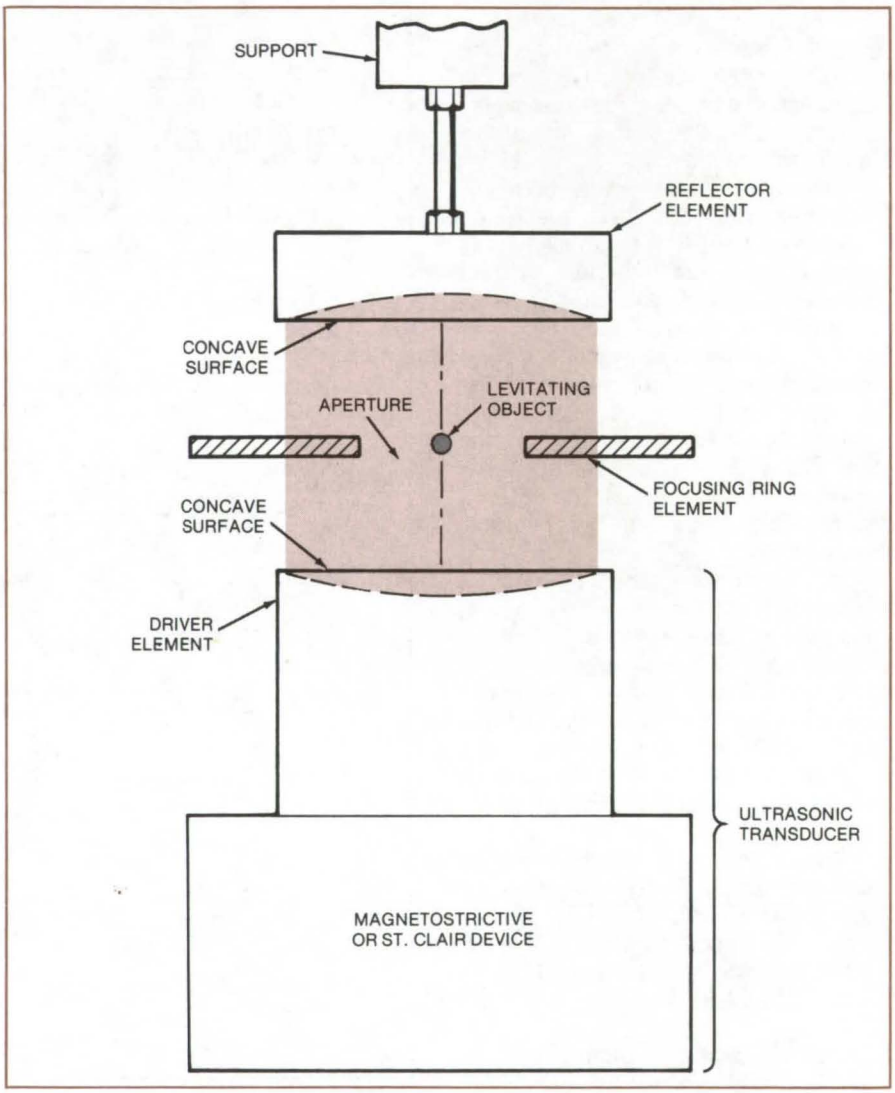
A proposed single-axis acoustic resonance system incorporates concave drivers and reflectors to increase the levitation force up to a factor of 6 as compared to conventional flat-shaped elements. A ring element inserted between the concave surfaces controls the standing-wave pressure pattern, particularly critical in levitating liquids.

In the new arrangement (see figure) a cylindrical aluminum reflector and a driver have spherically-machined concave surfaces facing each other and separated by a distance equal to the smaller radius of curvature of one of the elements. Generally, the reflector surface has the greater radius of curvature for a more stable radiation pressure. The driver is coupled with a magnetic driving device (e.g., magnetostrictive or St. Clair device) to form an ultrasonic transducer.

A single levitation node is formed by the standing-wave field between the driver and the reflector. The field is shaped by a ring element between the driver and the reflector. All of the pressure-wave patterns are focused or shaped within the ring as it is moved between the driver and the reflector. The levitated object generally remains inside this ring.

The apparatus may be modified to a lesser extent by using one concave and one flat opposing surfaces. This would increase the levitating force by about a factor of 2 as compared with the conventional flat elements.

Another alternative involves using concave elliptical surfaces to obtain multiple off-axis levitation nodes. This more complex field may be controlled by similar washer elements, screens, or other passive or secondary reflectors positioned at different points about the axes. This configuration would be favorable in levitating two different liquids or materials that are heated separately and then brought together to determine the heat of the reaction.



Concave Driver and Reflector enhance and shape the levitation forces in an acoustic resonance system. A single-mode standing-wave pattern is "focused" by a ring element situated between the driver and the reflector. Concave surfaces increase the levitating forces up to a factor of 6 as opposed to conventional flat surfaces, making it possible to suspend heavier objects.

This work was done by L. H. Berge, J. L. Johnson, W. A. Oran, and D. A. Reiss of **Marshall Space Flight Center.** *For further information, Circle 69 on the TSP Request Card.*

This invention is owned by NASA, and a patent application has been filed. Inquiries concerning nonexclusive or exclusive license for its commercial development should be addressed to the Patent Counsel, Marshall Space Flight Center [see page A5]. *Refer to MFS-25050.*

A Plasma-Sprayed Valve Coating

A durable cobalt and carbide coating is applied to valve seats and poppets.

Marshall Space Flight Center, Alabama

The need to reduce wear on nickel alloy valve seats and poppets for the Space Shuttle main engine has led to a fused cobalt/tungsten carbide coating. The coating, which is dense, wear-resistant, and nonporous, can be applied in controlled amounts to various substrate configurations. The ease of application to parts with intricate shapes and contours should make the coating useful in automotive and aircraft manufacturing.

The fused cobalt and carbide hard facing coating is metallurgically bonded to valves and poppets, making it resistant to spalling and flaking. Also, it is resistant to thermal shock, and its mechanical shock characteristics are excellent at cryogenic temperatures (immersion in liquid oxygen and liquid hydrogen).

The hard-facing coating uses a nickel/boron/silicon braze alloy as a fusing medium. After the surface is grit-blasted, a plasma gun applies a precoat of the braze alloy and then a mixture of the braze alloy with the cobalt/tungsten carbide alloy. (Both alloys are commercially available.) The coating is subsequently fused at 1,925° F (1,051° C) in a vacuum, argon, or hydrogen atmosphere. The choice of atmosphere depends on the desired cooling rate.

The plasma gun applies a uniform distribution of the carbide in the nicket/boron/silicon matrix, which is essential for good bonding. The braze-alloy precoat helps wet the nickel alloy base, eliminating the need to nickelplate the substrate.

To obtain uniform nonporous hard facing overlays, the carbide/braze-alloy ratio is controlled so that the fused coating has a slightly wet appearance. An excess of carbide gives a dry appearance. The alloy ratio is controlled by varying the plasma-gun power level. The deposition efficiency is also a function of the gases and type of plasma gun being used.

An argon gas atmosphere prevents oxidation of the cobalt and tungsten carbide layer, which in turn promotes excellect wetting of the braze alloy with the carbide. With regard to oxidation of the carbide, the control of part temperature, gun distance, and deposition efficiency of the mixture being sprayed is critical.

This work was done by Alexander Brennan and Arthur B. Olmore of Rockwell International Corp. for **Marshall Space Flight Center.** *For more details on the hard-facing process, Circle 70 on the TSP Request Card.*

Inquiries concerning rights for the commercial use of this invention should be addressed to the Patent Counsel, Marshall Space Flight Center *[see page A5].* *Refer to MFS-19494.*

Inhibiting Oxidation of Tungsten at High Temperatures

A ceramic coating protects tungsten from oxidation.

Marshall Space Flight Center, Alabama

A coating of mixed ceramics protects tungsten from oxidation. Originally suggested for critical tungsten components on the Space Shuttle, the mixture consists of 98.5 percent aluminum oxide and 1.5 percent silicon dioxide. It is particularly useful in welding when there is a danger that the welding arc can burn adjacent components. If the coating is applied to nearby tungsten parts, it prevents arcing.

Although very pure tungsten can be forged, spun, drawn, and extruded, the impure metal is brittle and can be worked only with difficulty. Moreover, because tungsten is refractive, it is difficult to process, and powder metallurgical techniques are often necessary. Above 1,650° C it has the highest tensile strength of all elements and has excellent corrosion resistance over the entire temperature range, being attacked only slighty by mineral acids.

Because of its excellent high-temperature mechanical properties, tungsten is useful for glass-to-metal seals, for numerous aerospace applications, and for radioactive shields. However, its susceptibility to oxidation is often a problem at elevated temperatures.

In the new treatment, the tungsten is initially cleaned with acetone and grit-blasted with clean 60-grit aluminum oxide. The coating is then applied by using an arc-plasma gun.

This work was done by J. Lombard and M. Moynahan of Rockwell International Corp. for **Marshall Space Flight Center.** *No further documentation is available.*
MFS-19347

Electrodeposition Process Reduces Cost of Cold Plates

Efficient nickel heat-exchanger cold plates can be fabricated less expensively than stainless steel plates.

Lyndon B. Johnson Space Center, Houston, Texas

Experimental pure-nickel pin-fin cold plates for heat exchangers have been fabricated by electrodepositing nickel covers on machined nickel cores. The process uses lower-cost production equipment than required for vacuum-retort-brazed stainless-steel cold plates. Furthermore, the frequent replacement of short-life retorts required in vacuum brazing is eliminated. Other advantages of electrodeposition are the ability to produce different types and shapes of plates and the smaller size and weight of the plates due to the better heat-transfer characteristics of nickel versus the steel. If adapted to mass production, it is estimated that nickel cold plates might be made for about 30 percent less than stainless-steel plates.

The process (see Figure 1) is initiated by machine-tooling holes and port openings in the surfaced nickel plate that forms the core. Next the pin-core gap is electric-discharge-machined on both sides of the nickel plate and filled with a rigid wax. One commercially available wax that has been used for this application solidifies into a hard, machinable filler at approximately 155° F (68° C). Next, excess wax is scraped from both faces, and silver powder is burnished into the surfaces. The plate is then immersed into an electrolytic bath for electrodepositing nickel. The cold plate (Figure 2) is finished by melting the wax out of the passages and by cleaning the passages with an appropriate solvent.

The resulting electrodeposited bond in pure nickel has a minimum ultimate tensile strength of 90,000 psi (621×10^6 N/m^2), a yield of 60,000 to 65,000 psi (414×10^6 to 448×10^6 N/m^2), an elongation of 25 percent, and 85 percent reduction in area. Solid copper plates can be made by the same method. Alternately, this flash nickel plating can be applied to stainless-steel cores following step g.

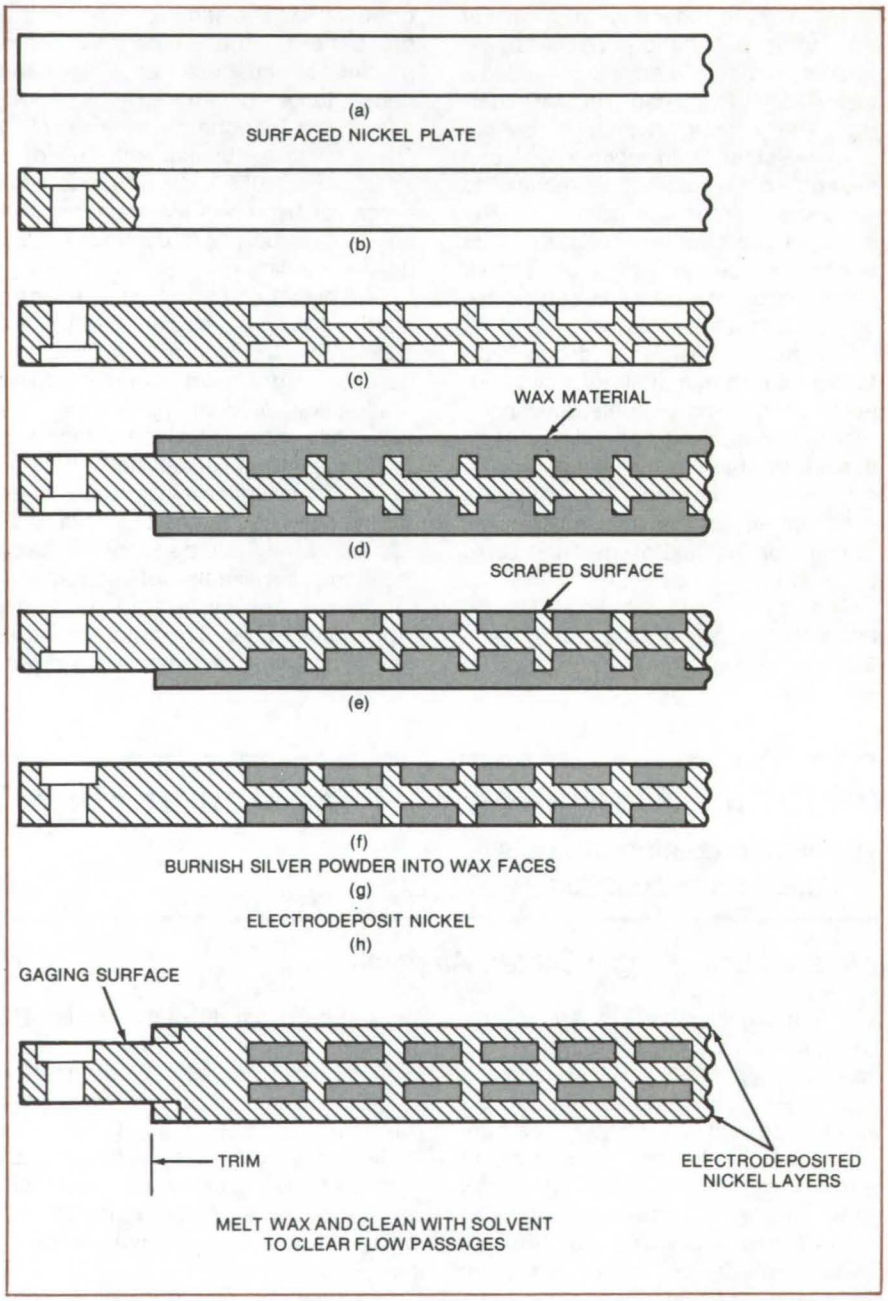


Figure 1. **Experimental Nickel Cold Plates** have been successfully produced at reduced costs by the electrodeposition of nickel cover plates. The process involves the machine-tooling of holes and port openings (step b) of a surfaced nickel plate (a), forming the pin core on both sides (step c), filling the core with commercially-available wax material (step d), scraping both sides to remove the wax (e and f), the burnishing of silver powder into the wax faces (g), and electrodepositing nickel (h). Wax is melted out of the flow passages and cleaned out with appropriate solvent.

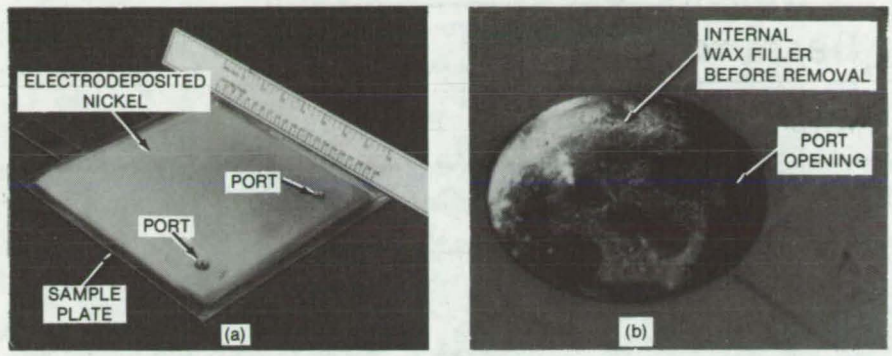


Figure 2. **Photographs of Electroformed Nickel Cold Plate** show the plate sample with electrodeposited nickel (a) and one port after the wax has been machined from the opening (b). The internal wax filler has not been removed and is visible in picture (b).

This work was done by Emil P. Ruppe of Rockwell International Corp. for **Johnson Space Center.** *No further documentation is available.*
MSC-19524

Tube-Shape Verifier

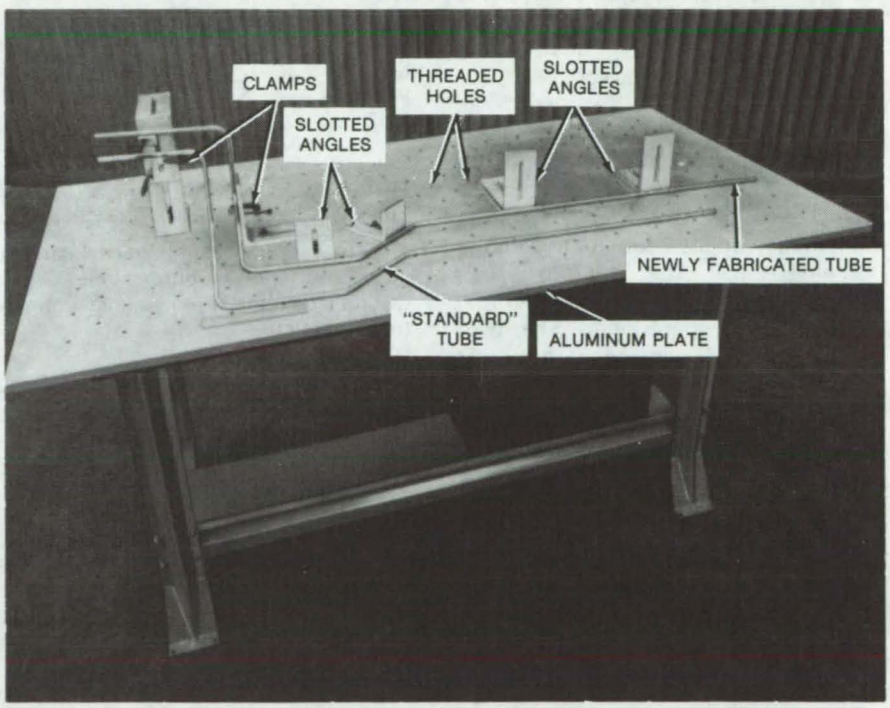
An inexpensive apparatus for checking the accuracy of bent tubes

Lyndon B. Johnson Space Center, Houston, Texas

A relatively simple apparatus can speed up the quality control in tube-bending shops. The accuracy of bent tubes is verified on a flat aluminum tabletop supporting a set of attachments. An assortment of clips, slotted angles, clamps, and bolts is secured to threaded holes on the tabletop (see figure) according to the shape of a "standard" tube bent and measured exactly to the required configuration. Once the setup is fixed, other tubes can be quickly inserted to see if they are bent to the same shape.

The apparatus, developed for the Space Shuttle tube-bending operation, has reduced the rework/rejection rate from over 20 percent to near zero percent. An earlier method of checking bent tubes used standard loose blocks, vees, and other devices that could be accidentally shifted during the tests. On the new apparatus the attachments are bolted down, remaining fixed throughout the tests.

This work was done by August N. Anderson and Charles R. Christ of Rockwell International Corp. for **Johnson Space Center.** *No further documentation is available.*
MSC-19623



Inexpensive Tube-Shape Verifier is used to check the accuracy of bent tubes. An assortment of slotted angles and clamps is bolted down to a flat aluminum plate outlining the shape of a "standard" tube bent to the desired configuration. Newly bent tubes are then checked against this outline. Because the parts are bolted down, the tubes can be checked very rapidly without disturbing the outline. One verifier per tube-bending machine can really speed up production in a tube-bending shop.

Adjusting an Electron Beam for Drilling

A new reticle simplifies the adjustment of the beam and alinement of the workpiece.

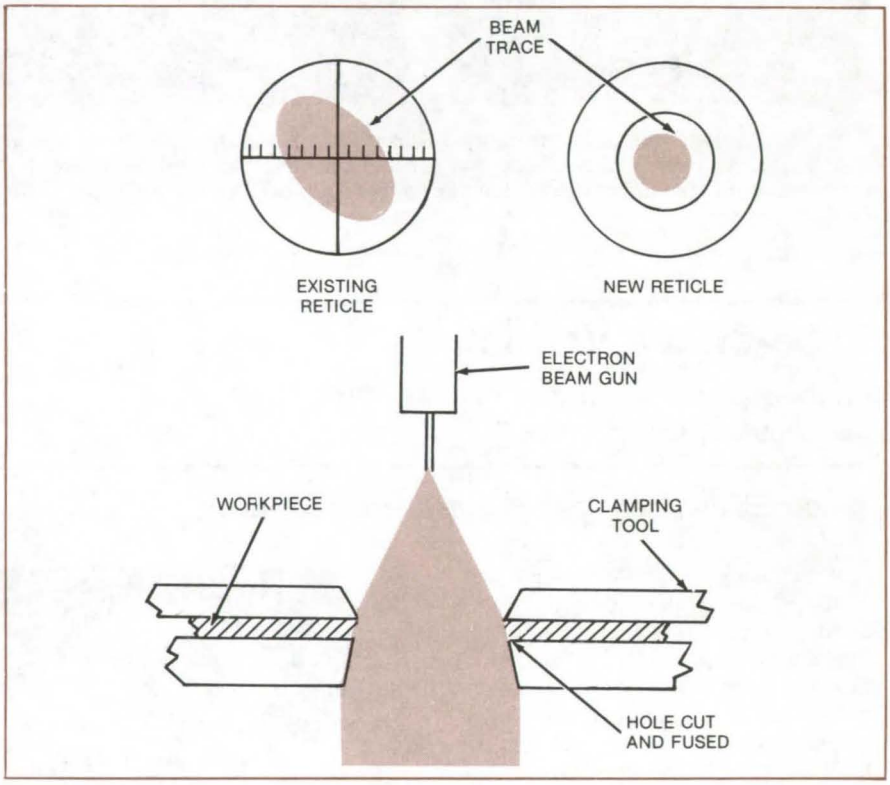
Marshall Space Flight Center, Alabama

A new reticle quickly alines an electron beam for drilling. The glass reticle, which fits into a microscope eyepiece, contains two etched concentric circles.

Looking through the microscope, the operator of the electron-beam drilling machine determines that the electron-beam trace on a target is within the inner circle, adjusting the beam size and shape as necessary (see figure). Then the operator inserts the workpiece and its clamping tool on the machine and looks through the microscope to make sure that the clamp does not extend within the reticle outer circle (adjusting the clamp as necessary). This simple procedure ensures that the electron beam has the proper size and circularity for the hole to be drilled and prevents the electron beam from damaging the clamping tool.

The reticle previously used has crosshairs with a scale on one of the hairlines. To check the beam for circularity and diameter, the operator first directed the beam on a tungsten target and measured the beam trace with the reticle scale. The operator then rotated the eyepiece 90 degrees and measured the trace again. This two-step procedure was repeated for the clamping tool to ensure that the beam would not strike it when drilling commenced.

The new reticle speeds up the electron-beam drilling process by eliminating the need to rotate the eyepiece to make measurements against the reticle scale.



The **New Reticle** contains two concentric circles: The inner circle insures beam circularity, and the outer circle is a guide to prevent the beam from cutting the workpiece clamp. Precise measurement of the beam and clamp was required with the old reticle.

This work was done by Charles L. Childress of Rockwell International Corp. for **Marshall Space Flight Center.** *No further documentation is available.*
MFS-19326

Repairing Sealing Surfaces on Aluminum Castings

New method reduces repair time.

Marshall Space Flight Center, Alabama

Damaged sealing surfaces on aluminum castings used on spaceflight rocket engines have been experimentally repaired using stylus copper plating. In the original procedure, voids were filled with copper, and a stylus cadmium-plating cap was applied over the copper to prevent galvanic corrosion by the large electromotive potential difference between the copper and aluminum. Unfortunately, the cadmium would vaporize in a flight environment (vacuum) and could not be used on flight-scheduled engines. In addition

the repaired area had to be remachined or lapped extensively to eliminate porous and scratched areas.

A new approach using stylus nickel plating instead of the copper and cadmium plating has simplified the repair procedure and allowed the casting to be used in flight. The damaged sealing surfaces are stylus nickelplated in one step. Superficial scratches and porous areas are removed more easily from the repaired surface by simply lapping the sealing areas to the required finish.

Although the method is aimed for aerospace components, it may be easily incorporated into conventional aluminum-casting technology. This one-step repair can be considered for cast-aluminum automobile and aircraft engines to reduce the time and costs.

This work was done by Timothy L. Hanna of Rockwell International Corp. for **Marshall Space Flight Center.** *No further documentation is available.*

Inquiries concerning rights for the commercial use of this invention should be addressed to the Patent Counsel, Marshall Space Flight Center [see page A5]. Refer to MFS-19455.

Protecting Brazing Furnaces From Air Leaks

An envelope of inert gas avoids process interruption in the event of a leak.

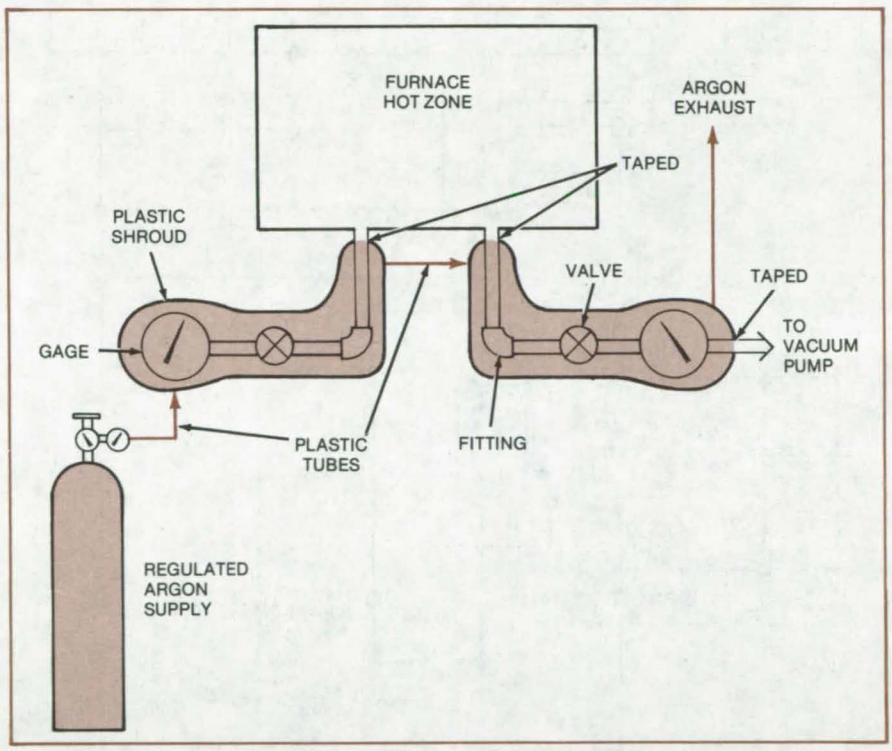
Marshall Space Flight Center, Alabama

Leakage in vacuum brazing furnaces most likely occurs around instrumentation and plumbing. Air entering the chamber through deteriorated pipefittings, valves, and gages can oxidize the hot metal surfaces of parts being brazed or heat-treated. Then the process must be interrupted because oxidized surfaces will not wet with the molten braze alloy nor will they qualify as heat-treated components.

An economical procedure used with the brazing furnace for the Space Shuttle main-engine nozzle eliminates this costly problem. A plastic shroud filled with neutral gas (e.g., argon) encases all the critical external components that may spring a leak. If the leak occurs, harmless argon will enter the chamber, making it possible to finish the process before the shutdown.

All the fittings, valves, and gages are shrouded in transparent plastic sheet and sealed with tape (see figure). The encased areas are interconnected with plastic tubes tape-sealed to the sheets. Then covered areas are flushed with argon and kept inflated with it by a continuous "soft flow" [e.g., 10 ft^3/h (0.3 m^3/h)] circulated through the plastic tubes.

The cover does not interfere with the furnace operation. Gages may be read and valves adjusted through the clear plastic without rupturing the argon envelope. As an added protection against leakage, it is suggested that pipefittings be eliminated from the hot zone by using solid pipes and welded joints.



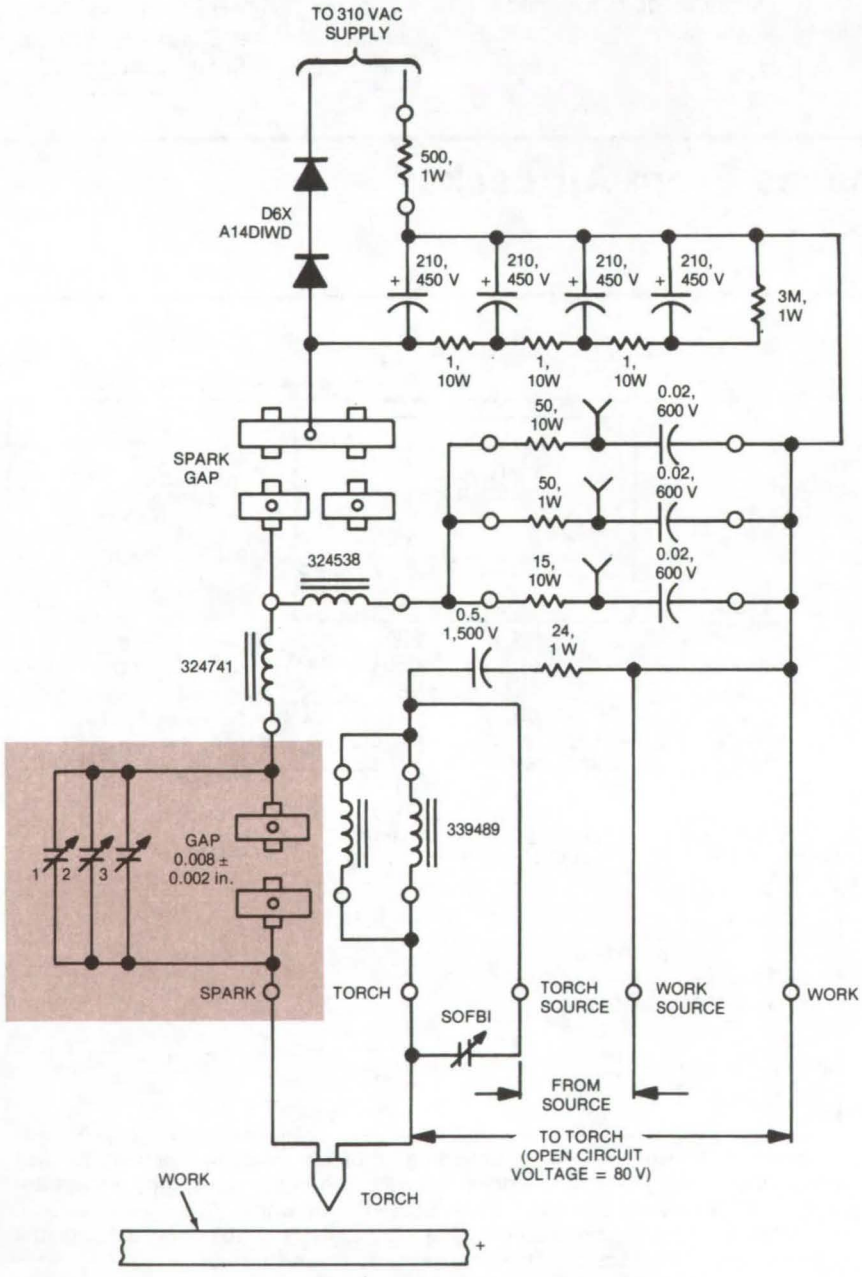
An **Inexpensive Inert-Atmosphere Shielding** protects vacuum brazing-furnace components that are likely to spring a leak. Pipefittings, gages, and valves are encased in a transparent plastic shroud inflated with argon. If a leak develops, harmless argon will enter the vacuum chamber, making it possible to finish the ongoing brazing or heat treatment before shutting down for repair.

This work was done by Carl T. Armenoff and Ross D. McKown of Rockwell International Corp. for **Marshall Space Flight Center.** *No further documentation is available.*
MFS-19379

An Improved Welding-Arc Starter

A simple circuit modification makes the pulse-arc starters more reliable at low currents.

Lyndon B. Johnson Space Center, Houston, Texas



NOTE: ALL RESISTANCE VALUES ARE IN OHMS AND ALL CAPACITOR VALUES IN MICROFARADS UNLESS OTHERWISE STATED.

A **Spark Gap** has been installed in the commercially-developed pulse-arc starter circuit above. The colored area in the capacitive discharge circuit shows where a fixed 1-ohm, 20-W resistor was replaced by the gap. The gap allows sufficient time for the charge to build up to initiate a welding arc. The arc is initiated for a longer time to assure a reliable start at currents as low as 10 A from the welder power supply.

Pulse-arc starters used in high-current (800- to 1,000-A), automatic, fusion-welding apparatus frequently failed to activate arcs, particularly at welding-supply currents below the 100- to 150-A range. That problem has been solved (see figure) by using a spark gap instead of a dropping resistor in the spark-discharge leg of the starter circuit. The gap modifies the discharge-circuit time constant by presenting an inversely-resistive discharge path. The net effect is that the conductance between the tungsten electrode (torch) and the work surface is increased and that the current is applied for a longer time, making it possible to develop an arc at inputs as low as 10 A.

Basically the starter ionizes helium shield gas to create a conductive path for the current generated by the welding-machine power supply. The spark gap is set at 0.008±0.002 in. (0.20±0.05 mm). As the power is applied, no conduction occurs at the gap until the voltage reaches approximately 2,000 V; i.e., the breakdown, or ionization, level. The delay allows the initial arc to occur with an increased-voltage rise time at the tungsten electrode. Sufficient charge is then developed between the electrode and the work surface to initiate an arc for a prolonged time. Once the arc is started, it is maintained at a lower voltage level than in the previous arrangement due to sufficient concentration of metallic vapor between the electrode and the working surface as a result of the improved conduction.

This work was done by Thomas J. Taufer of Rockwell International Corp. for **Johnson Space Center.** *No further documentation is available. MSC-17415*

Microscope for High-Temperature Welding

Dark glass in eyepieces lets welder look at fine parts without eye damage.

Lyndon B. Johnson Space Center, Houston, Texas

A conventional binocular microscope has been adapted for use in microwelding. Dark glass, of the same type used in welder's goggles, is inserted under the rubber cushions on the microscope eyepieces (Figure 1). The dark glass filters out harmful intense light from the welding torch and allows the welder to work on small parts at magnifications of 10 to 30 times. Viewed without the dark glass, the torchlight can cause temporary blindness.

The filtered microscope makes it possible to weld miniature parts or repair fine defects and at the same time affords eye protection. The filters are made by cutting disks 1 inch (2.5 centimeters) in diameter from standard welder's goggles.

The binocular microscope was adapted for repairing hairline crasks in the heat-resistant tiles that insulate the Space Shuttle. In this operation, a fine-tip oxyacetylene torch at a temperature of about 2,500° F (1,370° C) is applied to the crack so that the surrounding material fuses and fills the hairline void (Figure 2). By observing the process through the microscope, the welder is able to confine the flame tip to the immediate area of the crack, thus preventing further damage to the tile.



Figure 1. **Dark-Glass Disks** cut from welder's goggles are inserted in binocular-microscope eyepieces.

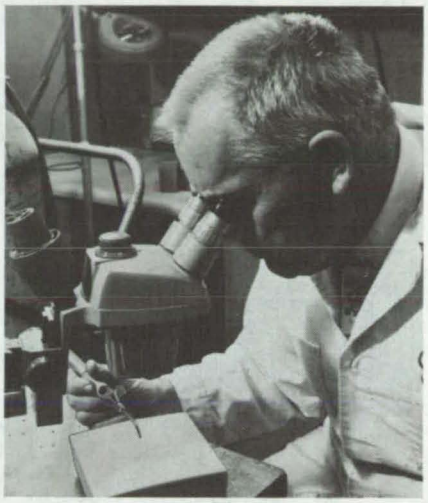


Figure 2. **With the Aid of a Filtered Microscope,** a welder has far better control in fusing hairline cracks.

Previously, the welder had to repair the barely visible crack without magnification, because the necessary goggles kept the eyes too far from the microscope eyepieces.

This work was done by Oliver E. Accountius of Rockwell International Corp. for **Johnson Space Center.** *No further documentation is available.*
MSC-19572

Brazing Titanium to Stainless Steel

A new approach makes it possible to braze the two metals.

Langley Research Center, Hampton, Virginia

Titanium and stainless-steel members are usually joined mechanically for lack of any other effective method. This approach adds weight and bulkiness to the joined assembly. Conventional welding and brazing techniques have not been entirely effective or efficient due to the different melting points of the two metals and other metallurgical incompatibilities that can arise among the titanium, steel, and braze alloys that would weaken or break the bond.

A new approach using a different brazing alloy and plating the steel member with nickel resolves the problem. The new braze alloy is made of silver, 9 percent palladium, and 9 percent gallium. Before the brazing, the stainless-steel member is plated with a coat of nickel 0.05 to 0.1 mil (0.001 to 0.002 mm) thick. The nickel makes the steel wettable at the brazing temperature.

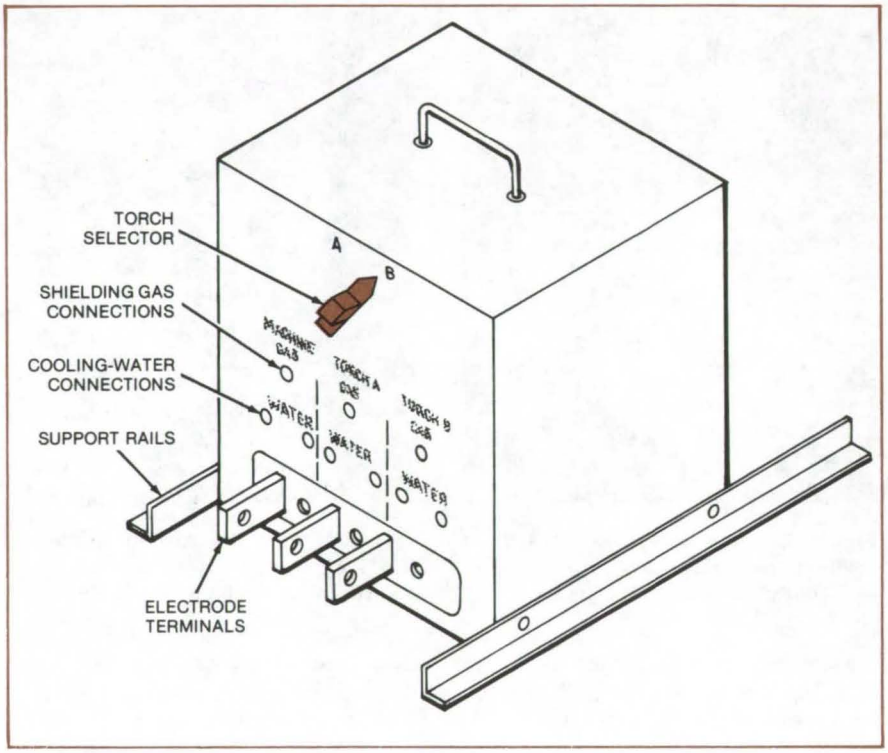
Once these conditions are met, stainless steel can be bonded to titanium in either a conventional brazing furnace or via induction heating. The process must be carried out in vacuum or in an inert atmosphere.

This work was done by Roy I. Batista of TRW, Inc., for **Langley Research Center.** *No further documentation is available.*
LAR-11441

Switchbox for Welding Torches

A proposed switchbox speeds up changeover from one torch setup to another.

Marshall Space Flight Center, Alabama



This **Proposed Switchbox** can be used to change from one welding torch setup to another without stopping the production line. A simple flip of a switch connects gas, water, and power to the selected torch. In conventional systems, production must be stopped so that maintenance people can disconnect one and reconnect another torch.

Welding production lines sometimes require a changeover from one torch setup to another to weld different parts of an assembly. Normally two separate torch systems are used with their own water, gas, and power supplies; or one setup is removed, and a second is connected to the same supply system. Separate systems are expensive, and connecting and disconnecting systems require costly time.

A proposed low-cost approach to the problem is a switchbox as shown in the illustration. The box would be connected simultaneously to two torch setups fed by a single supply system. A switch would automatically shut off gas, water, and power supplies to one torch and connect them to the other. A production line need not be stopped to call maintenance personnel for the changeover. The line operator would simply flip the swtich and proceed working with the selected torch.

This work was done by R. K. Burley of Rockwell International Corp. for **Marshall Space Flight Center.** *No further documentation is available.*
MFS-19354

Thermal Jack

A brazing-furnace fixture keeps parts together during brazing.

Marshall Space Flight Center, Alabama

An auxiliary furnace tool called the "thermal jack" forces a part to match the length of a mating part during brazing. Without this jack, parts with unequal coefficients of expansion may buckle and separate during the brazing process. The thermal jack compensates for this difference.

The illustration shows how the thermal jack has been applied in brazing tubes made from stainless steel (A-286) into a jacket made from Inconel 718 (which has a lower coefficient of expansion than the tube material) for the 10-ft (3-m) Space Shuttle main-engine flight nozzle. In this case, the jack was made from austenitic stainless steel (RA-330) to match the expansion of the tubes.

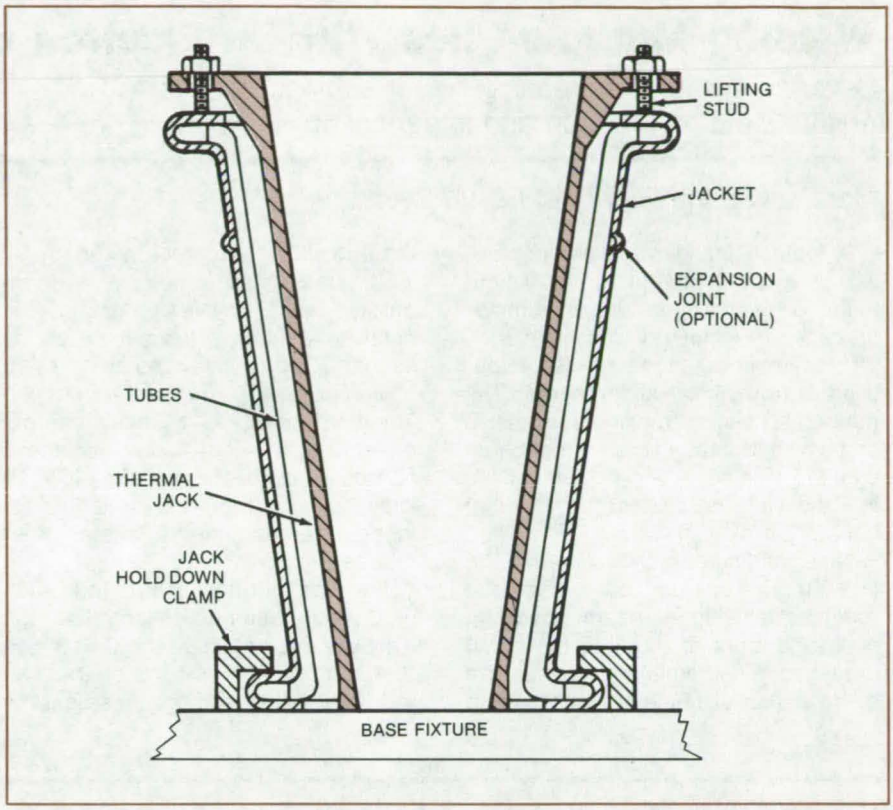
The assembly to be brazed was held on the bottom by the furnace base fixture. The thermal jack was installed resting against the base fixture. It was coupled to the jacket by lifting studs secured on top by nuts.

As the assembly was heated, the thermal jack pushed against the base fixture and lifting studs, stretching the jacket to expand at the same rate as the tubes. Thus the tubes did not buckle and disengage from their intended end locations.

After brazing, the assembly was cooled; and the thermal jack contracted more rapidly than the brazed composite assembly, disengaging the jack from the lifting studs. This is due to the fact that the brazed composite acquires a new linear thermal coefficient that is less than that of the thermal jack.

The thermal coefficients of the jack and the tubes need not be perfectly matched. Minor differences may be compensated by adjusting the length and thermal coefficient of the lifting studs. For example, to increase the expansion of the jack, the length of the lifting stud is increased by using a stud material with a lower thermal coefficient than that of the jack. Conversely, opposite measures are taken to increase the thermal coefficient of the jack. Thus there is some leeway in selecting the thermal jack material.

This work was done by Carl T. Armenoff and Ross D. McKown of Rockwell International Corp. for **Marshall Space Flight Center.** *No further documentation is available.*
MFS-19365



The **Thermal Jack** shown in this example has a coefficient of expansion matching that of the tubes to be brazed. As the furnace is heated, the jack expands and stretches the lower-expanding-coefficient jacket so that the jacket and the tubes stay together during the brazing process [1,900° F (1,038° C)]. The total compensation in this case is 0.2 in. (5 mm) for the 10-ft (3-m) assembly. As the brazed assembly cools, the jack contracts faster and disengages from the lifting studs.

Viewing Electron-Beam Welds In Progress

A filter prevents "blooming" in a TV image of the weld.

Marshall Space Flight Center, Alabama

With the aid of an optical filter, the operator of an electron-beam welding machine can view a TV image of a joint that is being welded and can make corrections as necessary. The operator can see when the weld bead gets out of alinement, for example, and compensate for deflection of the electron beam caused by changes in magnetic field.

The optical filter is placed over the lens of a closed-circuit television camera that views the electron beam and the workpiece. The Wratten 53 filter blocks the intense light emanating from the weld; the light would otherwise overload the vidicon camera and its electronic circuits, causing the image on the TV screen to "bloom" (i.e., white out) so that the weld joint would be obscured.

Although the filter blocks light from the electron-beam weld, it does transmit light in the wavelength range from 520 to 570 nanometers. Therefore, to permit viewing of the weld in progress, the work is illuminated by a mercury-vapor arc lamp, which has a strong emission peak at 546 nm. The filter permits the mercury-vapor light reflected from the joint to reach the TV camera. The operator thus has a clear view of the joint on the screen.

This work was done by C. T. Armenoff of Rockwell International Corp. for **Marshall Space Flight Center.** *No further documentation is available.*
MFS-19364

Welding Multiple Plies With an Electron Beam

Several passes at increasing power settings ensure weld penetration and integrity.

Marshall Space Flight Center, Alabama

A method for electron-beam welding of multi-ply metal sheets eliminates ply separation and minimizes porosity. The method was developed for assembling bellows made of four plies of iron/nickel alloy sheets. The method consists of making successive stitch welds with the electron beam until the weld seam is completely filled in and all the plies have been penetrated.

Nine welding passes are made. The first three passes are made at progressively higher beam power to penetrate more deeply into the metal in stages. The remaining passes are made a short distance on either side of the original weld to seal the seam.

The first pass, made at a beam current of 5 milliamperes in the bellows fabrication, fuses the first and second plies. The second pass, at 10 milliamperes, penetrates the third ply. The third pass, at 13 milliamperes, penetrates the fourth ply. For these passes, the beam voltage is 120 kilovolts, and the weld speed is 80 inches per minute (2 meters per minute).

For the fourth, fifth, and sixth passes, the beam is deflected so that it strikes the metal surface 0.010 inch (0.25 millimeter) inboard of the first weld. Beam currents for these passes are 3, 6, and 6 to 8 milliamperes, respectively. As before, beam voltage is 120 kilovolts, but weld speed is only 30 inches per minute (0.75 meter per minute).

For the seventh, eighth, and ninth passes, the beam is deflected to strike the metal 0.010 inch outboard of the first weld. Weld conditions are the same as in the fourth, fifth, and sixth passes.

This work was done by F. J. Kiluk of Rockwell International Corp. for **Marshall Space Flight Center.** *No further documentation is available.*
MFS-19428

Bonding Soft Rubber or Plasticized Elastomers to Metal

A technique of obtaining durable bond that will withstand loads

Marshall Space Flight Center, Alabama

During the Space Shuttle program, soft-rubber flex seals were bonded to the metal exhaust nozzle of the solid-fuel rocket motor. A primer and adhesive were applied to the cleaned metal surface. The rubber was then pressed to the adhesive and cured at 300° F (150° C) for 1 hour. This type of bond frequently failed under pressure or other loads. The weakness was due to the diffusion of soft-rubber plasticizing agents into the adhesive.

A new approach using a bond-cover coat of unplasticized rubber between the soft rubber and the adhesive eliminated the diffusion problem. The resulting bond is much stronger and more durable.

First the metal surfaces [in this case two disks 2 in. (5 cm) in diameter] are prepared by sandblasting, washing with toluene, and drying with acetone. The surfaces are conditioned by applying a coat of metal primer (Chemlok-205 or equivalent) and drying for 30 min. Next an adhesive coat (Chemlok-220 or equivalent) is applied over the primed surface and dried for 1 hour. The adhesive layer will be covered with a coat of unplasticized rubber.

The bond-cover coat is prepared by dissolving a quantity of milled and mixed rubber in the adhesive. The milled and mixed rubber is prepared by dissolving Norsorex rubber, or equivalent, containing plasticizers and curing agents, in toluene and exposing the mixture to vacuum for 1.5 hours. The rubber then is mixed with the adhesive and poured on an aluminum foil to dry overnight at room temperature. The resulting dried sheets are about 30 mils (0.8 mm) thick and are cut and removed from the foil to cover the size of the bond area.

The cover coats are placed on adhesive surfaces of both metal pieces, and the soft rubber to be bonded to the metal is sandwiched in between the cover coats. The entire assembly is molded and cured at 300° F (150° C) for 1 hour.

This approach would be useful in making improved seals in automobile engines, industrial and public plumbing, and in other areas using soft-rubber-to-metal bonds. Seals and gaskets made this way would not have to be replaced very often, reducing the cost of maintenance.

This work was done by Johnny M. Clemons, Frank E. Ledbetter III, and William T. White of **Marshall Space Flight Center.** *No further documentation is available.*

Inquiries concerning rights for the commercial use of this invention should be addressed to the Patent Counsel, Marshall Space Flight Center *[see page A5].* *Refer to MFS-25181.*

Vacuum-and-Pressure Laminating Polymer Materials

Outgassing prior to bonding reduces voids.

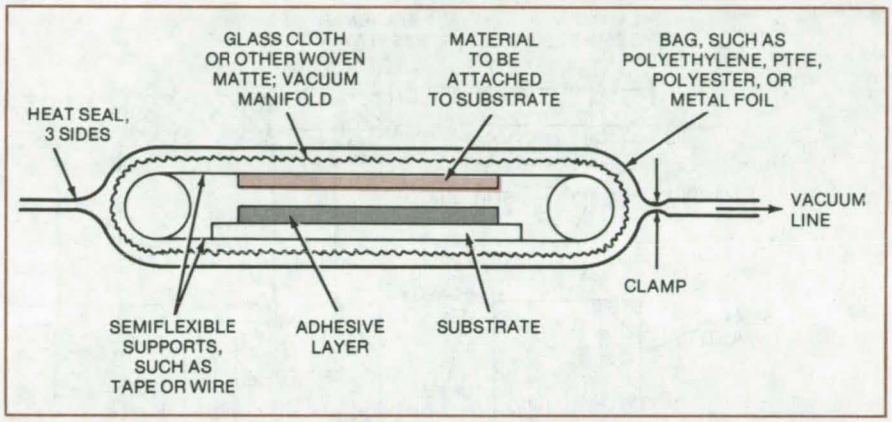
Lewis Research Center, Cleveland, Ohio

A technique that eliminates voids in either the base material or the bonding adhesive has been developed for laminating two or more polymer materials in a vacuum environment. Existing techniques utilize a vacuum environment simply as a means of applying pressure to the parts being bonded, and gases coming from adhesives or from the material surface frequently are trapped. Ultimately these gases would migrate or diffuse, causing large voids with resulting part failure.

The new technique involves manipulating the materials in such a manner that all gas-containing materials are outgassed by exposure to vacuum prior to bonding, thus eliminating the potential voids or void formations. The void-free process consists of the following steps (see figure).

Step 1: Surfaces of materials to be bonded are prepared to insure cleanliness. The cleaning process depends on the type of material to be bonded. The adhesive used should be viscous (greater than 100,000 cps) to minimize handling problems.

Step 2: The parts are attached to a rolled metal picture frame that is approximately 10 percent longer and wider than the parts, to permit the bonded material to stretch. The thickness or strength of the frame depends on the size and weight of the parts, on the final orientation of the bagged assembly during step 4, and on the flexibility of the supports for the parts. The substrate is centered in the frame. Masking tape is attached to the back of the substrate and to each end of the frame. Adhesive is applied to the substrate. The material to be bonded to the substrate is taped across the frame with a gap left between this material and the adhesive.



Lamination Setup is used to produce void-free bonds by first employing a vacuum to outgas the materials and adhesive at a temperature below the curing temperature and then subjecting the assembly to pressure and temperature necessary for cure.

Step 3: The frame assembly is wrapped with one layer of fiberglass cloth, which augments vacuum pumping of large areas ($\cong$>50 in.^{2}) during step 5. The assembled unit is then inserted into a plastic bag. The bag material depends on subsequent bakeout and cure requirements. A tube with a quick-disconnect attachment is inserted several inches into the bagged assembly. Two flat pieces of metal with recesses to accommodate the tube are clamped to the bag in order to seal the bag for evacuation.

Step 4: The bagged assembly is inserted into a vacuum chamber, and the quick-disconnect fitting of the assembly is attached to a closed vacuum line, which is accessible from the top of the chamber. The bagged assembly is then lowered into the vacuum chamber. Next, the vacuum chamber is sealed and evacuated, so that the bagged assembly expands. Care must be taken not to rupture the bag. The vacuum line is then opened so that a vacuum is applied to the interior of the bagged assembly. The evacuated assembly is exposed to temperatures for times sufficient to remove contaminants without curing the adhesives.

Step 5: While maintaining the vacuum in the vacuum line, the exterior of the assembly is subjected to pressure. Either gas or liquid may be used for pressurization, depending on further processing requirements.

Variations of the vacuum-and-pressure laminating process are possible as long as the basic concept of step 4 is retained. The process can be successfully utilized for either continuous or batch production.

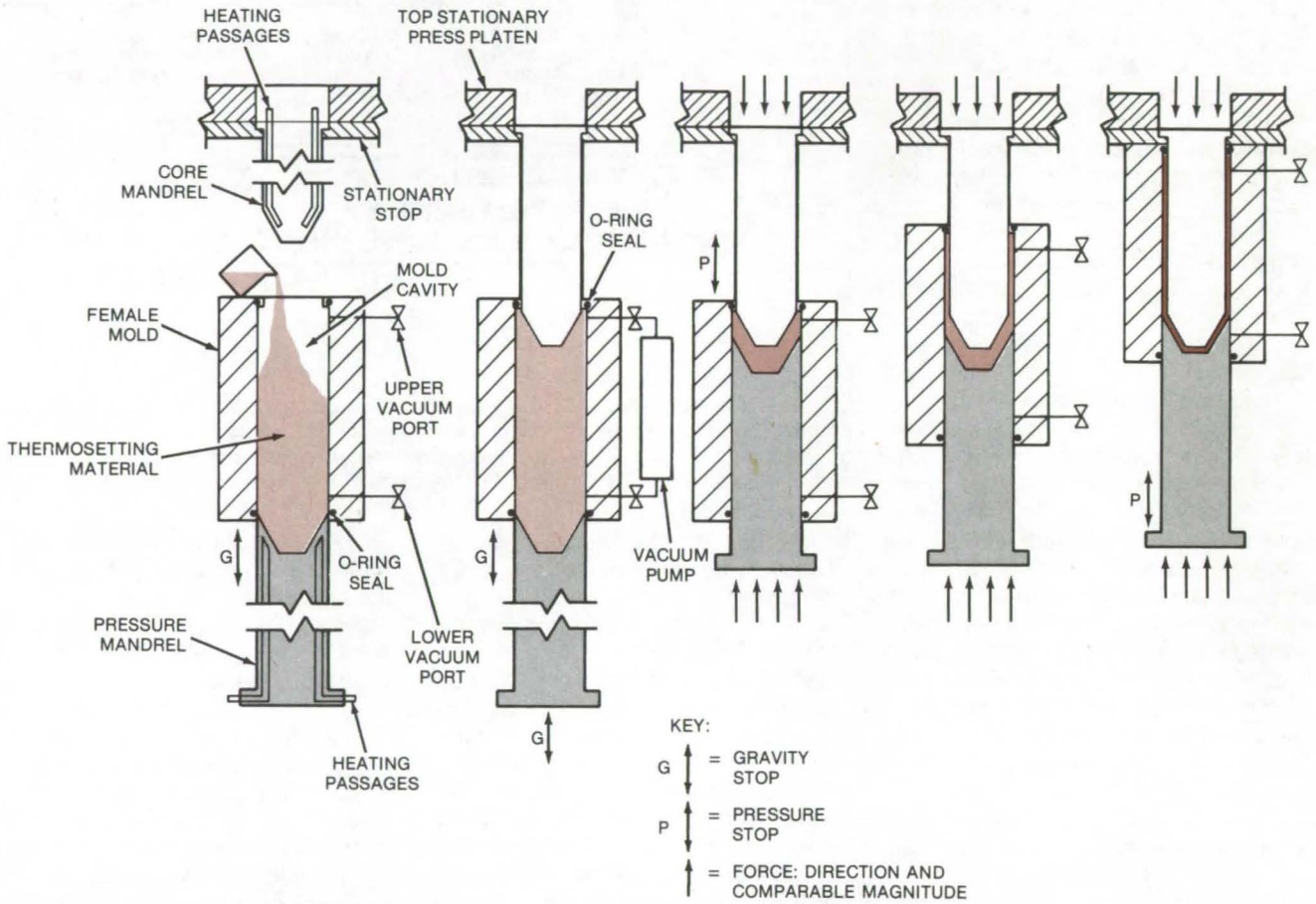
This newly developed technique permits the use of adhesive systems having a high solvent content that previous systems did not allow. It should be of interest to producers of rigid or flexible printed circuits, solar-collector coatings, or similar composite-bonding operations.

This work was done by David R. Hoffman and Thomas J. Riley of **Lewis Research Center.** *No further documentation is available.*
LEW-12721

Evacuated-Displacement Compression Molding

Floating female mold prevents increase in cavity volume.

Langley Research Center, Hampton, Virginia



Compression-Molding Process, as described in the text, comprises (a) loading the molding compound, (b) evacuation, (c) applying pressure to shape the softened compound, (d) further compressing the compound while using the compound as a hydraulic fluid, and (e) applying heat and pressure for cure.

A new approach to evacuated-displacement compression molding prevents an increase in cavity volume. When molding long, thin-walled tubular shapes from thermoset resin, the female mold is allowed to "float," and the softened resin charge acts as a hydraulic fluid.

A predetermined quantity of molding compound is loaded into a female cavity closed at one end by a pressure mandrel. After closing the other end of the female mold with a core mandrel, the loaded cavity is evacuated by applying a vacuum of 1 to 5 mm Hg for 15 to 30 minutes. The mold temperature is raised to the minimum temperature at which the resin constituent of the compound will soften or plasticize, and a pressure of 2,500 psi (173×10^6 N/m^2) applied by the pressure mandrel for 5 to 15 minutes. While maintaining vacuum and temperature, the pressure mandrel force is reduced sufficiently to remove the female pressure stop. When the 2,500-psi force is reapplied, the compound, acting as a hydraulic fluid, propels the female as the mandrel ends converge. This movement continues until the female mandrel again lands on a preselected pressure stop. At that point a second pressure stop is placed to prevent further penetration of the female mandrel by the pressure mandrel.

Pressure mandrel force is then increased by about 10 percent, and that of the core-mandrel pressure is reduced to assume the 2,500-psi molding pressure. The mold temperature is then increased to and maintained at 300° to 350° F (149° to 176° C) for a period of 30 to 60 minutes while maintaining the vacuum and pressure of both mandrels. The core mandrel is then force-cooled to help remove it easily from the tubular article, which remains in the female mold. By opening the press to the starting position (a, in the figure) and installing a pressure stop to lock the female against its lower gravity stops, the molded article is pushed from the cavity by the pressure mandrel.

The major advantage of this method is that it prevents an increase in cavity volume (sporadic or general) throughout the transformation phase of molding. The cavity volume is determined by the compound volume. Also, as required, the speed of transformation at a given pressure depends on the viscosity of the plasticized compound. Transformation of the compound from billet to tubular article is inherent, and the resin constituent is at the best possible stage of polymerization as the full formed part is completed.

This work was done by Wilbur C. Heir of **Langley Research Center.** *No further documentation is available.*

Inquiries concerning rights for the commercial use of this invention should be addressed to the Patent Counsel, Langley Research Center [see page A5]. Refer to LAR-12523.

Electromagnetic Bonding of Plastics to Aluminum

High-temperature-cure adhesives are bonded to aluminum surface without degrading its heat-treatment condition.

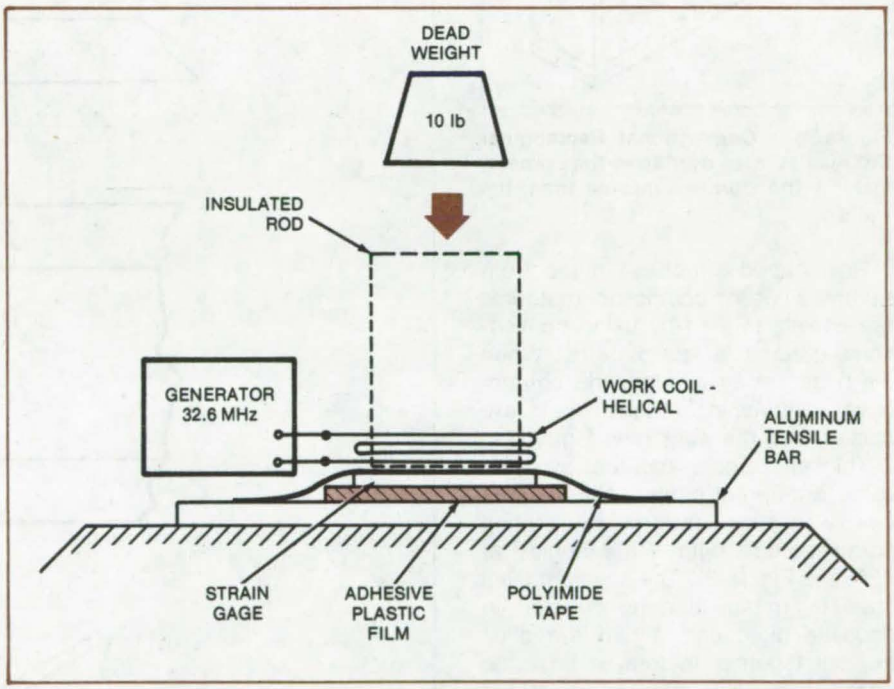
Marshall Space Flight Center, Alabama

A new process based on an earlier study incorporates electromagnetic energy for bonding high-temperature-cure [above 350° F (175° C)] plastic adhesives to aluminum surfaces without affecting the heat-treatment condition of the aluminum. Electromagnetic energy heats only the plastic/metal interface, by skin effect. The process has been shown to work with polyimide and polyamide/imide adhesives and has been used to bond strain gages to 2219-T87 aluminum. It replaces a more complex procedure using electromagnetic or ceramic powder materials dispersed in the plastic adhesives for electromagnetic bonding.

The setup as shown in the illustration incorporates a helical induction coil fed by a 32.5-MHz, or greater, generator. The top part of the core forms an insulated rod.

An aluminum tensile bar is laid on a working level, and the polymer adhesive is applied to the aluminum surface. The strain gage is placed on top of the adhesive and covered by a polyimide tape. Next the coil and a weight are placed on top of the assembly. Electromagnetic energy applied at 32.6 MHz cures the adhesive in 2.5 to 2.8 s at about 500° F (260° C) without affecting the aluminum.

The finished specimens were successfully tested in liquid hydrogen and exhibited no creep to 400° F (205° C).



Electromagnetic Curing is used to bond a strain gage to an aluminum tensile bar. Electromagnetic energy heats only the plastic/metal interface by means of a skin effect, preventing degradation of the heat-treated aluminum. The process can be easily applied to other metals joined by high-temperature-curing plastic adhesives.

The process could be applied in bonding plastic-to-plastic components and in metal-to-metal bonding/joining when the finish of the joined metals is not to be altered by such high-temperature processes as soldering, brazing, or welding.

This work was done by Alvin T. Sheppard and Len Silbert of Martin Marietta Corp. for **Marshall Space Flight Center.** *For further information, Circle 72 on the TSP Request Card.*

Inquiries concerning rights for the commercial use of this invention should be addressed to the Patent Counsel, Marshall Space Flight Center [see page A5]. Refer to MFS-25083.

Structurally-Continuous Composite Corners

Flat composite materials are cut at certain angles to form boxes with corners as thick as the walls.

Langley Research Center, Hampton, Virginia

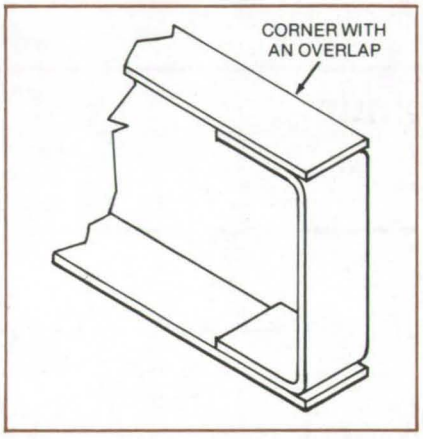


Figure 1. A **Conventional Rectangular Cut** results in an overlap at the corners, making the corners thicker than the walls.

Box-shaped structures made from several plies of composite materials are usually formed by using conventional rectangular-cut patterns. When the plies are assembled, the corners have overlapping edges that are thicker than the walls (see Figure 1).

Thicker corners can be avoided, using a different cutting pattern. The box walls are formed by cutting parallelograms with acute angles at 45° (see Figure 2). The adjacent plies have the parallelograms oriented in opposite directions. When the plies are put together to form a box, the edges with acute angles are folded over around the corners and bonded without overlap. A somewhat different rectangular cut can be used to enclose the entire assembly, also with no overlap.

The proposed patterns produce uniform corners, and the cuts are structured so that shear loads are transferred from ply to ply instead of across one surface. The technique has been proposed for an aircraft aileron rib structured from alternately-oriented + 45°, -45° composite plies.

This work was done by Anthony C. Jackson and John A. Van Hamersveld of Lockheed Aircraft Corp. for **Langley Research Center.** *No further documentation is available.*
LAR-11942

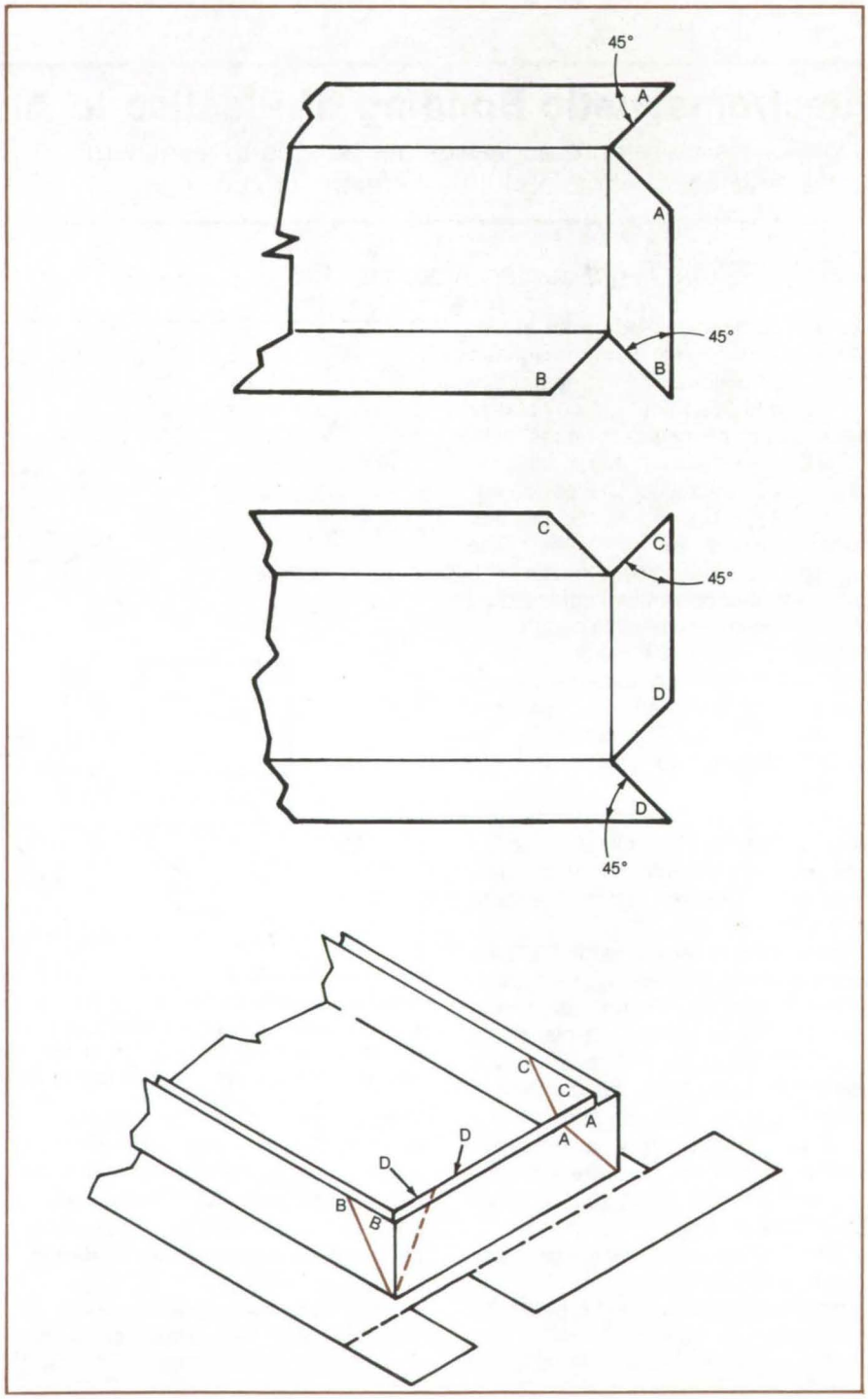


Figure. 2. **Parallelogram-Shaped Walls** fold neatly over, making the corners uniformly thick with the walls. The adjacent composite plies have parallelograms cut in opposite directions, improving the strength of the box. A modified rectangular cut can be used to enclose the entire structure with no added thickness at the corners.

Removing Bonded Skin From a Substrate

Metal skin is peeled off like a sardine-can cover with a key.

Lyndon B. Johnson Space Center, Houston, Texas

An inexpensive and relatively fast method has been used in removing bonded skin from a metal substrate. A saw is used to cut parallel grooves into the skin surface along its entire length. The depth of the saw cuts is about one-half the skin thickness, and the width between the cuts is chosen such that the strips will be easily peeled off. The strips are then peeled off one by one with a slotted pipe by inserting the edge of the skin into the slot and peeling it off like a sardine-can cover.

This method was successfully used in replacing aluminum alloy skin 0.032 in. (0.81 mm) thick with a heavier gage skin on a Shuttle-wing test panel. Two conventional alternatives of either fabricating a completely new assembly or chemically milling the skin off without damaging the substrate were less economical.

The 32- by 80-in. (81- by 203-cm) test panel was grooved into 5-in. (13-cm) strips along its entire length by cutting grooves 0.016 in. (0.41 mm) deept. A 3/4-in. (1.9-cm) steel pipe (a slotted bar may also be used) slotted on one end to accommodate the skin thickness was then applied by inserting the skin edge into the slot. Using a pipe wrench the skin was then peeled off section by section. The substrate was then cleaned and the new skin bonded in place.

The entire operation of grooving, peeling, and fabricating the slotted pipe took about 2 hours. Chemical milling or replacement would have taken much longer.

The method may be useful in removing bonded skins from any substrate where the substrate is strong enough not to buckle or tear when bonded skin is "rolled" free. Also it may be useful for removing sections of damaged skin where bladders or other equipment below the substrate might be damaged if a saw or router were used to cut completely through the skin.

This work was done by Eldon N. Chartier of Rockwell International Corp. for **Johnson Space Center.** *No further documentation is available. MSC-19664*

Books and Reports

These reports, studies, and handbooks are available from NASA as Technical Support Packages (TSP's) when a Request Card number is cited; otherwise they are available from the National Technical Information Service.

Arc-Termination Cracks in Inconel 718 and Incoloy 903

A study investigates the causes of crater cracks and the means to repair the cracks.

Arc-termination crater cracks have been reported in Inconel 718 and Incoloy 903 materials during the welding assembly of the Shuttle main engine. These cracks form at the weld-termination points and if undetected can cause a serious breakdown. Recently a four-phase study was launched to determine the welding conditions conducive to the crater cracks and to establish procedures for fixing them. The results of this study are published in a brief report.

Phase 1 of the program investigated several weld-termination techniques in Inconel 718 to determine the frequency and the degree of crater cracks. The following cases were considered: (a) weld termination without decreasing the welding current, (b) weld termination with a 50-percent reduced welding current, and (c) weld termination using current decay to 5 to 6 A. A total of 16 samples was studied in each case, with 8 samples welded manually and 8 automatically. In the first group, all the weld terminations had crater cracks, most being very deep and some completely through the weld nugget. The second group had detectable cracks in 50 percent of the terminations, while the third group had practically none.

Phase 2 investigated a weld-termination buildup technique using eight manually- and eight machine-welded Inconel 718 samples. This technique involved a weld-movement dwell and buildup by adding an Inconel wire to the weld zone while the current was uniformly reduced to about 5 to 6 A. None of these samples had cracks.

Phase 3 examined a repair procedure to eliminate the crater cracks. Three weld passes were made over each detected crack using one manual- and two machine-welding procedures. The repaired samples had no detectable cracks, but the welded areas exhibited porosity and oxide contamination.

Phase 4 determined the crater-cracking sensitivity of Incoloy 903 as compared to Inconel 718. The former developed crater cracks in 100 percent of the terminations at full welding current. Cases at lower welding currents were not studied. As in Inconel 718, the weld buildup technique eliminated cracks in the Incoloy.

The general observation shows that temperature control of the cooling puddle seems to be the key to obtaining crack-free terminations. An optimum condition is to have a minimum of temperature variations throughout the puddle when the arc is terminated. Crack repairs by welding are not recommended. The cracks should be removed mechanically by etching the area and checking it with a dye penetrant for proper removal.

(continued on next page)

This work was done by E. Bayless, J. McCaig, and R. Poorman of **Marshall Space Flight Center.** *To obtain a copy of the report, "Arc Termination Cracks in Inconel 718 and Incoloy 903," Circle 73 on the TSP Request Card.*
MFS-25089

Cost Savings in LSI Fabrication

Some promising areas of cost reduction in packaging the LSI microcircuits

A 1-year study program was devoted to large-scale integrated (LSI) microcircuits to identify major areas affecting their costs. The program was divided into three tasks: (1) to identify the cost factors involved in packaged electronic subsystems as a function of LSI density and reliability, (2) to select the most promising factors that might be modified to reduce costs in high-density packaging, and (3) to investigate the cost-saving beam tape technology for producing high-volume discrete-device packages. The results of this program are published in a 67-page report.

The first two tasks were combined into a cost factors study. The study encompassed both hybrid and standard discrete LSI devices. Most of the data were obtained from 225 reviewed reference articles and organized in the form of a data summary. The cost factors were divided into three basic classifications: (1) nonrecurring, (2) manufacturing, and (3) production. These classifications were examined in detail and were further broken down to define mathematical cost models that may form the basis of future computerized detailed studies.

Cost equations have been worked out for substrate processing based on the costs of substrate material, circuit processing, circuit complexity, resistor trimming, and quality-control inspection. Cost equations for assembly and test are based on package cost, active and passive chips, package lid, pretin cost, bonding chips, wire bonding, nondestructive pull test, preseal visual quality control, preseal electrical test, troubleshooting before sealing, rework before sealing, preseal inspection, sealing, postseal acceptance test, troubleshooting after sealing, rework after sealing, and final quality-control inspection.

The study recommends that these models be refined and broadened to include such other packaging techniques as ceramic-chip carriers, multichip LSI "subassembly" arrays, and plastic LSI packages. The developed cost factors will be further refined and reduced to formulas for computer solution.

The evaluation of tape chip-carrier technology has shown that this is a viable approach to low-cost LSI packaging and could also reduce hybrid microcircuit costs. The recommended areas for future investigation include: wafer bumping, inner/outer lead bonding, testing, and tape processing. To develop this technology, studies should be made to check the feasibility of interconnecting an array of two, four, or more LSI chips on a tape carrier. These arrays would form standard building blocks for minicomputers and high-density arrays.

This work was done by R. P. Himmel, S. Salmassy, and S. M. Stuhlbarg of Hughes Aircraft Co. for **Marshall Space Flight Center.** *For a copy of the report, NASA CR-150832 [N79-10341/NSP] "Design, Processing and Testing of LSI Arrays Hybrid Microelectronics task," Circle 74 on the TSP Request Card.*
MFS-25079

Mathematics and Information Sciences



Hardware, Techniques, and Processes

583 Optical Comparator Uses Holographic Subtraction
584 Numerical Analysis of Complex Fluid-Flow Systems

Computer Programs

584 Generalized Plotting and Contouring Package
585 Viterbi/Algebraic Hybrid Decoder

Optical Comparator Uses Holographic Subtraction

Integrated optics are combined with holography to process optical data.

Langley Research Center, Hampton, Virginia

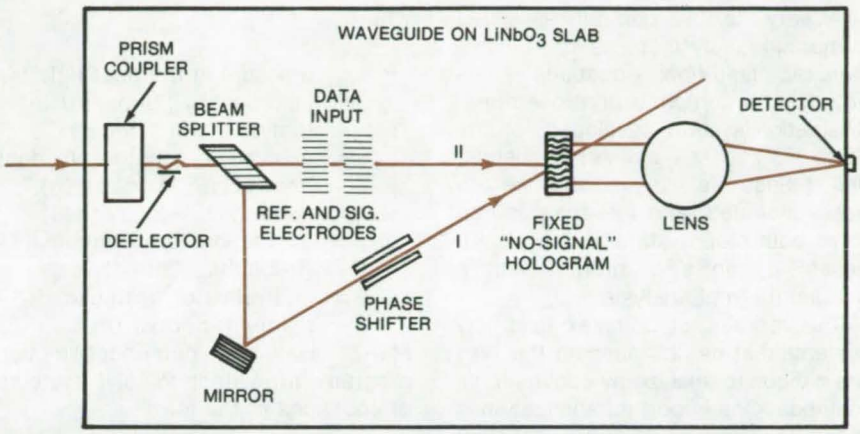
As space missions and Earth-resources surveillance techniques become more sophisticated, NASA is finding itself in the position of being able to gather more data than can be conveniently transmitted, able to transmit more data than can be stored, and able to store more data than can be processed in a reasonable length of time.

A typical example of this problem occurred with a multichannel scanning system called MOCS: Multichannel Ocean Color Sensor. The MOCS lacked a preprocessor to distinguish useful from unuseful data: As a consequence considerable time and effort were required to recover the useful portion of a large data set.

The key to this type of problem is the development of onboard data processors that reduce the amount of transmitted data without losing significant information. An integrated optical comparator (IOC) developed for this purpose is a holographic subtraction device.

The IOC is a preprocessor that signals the MOCS when the information being processed warrants recording. In this way, data that have no desired information are discarded. The IOC compares two sets of voltages: one set, the reference, is characteristic of data that should not be recorded based on some predetermined criteria; the other set, the signal, is characteristic of the information to be processed by the MOCS. When the reference voltage is identical to the data set, the IOC deactivates the MOCS recording system.

The operation of the IOC is based on the principle of holographic subtraction. As shown in the diagram, two coherent guided beams intersect within a photorefractive waveguide to produce a hologram. Beam I traverses a path with an optical length that may be varied by distances on the order of a wavelength. Beam II passes beneath two sets of electrodes to which the reference and signal voltages are applied after the hologram is recorded. For an electro-optic waveguide, these voltages will produce a change in the wave front of beam II. However, if each of the reference and signal voltages match, the phase wave front will be essentially unperturbed.



Integrated Optical Comparator compares reference and signal voltages by their effects on a coherent light beam (beam II above). If both voltages are the same, the beam is essentially unperturbed. If the voltages differ, light is deflected by a previously recorded hologram to a detector.

When at least one of the signal and reference voltages differs in magnitude, the resulting phase perturbation of beam II results in some light being deflected by the hologram toward the detector. Holographic subtraction is frustrated. This is the condition under which the MOCS device operates its record mode.

The IOC effectively combines two existing technologies, integrated optics and holography, for the purpose of processing optical data. The integrated optical configuration offers the advantages of size and ease of alinement. This device will greatly reduce the amount of useless data accumulated in remote-sensing operations such as are performed by the MOCS.

This work was done by David W. Vahey and Carl M. Verber of Battelle Memorial Institute for **Langley Research Center.** *Further information may be found in NASA CR-2829 [N77-28471/NSP], "Feasibility Investigation of Integrated Optics Fourier Transform Devices"* [**$9**]. *A copy may be purchased [prepayment required] from the National Technical Information Service, Springfield, Virginia 22161.*

LAR-12126

Numerical Analysis of Complex Fluid-Flow Systems

An analytical approach with quick answers to a wide variety of heating and cooling problems

Marshall Space Flight Center, Alabama

A very flexible computer-assisted numerical analysis is used to solve dynamic fluid-flow equations characterizing a computer-controlled heat dissipation system developed for the Spacelab. Losses caused by bends, ties, fittings, valves, and the like are easily included, and the analysis can solve both steady-state and transient cases. It can also interact with a parallel thermal analysis.

The varieties of complex fluid-flow systems that can be handled this way are difficult to analyze by conventional methods. One important application is in the development of energy-efficient environmental control systems for heating and cooling homes and buildings.

The analysis uses a finite-differencing technique that can be readily handled by available computer programs. The fluid flow is assumed to be turbulent and incompressible throughout the system.

The basic equation describing a pressure drop for a fluid flowing in a duct from point i to point j may be expressed as

$$P_i - P_j = \frac{\varrho f L_e V^2}{2 g_c D_e} \qquad (1)$$

where

- P = pressure in the duct (lbf/ft^2)
- ϱ = fluid density [lb(mass)/ft^3]
- f = friction factor (Moody)
- L_e = equivalent length of duct from point i to point j (ft)
- V = mean fluid velocity (ft/s)
- g_c = gravitational constant [ft-lb(mass)/lbf-s^2]
- D_e = equivalent or hydraulic diameter of duct (ft)

Many available numerical-solution programs are written to solve systems of equations of the form

$$X = Z(Y_i - Y_j) \qquad (2)$$

where

- X = heat, electric current, or fluid-flow rate
- Z = thermal, electrical, or fluid-flow conductance
- Y = temperature, voltage, or pressure

Equation (1) therefore may be expressed in the form of equation (2) as

$$\dot{m} = \left[\frac{\sigma G}{(P_i - P_j)}\right]^{1/2} (P_i - P_j) \qquad (3)$$

where

- $\dot{m}$ = fluid mass-flow rate [lb(mass)/s]
- G = flow coefficient $= \dfrac{\varrho_0 2 g_c D_e A^2}{f L_e}$ [ft^2 - lb^2(mass)/lbf - h^2]
- σ = density ratio = ϱ / ϱ_0, where ϱ = the local air density [lb(mass)/ft^3] and ϱ_0 is the reference air density for loop simulation [lb(mass)/ft^3]

Using equation (3), a network representing any flow system may be developed. Performance curves for any components, such as fan or heat-exchanger performance, and valve or equipment pressure-drop characteristics may be input as arrays to be used in the solution process to determine system performance. Once a network is established, parametric studies may be rapidly and easily performed by changing component (valve, heating units, fan, diffusers, heat, ducting exchanger, and the like) input data. A fluid-flow system may thus be optimized without very complex analytical techniques.

This work was done by Ronald L. Holland of McDonnell Douglas Corp. for **Marshall Space Flight Center.** *For further information, Circle 71 on the TSP Request Card.*
MFS-25125

Computer Programs

These programs may be obtained at very reasonable cost from COSMIC, a facility sponsored by NASA to make new programs available to the public. For information on program price, size, and availability, circle the reference letter on the COSMIC Request Card in this issue.

Generalized Plotting and Contouring Package

Wide range of graphics capabilities

PLOTPAK is a complete general-purpose plotting and contouring package. A flexible and easy-to-use system, it produces line-printer, television-screen, and DICOMED plots. Plots, from the quick and simple to the complex and sophisticated, can be generated with only a basic knowledge of FORTRAN and the PLOTPAK commands. Offering several advantages over standard hardware-support packages, the wide range of ready-to-use graphics saves program-development time. PLOTPAK has proved to be a useful part of the Atmospheric and Oceanographic Information Processing System (AOIPS) in use at the NASA Goddard Space Flight Center.

The PLOTPAK package has a plotting segment and a contouring segment. The plotting segment includes ready-to-use commands for producing linear, semilog, log/log, and polar plots. The user may specify horizontal labels, vertical labels, and vector characters of any size. These may be placed either in terms of device coordinates or the user's plotting coordinates.

Gridding routines automatically generate full grids, open grids, and axes with or without tick marks. Special line features include solid, dashed, multiple-character printer, and character plotter lines. The contouring segment can contour any regularly spaced or random data. The data are fitted to the desired grid, and the contour is generated at specified values. The contouring segment uses the plotting segment for actual plot generation; therefore all of the plotting-segment features are available during the contour plotting.

The PLOTPAK system is written in FORTRAN IV PLUS and has been implemented on a PDP 11/70 computer under control of RSX 11D with a central memoury requirement of approximately 32K of 16-bit words. Plotted output is generated for either the line printer, the Hazeltine graphics terminal, the DICOMED plotter, or any combination of these three simultaneously. The PLOTPAK system was developed in 1977.

This program was written by D. Rubin of Computer Sciences Corp. for **Goddard Space Flight Center.** *For further information, Circle R on the COSMIC Request Card.*
GSC-12367

Viterbi/Algebraic Hybrid Decoder

Hybrid decoder for compound channels

In recent years the demand for efficient and reliable digital transmission systems has been accelerated by the increased use of automatic data processors. The need for long-range transmissions has been increased to support global crop-production forecasting, local weather forecasting, severe storm tracking and prediction, water availability studies, land-use surveys, and pollution monitoring. These applications involve high data volumes, high transmission rates, and the need for rapid throughput.

The most serious problems encountered in any high-speed data-transmission system are the occurrence of errors and the need for bandwidth compression. The most promising approach to eliminating, or at least significantly reducing, both of these problems is the use of encoding and decoding algorithms to compress the data for transmission and to correct errors upon receipt.

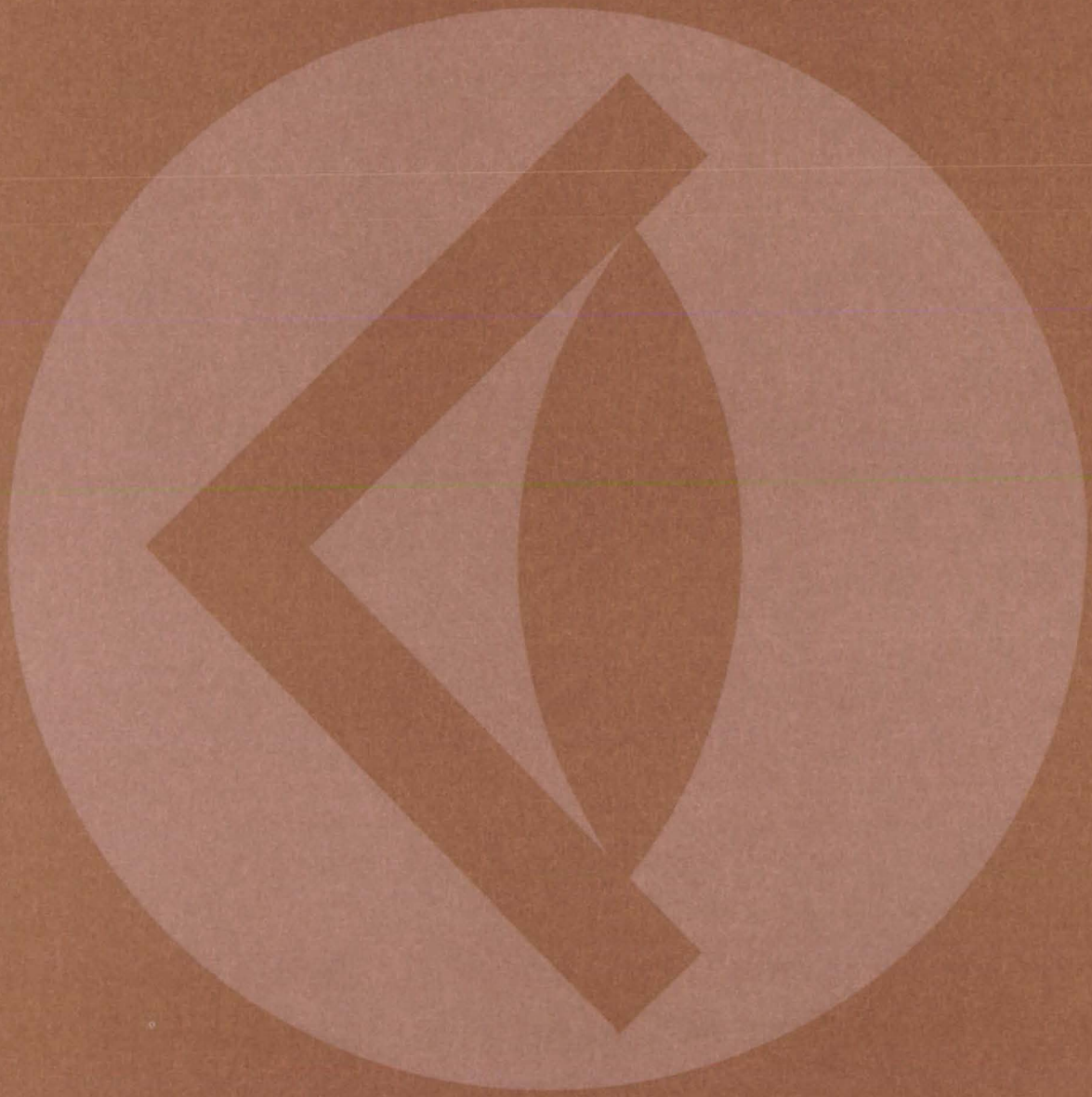
A new decoder computer program is a hybrid between the optimal Viterbi and the optimal algebraic decoders. Tests have shown that the hybrid decoder outperforms any strictly Viterbi or strictly algebraic decoder and effectively handles compound channels. The algorithm developed uses syndrome-detecting logic to direct the two decoders to assume the decoding load alternatively, depending on the real-time channel characteristics.

The algebraic decoder component of the hybrid decoder is an optimal "B2" burst corrector suitable for decoding nonsystematic convolution codes. The algebraic decoder is capable of correcting any short burst that does not exhaust the storage capacity of the decoder. It can also correct long bursts with a high probability without sacrificing the random-error-correcting capability of the code. The Viterbi decoder component of the hybrid decoder handles random channel errors. When encountering long bursts that are beyond the capability of the algebraic decoder, the overall system still tends to outperform a stand-alone Viterbi because error propagations are suppressed.

The decoder algorithm is written in FORTRAN IV for batch execution and has been implemented on the UNIVAC 1108 with a central memory requirement of approximately 55K of 36-bit words. Access to the UNIVAC MATHPACK library is required. This program was developed in 1978.

This program was written by Robert W. Boyd, Frank M. Ingels, and Chung-Dau Mo of Mississippi State University for **Marshall Space Flight Center.** *For further information Circle S on the COSMIC Request Card.*
MFS-25095

SUBJECT INDEX



ACOUSTIC PROPERTIES
Measuring acoustic properties of materials and jet nozzles
page 523 LEW-13265

ADDITIVES
Scratch encourages selective doping
page 557 LAR-11590

ADHESIVE BONDING
Bonding soft rubber or plasticized elastomers to metal
page 574 MFS-25181

Electromagnetic bonding of plastics to aluminum
page 577 MFS-25083

Vacuum-and-pressure laminating polymer materials
page 575 LEW-12721

AERODYNAMIC LOADS
Aerodynamic performance of jet-flap wings
page 538 ARC-11215

AILERONS
Structurally-continuous composite corners
page 578 LAR-11942

AIR CARGO
Helicopter sling loads
page 540 LAR-12557

AIRCRAFT TIRES
Tire-pressure measuring concept
page 524 MSC-18490

AIRFOILS
Transonic airfoil analysis and design
page 540 LAR-12354

ALGORITHMS
Viterbi/algebraic hybrid decoder
page 585 MFS-25095

ALIGNMENT
Adjusting an electron beam for drilling
page 568 MFS-19326

ALLOYS
Alloys of immiscible metals
page 508 MFS-23816

ALUMINUM ALLOYS
Synthetic seawater as stress-corrosion test medium
page 525 MFS-22706

AMPLIFIERS
Rise-time control in saturated amplifiers
page 470 MSC-14934

ANALYZERS
Detector verifier for circuit analyzers
page 530 MSC-19669

ARC WELDING
An improved welding-arc starter
page 570 MSC-17415

Arc-termination cracks in Inconel 718 and Incoloy 903
page 576 MFS-25089

ATMOSPHERIC TEMPERATURE
Rugged fast-response temperature probe
page 531 ARC-11289

AUTOMATIC TEST EQUIPMENT
Detector verifier for circuit analyzers
page 530 MSC-19669

AZIMUTH
Azimuth correlator device
page 469 NPO-14614

BAFFLES
A tool for installation/removal of cylindrical baffles
page 551 MFS-19508

BELLOWS
Welding multiple plies with an electron beam
page 574 MFS-19428

BENDING
Tube-shape verifier
page 567 MSC-19623

BINARY ALLOYS
Single-, two-, and three-phase binary-alloy systems
page 511 LAR-12381

BODY FLUIDS
Extracting trace substances from biological fluids
page 516 MSC-18522

BRAZING
Brazing titanium to stainless steel
page 571 LAR-11441

Electrodeposition process reduces cost of cold plates
page 556 MSC-19524

Protecting brazing furnaces from air leaks
page 569 MFS-19379

Thermal jack
page 572 MFS-19365

CADMIUM SULFIDES
CdSInP semiconductor alloy
page 494 LAR-12405

CALIBRATING
A practical Josephson voltage standard
page 488 MFS-23845

CARBON FIBER REINFORCED PLASTICS
Graphite/epoxy-type test specimens
page 528 MSC-18495

CARDIOVASCULAR SYSTEM
Trifunctional transducer for myocardial monitoring
page 517 NPO-14329

CARRIER INJECTION
Improved degradation resistance of (AlGa)As lasers
page 491 LAR-12242

CERAMIC COATINGS
Inhibiting oxidation of tungsten at high temperatures
page 565 MFS-19347

Longer shelf life for ceramic slurries
page 509 MSC-18543

CIRCUIT PROTECTION
Overload protection for switching regulators
page 468 MSC-18513

CLOSED CIRCUIT TELEVISION
Viewing electron-beam welds in progress
page 573 MFS-19364

CODING
Digital generation of command-encoder waveforms
page 482 GSC-12203

COMMUNICATION CABLES
High-acceleration cable deployment
page 545 ARC-11256

COMPARATOR CIRCUITS
Window comparator for voltages
page 464 FRC-10090

COMPONENT RELIABILITY
JANTX1N3893 diode
page 476 MFS-25266

JANTX1N5415 diode
page 476 MFS-25270

JANTX1N5417 diode
page 476 MFS-25271

JANTX1N5420 diode
page 476 MFS-25272

JANTX1N5550 switching diode
page 476 MFS-25273

JANTX1N5552 switching diode
page 477 MFS-25274

JANTX1N5554 switching diode
page 477 MFS-25275

JANTX1N5614 switching diode
page 477 MFS-25276

JANTX1N5615 switching diode
page 477 MFS-25277

JANTX1N5618 switching diode
page 478 MFS-25278

JANTX1N5619 diode
page 478 MFS-25279

JANTX1N645-1 diode
page 474 MFS-25243

JANTX1N649-1 diode
page 474 MFS-25244

JANTX1N746A diode
page 474 MFS-25245

JANTX1202A switching diode
page 475 MFS-25250

JANTX1N759A voltage-regulating diode
page 475 MFS-25246

JANTX1N937B Zener diode
page 475 MFS-25247

JANTX1N972B Zener diode
page 475 MFS-25248

JANTX1N981B Zener diode
page 475 MFS-25249

JANTX1N4570A Zener diode
page 476 MFS-25268

Semiconductor step-stress testing
page 473 MFS-25329

COMPOSITE MATERIALS
Liquid-oxygen-compatible covering material
page 509 MSC-16235

Structurally-continuous composite corners
page 578 LAR-11942

COMPOSITE STRUCTURES
Graphite/epoxy-tape test specimens
page 528 MSC-18495

COMPRESSION LOADS
Mechanical-load indicator
page 534 MSC-19511

COMPUTER DESIGN
Switching reduces computer power requirement
page 484 LAR-11958

COMPUTER GRAPHICS
Generalized plotting and contouring package
page 584 GSC-12367

COMPUTER STORAGE DEVICES
Conserving power in computer memories
page 482 LAR-11952

COMPUTERIZED SIMULATION
Spacecraft trajectory
page 541 LEW-13248

CONNECTORS [ELECTRIC]
Crimped thermocouple connections
page 559 MSC-18489

CONTOURS
Generalized plotting and contouring package
page 584 GSC-12367

CORNERS
Structurally-continuous composite corners
page 578 LAR-11942

CORRELATORS
Azimuth correlator device
page 469 NPO-14614

CORROSION PREVENTION
Simplified installation of thrust bearings
page 552 MFS-19473

COST REDUCTION
Fabrication cost savings in LSI microcircuits
page 580 MFS-25079

COUNTERS
Variable-resolution counter
page 463 LAR-12530

COUPLING CIRCUITS
Biased-receiver digital interface
page 466 MSC-14968

CRACK INITIATION
Arc-termination cracks in Inconel 718 and Incoloy 903
page 579 MFS-25089

CRACKING [FRACTURING]
Resonant-fatigue cracking apparatus
page 522 LEW-13037

CROSS CORRELATION
Acoustical measurement separates core noise and jet noise
page 526 NPO-14698

CROSSLINKING
Self-curing plastic foam
page 507 ARC-11170

CRYOGENIC EQUIPMENT
Liquid-oxygen-compatible covering material
page 509 MSC-16235

CRYSTAL GROWTH
Alloys of immiscible metals
page 508 MFS-23816

CURING
Self-curing plastic foam
page 507 ARC-11170

CURRENT REGULATORS
Rise-time control in saturated amplifiers
page 470 MSC-14934

CUTTING
Wire stripper
page 557 FRC-10111

CYLINDRICAL BODIES
Determining radii of cylindrical segments
page 536 LEW-12826

DATA COLLECTION PLATFORMS
Conserving power in computer memories
page 482 LAR-11952

DATA TRANSMISSION
Binary synchronous simulator
page 483 KSC-11096

Viterbi/algebraic hybrid decoder
page 585 MFS-25095

DECODERS
Viterbi/algebraic hybrid decoder
page 585 MFS-25095

DEPLOYMENT
High-acceleration cable deployment
page 545 ARC-11256

DIFFUSION
Single-, two-, and three-phase binary-alloy systems
page 511 LAR-12381

DIGITAL INTEGRATORS
Real-time digital integrator
page 465 NPO-14530

DIODES
JANTX1N3893 diode
page 476 MFS-25266

JANTX1N5415 diode
page 476 MFS-25270

JANTX1N5417 diode
page 476 MFS-25271

JANTX1N5420 diode
page 476 MFS-25272

JANTX1N5550 switching diode
page 476 MFS-25273

JANTX1N5552 switching diode
page 477 MFS-25274

JANTX1N5554 switching diode
page 477 MFS-25275

JANTX1N5614 switching diode
page 477 MFS-25276

JANTX1N5615 switching diode
page 477 MFS-25277

JANTX1N5618 switching diode
page 478 MFS-25278

JANTX1N5619 diode
page 478 MFS-25279

JANTX1N645-1 diode
page 474 MFS-25243

JANTX1N649-1 diode
page 474 MFS-25244

JANTX1N202A switching diode
page 475 MFS-25250

JANTX1N746A diode
page 474 MFS-25245

JANTX1N759A voltage-regulating diode
page 475 MFS-25246

JANTX1N4570A Zener diode
page 476 MFS-25268

JANTX1N937B Zener diode
page 475 MFS-25247

JANTX1N972B Zener diode
page 475 MFS-25248

JANTX1N981B Zener diode
page 475 MFS-25249

DOPING
Scratch encourages selective doping
page 557 LAR-11590

DRILLING
Adjusting an electron beam for drilling
page 568 MFS-19326

ELASTOMERS
Bonding soft rubber or plasticized elastomers to metal
page 574 MFS-25181

ELECTRIC BATTERIES
Nuclear electro-optic power
page 487 LAR-12496

ELECTRIC CONNECTORS
Securing connector pins to a PC board
page 561 MSC-16059

ELECTRIC CONTACTS
Stress-relieved solder joints
page 555 MSC-14981

ELECTRIC EQUIPMENT TESTS
Rapid testing of pulse transformers
page 529 MSC-18202

ELECTRIC RELAYS
Low-cost, lightweight RF transfer switch
page 472 MSC-16907

Low-EMI solid-state relay
page 465 MSC-12698

ELECTRIC WIRE
Wire stripper
page 557 FRC-10111

ELECTRIC WIRING
Stitch-bond/parallel-gap welding for IC circuits
page 558 MSC-16459

ELECTRODEPOSITION
Electrodeposition process reduces cost of cold plates
page 556 MSC-19524

Repairing sealing surfaces on aluminum castings
page 568 MFS-19455

ELECTROLYTES
A method increases fuel-cell pressure limit
page 490 MFS-25196

ELECTROMAGNETIC CURING
Electromagnetic bonding of plastics to aluminum
page 577 MFS-25083

ELECTROMAGNETIC INTERFERENCE
Low-EMI solid-state relay
page 465 MSC-12698

Low-noise sensor/amplifier for weak light sources
page 467 MFS-25025

ELECTROMAGNETIC SHIELDING
Wire stripper
page 557 FRC-10111

ELECTRON BEAMS
Adjusting an electron beam for drilling
page 568 MFS-19326

ELECTRONIC EQUIPMENT TESTS
Detector verifier for circuit analyzers
page 530 MSC-19669

ELECTRONIC PACKAGING
Fabrication cost savings in LSI microcircuits
page 580 MFS-25079

Improved switch-resistor packaging
page 562 MSC-19531

ENERGY CONVERSION EFFICIENCY
High-efficiency wind turbine
page 489 MFS-23830

ENERGY STORAGE
Wind-energy storage
page 499 LEW-13097

EVACUATING [VACUUM]
Evacuated-displacement compression molding
page 576 LAR-12523

FACSIMILE COMMUNICATION
Variable-resolution facsimile system
page 481 MSC-18516

FATIGUE TESTS
Resonant-fatigue cracking apparatus
page 522 LEW-13037

FETUSES
Monitoring fetal pH by telemetry
page 517 GSC-12507

FIELD EFFECT TRANSISTORS
Improved process control for VMOS FET's
page 561 GSC-12515

FILLETS
Shear strength of aluminum fillet welds
page 510 MFS-23946

FILTRATION
A method increases fuel-cell pressure limit
page 490 MFS-25196

FINITE DIFFERENCE THEORY
Numerical analysis of complex fluid-flow systems
page 584 MFS-25125

FINITE ELEMENT METHOD
Nonlinear structural analysis
page 537 MFS-25122

FLAT CONDUCTORS
Repairing flat cables
page 556 LAR-11950

FLUID AMPLIFIERS
Controlling subsynchronous whirl in turbopumps
page 533 MFS-19423

FLUID FILTERS
Indirect microbial detection
page 515 LAR-12520

FLUID FLOW
Numerical analysis of complex fluid-flow systems
page 584 MFS-25125

FOAMS
Self-curing plastic foam
page 507 ARC-11170

FREQUENCY SYNTHESIZERS
Digital generation of command-encoder waveforms
page 482 GSC-12203

FUEL CELLS
A method increases fuel-cell pressure limit
page 490 MFS-25196

GAS CHROMATOGRAPHY
Extracting trace substances from biological fluids
page 516 MSC-18522

GAS MASERS
PTFE plug protects H_2 masers
page 497 GSC-12552

GERMANIUM
Germanium-on-InP heterojunction-structure LED
page 492 LAR-12349

GUARDS [SHIELDS]
Improved table-saw guard
page 549 MSC-19550

HEAT EXCHANGERS
Electrodeposition process reduces cost of cold plates
page 556 MSC-19524

HEAT RESISTANT ALLOYS
Engineering properties of Incoloy-903 and CTX-1
page 510 MFS-23359

HEATING EQUIPMENT
Installation package-home solar heater
page 498 MFS-25338

Programable solar-energy controller
page 497 MFS-25189

HELICOPTERS
Helicopter sling loads
page 540 LAR-12557

HIGH PRESSURE
High-temperature high-pressure magnetic pickup
page 532 MSC-18389

Sealed high-pressure X-ray detector
page 495 GSC-12519

HIGH TEMPERATURE
High-temperature high-pressure magnetic pickup
page 532 MSC-18389

HOLDERS
Adjustable holder for transducer mounting
page 535 MSC-18371

HOLOGRAPHIC INTERFEROMETRY
Triple-exposure holography for materials tests
page 521 MFS-25180

HOLOGRAPHY
Optical comparator uses holographic subtraction
page 583 LAR-12126

HYDRAZINES
Low-cost scrubbing of monomethylhydrazine
page 504 KSC-11135

HYPERFINE STRUCTURE
Unresolved Mossbauer hyperfine spectra
page 511 LAR-12439

IMAGERY
Optical comparator uses holographic subtraction
page 583 LAR-12126

IMAGING TECHNIQUES
Automatically classifying Earth features from orbit
page 496 LAR-12589

INCONEL [TRADEMARK]
Arc-termination cracks in Inconel 718 and Incoloy 903
page 579 MFS-25089

Engineering properties of Incoloy-903 and CTX-1
page 510 MFS-23359

INDICATING INSTRUMENTS
Mechanical-load indicator
page 534 MSC-19511

INDIUM PHOSPHIDES
Ohmic contact to p-type indium phosphide
page 494 LAR-12351

INDUCTORS
Rise-time control is saturated amplifiers
page 470 MSC-14934

INITIATORS [EXPLOSIVES]
"Three-dimensional" vibration fixture
page 529 MSC-16305

INSTRUMENT PACKAGES
An evaluation of low-cost payload carrier
page 536 MFS-25129

INSULATION
Detecting insulation defects in metal/plastic films
page 526 MFS-25127

INVISCID FLOW
Transonic airfoil analysis and design
page 540 LAR-12354

ION IMPLANTATION
Improved process control for VMOS FET's
page 561 GSC-12515

IONIZATION
An improved welding-arc starter
page 570 MSC-17415

JACKS [LIFTS]
Thermal jack
page 572 MFS-19365

JET AIRCRAFT NOISE
Acoustical measurement separates core noise and jet noise
page 526 NPO-14698

JET ENGINES
Measuring acoustic properties of materials and jet nozzles
page 523 LEW-13265

JET FLAPS
Aerodynamic performance of jet-flap wings
page 538 ARC-11215

JOSEPHSON JUNCTIONS
A practical Josephson voltage standard
page 488 MFS-23845

LAMINATES
Detecting insulation defects in metal/plastic films
page 526 MFS-25127

Vacuum-and-pressure laminating polymer materials
page 575 LEW-12721

LANDSAT SATELLITES
Automatically classifying Earth features from orbit
page 496 LAR-12589

Landsat signature development program
page 500 KSC-11113

LARGE SCALE INTEGRATION
Fabrication cost savings in LSI microcircuits
page 580 MFS-25079

LASERS
CdSinP semiconductor alloy
page 494 LAR-12405

Improved degradation resistance of (AlGa)As lasers
page 491 LAR-12242

Improved thermal-conducting and current-confining film
page 493 LAR-12350

Improved vapor-growth technique for III-V compound lasers
page 492 LAR-12255

Ohmic contact to p-type indium phosphide
page 494 LAR-12351

LEAKAGE
Protecting brazing furnaces from air leaks
page 569 MFS-19379

LEVITATION
Improved acoustic levitation apparatus
page 564 MFS-25050

LIGHT EMITTING DIODES
Germanium-on-InP heterojunction-structure LED
page 492 LAR-12349

LIGHT SOURCES
Low-noise sensor/amplifier for weak light sources
page 467 MFS-25025

LIGUID-GAS MIXTURES
Separating liquid and gaseous solutions
page 506 MFS-23368

LOGIC CIRCUITS
Biased-receiver digital interface
page 466 MSC-14968

Real-time digital integrator
page 465 NPO-14530

LOUDNESS
Overall loudness of steady sounds
page 537 LEW-12914

LOW GRAVITY MANUFACTURING
Separating liquid and gaseous solutions
page 506 MFS-23368

MAGNETIC TRANSDUCERS
High-temperature high-pressure magnetic pickup
page 532 MSC-18389

MAINTENANCE
Repairing flat cables
page 556 LAR-11950

MARKING
Precision scriber
page 563 LEW-12976

MASS SPECTROMETERS
A low-cost molecular-leak valve
page 505 LAR-12249

MATERIALS HANDLING
Helicpoter sling loads
page 540 LAR-12557

METAL BONDING
Electromagnetic bonding of plastics to aluminum
page 577 MFS-25083

METAL COATINGS
A plasma-sprayed valve coating
page 565 MFS-19494

METAL FILMS
Improved thermal-conducting and current-confining film
page 493 LAR-12350

METAL MATRIX COMPOSITES
Alloys of immiscible metals
page 508 MFS-23816

METAL OXIDE SEMICONDUCTORS
Improved process control for VMOS FET's
page 561 GSC-12515

Multilayer metalization of MOS IC's
page 560 MFS-23541

METAL SHEETS
Welding multiple plies with an electron beam
page 574 MFS-19428

METAL-METAL BONDING
Removing bonded skin from a substrate
page 579 MSC-19664

METALLIZING
Multilayer metalization of MOS IC's
page 560 MFS-23541

MICROMETERS
Determining radii of cylindrical segments
page 536 LEW-12826

MICROORGANISMS
Indirect microbial detection
page 515 LAR-12520

MICROSCOPES
Microscope for high-temperature welding
page 571 MSC-19572

MICROWAVE AMPLIFIERS
PTFE plug protects H_2 masers
page 497 GSC-12552

MODULATORS
Digital generation of command-encoder waveforms
page 482 GSC-12203

MOLDS
Evacuated-displacement compression molding
page 576 LAR-12523

MOLECULAR FLOW
A low-cost molecular-leak valve
page 505 LAR-12249

MONOMERS
Improved synthesis of polyformals
page 506 ARC-12244

MONTE CARLO METHOD
Monte Carlo variance reduction
page 499 MFS-23645

MOSSBAUER EFFECT
Unresolved Mossbauer hyperfine spectra
page 511 LAR-12439

MOUNTING
Adjustable holder for transducer mounting
page 535 MSC-18371

MULTISPECTRAL PHOTOGRAPHY
Landsat signature development program
page 500 KSC-11113

MYOCARDIUM
Trifunctional transducer for myocardial monitoring
page 517 NPO-14329

NEWTON-RAPHSON METHOD
Nonlinear structural analysis
page 537 MFS-25122

NICKEL ALLOYS
Engineering properties of Incoloy-903 and CTX-1
page 510 MFS-23359

NICKEL PLATE
Repairing sealing surfaces on aluminum castings
page 568 MFS-19455

NODES [STANDING WAVES]
Improved acoustic levitation apparatus
page 564 MFS-25050

NOISE MEASUREMENT
Acoustical measurement separates core noise and jet noise
page 526 NPO-14698

NOISE THRESHOLD
Overall loudness of steady sounds
page 537 LEW-12914

NONDESTRUCTIVE TESTS
Triple-exposure holography for materials tests
page 521 MFS-25180

NUCLEAR ELECTRIC POWER GENERATION
Nuclear electro-optic power
page 487 LAR-12496

NUMERICAL ANALYSIS
Numerical analysis of complex fluid-flow systems
page 584 MFS-25125

NUMERICAL CONTROL
Programable solar-energy controller
page 497 MFS-25189

OHMIC CONTACT
Ohmic contact to p-type indium phosphide
page 494 LAR-12351

OPTICAL DATA PROCESSING
Optical comparator uses holographic subtraction
page 583 LAR-12126

Variable-resolution facsimile system
page 481 MSC-18516

OPTICAL FILTERS
Microscope for high-temperature welding
page 571 MSC-19572

Viewing electron-beam welds in progress
page 573 MFS-19364

OUTGASSING
Vacuum-and-pressure laminating polymer materials
page 575 LEW-12721

OXIDATION RESISTANCE
Inhibiting oxidation of tungsten at high temperatures
page 565 MFS-19347

Single-, two-, and three-phase binary-alloy systems
page 511 LAR-12381

PACKAGING
An evaluation of low-cost payload carrier
page 536 MFS-25129

PAINTS
Recirculating sprayer for fiber-filled paints
page 550 KSC-11146

PAYLOADS
An evaluation of low-cost payload carrier
page 536 MFS-25129

PEELING
Removing bonded skin from a substrate
page 579 MSC-19664

PERFORMANCE TESTS
Testing of a solar collector with concentrating mirrors
page 498 MFS-25310

PH
Monitoring fetal pH by telemetry
page 517 GSC-12507

PHOSPHORYLATION
Improved synthesis of polyformals
page 506 ARC-11244

PINS
Securing connector pins to a PC board
page 561 MSC-16059

PIPELINES
Liquid-oxygen-compatible covering material
page 509 MSC-16235

PIPES [TUBES]
Tube-shape verifier
page 567 MSC-19623

PLASMA SPRAYING
A plasma-sprayed valve coating
page 565 MFS-19494

PLOTTING
Generalized plotting and contouring package
page 584 GSC-12367

PLUGS
A simple self-sealing plug
page 546 MSC-19635

POLLUTION MONITORING
Indirect microbial detection
page 515 LAR-12520

POLYFORMALS
Improved synthesis of polyformals
page 506 ARC-11244

POLYIMIDES
Self-curing plastic foam
page 507 ARC-11170

POLYMERIC FILMS
Detecting insulation defects in metal/plastic films
page 526 MFS-25127

PORTS [OPENINGS]
A simple self-sealing plug
page 546 MSC-19635

POWER EFFICIENCY
Switching reduces computer power requirement
page 484 LAR-11958

PRESSING [FORMING]
Evacuated-displacement compression molding
page 576 LAR-12523

PRESSURE MEASUREMENTS
Tire-pressure measuring concept
page 524 MSC-18490

PRESSURE SENSORS
Miniature motor-driven instrument valve
page 547 LEW-13195

Onsite testing of pressure-sampling valves
page 527 LAR-12428

PRINTED CIRCUITS
Securing connector pins to a PC board
page 561 MSC-16059

PROJECTILES
High-acceleration cable deployment
page 545 ARC-11256

PROPULSIVE EFFICIENCY
Spacecraft trajectory
page 541 LEW-13248

PROTECTIVE COATINGS
PTFE plug protects H_2 masers
page 497 GSC-12552

PULSE MODULATION
Rapid testing of pulse transformers
page 529 MSC-18202

PUMPS
Recirculating sprayer for fiber-filled paints
page 550 KSC-11146

PURIFICATION
Low-cost scrubbing of monomethylhydrazine
page 504 KSC-11135

PYROLYSIS
Improved vapor-growth technique for III-V compound lasers
page 492 LAR-12255

PYROTECHNICS
"Three-dimensional" vibration fixture
page 529 MSC-16305

RADAR TRACKING
Azimuth correlator device
page 469 NPO-14614

RADIATION DETECTORS
Sealed high-pressure X-ray detector
page 495 GSC-12519

RADIATIVE RECOMBINATION
Improved degradation resistance of (AlGa)As lasers
page 491 LAR-12242

RADII
Determining radii of cylindrical segments
page 536 LEW-12826

RADIO FREQUENCIES
A reliable solid-state RF transfer switch
page 472 MSC-16890

Low-cost, lightweight RF transfer switch
page 472 MSC-16907

RANDOM SAMPLING
Monte Carlo variance reduction
page 499 MFS-23645

REAL TIME OPERATION
Real-time digital integrator
page 465 NPO-14530

RECEIVERS
Biased-receiver digital interface
page 466 MSC-14968

REDUNDANT COMPONENTS
Redundant structures at elevated temperatures
page 538 MSC-18476

REGULATORS
Overload protection for switching regulators
page 468 MSC-18513

RESISTORS
Improved switch-resistor packaging
page 562 MSC-19531

RESOLUTION
Variable-resolution counter
page 463 LAR-12530

Variable-resolution facsimile system
page 481 MSC-18516

ROTARY STABILITY
Controlling subsynchronous whirl in turbopumps
page 533 MFS-19423

SAFETY DEVICES
Improved table-saw guard
page 549 MSC-19550

SAWS
Improved table-saw guard
page 549 MSC-19550

SCORING
Precision scriber
page 563 LEW-12976

SCREWS
Screw/stud removal tool
page 550 MFS-22957

SEA WATER
Synthetic seawater as stress-corrision test medium
page 525 MFS-22706

SEALS [STOPPERS]
A simple self-sealing plug
page 546 MSC-19635

Bonding soft rubber or plasticized elastomers to metal
Page 574 MFS-25181

Flexible sliding seal
page 548 MSC-18467

Repairing sealing surfaces on aluminum castings
page 568 MFS-19455

SEMICONDUCTOR DEVICES
JANTX1N3893 diode
page 476 MFS-25266

JANTX1N5415 diode
page 476 MFS-25270

JANTX1N5417 diode
page 476 MFS-25271

JANTX1N5420 diode
page 476 MFS-25272

JANTX1N5550 switching diode
page 476 MFS-25273

JANTX1N5552 switching diode
page 477 MFS-25274

JANTX1N5554 switching diode
page 477 MFS-25275

JANTX1N5614 switching diode
page 477 MFS-25276

JANTX1N5615 switching diode
page 477 MFS-25277

JANTX1N5618 switching diode
page 478 MFS-25278

JANTX1N5619 diode
page 478 MFS-25279

JANTX1N645-1 diode
page 474 MFS-25243

JANTX1N649-1 diode
page 474 MFS-25244

JANTX1N746A diode
page 474 MFS-25245

JANTX1N759A voltage-regulating diode
page 475 MFS-25246

JANTX1N202A switching diode
page 475 MFS-25250

JANTX1N4570A Zener diode
page 476 MFS-25268

JANTX1N937B Zener diode
page 475 MFS-25247

JANTX1N972B Zener diode
page 475 MFS-25248

JANTX1N981B Zener diode
page 475 MFS-25249

Semiconductor step-stress testing
page 473 MFS-25329

SEMICONDUCTOR LASERS
CdSInP semiconductor alloy
page 494 LAR-12405

SEMICONDUCTORS [MATERIALS]
Scratch encourages selective doping
page 557 LAR-11590

SEPARATORS
Separating liquid and gaseous solutions
page 506 MFS-23368

SEQUENTIAL CONTROL
Mechanical-load indicator
page 543 MSC-19511

SERUMS
Extracting trace substances from biological fluids
page 516 MSC-18522

SERVOMECHANISMS
Window comparator for voltages
page 464 FRC-10090

SHAPES
Tube-shape verifier
page 567 MSC-19623

SHEAR STRENGTH
Shear strength of aluminum fillet welds
page 510 MFS-23946

SIMULATORS
Binary synchronous simulator
page 483 KSC-11096

SKIN [STRUCTURAL MEMBER]
Removing bonded skin from a substrate
page 579 MSC-19664

SLIDING
Flexible sliding seal
page 548 MSC-18467

SLURRIES
Longer shelf life for ceramic slurries
page 509 MSC-18543

SOLAR CELLS
Measuring transmissivity of solar-cell covers
Page 490 NPO-14638

SOLAR ENERGY
Installation package-home solar heater
page 498 MFS-25338

Programable solar-energy controller
page 497 MFS-25189

Testing of a solar collector with concentrating mirrors
page 498 MFS-25310

Weathering of a liquid solar collector
page 498 MFS-25300

SOLDERED JOINTS
Stress-relieved solder joints
page 555 MSC-14981

SOUND GENERATORS
Improved acoustic levitation apparatus
page 564 MFS-25050

SOUND PRESSURE
Overall loudness of steady sounds
page 537 LEW-12914

SOUND TRANSMISSION
Measuring acoustic properties of materials and jet nozzles
page 523 LEW-13265

SPACEBORNE PHOTOGRAPHY
Automatically classifying Earth features from orbit
page 496 LAR-12589

SPACECRAFT TRAJECTORIES
Spacecraft trajectory
page 541 LEW-13248

SPARK GAPS
An improved welding-arc starter
page 570 MSC-17415

SPECTRAL SIGNATURES
Landsat signature development program
page 500 KSC-11113

SPECTRUM ANALYSIS
Unresolved Mossbauer hyperfine spectra
page 511 LAR-12439

SPLICING
Crimped thermocouple connections
page 559 MSC-18489

SPRAYERS
Recirculating sprayer for fiber-filled paints
page 550 KSC-11146

SPUTTERING
Multilayer metalization of MOS IC's
page 560 MFS-23541

STACK-GAS PURIFICATION
Simultaneous stack-gas scrubbing and wastewater treatment
page 503 MSC-16258

STAINLESS STEELS
Brazing titanium to stainless steel
page 571 LAR-11441

STANDARDS
A practical Josephson voltage standard
page 488 MFS-23845

STATISTICAL ANALYSIS
Monte Carlo variance reduction
page 499 MFS-23645

STRESS CORROSION
Synthetic seawater as stress-corrosion test medium
page 525 MFS-22706

STRESS RELIEF
Stress-relieved solder joints
page 555 MSC-14981

STRUCTURAL ANALYSIS
Nonlinear structural analysis
page 537 MFS-25122

Redundant structures at elevated temperatures
page 538 MSC-18476

STUDS [STRUCTURAL MEMBERS]
Screw/stud removal tool
page 550 MFS-22957

SULFUR OXIDES
Simultaneous stack-gas scrubbing and wastewater treatment
page 503 MSC-16258

SUPERSONIC SPEEDS
Wing and leading-edge thrust
page 541 LAR-12516

SURFACE CRACKS
Resonant-fatigue cracking apparatus
page 522 LEW-13037

SURFACE DEFECTS
Triple-exposure holography for materials tests
page 521 MFS-25180

SWEPT WINGS
Transonic flow past swept wings
page 539 LAR-12446

SWITCHES
A reliable solid-state RF transfer switch
page 472 MSC-16890

Low-cost, lightweight RF transfer swtich
page 472 MSC-16907

SWITCHING
Low-EMI solid-state relay
page 465 MSC-12698

Switchbox for welding torches
page 572 MFS-19354

Switching reduces computer power requirement
page 484 LAR-11958

SWITCHING CIRCUITS
Conserving power in computer memories
page 482 LAR-11952

Improved switch-resistor packaging
page 562 MSC-19531

Overload protection for switching regulators
page 468 MSC-18513

SYNCHRONOUS COMMUNICATIONS
Binary synchronous simulator
page 483 KSC-11096

TELEMETRY
Monitoring fetal pH by telemetry
page 517 GSC-12507

TEMPERATURE CONTROL
Installation package-home solar heater
page 498 MFS-25338

TEMPERATURE PROBES
Rugged fast-response temperature probe
page 531 ARC-11289

TEMPERATURE TESTS
Semiconductor step-stress testing
page 473 MFS-25329

TENSILE TESTS
Graphite/epoxy-tape test specimens
page 528 MSC-18495

TEST FACILITIES
Graphite/epoxy-tape test specimens
page 528 MSC-18495

THERMAL CONDUCTORS
Improved thermal-conducting and current-confining film
page 493 LAR-12350

THERMAL EXPANSION
Thermal jack
page 572 MFS-19365

THERMAL INSULATION
Liquid-oxygen-compatible covering material
page 509 MSC-16235

THERMAL [STRESSES]
Redundant structures at elevated temperatures
page 538 MSC-18476

THERMOCOUPLES
Crimped thermocouple connections
page 559 MSC-18489

THERMODYNAMIC EFFICIENCY
Weathering of a liquid solar collector
page 498 MFS-25300

THRUST
Wing and leading-edge thrust
page 541 LAR-12516

THRUST BEARINGS
Simplified installation of thrust bearings
page 552 MFS-19473

TIME MEASUREMENT
Variable-resolution counter
page 463 LAR-12530

TIRES
Tire-pressure measuring concept
page 524 MSC-18490

TITANIUM
Brazing titanium to stainless steel
page 571 LAR-11441

TOOLS
A tool for installation/removal of cylindrical baffles
page 551 MFS-19508

Precision scriber
page 563 LEW-12976

TORCHES
Switchbox for welding torches
page 572 MFS-19354

TRANSDUCERS
Adjustable holder for transducer mounting
page 535 MSC-18371

Low-noise sensor/amplifier for weak light sources
page 467 MFS-25025

Trifunctional transducer for myocardial monitoring
page 517 NPO-14329

TRANSFORMERS
Rapid testing of pulse transformers
page 529 MSC-18202

TRANSMISSION LINES
Repairing flat cables
page 556 LAR-11950

TRANSONIC FLOW
Transonic airfoil analysis and design
page 540 LAR-12354

Transonic flow past swept wings
page 539 LAR-12446

TRANSPARENCE
Measuring transmissivity of solar-cell covers
page 490 NPO-14638

TUNGSTEN
Inhibiting oxidation of tungsten at high temperatures
page 565 MFS-19347

TURBINE PUMPS
Controlling subsynchronous whirl in turbopumps
page 533 MFS-19423

Simplified installation of thrust bearings
page 552 MFS-19473

High-efficiency wind turbine
page 489 MFS-23830

VACUUM FURNACES
Protecting brazing furnaces from air leaks
page 569 MFS-19379

VALVES
A low-cost molecular-leak valve
page 505 LAR-12249

A plasma-sprayed valve coating
page 565 MFS-19494

Miniature motor-driven instrument valve
page 547 LEW-13195

Onsite testing of pressure-sampling valves
page 527 LAR-12428

VAPOR DEPOSITION
Germanium-on-InP heterojunction-structure LED
page 492 LAR-12349

Improved vapor-growth technique for III-V compound lasers
page 492 LAR-12255

VIBRATION TESTS
"Three-dimensional" vibration fixture
page 529 MSC-16305

VISCOUS FLUIDS
Longer shelf life for ceramic slurries
page 509 MSC-18543

VOLTAGE REGULATORS
Window comparator for voltages
page 464 FRC-10090

WASTE DISPOSAL
Low-cost scrubbing of monomethylhydrazine
page 504 KSC-11135

WATER TREATMENT
Simultaneous stack-gas scrubbing and wastewater treatment
page 503 MSC-16258

WEATHERING
Measuring transmissivity of solar-cell covers
page 490 NPO-14638

Testing of a solar collector with concentrating mirrors
page 498 MFS-25310

Weathering of a liquid solar collector
page 498 MFS-25300

WELD STRENGTH
Shear strength of aluminum fillet welds
page 510 MFS-23946

WELDING
Inhibiting oxidation of tungsten at high temperatures
page 565 MFS-19347

Microscope for high-temperature welding
page 571 MSC-19572

Stitch-bond parallel-gap welding for IC circuits
page 558 MSC-16459

Switchbox for welding torches
page 572 MFS-19354

Viewing electron-beam welds in progress
page 573 MFS-19364

Welding multiple plies with an electron beam
page 574 MFS-19428

WIND TUNNEL CALIBRATION
Onsite testing of pressure-sampling valves
page 527 LAR-12428

WIND TUNNELS
Miniature motor-driven instrument valve
page 547 LEW-13195

Rugged fast-response temperature probe
page 531 ARC-11289

WINDPOWER UTILIZATION
Wind-energy storage
page 499 LEW-13097

WINDPOWERED GENERATORS
High-efficienty wind turbine
page 489 MFS-23830

WING LOADING
Aerodynamic performance of jet-flap wings
page 538 ARC-11215

WING PLANFORMS
Wing and leading-edge thrust
page 541 LAR-12516

WIRE
Wire stripper
page 557 FRC-10111

WRENCHES
A tool for installation/removal of cylindrical baffles
page 551 MFS-19508

Screw/stud removal tool
page 550 MFS-22957

X-RAY APPARATUS
Sealed high-pressure X-ray detector
page 495 GSC-12519

*U.S. GOVERNMENT PRINTING OFFICE: 1980-311-486/2

National Aeronautics and
Space Administration

Washington, D.C.
20546

Official Business
Penalty for Private Use, $300

THIRD-CLASS BULK

THIRD-CLASS BULK RATE
POSTAGE & FEES PAID
NASA
WASHINGTON, D.C.
PERMIT No. P-154

NASA

Four high-intensity floodlights on the roof of this emergency vehicle are elevated by an extendable mast, originally developed to deploy antennas on NASA spacecraft. The lights are part of a commercial system that includes a generator and a dashboard-mounted control panel. [*See page A1.*]



